AN ABSTRACT OF THE THESIS OF

Cristina M. Darr for the degree of Masters of Science in Geology presented on December 6, 2006.

Title: Magma Chamber Processes Over the Past 475,000 Years at Mount Hood, Oregon: Insights From Crystal Zoning and Crystal Size Distribution Studies

Abstract approved:

Adam J.R. Kent

Several different petrological techniques have been applied to lava flows between 200 to 475,000 years old from Mount Hood, Oregon. Mount Hood is unusual, in comparison to nearby Mount St. Helens and Mount Jefferson, in that it has produced relatively homogeneous lava compositions over 475,000 years. Erupted lavas are mostly crystal rich andesites and in total vary between 53 and 63 weight percent silica, with ~85% of the lavas having silica between 58-62 wt. %. The most evolved lavas have only erupted within the past 15,000 years. Despite this homogeneity, and as with many other silicic volcanoes, petrographic features such as mineral zoning, sieved textures and dissolution surfaces, suggest a more complex magmatic history. Crystal Size Distribution (CSD) studies have been used to identify different plagioclase crystal populations, to recognize mixing of these populations and to estimate crystal residence times within the magma chamber. The major and trace element compositions of crystal populations have also been determined using Electron Microprobe Analysis (EMPA) and Laser Ablation Inductively Coupled Plasma Mass Spectrometry (LA-ICP-MS).

Results show that the lavas at Mount Hood are derived from mixing of two end member magmas. Each of the end members contribute a plagioclase crystal population to

the final erupted lava that is distinguishable in the lavas by CSD studies and trace element compositions. The first crystal population belongs to a relatively undepleted mafic end member that has only been crystallizing plagioclase for approximately 3.9 – 5.5 years, assuming a crystal growth rate of 10^{-9} mm/sec, while the other is from a more silicic end member that has been crystallizing plagioclase for 177 – 227 years, assuming a crystal growth rate of 10^{-10} mm/sec. Textural disequilibrium textures are found near the rim of plagioclase phenocrysts from the second populations of crystals and correlate to increases in anorthite, MgO, FeO, Ti, and Sr and decreases in Ba and Ce indicating that the plagioclase have recorded a mixing event between the host and a relatively more mafic magma during the later stages of crystallization, which may have triggered eruptions. Eruptions of these mixed magmas occur approximately 3 – 0.2 years after the mixing event takes place.

Magma Chamber Processes Over the Past 475,000 Years at Mount Hood, Oregon: Insights From Crystal Zoning and Crystal Size Distribution Studies

by
Cristina M. Darr

A THESIS

submitted to

Oregon State University

in partial fulfillment of
the requirements for the
degree of

Master of Science

Presented December 6, 2006
Commencement June 2007

Master of Science thesis of Cristina M. Darr presented on December 6, 2006

APPROVED:

Major Professor, representing Geology

Chair of the Department of Geosciences

Dean of the Graduate School

I understand that my thesis will become part of the permanent collection of Oregon State University libraries. My signature below authorizes release of my thesis to any reader upon request.

Cristina M. Darr, Author

ACKNOWLEDGMENTS

I would like to thank Adam Kent, Anita Grunder, and Frank Tepley for all of their support, advice, and funding with the research involved in this project. I would also like to thank William Scott and Cynthia Gardner of the USGS Cascade Volcanic Observatory for all of their time and knowledge when leading me and others around Mount Hood to collect samples. To my friends in the Geology Department at Oregon State University and all around the country, thank you for your help and support with all aspects of my work.

Lastly, I'd like to thank my Mom, Dad, Sister, and Mike for their continued support that helped me get through my Masters work, and my Grandmother who passed on her love of rocks to me.

TABLE OF CONTENTS

TABLE OF CONTENTS (Continued)

LIST OF FIGURES

LIST OF FIGURES (Continued)

LIST OF FIGURES (Continued)

LIST OF TABLES

Introduction

Compositional Homogeneity in Mount Hood Lavas

Mount Hood is composed of lavas with a very restricted range (53 – 63 weight percent silica. This is a large difference when compared to the range of lava compositions from neighboring volcanoes in the Cascade Volcanic Arc (Cribb and Barton, 1997; Crandell, 1980; Sherrod and Smith, 1990; Wood, 1990). Understanding the origin of what is producing the lack of magma diversity at Mount Hood requires an understanding of both the magma chamber processes that control composition and the link between these and the processes that lead to eruptions. This study will investigate the timing of mixing and eruption in more detail. The goal is to identify crystal populations within individual magmas using geochemical and textural analysis techniques, and to use this information to constrain the timing of crystal growth and mixing.

This study will focus on plagioclase phenocrysts and microphenocryts. Compositional changes in the magma chamber are recorded in plagioclase crystals that nucleate and grow within the chamber and then subsequently erupt. Plagioclase is suited to such studies because it is stable over a broad range of magmatic conditions, is resistant to re-homogenization via diffusion, and through mineral partition coefficients may record the composition of melt from which it has crystallized, although plagioclase compositions are also susceptible to changes in T and fluid pressure. Plagioclase can thus provide a means to investigate the range of magma compositions present in the magma chamber through time.

Geochemical evidence recorded in plagioclase such as changing anorthite or trace elements compositions could be interpreted as changes in the composition of the magma in the chamber due to physical processes such as crystal fractionation or recharge magma. Textural evidence such as dissolution surfaces and oscillatory zoning can represent times of disequilibrium within the magma chamber. Geochemical and textural evidence may lead to a better understanding of different processes occurring in the chamber as phenocrysts are crystallizing and what has and may still trigger an eruption at Mount Hood.

Geologic Background of the Cascades

Mount Hood is a stratovolcano and is part of the Cascade Volcanic Arc that extends from southern British Columbia to northern California, approximately 1000 km in length. Activity along the arc began approximately 40 million years ago and continues into modern times (McBirney, 1978; Guffanti and Weaver, 1988; Priest, 1990; Taylor, 1990). The Cascade Volcanic Arc was first formed by the subduction of the Farallon Plate beneath the North American plate, which was then split into two micro-plates when subduction ended in California and the San Andreas Fault was formed approximately 30 Ma (McBirney, 1978, Guffanti and Weaver, 1988, Taylor, 1990). The Juan de Fuca Plate, the northern remnant of the Farallon Plate, is currently being subducted at a rate of 3.8 cm/yr to 4.6 cm/yr and is currently underlying the Cascade Volcanic Arc (Guffanti and Weaver, 1988; McBirney, 1978; Priest, 1990, Rogers, 1985; Taylor, 1990) (Figure 1).

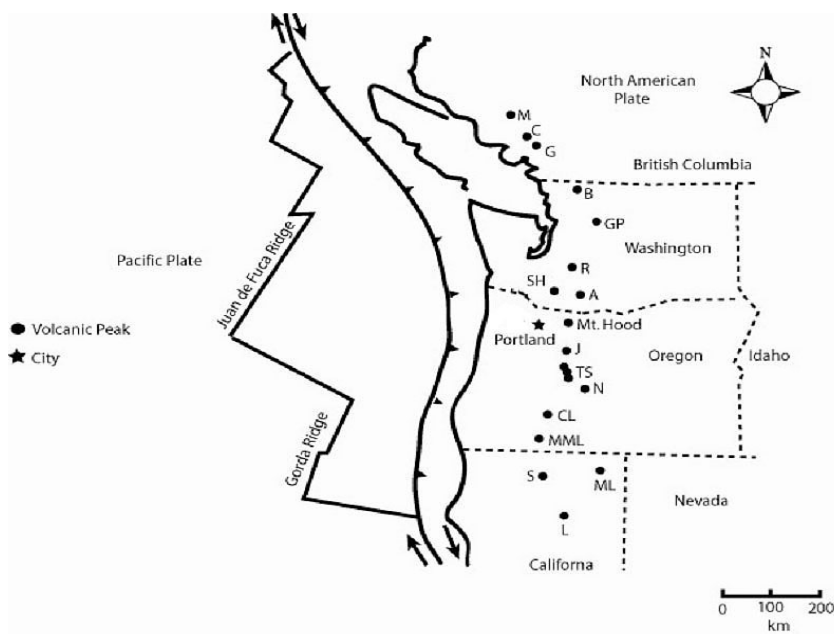

Figure 1: Map of Pacific Northwest with locations of plates and volcanoes of the Cascade Volcanic Arc. Abbreviations for volcanoes are a follows: M = Mt. Meager, C = Mt. Cayley, G = Mt. Girabaldi, B = Mt Baker, GP = Glacier Peak, R = Mt. Rainier, SH = Mt. St. Helens, A = Mt. Adams, J = Mt. Jefferson, TS = Three Sisters, N = Newberry, CL = Crater Lake, MML = Mt. mc Laughlin, S = Mt. Shasta, ML = Medicine Lake, L = Lassen Peak.

The following description of the formation of the Cascade Volcanic Arc is a summary from several papers (Blakely and Jachens, 1990; McBirney, 1978; Guffanti and Weaver, 1988; Priest, 1990; Rogers, 1985; Sherrod and Smith, 1990; Taylor, 1990).

The arc consists of two distinct volcanic assemblages, the older Western Cascades and the younger High Cascades. Development of the Western Cascades began approximately 35 million years ago when large amounts of tholeiitic lavas were erupted, which reflects the initial arc with an oceanic section behind it in the Columbia Embayment. Calc-alkaline compositions became dominant in the late Eocene. Over the next 30 Ma the Western Cascades rotated clockwise into their present position while the subducting slab began to flatten out below the arc and the convergence rate decreased to the present day rate. These changes moved the volcanic arc eastward, created a more oblique convergence zone, and decreased the amount of volcanic material that was being erupted from the arc. Due to these changes within the subduction zone there is a decrease in the amount of volcanism when the older Western Cascades are compared to the younger High Cascades.

Between 10 and 5 Ma, two major tectonic developments occurred. The Western Cascades were uplifted and tilted to the west, while at approximately the same time an intra-arc graben was formed in the High Cascades. This was followed by the development of the High Cascades. The graben itself was probably a result of extensional forces from the oblique subduction of the Juan de Fuca Plate, and the empting of magma chambers that resided below the arc (Figure 2). The graben is best developed in the central Cascade Range where several large volcanoes reside in close proximity to each other, and is less developed in the northern and southern sections of the Cascade Range where the major volcanoes are situated farther from each other. The graben down dropped some areas in the central Cascade Range up to 700 meters. The propagation of the intra-arc graben is continuing to move northward with the approximate position of the modern rift opening situated just south of Mount Hood. A period of increased eruptions and volcanic products around 7.4 Ma characterized by large amounts of basalt, basaltic andesite, and minor amounts of silicic ash flows filled in parts of the graben that would later serve as a platform for the modern High Cascade stratovolcanoes to build upon. The large stratovolcanoes that form the crest of the Cascade Range began to develop within the last 1 Ma. These volcanoes themselves are predominantly calc-alkaline andesite with a total compositional range covering basalt to more infrequent rhyolite.

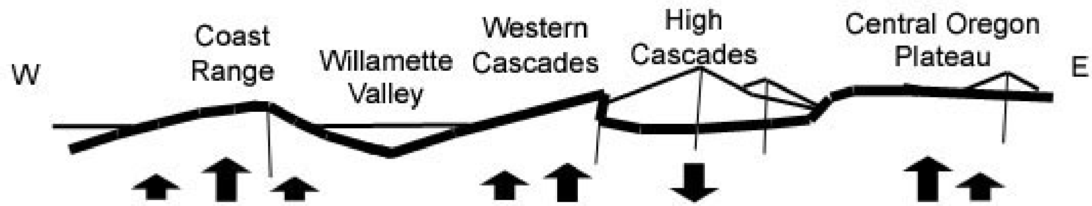

Figure 2: Graben formation in the High Cascades. Modified from McBirney (1978), and Taylor (1990).

Over the eruptive lifespan of the Cascade Volcanic Arc the frequency of large explosive eruptions and overall volcanic activity has decreased, yet there still has been several notable eruptions during the Holocene and also during recorded history, including Mount Mazama (7,600 BP), which formed Crater Lake Caldera; Mount St. Helens (May 18, 1980 and currently active); Mount Hood (~200 BP); Mount Rainer (2,300 and 1,000 BP); and Lassen Peak (1914 – 1917). Mount Hood has active fumaroles near Crater Rock.

Geologic Background of Mount Hood

Mount Hood is located 75 km east-southeast of Portland, Oregon in the Cascade Range. It is the highest (3,426 meters) and most northern peak of the Cascade Range in Oregon (Cribb and Barton, 1997; Scott, et al., 1997, 2003). It has been built upon basaltic lava flows from Miocene to Pliocene in age. The oldest exposed rocks in the Mount Hood area are unrelated Miocene tholeiitic lavas that belong to the Columbia River Basalt Group (~15.3 Ma). The mountain itself is less than 730,000 years old (Hoblitt, et al., 1987; Wise, 1969; Wood, et al., 1990); however, the scope of this paper deals with lavas as old as 475,000 years. The bulk of the volcano is made of calc-alkaline andesite lava flows and deposits ranging in composition from 53 – 63 weight percent silica. Overall, the compositions of the erupted materials are restricted. The most evolved dacite compositions have only erupted with in the last 15,000 years and make up only a small fraction of the entire bulk of Mount Hood (Cribb and Barton, 1997; Crandell, 1980; Sherrod and Smith, 1990; Wood, 1990).

The eruptive history of Mount Hood can be divided into five eruptive stages, with each separated by periods of relative inactivity (Table 1): Main Stage or Pre-Polallie (>29,000 years); Polallie (15,000 – 12,000 years); Timberline (1,800 – 1,400 years); Zigzag (600 – 400 years); and Old Maid (250 – 180 years). The ages of the eruptive periods were dated using K/Ar dating (Cribb and Barton, 1997; Cameron and Pringle, 1986, 1987; Crandell, 1980; Hoblitt, et al., 1987; Priest, 1982; Scott, et al., 1997, 2003; White, 1980; Wood, 1990).

Table 1: Eruptive history of Mount Hood, Oregon, including other major events.

Eruptive Stage/Events	Age Range	Eruptive Products
Pumice Eruption	1859 - 1865	Scattering of gray pumice fragments
Old Maid	250 - 180 years	Pyroclastic Flows Lahars Dome Growth and Collapse Crater Rock Formed
Zigzag	600 - 400 years	Lithic-rich lahars Pyroclastic flows Dome Growth and Collapse
Timberline	1.8 - 1.4 ka	Pyroclastic Flows Dome Growth and Collapse
Parkdale Lava Flow	7.7 - 7.5 ka	Lava Flow
Polallie	15 - 12 ka	Pyroclastic Flows Dome Growth and Collapse
Fraser Glaciation	29 - 10 ka	
Main Stage (Pre-Polallie)	>29 ka	Lava Flows Pyroclastic flows

The Main Stage or the Pre-Polallie eruptive period (>29 ka) makes up approximately 90% of the volume of Mount Hood. The eruptive products are typically either lava flows or pyroclastic debris flows, and are overall andesite in composition. The majority of the lavas from this study are from Main Stage. Typically, the lavas from this eruptive period are medium grained, porphyritic and contain phenocrysts of plagioclase, orthopyroxene with minor amounts of clinopyroxene and hornblende. The hornblende typically has an oxide reaction rim, and may be completely reacted into Fe-Ti oxides. The groundmass is hypocrystalline with plagioclase laths (Cribb and Barton, 1997; Priest, 1982; White, 1980).

The Polallie eruptive period (15 ka – 12 ka) is separated from the Pre-Polallie eruptive period by the Fraser Glaciation between 29 ka and 10 ka, which reached its maximum around 18 ka. Eruptive products from this period were mostly pyroclastic flows formed by the collapse of extruding summit domes. These deposits have been found on all sides of Mount Hood, but primarily occur on the east and northeast flanks. Rocks from this period have an andesite to dacite composition and are porphyritic with phenocrysts of plagioclase, orthopyroxene, clinopyroxene, and hornblende. The groundmass is typically holocrystalline with microlites of plagioclase, orthopyroxene, and clinopyroxene (Cameron and Pringle, 1987; Crandell, 1980; Cribb and Barton, 1997; Hoblitt, et al., 1987; White, 1980).

A 10 ka gap of relative inactivity exists between the end of the Polallie eruptive period and the start of the Timberline eruptive stage (1.8 ka – 1.4 ka). Eruption style and products from this time period are similar to those from the Polallie eruptive period. The major difference between the two is the absence of phenocrystic hornblende in Timberline products, and the minor amount of hornblende that is present is surrounded by oxide reaction rims. The vent during this eruptive period was located on the southwest side just below the summit and is known for creating the main debris fan seen today on the south flank of Mount Hood (Cameron and Pringle, 1986, 1987; Crandell, 1980; Cribb and Barton, 1997).

Between the Polallie eruptive period and the following Timberline eruptive period, the only known lava flow to occur during postglacial time was the Parkdale lava flow located about 11 km north of Mount Hood. It was dated as having erupted around 7.7 – 7.5 ka. The flow is andesite (silica ~58 weight percent) with a blocky surface. It is approximately 7 km long and 0.3 km^3 in volume (Hoblitt, et al., 1987; Scott, et al., 2003). It is believed that the Parkdale flow post-dates the eruption of Mount Mazama since there is no indication of tephra associated with the Mazama eruption on the surface of the flow, unlike elsewhere in the area, where tephra can be as thick as 10 cm thick (Scott, et al., 2003).

After Timberline, another time gap exists prior to the Zigzag eruptive period (600 – 400 years ago). This eruptive period has the lowest volume and extent of eruptive products than any of the other eruptive periods. Products from this period were lithic-rich lahars and pyroclastic flows formed by dome collapses (Cameron and Pringle, 1986, 1987). Lahar and pyroclastic flow deposits from this period have only been identified in the Sandy and Zigzag River basins.

The last documented eruptive period is the Old Maid eruptive period (250 – 180 years ago). Characterized by pyroclastic flows and lahars similar to the previous eruptive periods, the most distinctive remnant of this period was the creation of Crater Rock. Crater Rock is a dacite dome near the summit on the south side of Mount Hood. Rocks from Crater Rock are rich in phenocrysts of plagioclase, orthopyroxene, and hornblende (Crandell, 1980; Cribb and Barton, 1997). The pyroclastic flows and lahars formed by dome collapses were large enough to change the river morphology of the Sandy, Zigzag, and White rivers. The effects of these flows were noted in the journals of Captain William Clark during the Lewis and Clark expedition through the Pacific Northwest in the early 1800's (Cameron and Pringle, 1986, 1987). Between the years of 1859 – 1865 a small eruption known as the Pumice Eruption occurred. This scattered gray pumice with a composition of ~62.6 weight percent silica, and the largest piece was approximately 2 cm in diameter (Crandell, 1980).

In contrast to Mount St. Helens, located to the northwest in Washington, Mount Hood is not known for violent explosive eruptions; however, with the slow evolution to more dacitic lava compositions, the possibility of a more explosive eruption exists. To date, most eruptions consist of lava flows, pyroclastic flows, debris avalanches, lava dome collapse, and lahars. Today the greatest hazards posed by Mount Hood are lava dome collapses resulting pyroclastic flows, which in turn, would melt glaciers and snow creating lahars. These lahars may be strong enough to disrupt and change river channels. Another likely hazard would be debris avalanches with similar general consequences as a pyroclastic flow (Crandell, 1980; Gardner, et al., 2000; Hoblitt, 1987; Scott, et al., 1997, 2003).

Previous Works on Mount Hood and Other Similar Volcanoes

As stated earlier, the compositional range of lavas erupted from Mount Hood over its entire eruptive lifespan is relatively restricted with a total range of 53 – 63 weight percent silica (Cribb and Barton, 1997). Furthermore, the majority of the lavas (85%) are between 58 – 62 weight percent silica and the most silicic lavas have only been erupted within in the past 15 ka (Scott, et al., 1997, 2003). The lack of compositional range in lavas from Mount Hood over a long eruptive time period is unusual when Mount Hood is compared to neighboring Cascade volcanoes. Mount Jefferson, approximately 80 km to the south of Mount Hood, has a much broader lava composition over its eruptive history (50 – 71 weight percent silica) (Conrey, et al., 2001). Intermediate and silicic volcanism has persisted at Mount Jefferson for about 1 million years (Conrey, et al., 2001). Lavas erupted from Mount Jefferson are hypothesized to be derived from two types of crustal melting beneath the arc (Conrey, et al., 2001). Mount St. Helens, approximately 100 km to the north of Mount Hood, has compositions between 48 – 69 weight percent silica (Hoblitt, et al., 1980; Smith and Leeman, 1993) (Figure 3). The basaltic and dacitic magmas are thought to be derived from partial melts of distinct mantle and crustal sources, while the intermediate magmas are formed by the mixing between the mafic and silicic magmas (Smith and Leeman, 1993). It might be suspected that the homogeneous compositions erupted from Mount Hood are the result of a relatively simple magmatic evolution path; however, petrographic features such as mineral zoning, sieved textures and dissolution surfaces appear indicative of a more complex magmatic history.

Several works have noticed this paradox. Cribb and Barton (1997) suggested that repeated cycles of mixing within the magma chamber at Mount Hood accompanied by fractionation of plagioclase, orthopyroxene, clinopyroxene, and ilmenite resulted in the eruption of compositionally homogeneous lavas. Their evidence for this included the presence of olivine and plagioclase phenocrysts with partially resorbed rims. Cribb and Barton (1996) showed that these repeated cycles of mixing at a constant host magma to recharge magma ratio results in a buffered system that produces homogeneous magma compositions. Cribb and Barton (1997) were also able to determine that there had been small amounts of assimilated volcanic upper crust added to the system and negligible assimilation of subducted sediments or upper mantle sources due to the absence of high field strength elements (HFSE) depletions in the lavas.

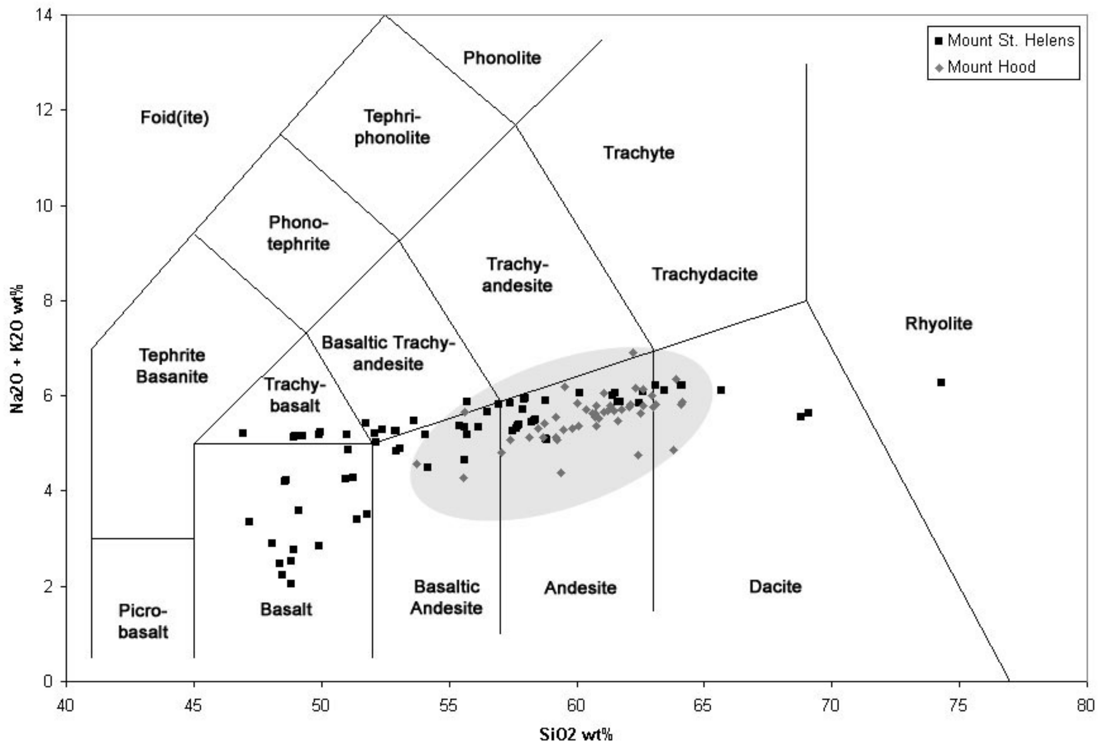

Figure 3: Compositional range of lavas from Mount Hood and Mount St. Helens. Shaded area shows the restricted range of compositions from Mount Hood when compared to the wider range of Mount St. Helens. Composition data for Mount St Helens and Mount Hood from the GeoRock database (Mount St. Helens – Halliday, et al., 1983; Heliker, 1995; Leeman, et al.,1990; Melson, 1983; Smith, 1986, 1987; Mount Hood – Cribb and Barton, 1997; Wise, 1969).

Woods (2004) continued to research this hypothesis and concluding that the lavas from Mount Hood were formed by a combination of crystal fractionation and magma mixing plus magma recharge. The presence of mafic inclusions in the lavas was interpreted to represent a recharging magma quenched in the original host magma. These mafic inclusions were found to be only slightly more mafic than the host rock and had a mineralogy that was similar to the host lavas. These were then considered to be a parental magma. Woods (2004) modeled crystal fractionation of the Mount Hood lavas, and showed that crystal fractionation of magmas depleted in silica could reproduce observed lava compositions. To support the idea of magma mixing in the chamber, Woods (2004) used the composition of the inclusion as the mafic end member and the host rock andesite composition as the mixed product and defined a hypothetical silicic end member (66 weight percent silica). Assuming that the inclusions were also formed by mixing, two hypothetical mafic end members were calculated (one basaltic at 49 weight percent silica and one basaltic andesite at 54 weight percent silica). The two mafic end members varied by the amount of the hypothetical silicic end member that was added. Both the host rock and the inclusions generally fell along the mixing line formed by the silicic end member and the mafic end members.

Another way to determine what is occurring in the chamber to produce homogeneous compositions is to examine the minerals in lavas for textural and compositional variations. Different types of zoning found in plagioclase, due to periods of growth alternating with periods of dissolution, reaction, or slow growth, can be used to interpret what has occurred in the chamber to bring about such zoning. Any interpretation would have to take into account the width of the zones and compositional changes. Pearce and Kolisnik (1990) divided different types of plagioclase zoning into two main types. Type 1 zoning is characterized by small scale changes (1 – 10 μm wide zones and 1 – 10 An % changes) and is due to near equilibrium diffusion controlled growth along the boundary layer. Type 2 zoning (up to 100 μm wide zones and 10 – 25 An % changes), however, is caused by larger scale disturbances, such as magma mixing, or changes in T, P, or P_{H2O}.

There are several examples of the use of plagioclase zoning to investigate magma chamber processes in the literature (Browne, et al., 2006; Davidson and Tepley, 1997; Landi, et al., 2004; Morgan, et al., 2004; Tepley, et al., 1997, 2000; Triebold, et al., 2006). Landi et al., (2004) interpreted abrupt compositional and textural changes in the plagioclase phenocrysts in scoria samples from Stromboli, Italy to reflect recharge of a magma chamber containing an evolved silicic magma with a new hotter and more primitive magma. The plagioclase are complexly zoned with layer thicknesses ranging from <10 to 100 μm and anorthite variations in the rings ranged from An_{62} to An_{88}. The most common textural changes within the crystals include sieve textures that were derived from plagioclase dissolution followed by crystal growth. Similar textures have been observed in plagioclase from Mt. Hood.

According to Tepley, et al. (2000) plagioclase crystals in the homogeneous lavas at El Chichón in Mexico show large (10 – 25 An %), sharp, type 2 zoning variations in the anorthite content from the core to the rim. These changes in plagioclase compositions would indicate that there have been large perturbations occurring within the chamber, however, compositional changes are not evident in the bulk rock itself. These spikes in the anorthite content show influences of magma injections on the magma chamber. Influx of hotter volatile-rich magmas would effectively lower the plagioclase solidus and stabilize a more anorthite-rich plagioclase composition. A baseline anorthite content of $\sim An_{40}$ is seen after each of the major spikes within the plagioclase, showing a return to equilibrium state within the chamber. There are also textural discontinuities seen within the plagioclase crystals due to dissolution of the crystals during periods associated with mixing and temperature fluctuations.

Recharge of a mafic magma into a more silicic magma is one likely trigger of an eruption (Eichelberger, 1995; Izbekov, et al., 2004; Murphy, et al., 1998; Sparks, et al., 1977; Watts, et al., 1999). The recharge and mixing of magmas causes several parameters of a magma chamber to change, creating more favorable conditions for an eruption to occur. These include increase in the volume of magma chamber, superheating of resident magma, and volatile exchange during recharge (Watts, et al., 1999). Increasing the volume of magma within a chamber will increase the magmatic pressure which may than exceed the principal stress and tensile strength of the surrounding rock causing failure of the rock and an eruption to take place (Bindeman, 1993; Eichelberger, 1995; Murphy, et al., 1998; Watts, et al., 1999). Superheating of a magma would induce convection of the host magma, reduce viscosity, and lower the solubility of volatiles, which in turn would increase vapor pressure that may trigger an eruption (Eichelberger, 1995; Murphy, et al., 1998; Sparks, et al., 1977; Watts, et al., 1999). Lastly, as a cooler silicic magma meets with a hotter mafic recharge magma a mixing zone may develop along the interface of the two systems possibly promoting crystallization and volatile saturation in the melt. This would increase the volume of the magma and may create vapor overpressures large enough to trigger an eruption (Watts, et al., 1999).

Cerro Chascon-Runtu Jarita Complex, Southwest Bolivia (Watts, et al., 1999), Soufriere Hills, Montserrat, West Indies (Murphy, et al., 1998), and Karymsky Volcano, Kamchatka (Izbekov, et al., 2004) all show evidence for a mafic recharge magma entering a more silicic magma system, which may have lead to an eruption. At Soufriere Hills, Montserrat, West Indies, observations of reversely zoned plagioclase (lacking sodic overgrowths) and reversely zoned orthopyroxenes from andesite lavas suggests that the recharge event occurred just prior to the eruption. Similar mineral compositional changes can also be seen in the andesite lavas from Karymsky, Kamchatka. There are also xenocrysts of basaltic origin, and olivine that has been found as resorbed cores in pyroxene phenocrysts.

Methods

Sample Collection

Lava samples of varying ages were collected from around Mount Hood during the summers of 2004 and 2005. Nine different lava flows and one sample from the Crater Rock were sampled from various locations along the length of the flows (Figure 4). Ages of the flows range from 475 ka to approximately 215 year old. Ages for these flows are based on K/Ar dating with one-sigma error (Scott, et al., 2003). Several samples were collected from each of the sampled lava flows in order to obtain samples that contained inclusions and were inclusion free. For the Parkdale lava flow, several samples were taken from along the length of the flow to use in determining compositional changes within the flow (Figure 5). Table 2 lists each lava sample along with several other characteristics of each sample. Figure 6 is a simplified geologic map of the Mount Hood region that shows the approximate location of the sample locations (excluding the four Parkdale samples). Explanations of map units are in Table 3.

Table 2: Samples from Mount Hood, Oregon.

Sample Label	Date Collected	Age	Eruptive Period	Location GPS	SiO_2	EMPA Plag	XRF	CSD	LA-ICP-MS
CD-04-01	9/21/04	~225 ka	Main Stage	N 45 19.048, W 121 48.637	60.0	x	x	x	
TL-04-01	9/21/04	1.5 ka	Timberline	N 45 19.944, W 121 42.489	63.4		x		
HW-04-01	9/21/04	120 ka	Main Stage	N 45 17.419, W 121 44.087	61.9	x	x		
HM-04-01	9/21/04	50 ka	Main Stage	N 45 19.070, W 121 37.921	60.1	x	x	x	x
CS-04-01	9/21/04	425 ka	Main Stage	N 45 25.551, W 121 34.750	58.9		x		
CS-04-02	9/21/04	475 ka	Main Stage	N 45 25.636, W 121 35.184	59.2	x	x	x	
CC-04-01	9/21/04	55 ka	Main Stage	N 45 27.384, W 121 35.903	55.7	x	x	x	x
EB-04-01	9/21/04	35 ka	Main Stage	N 45 27.695, W 121 38.420	61.9	x	x	x	
PD-04-01	9/21/04	7.5 ka	Parkdale Flow	N 45 30.162, W 121 36.917	58.8	x	x	x	x
PD-05-02	7/22/05	7.5 ka	Parkdale Flow	N 45 31.177, W 121 37.280	58.6	x	x		x
PD-05-03	7/22/05	7.5 ka	Parkdale Flow	N 45 29.472, W 121 37.288	58.1	x	x		
PD-05-04	7/22/05	7.5 ka	Parkdale Flow	N 45 29.629, W 121 37.475	58.1	x	x		
MHM-05-05	9/19/05	50 ka	Main Stage	N 45 20.639, W 121 40.333	61.1		x		
WR-05-01	9/19/05	~215	Old Maid	N 45 18.492, W 121 40.971	63.7	x	x		x

Sample Preparation

Sixteen thin sections were made after cutting the samples into 2.5 x 4.5 cm billets. The billets were sent to Petrographic International in Saskatchewan, Canada to be made into thin sections for petrographic and geochemical analyses using the petrographic microscope, Electron Microprobe Analysis (EMPA), Laser Ablation Inductively Coupled Plasma Mass Spectrometry (LA-ICP-MS), and Crystal Size Distribution (CSD) analytical methods.

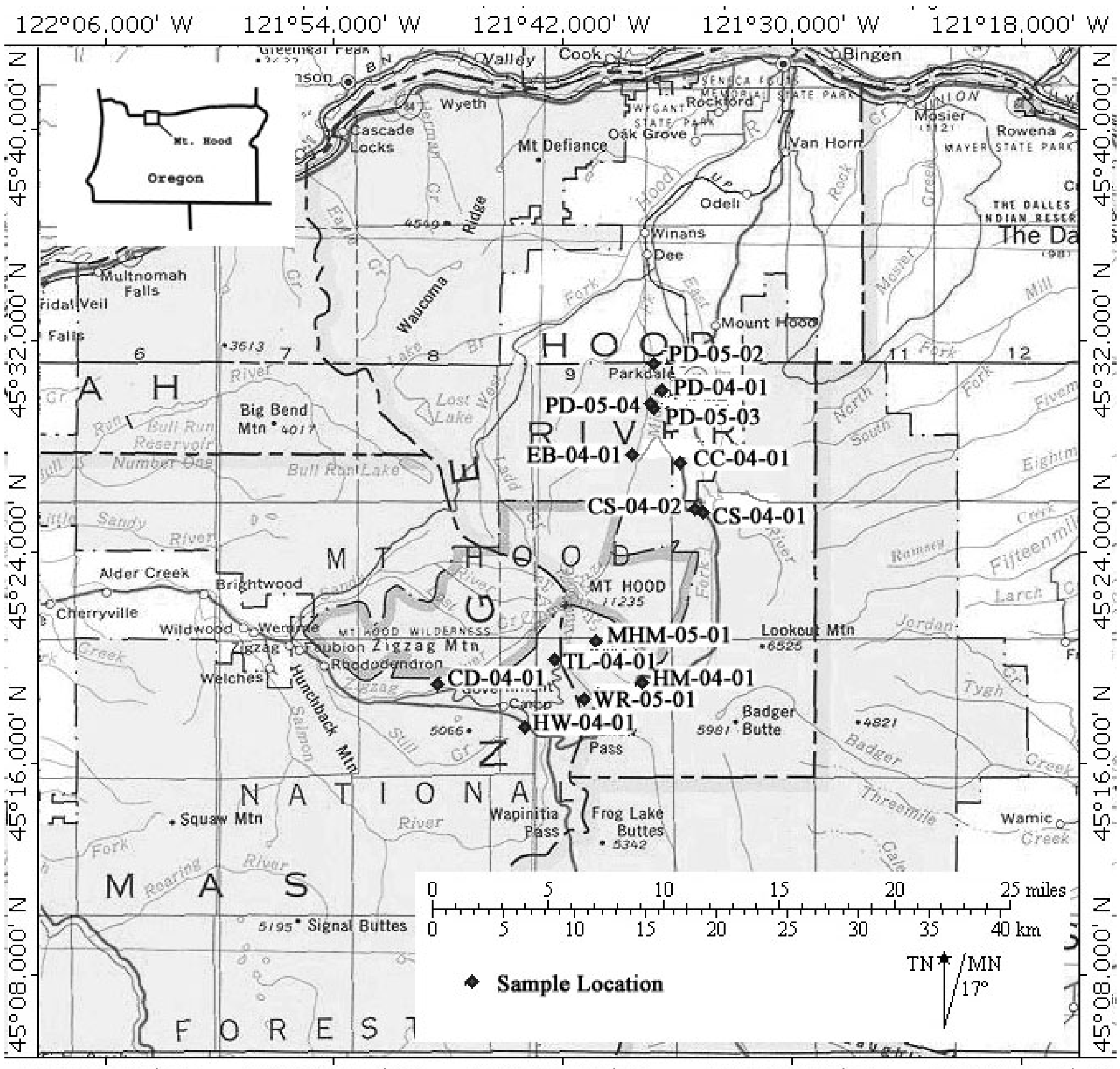

Figure 4: Location of samples collected from Mount Hood for this study. Map modified from National Geographic Topo! (2000).

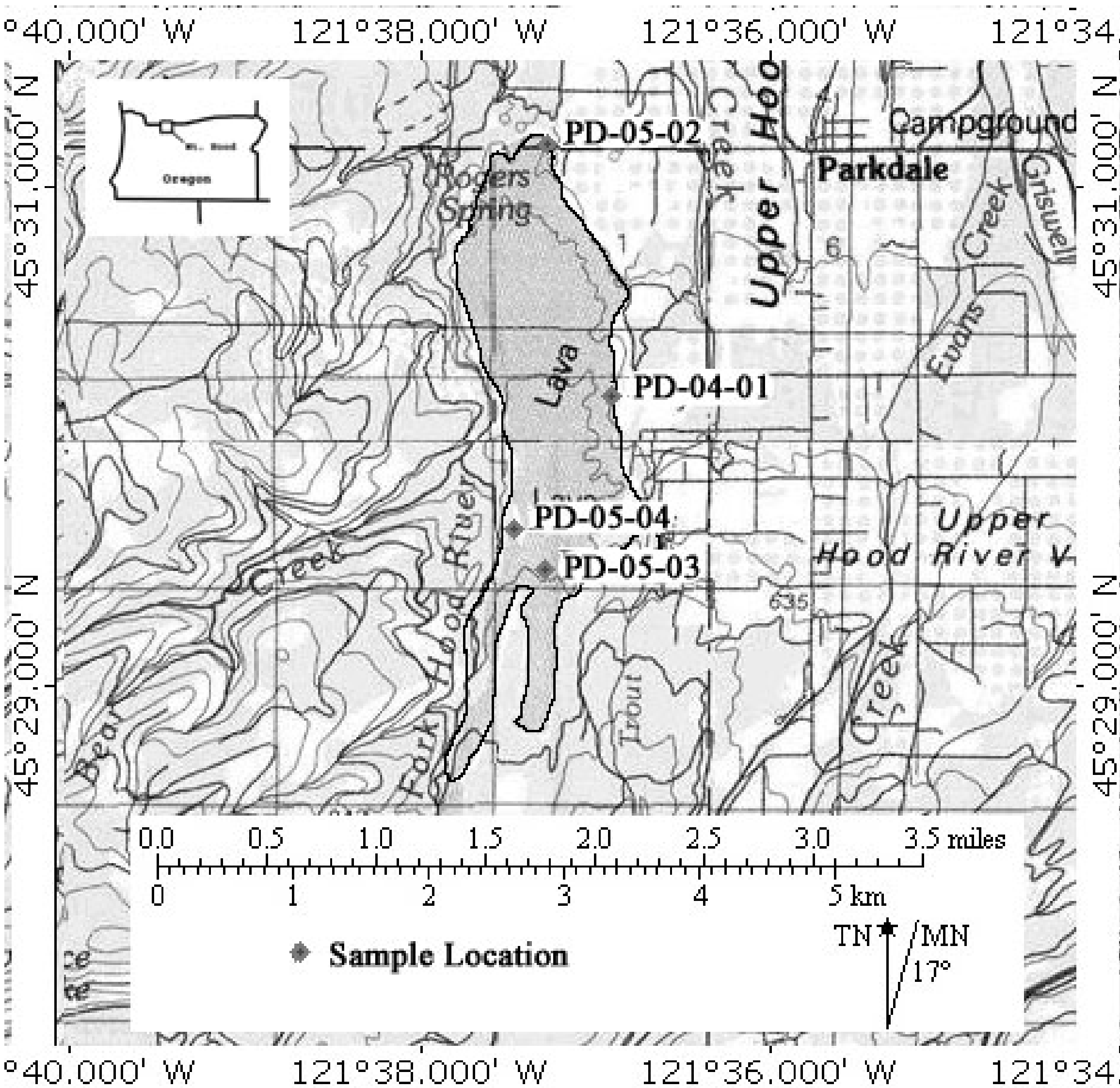

Figure 5: Detailed location map for Parkdale lava samples. Lava flow has been outlined in black. Map modified from National Geographic Topo! (2000).

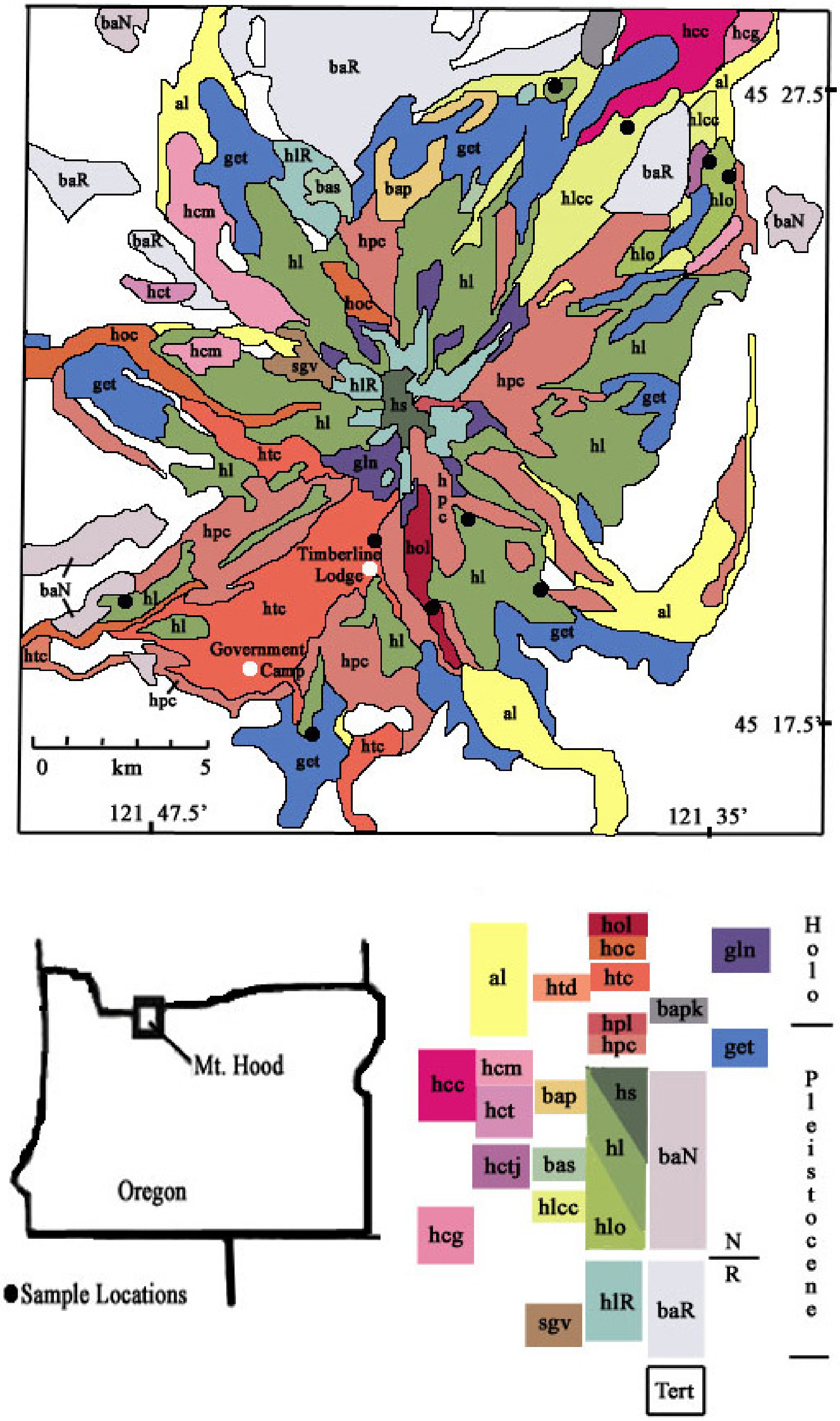

Figure 6: Geologic map of Mount Hood. Samples locations shown as black dots. Parkdale samples not included in this figure. Modified from Scott, et al. (2000).

Table 3: Explanation of geologic map units for Figure 6. Modified from Scott, et al. (2000).

Explanation of Map Units

Alluvial an Glacial Deposits		Mount Hood Volcano:	Clastic deposits	Lava flows and domes	Lava flows and pyroclastic deposits of other vents in map area	
		hol		Of Old Maid Eruptive Period		
al	Alluvium	hoc	Of Old Maid Eruptive Period			
gln	Till of neoglacial age	htc	Of Timberline Eruptive Period			
		htd	Debris avalanche of Ladd Creek		bapk	Basaltic andesite of Parkdale
		hpl		Of Polallie Eruptive Period		
		hpc	Of Polallie Eruptive Period			
ge	Till, Evans Creek Advance					
		hcm	Of McGee Creek			
		hs		Undivided; of summit		
		hcc	Of Clear Creek		bap	Basaltic andesite of the Pinnacle
		hct	Of Top Spur			
		hctj	Of Tilly Jane Creek		bas	Basaltic andesite of Stump Creek
		hcg	Of Griswell Creek			
		hl		Undivided; of main cone	hlcc	Basaltic andesite of Cloud Cap
		hlo		Older Units; N Polarity	baN	Basaltic andesite; N Polarity
		hlR		Older Units; R polarity	sgv	Basaltic to andesite of Sandy Glacier Volcano
					baR	Basalt and basaltic andesite; R polarity
					Tert	Pre-Quaternary lava flows and sedimentary rocks

X-ray Fluorescence

Fourteen sampled lavas were analyzed by XRF. These consisted of samples from ten different flows with two samples from a 50 ka year old flow, which goes through Mount Hood Meadows Ski area and 4 from the Parkdale flow. The multiple samples from a single lava flow were analyzed to determine chemical variations within the flow. The samples were first broken down into small chips using a sledgehammer and chips were selected that were free of inclusions, weathered surfaces, and saw marks. Further preparation and analyses were performed at Washington State University. The chips were ground in a swing mill with tungsten carbide surfaces. Once powdered, 3.5 g of the sample were put into a plastic jar with 7.0 g of spec pure dilithium tetraborate ($Li_2B_4O_7$), and mixed with the aid of a small plastic ball. The mixed powders were then placed in graphite crucibles and placed in a furnace for 5 minutes at 1000°C. Once cooled the beads were reground in the swing mill, and then re-fused in the furnace. The beads then had their lower surface ground on 600 silicon carbide grit, washed with alcohol, and dried. The beads were then analyzed on an Advant'XP+ ThermoARL sequential wavelength-dispersive X-ray spectrophotometer, which analyzes each sample for 10 major and minor elements and 18 trace elements, and is run at 60kV/60mA for all elements. Precision data for this technique for each element is in Table 4.

Table 4: Analytical Precision for XRF analysis (Standard BCR-2 basalt (unnormalized) from Johnson, et al., 1999).

Element	Standard Deviation Weight Percent	Element	Standard Deviation ppm
SiO2	0.159	Ni	1.7
TiO2	0.006	Cr	1.0
Al2O3	0.060	Sc	1.4
FeO*	0.040	V	3.6
MnO	0.001	Ba	6.2
MgO	0.038	Rb	0.9
CaO	0.024	Sr	0.9
Na2O	0.031	Zr	0.9
K2O	0.008	Y	1.4
P2O5	0.002	Nb	0.5
		Ga	2.5
		Cu	1.6
		Zn	2.3
		Pb	2.5
		La	3.8
		Ce	5.9
		Th	1.4
		Nd	3.0

Electron Microprobe Analysis

Electron Microprobe analyses were conducted at Oregon State University using a Cameca SX 100 microprobe. Plagioclase and pyroxenes phenocrysts were analyzed using 1 μm beam with a sample current of 15 nA with an accelerating voltage of 15kV for plagioclase and 30 nA at 15kV for pyroxenes. For pyroxenes (both orthopyroxene and clinopyroxene) analyses were done at the core and the rim to determine changes in composition over the crystals crystallization period within the magma chamber. The same was done for plagioclase microlites and several plagioclase phenocrysts in each sample. For four samples (the most mafic sample, the most evolved sample, and two from the Parkdale flow) more detailed traverses were performed on zoned plagioclase phenocrysts. A Backscattered Electron (BSE) image was taken of the plagioclase prior to analysis. Traverses were conducted from the core of the phenocrysts to the rim at 5 μm spacing.

The Electron Microprobe was also used to create X-ray maps of six thin sections at high and low magnifications. These yielded detailed maps of the thin sections encompassing a ~5 mm x 7 mm area for high magnification and a ~20 mm x 23 mm area for low magnification. Each thin section had an X-ray map of Al, Ca, K, and Fe for use in crystal size distribution created in both high and low magnifications. Precision data for the Cameca SX 100 microprobe is given in Table 5.

Table 5: Analytical precision for EMPA. Standard Labradorite analyzed six times

	Average Calculated (Weight Percent)	Standard Labradorite (Weight Percent)	Standard Deviation (1 sigma)	Standard Deviation %	Average Detection Limit (ppm)
Na	2.64	2.56	0.0094	0.36	246
Mg	0.09	0.08	0.0074	8.04	140
Al	16.31	16.36	0.0132	0.08	280
Si	24.00	23.96	0.0358	0.15	331
K	0.10	0.15	0.0081	8.07	189
Fe	0.33	0.34	0.0046	1.37	712
Ca	9.64	9.75	0.0122	0.13	233
O*	46.75	47.61	0.0663	0.14	
Total	99.85	100.81			

*** O calculated as summary Fe = FeO**

Crystal Size Distribution

Background

Crystal size distribution (CSD) can be used to yield quantitative information using the dimensions and relationship of crystals within igneous rocks. The main goal of CSD studies is to examine the relationship between crystal size (mm) and crystal population densities (ln(n)) (crystals per size per volume) (Marsh, 1988) where n is defined as dN/dL and N is the number of crystals of a certain crystal size (L) (Marsh, 1998). Graphs of crystal size versus density usually show clear correlations (Cashman and Marsh, 1988; Higgins, 1994, 1998, 2000, 2002; Marsh, 1988, 1998). These plots describe the changes in frequency and sizes of crystals as a function of their residence times in the system and as a function of influx and loss of crystals to the system (Marsh, 1988).

The data gathered for CSD, however, is only a 2D representation of the crystal population in the rock. The long axis length measured in a 2D section is not always the true long axis length in a 3D crystal. This is known as the cut section effect (Higgins, 1998). This measured length in 2D is most likely the intermediate axis length. To have more representative data, the 2D sectional data has to be converted to 3D. Higgins (2000) has designed a program known as CSDCorrections, which allows the user to convert 2D data to 3D data. This is done using a parallelepiped model that assumes that the section measured is thin compared with the dimension of the entire rock. The fabric of the rock, quality of the fabric, and the orientation of the crystals to the fabric must be characterized as well.

The crystal number and length are probably the most sensitive part of a magmatic system to the kinetic processes within a system (Marsh, 1988, 1998). Nucleation density, nucleation and growth rates, and orders of kinetic reactions can be estimated from the data derived from CSD. The pattern the plots form can also describe several physical properties, such as residence time, growth rate, number of crystal populations, mixing histories, and textural coarsening (Higgins, 1998; Marsh, 1988).

A typical CSD graph, characteristic of a mature open steady-state system with continuous crystallization of one population of crystals, is a straight line with a negative slope (Marsh, 1988, 1998; Higgins, 2000) (Figure 7). This shows that the larger crystals in a given rock have a smaller population density than that of the smaller sized crystals. In other words, more crystals have nucleated than those that have grown in size. Another way to understand why these plots have negative slopes is to realize that the larger a crystal grows, the larger its chances become of being removed from the system in which it first nucleated by either eruption or crystal settling. The probability of a crystal to remain in the system is inversely proportional to its age and

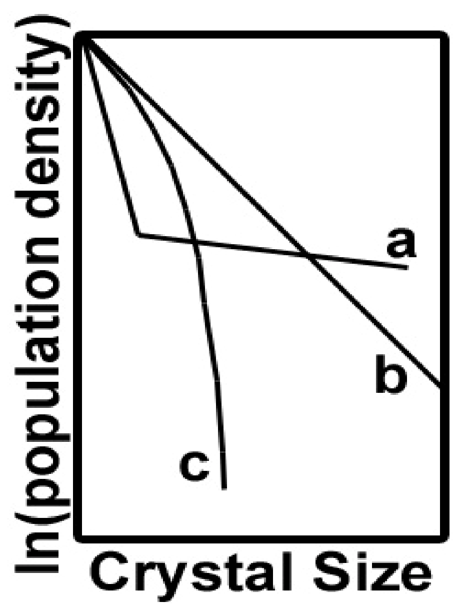

Figure 7: Typical patterns seen in CSD plots. a) Mixing between two magmas with different crystal population sizes, b) Crystallization of one population of crystals, c) fractionation and removal of large crystals. Modified from Marsh, 1988).

size (Marsh, 1988).

Variations from this typical pattern result from physical process inside the chamber, such as mixing of two crystal populations, crystal fractionation, or textural coarsening. Any of these processes can affect CSD by changing properties such as style of circulation, holding regime (Marsh, 1988). Thus, the variations can represent magma chamber processes (Figure 7).

A commonly seen variation in a CSD plot is a curved convex up line. This curved convex up CSD can reflect several different physical processes. One is sequential periods of cooling during the ascent and emplacement of the magma. Another is mixing of magmas with different size populations. If a magma with a majority of small crystals is mixed with a magma dominated by larger crystals, the CSD plot would have a kink in the line where the slope of the line changes from one crystal population to the other. The first magma would have a steeper slope, while the second would have a much shallower slope (Figure 8).

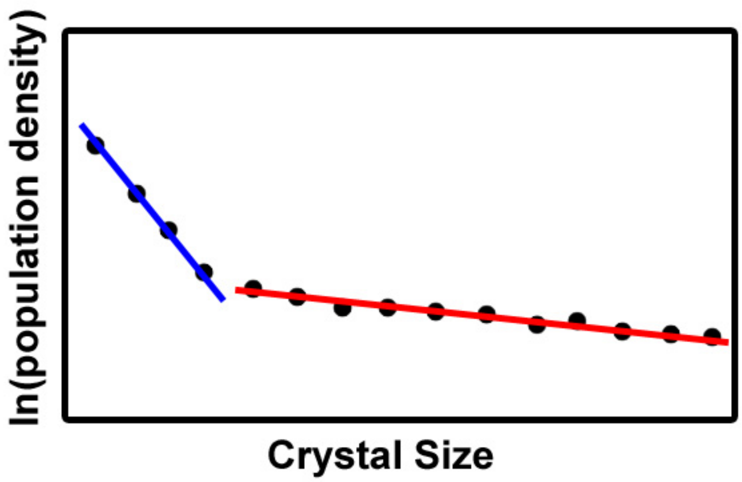

Figure 8: Example of the pattern formed by mixing two magmas with different sized crystal populations. The division between the two populations is found at the kink in the curve. Each crystal population can be characterized by different slopes. Crystal population 1 is in blue and crystal population 2 is in red.

Slopes in CSD plots can represent amount of undercooling in the system and the slope's linear relationship can be related to the average residence time of the crystals by the use of a simple equation (Marsh, 1988, 1998):

$$t_r = \frac{-1}{G * m * 31,536,000} \tag{1}$$

where t_r is the residence time of the crystals in a magma prior to eruption in years, G is the growth rate of the crystals in mm/s, m is the slope of the CSD linear relationship, and 31,536,000 is a constant to change the result from seconds to years (Cashman and Marsh, 1988). A CSD plot with a steep slope would correlate to a short residence time and a greater degree of undercooling in the system. A flatter slope would have a longer residence time and smaller degrees of undercooling associated with it. Since the CSD slope represents the amount of undercooling in the system it can also represent the amount of nucleation in the system. Steeper slopes represent greater degrees of undercooling, which favors higher nucleation rates of smaller crystals. On the other hand, shallower slopes would represent smaller degrees of undercooling which would indicate lower nucleation rates that would favor growth of crystals. This would lead to textural coarsening of minerals within the rock over nucleation.

An important assumption that must be made for this equation is the growth rate of the crystals. Using the appropriate growth rate is very important in the residence time calculation. There is an inverse correlation between growth rate and residence time. A larger growth rate would mean a shorter residence time and visa versa. Unfortunately, growth rates can be hard to determine. Larsen (2005) calculated experimental growth rates of plagioclase of 3.5 x 10^{-9} mm/sec to 60.6 x 10^{-9} mm/sec at pressures of 50 to 15 MPa and temperatures of 825°C - 850°C. Marsh (1988) observed through various studies that the growth rates for common silicates and oxides (plagioclase, olivine, clinopyroxene, orthopyroxene, ilmenite, magnetite, and garnet) are broadly similar at approximately 10^{-9} mm/s. Higgins and Roberge (2006) used a slower growth rate of 10^{-10} mm/s in order to calculated the average residence time of lavas from Eldfell volcano in Iceland. This growth rate was used as to model a deeper silicic magma chamber that had been cooling slowly. These are however only approximations of the growth rates, and each study should estimate a growth rate that best satisfies the constraints for the study.

For this study a range of growth rates will be used to calculate an estimate of the average residence times for plagioclase crystals depending on which population they represent. Plagioclase will grow faster in mafic magmas and slower in silicic magmas. For plagioclase crystals from a mafic melt a faster growth rates of 10^{-9} mm/s will be used, while a slower growth rate of 10^{-10} mm/s will be used to calculate the average residence time for plagioclase from a more silicic melt.

Increasing the growth rates by a magnitude will decrease the average residence time by a factor of 10, while decreasing the growth rates by a magnitude will increase the average residence time by a factor of 10. Due to the sensitivity of the average residence times on the growth rate and the inability to assume the exact appropriate growth rate for the system, the calculated growth rates can only be viewed as a way to characterize different populations of crystals. This can be done because the growth rate for a single crystal population does not vary much across igneous rocks of similar cooling histories and suggests relatively small variations exist (Marsh, 1998).

CSD has also been used to study: order of crystallization of mineral phases, timing and speed of cooling and ascent of magmas, reversals and pauses during crystallization, magma mixing, fractional crystallization, textural coarsening, and magma and crystal deformation and fracturing (Higgins, 2000).

Methods

X-ray maps created by the Electron Microprobe were used to identify plagioclase crystals in the thin sections. Adobe Photoshop 7.0 was used to outline and color individual crystals within each of the Al X-ray maps. Vesicles were identified so that their area could be subtracted out of the whole rock area of the slide. High magnification maps were used to identify plagioclase microlites, where as low magnification maps were used to identify larger plagioclase phenocrysts. Once all plagioclase crystals were identified, the map was transferred to NIH Image 1.63, where the area, angle, major ellipsoid axis, and minor ellipsoid axis were measured for each of the colored plagioclase crystals. The major ellipsoid axis data was arranged into bins that increase by 0.1 mm each step using KaleidaGraph 3.6. This data was used to calculate the natural log of population density of the plagioclase crystals in the thin section, and plots of this versus the crystal length were created. The 2D data was converted to 3D data using CSDCorrections 1.37 (Higgins, 2000).

Laser Ablation Inductively Coupled Plasma Mass Spectrometry

Trace elements in plagioclase phenocrysts were analyzed using LA-ICP-MS in the W.M. Keck Collaboratory for Plasma Spectrometry at Oregon State University. Five thin sections were analyzed, four of which also had EMPA transects analyzed on plagioclase phenocrysts. The fifth thin section was HM-04-01 and only plagioclase microlites (length < 1 mm) were analyzed. Sample PD-04-01 was analyzed for both plagioclase transects and microlites. A NewWave UP-213 Frequency Quintupled 213 nm Nd-YAG Laser operated in Q-switch mode was used to ablate areas of plagioclase on the thin sections for analysis. The laser had a spot diameter of 25 μm and pulse rate of 5 Hz. Each analysis consisted of 40 second ablation period, preceded by a 45 second background measurement and followed by a 45 second washout period. Spots for plagioclase phenocrysts were chosen that corresponded to the EMPA transects at roughly 25 μm spacing between the spots, while spots for microlites were centered in the middle of the microlite. Once ablated, the sample was transferred to the VG Elemental PQ ExCell Quadrupole ICP-MS via He gas at 0.8 L/minute. The sample then traveled through Ar plasma and into the quadrupole mass spectrometer. Trace elements analyzed for were: Li, Mg, Si, Ca, Ti, Sr, Ba, La, Pb, Ce, Pr, Nd, and Eu. Precision data and detection limits for the standards analyses are in Table 6. Standard NIST-612 was used to calibrate all elements except for Ti and Mg where BCR-2G was used. This was because NIST-612 had low concentrations of Ti and Mg and could not accurately calibrate for these two elements.

Table 6: Analytical precision for LA-ICP-MS. Values from standards NIST-612 and BCR-2G are from Kent, et al., 2004).

	Day 1 (WR-05-01, PD-04-01)				Day 2 (PD-05-02, CC-04-01, HM-04-01)			
Element	Standard NIST-612 (ug/g)	Standard BCR-2G (ug/g)	Standard Deviation %	Estimated Detection Limit (ug/g)	Standard NIST-612 (ug/g)	Standard BCR-2G (ug/g)	Standard Deviation %	Estimated Detection Limit (ug/g)
7Li	41.5		12.67	0.82	41.5		7.95	0.59
25Mg		13026	0.44	1.84		13026	0.35	4.10
29Si	715000		0.00	237	715000		0.00	202
43Ca	114000		4.29	180	114000		7.84	152
47Ti		13500	1.12	1.39		13500	0.65	3.16
86Sr	76.5		4.49	2.24	76.5		9.34	1.90
88Sr	76.5		4.71	0.10	76.5		8.45	0.08
137Ba	37.7		6.87	0.60	37.7		6.25	0.47
139La	35.9		4.81	0.05	35.9		7.74	0.04
140Ce	38.7		5.43	0.01	38.7		7.53	0.02
141Pr	38.0		6.24	0.02	38.0		9.22	0.02
146Nd	35.6		6.90	0.09	35.6		8.65	0.06
153Eu	35.4		6.94	0.03	35.4		5.95	0.04
208Pb	38.9		8.96	0.05	38.9		5.10	0.04

Results

Whole Rock

Lithology

Lavas from Mount Hood (regardless of the age) are all typically light to medium gray, medium-grained porphyritic rocks and contain phenocrysts of plagioclase and orthopyroxene with minor amounts of clinopyroxene and hornblende. The groundmass is hypocrystalline with plagioclase microlites and glass. Weak alignment of plagioclase microlites in the groundmass can be found in several of the samples denoting flow direction. The lavas are typically vesicle poor and may contain inclusions of similar mineralogy and that are slightly more mafic than the host rock (typically 2 – 4 weight percent silica less than the host rock) (Woods, 2004).

Geochemistry

Lavas from Mount Hood are medium K, calk-alkaline andesites. Out of the 14 samples that were analyzed using XRF (Table 7), only one falls in the basaltic andesite range (CC-04-01) and two (TL-04-01 and WR-05-01) plot at the lower edge of the dacite field (Figure 9 and 10). These two dacite samples are the youngest samples collected for this study, having only erupted 1.5 ka and ~215 years ago respectively.

Major and Minor Element Trends

The Mount Hood lavas have a simple linear decreasing trend in Al_2O_3, MgO, FeO*, CaO, TiO_2, P_2O_5 as silica increases (Figure 11). K_2O is the only major oxide that clearly increases as silica increases, while Na_2O shows no clear correlation between it and SiO_2. Na_2O varies little. With the exception of K_2O and Na_2O, these correlations are significant at a confidence level greater than 99%.

Trace elements have a similar behavior to major elements, in that all of the elements linearly correlate between themselves and SiO_2. Rb is the only trace element that shows a positive correlation with SiO_2 at a significance level greater than 99%. Ni, Cr, V and Ba all have negative correlations with SiO_2 at a significance level greater than 93%.

Table 7: XRF whole rock data for Mount Hood samples. Total Fe expressed as FeO*.

	CD-04-01	TL-04-01B	HW-04-02	HM-04-01	MHM-05-05	CS-04-01	CS-04-02
Age	~225 ka	1.5 ka	120 ka	50 ka	50 ka	425 ka	475 ka
Location	N 45 19.048, W 121 48.637	N 45 19.944, W 121 42.489	N 45 17.419, W 121 44.087	N 45 19.070, W 121 37.921	N 45 20.639, W 121 40.333	N 45 25.551, W 121 34.750	N 45 25.636, W 121 35.184
Major Element (Weight %)							
SiO2	59.95	63.43	61.93	60.08	61.14	58.92	59.21
TiO2	0.87	0.74	0.85	0.99	0.94	0.99	0.99
Al2O3	18.04	16.83	17.31	17.64	17.37	17.73	18.00
FeO*	5.59	4.71	5.43	5.96	5.82	6.15	6.11
MnO	0.10	0.09	0.10	0.11	0.10	0.11	0.11
MgO	3.25	2.56	3.20	3.14	3.00	3.31	3.31
CaO	6.55	5.34	5.73	6.03	5.94	5.97	5.85
Na2O	4.02	4.32	4.26	4.17	4.23	3.99	4.17
K2O	1.34	1.52	1.27	1.38	1.46	1.56	1.24
P2O5	0.19	0.17	0.18	0.24	0.23	0.27	0.23
Sum	99.90	99.70	100.25	99.73	100.24	99.02	99.21
Trace Elements (ug/g)							
Ni	28	23	39	32	30	34	28
Cr	29	20	51	31	29	31	38
Sc	15	11	14	15	16	16	16
V	116	91	108	115	110	130	129
Ba	256	353	317	359	363	445	297
Rb	14	22	18	20	20	22	16
Sr	736	575	526	566	577	733	644
Zr	147	157	147	186	184	199	152
Y	15	15	16	20	20	19	18
Nb	7	8	9	11	10	9	9
Ga	22	20	20	21	20	22	20
Cu	43	25	29	32	35	27	38
Zn	60	65	70	76	72	81	75
Pb	5	7	6	5	5	7	5
La	16	15	15	18	22	21	20
Ce	37	39	34	47	47	59	34
Th	4	4	2	3	3	5	3
Nd	16	17	19	23	23	27	19
Sum of Trace	1565	1466	1442	1580	1587	1887	1561
Sum of M + T	100.06	99.85	100.40	99.89	100.40	99.20	99.37

Table 7 Continued: XRF whole rock data from Mount Hood. Total Fe expressed as FeO*.

	CC-04-01	EB-04-01	WR-05-01	PD-04-01	PD-05-02	PD-05-03	PD-05-04
Age	55 ka	35 ka	~215	7.5 ka	7.5 ka	7.5 ka	7.5 ka
Location	N 45 27.384, W 121 35.903	N 45 27.695, W 121 38.420	N 45 18.492, W 121 40.971	N 45 30.162, W 121 36.917	N 45 31.177, W 121 37.280	N 45 29.472, W 121 37.288	N 45 29.629, W 121 37.475
Major Element (Weight %)							
SiO2	55.66	61.86	63.67	58.78	58.57	58.19	58.09
TiO2	1.23	0.90	0.77	1.12	1.13	1.15	1.15
Al2O3	18.73	16.74	16.80	18.00	18.11	18.27	18.17
FeO*	7.34	5.00	4.82	6.32	6.30	6.47	6.42
MnO	0.12	0.09	0.09	0.11	0.10	0.11	0.11
MgO	4.37	2.56	2.47	3.41	3.36	3.39	3.41
CaO	7.04	5.71	5.13	6.62	6.65	6.67	6.70
Na2O	4.27	4.40	4.36	4.47	4.45	4.36	4.42
K2O	0.69	1.89	1.45	0.90	0.89	0.85	0.86
P2O5	0.24	0.31	0.17	0.26	0.26	0.27	0.27
Sum	99.69	99.46	99.72	100.00	99.83	99.73	99.59
Trace Elements (ug/g)							
Ni	59	23	23	32	32	32	32
Cr	79	19	22	49	51	47	48
Sc	18	11	12	15	14	16	14
V	143	103	86	118	119	116	122
Ba	252	550	344	283	286	291	285
Rb	7	25	20	10	11	10	9
Sr	629	902	537	645	647	649	646
Zr	119	201	152	143	142	145	143
Y	18	18	15	17	16	18	17
Nb	7	10	8	10	9	9	8
Ga	21	20	20	20	20	21	22
Cu	46	33	17	38	39	40	37
Zn	83	77	67	86	86	87	89
Pb	3	9	7	5	5	5	5
La	11	30	18	16	14	13	16
Ce	29	75	39	32	28	33	34
Th	1	7	2	1	1	1	2
Nd	18	36	18	17	19	17	19
Sum of Trace	1544	2147	1407	1538	1539	1550	1546
Sum of M + T	99.84	99.67	99.86	100.16	99.99	99.89	99.74

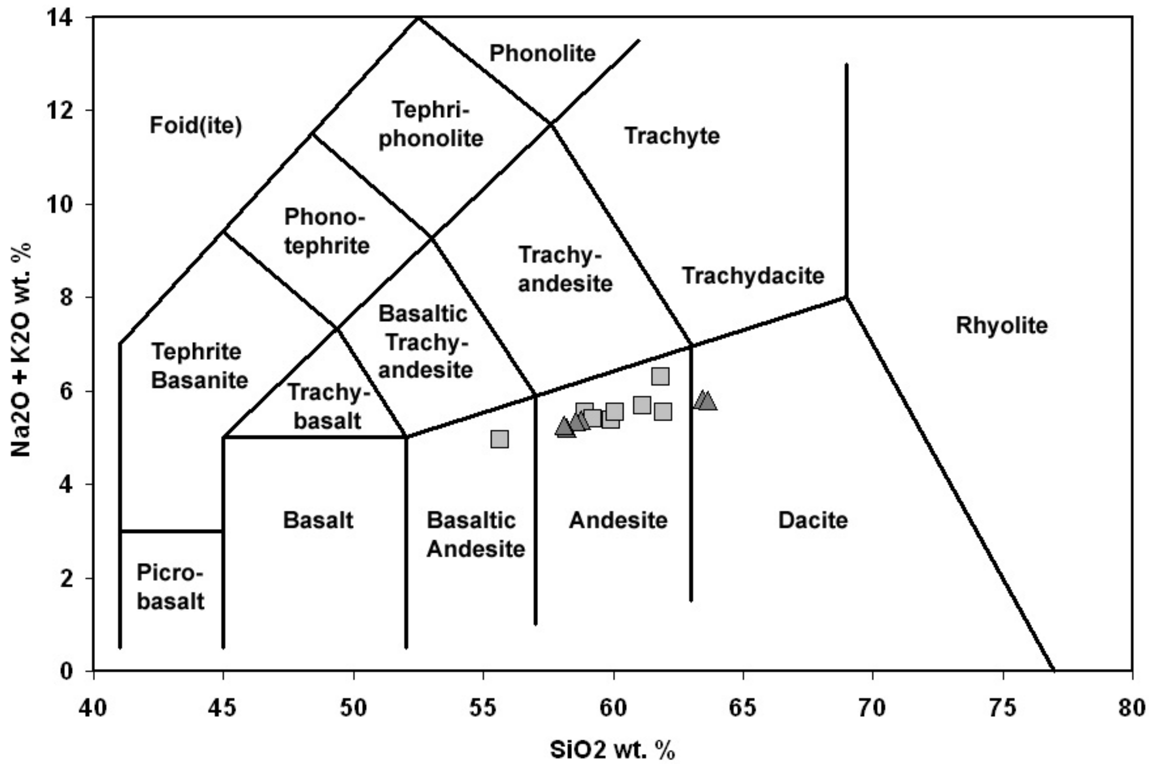

Figure 9: Lava samples on Total Alkali-Silica diagram. Squares represent samples from the Main Stage (Pre-Polallie) eruptive period. Triangles represent samples younger than 10 ka. Two young samples lie in lower dacite field and only one (CC-04-01) in the basaltic andesite field. After La Bas, et al. (1986).

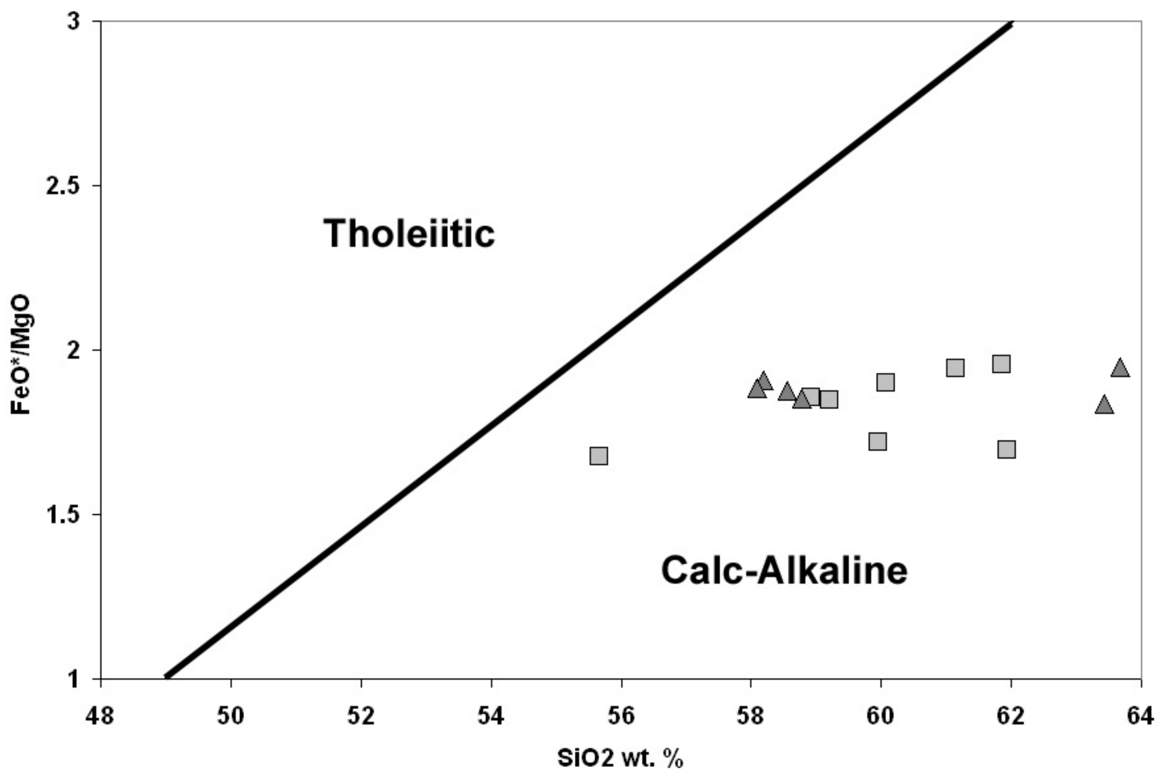

Figure 10: Lava samples plotted on FeO*/MgO versus SiO2 diagram showing calc-alkaline composition. Squares represent Main stage (Pre-Polallie) eruptive period, while triangles represent samples younger than 10 ka. After Miyashiro (1974).

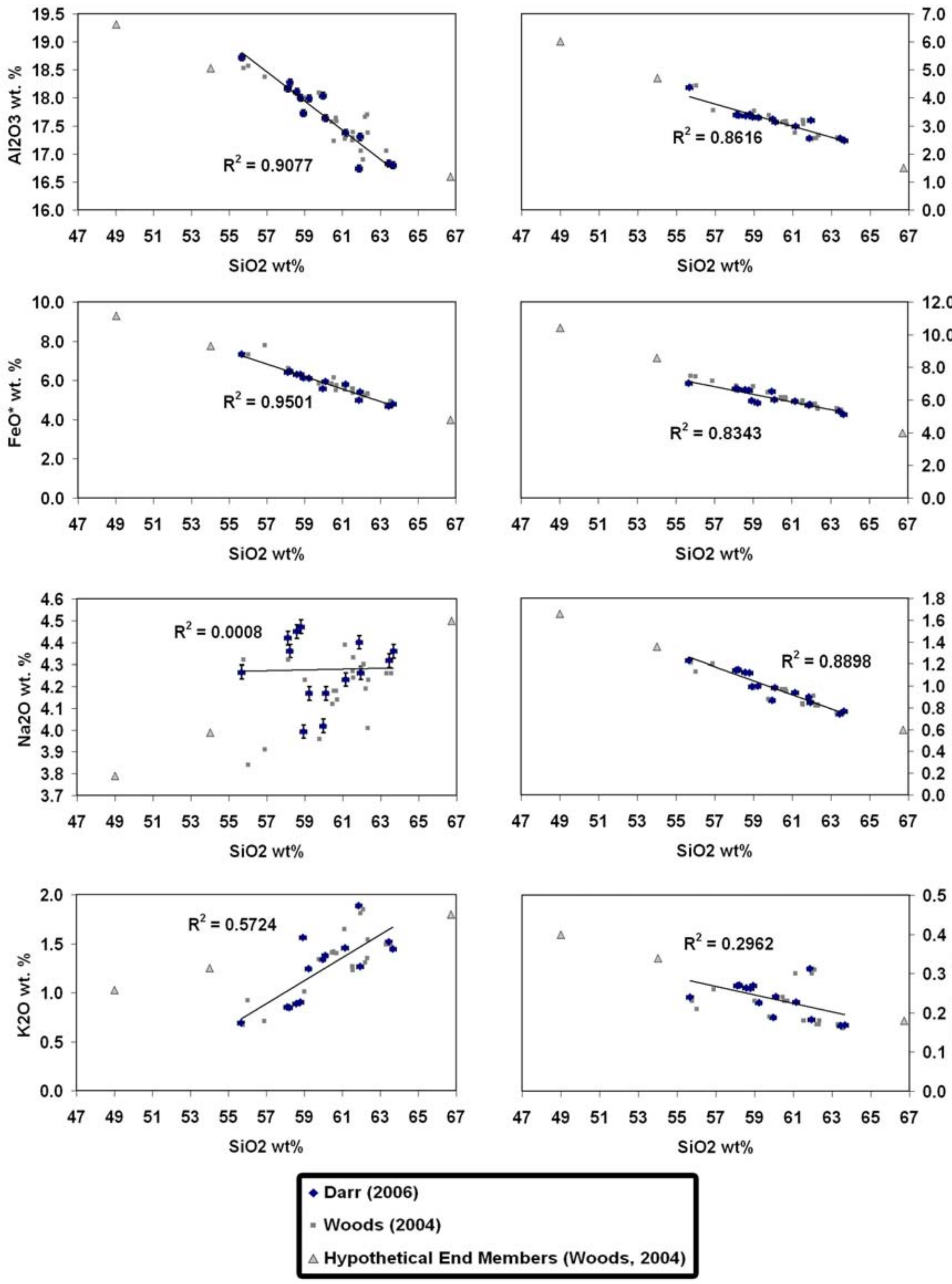

Figure 11: Major elements versus silica. Diamonds represent samples from this study; small dots represent samples from Woods (2004). Hypothetical end members from Woods (2004) are also shown. Lines represent the general trend formed by the whole rock data from this study. Analytical errors are shown on each of the diamond data points. In some plots the error is smaller than the data point.

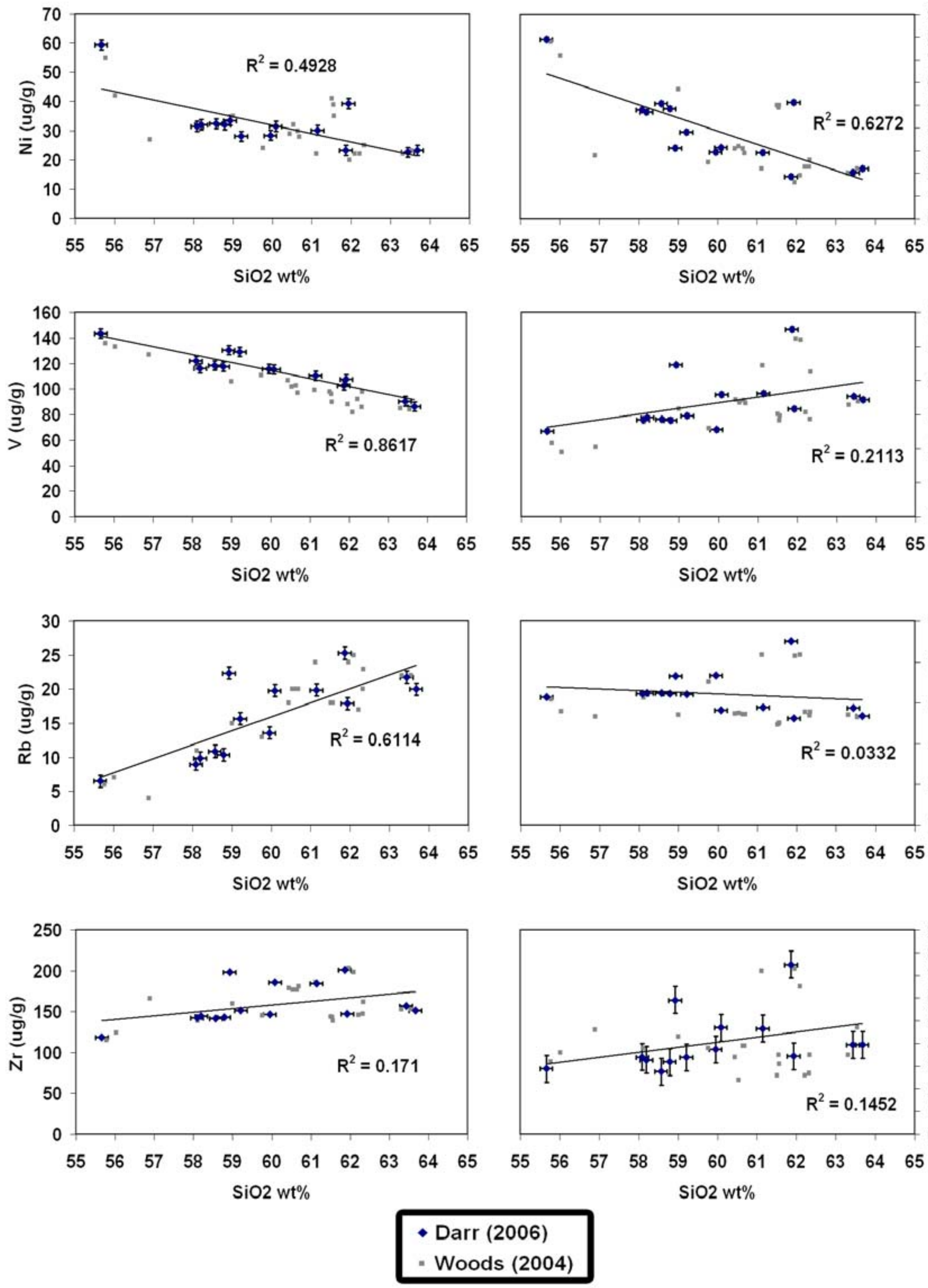

Figure 11 continued: Trace elements vs. silica. Diamonds represent samples from this study; small dots represent samples from Woods (2004). Lines represent the general trend formed by the whole rock data from this study. Analytical errors are shown on each of the diamond data points. In some plots the error is smaller than the data point. Woods (2004) end members are not shown in the trace element plots because not all of the trace elements were calculated for the end members.

Petrography and Mineral Chemistry

Plagioclase

Plagioclase is the dominant mineral as both phenocryst and microcryst phases in all of the Mount Hood lavas comprising approximately 50% – 70% of the phenocryst populations. Groundmass plagioclase crystals are euhedral and tabular in shape. Weak alignment of these plagioclase crystals is seen in several of the lava samples. Plagioclase phenocrysts range in size from 500 μm up to 5 mm in length. The shape of the phenocrysts can range from subhedral to euhedral, but the majority are closer to being euhedral in shape. The plagioclase phenocrysts usually have complex zonation patterns and typically also exhibit oscillatory zonation.

Several different types of textures have been observed in the plagioclase phenocrysts. The most common is zonation; normal, reverse, or oscillatory zonation patterns with no dissolution zones or sieved areas. These zonation patterns are commonly attributed to either changes in the physical condition of the magma chamber (T, P, P_{H2O}) and (or) to changes in the magma composition (Morgan, et al., 2004). Several of the larger phenocrysts have sieved textures near the rim of the phenocrysts. This type of texture represents the second most abundant texture seen in the plagioclase phenocrysts. These zones are approximately 50 – 100 μm thick and represent periods of either rapid crystal growth where equilibrium crystallization could not occur or dissolution of pre-existing plagioclase. In the first scenario the overall crystal shape would remain, but in the second scenario large embayments may form and the edge of the crystal and corners would be rounded. Both of these two processes are created in times of disequilibrium and are both found in plagioclase from Mount Hood. Plagioclase phenocrysts can also be found with sieved cores that also represents periods of fast growth. Plagioclase phenocrysts exhibiting this type of texture are far less abundant when compared to the two other types of textures. These sieved cores are typically then encompassed by oscillatory zoned plagioclase showing a return to equilibrium within the magma chamber. All three of these textures are present in the samples from Mount Hood, occasionally occurring in close proximity within the same thin section (Figure 12).

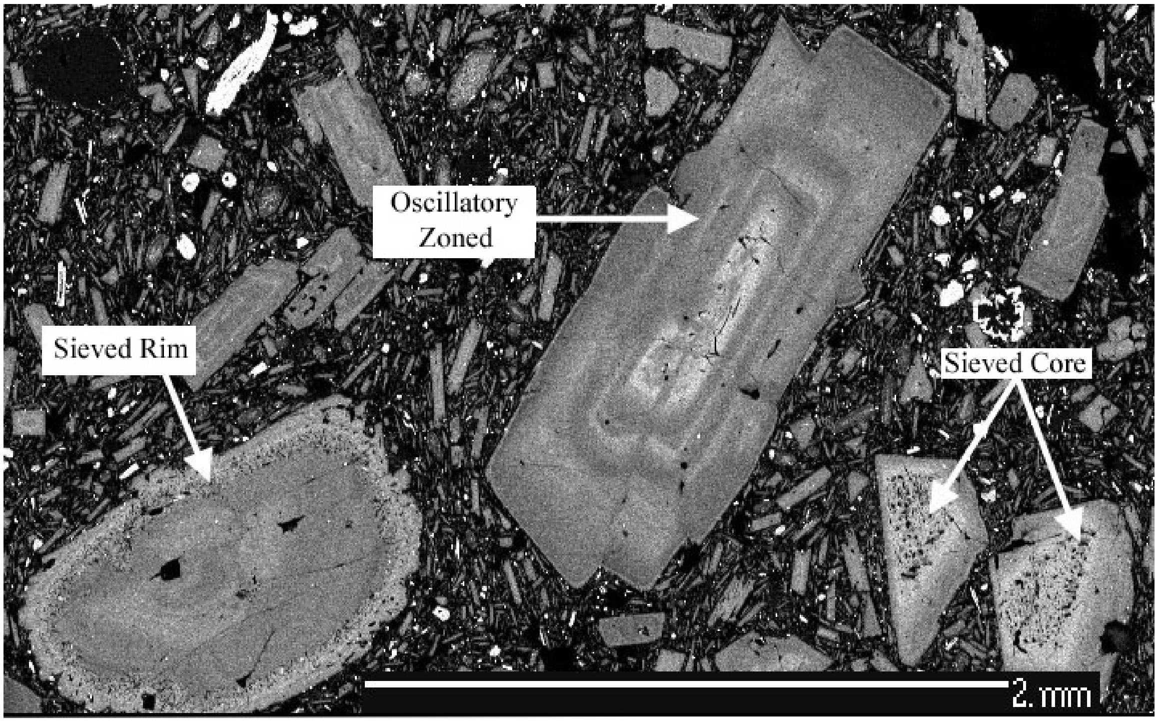

Figure 12: Ca X-Ray map from EB-04-01 showing all three plagioclase textures in the same sample in close proximity to each other.

Plagioclase crystals from eleven thin sections were analyzed for major elements by electron microprobe techniques. Most analyses consisted of a point in the center of the phenocryst and one on the edge. In four of the thin sections more detailed microprobe traverses were conducted on several phenocrysts. This will be discussed in more detail later in this chapter. Concerning only the core and rim analyses, the range of plagioclase compositions range from An_{22} – An_{83}. This range in anorthite is for samples that range in silica from 55.7 weight percent to 63.7 weight percent. Figure 13 breaks down the plagioclase analyses by sample. The core and rim analyses show both normal and reverse zonation overall (Figure 14).

Smaller plagioclase microlites (<1 μm in length) in the groundmass have anorthite compositions within the range of plagioclase phenocrysts but are typically normally zoned with no sieved textures. From core to rim, anorthite compositions change approximately 10%.

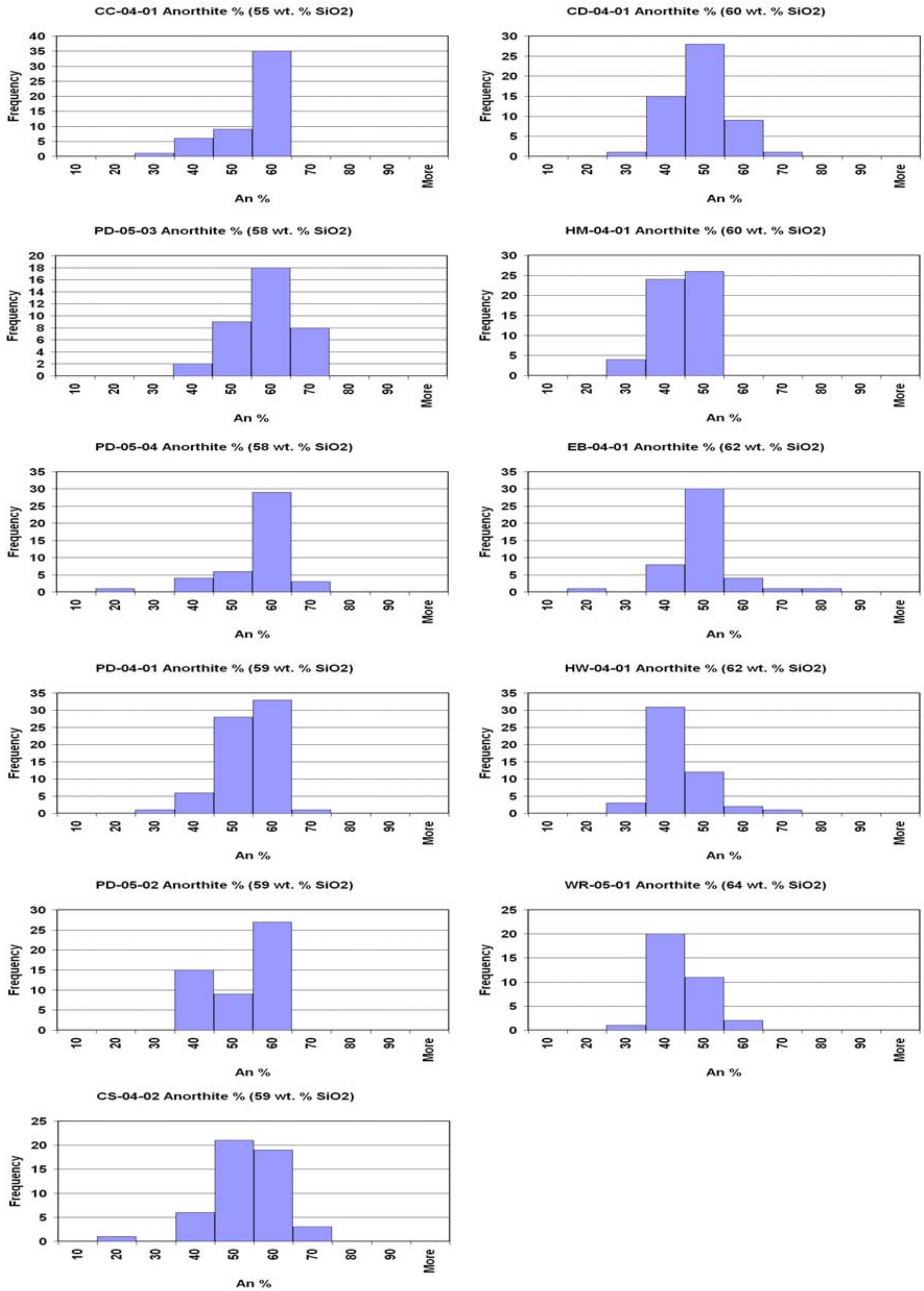

Figure 13: Anorthite for plagioclase from samples analyzed using EMPA techniques. Silica increases from top left graph to bottom right graph.

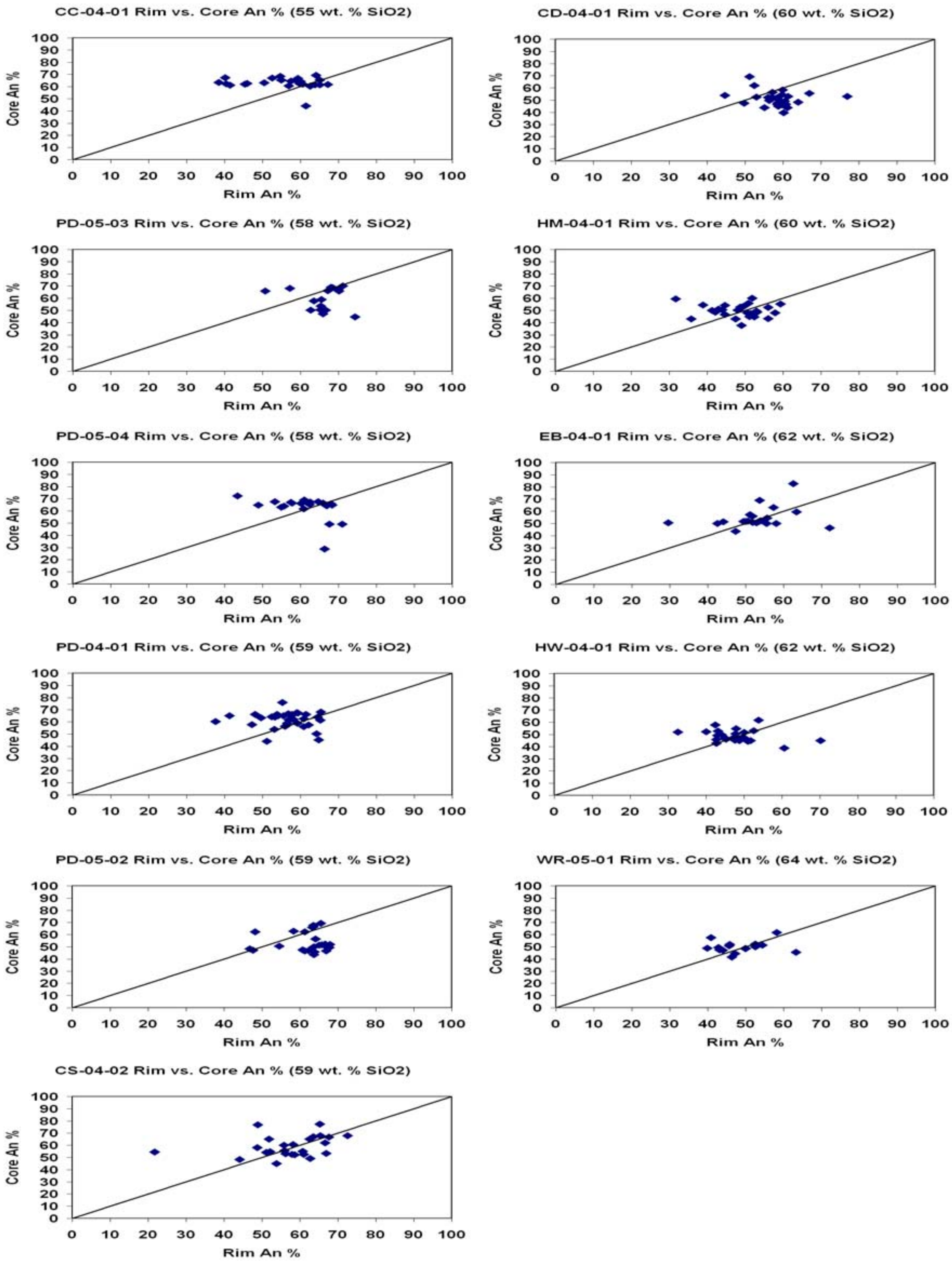

Figure 14: Rim anorthite versus core anorthite for analyzed plagioclase broken down by sample. Silica increases from top left graph to bottom right graph. Data points falling along the one to one line plotted have rim and core anorthite similar to each other. Those plotting above the line have higher anorthite in the core than rim (normal zonation) and those plotting below the line have higher anorthite on the rim than core (reverse zonation). However, the area between the core and rim show increases and decreases in anorthite creating oscillatory zonation.

Orthopyroxene

Orthopyroxene is the next most abundant mineral phase in lavas from Mount Hood comprising 10% to 25% of the phenocryst populations. Orthopyroxene phenocrysts and groundmass microlites are typically smaller than plagioclase phenocrysts, but as with the plagioclase, can be found as both euhedral to subhedral crystals. Resorbed rims on the orthopyroxene crystals can be observed within some samples. Typically, the zonation of the orthopyroxene follows the same zonation pattern in the plagioclase; normal, reverse, or oscillatory.

Orthopyroxene crystals were also analyzed using EMPA techniques, analyzing one point in the core and one on the rim. Mean composition value for orthopyroxene is En_{68} with a range of compositions encompassing En_{49-80}, Fs_{19-49}, Wo_{0-12}, plotting well within the enstatite field on a pyroxene ternary diagram (Figure 15). This range of orthopyroxene values is for samples with a silica range from 55.7 weight percent to 61.4 weight percent silica.

Clinopyroxene

Clinopyroxene is found in the more mafic samples with decreasing abundance as silica increases. Clinopyroxene comprises 0% to 10% of the phenocrysts populations. It is more common to find clinopyroxene crystals in the groundmass rather than as phenocrysts in the lavas. Crystal shapes again range from subhedral to euhedral and the crystals can be found with resorption rims. Very little zonation is found in the clinopyroxene crystals. Most are homogeneous from core to rim.

Clinopyroxene crystals were also analyzed using EMPA techniques, analyzing one point in the core and one on the rim. The range of compositions for the clinopyroxene was En_{38-45}, Fs_{13-21}, Wo_{40-45}, plotting within the augite field of the pyroxene ternary (Figure 15). Fewer clinopyroxene crystals were analyzed than orthopyroxene; however a similar composition range was reported in Woods (2004).

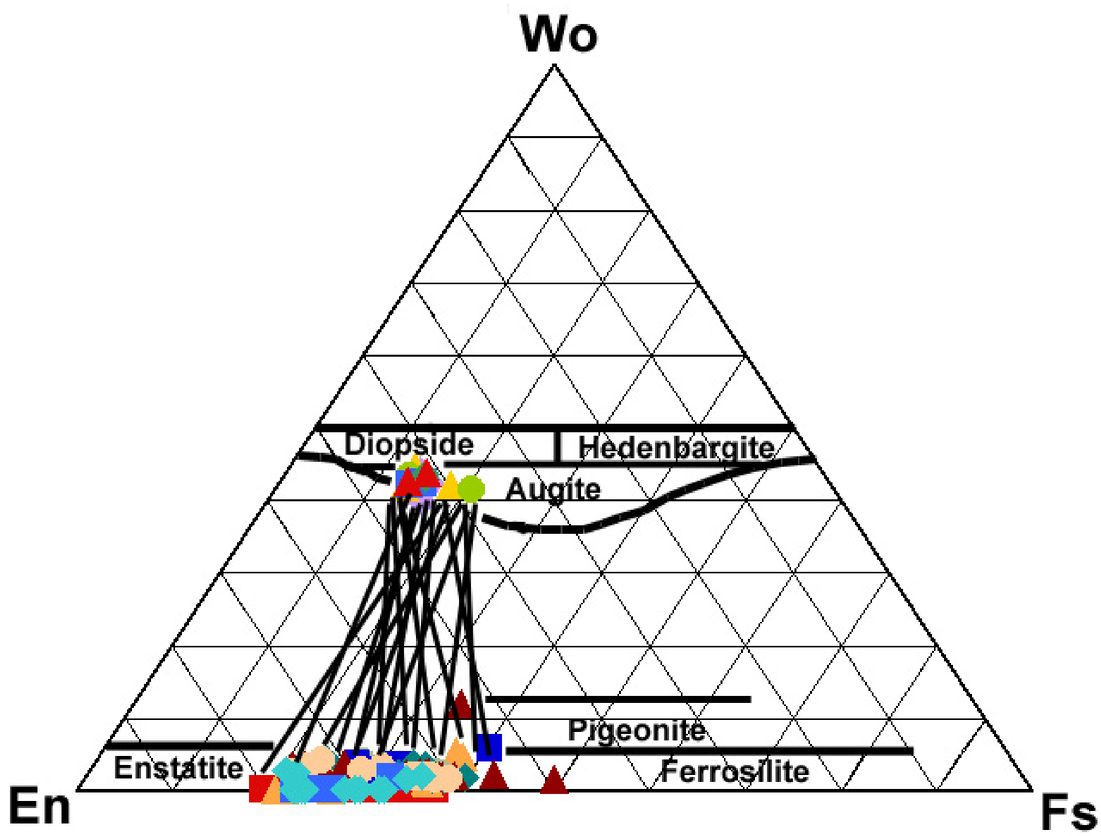

Figure 15: Pyroxene ternary showing the compositions of orthopyroxene (enstatite) and clinopyroxene (augite) phenocrysts. Tie-lines between the two groups of pyroxenes connect orthopyroxene and clinopyroxene crystals that coexist within the same sample.

Hornblende

Hornblende is found in abundance in lavas with silica greater than 62 weight percent comprising approximately 10% of the phenocryst populations and 0% in lavas less than 62 weight percent silica. Very few hornblende crystals are found in lavas with lower silica and when observed have thick oxide reaction rims, and some are completely reacted into oxides (Figure 16). The hornblende found in more silicic lavas tends to be elongated crystals with frayed ends. Oxidation rims are generally found around the hornblende in the more silicic lavas; but are thinner and in some cases completely absent. The width of the oxidation rims around hornblende crystals can be related to the ascent rate of the magma (Rutherford and Hill, 1993). Thicker oxidation rims represent a magma with a slow ascent rate, which allows for more time for the hornblende crystals to react and form the rims prior to eruption, while thinner oxide reaction rims represent hornblende that ascended rapidly to the surface, allowing for less reaction time prior to eruption (Rutherford and Hill, 1993). Hornblende will break down at a faster rate at higher pressures creating thicker rims then when at lower pressures when temperature is held constant. Hornblende from Mount Hood that have thick oxidation rims are typically observed in samples that are greater than 15 ka in age, while thinner rims, or lack of rims, are observed in younger samples. This indicates that ascent rates of magmas have increased through time. Woods (2004) performed a more extensive study of hornblende and found them to be calcic amphiboles (hornblende, paragasite, and tshermakite).

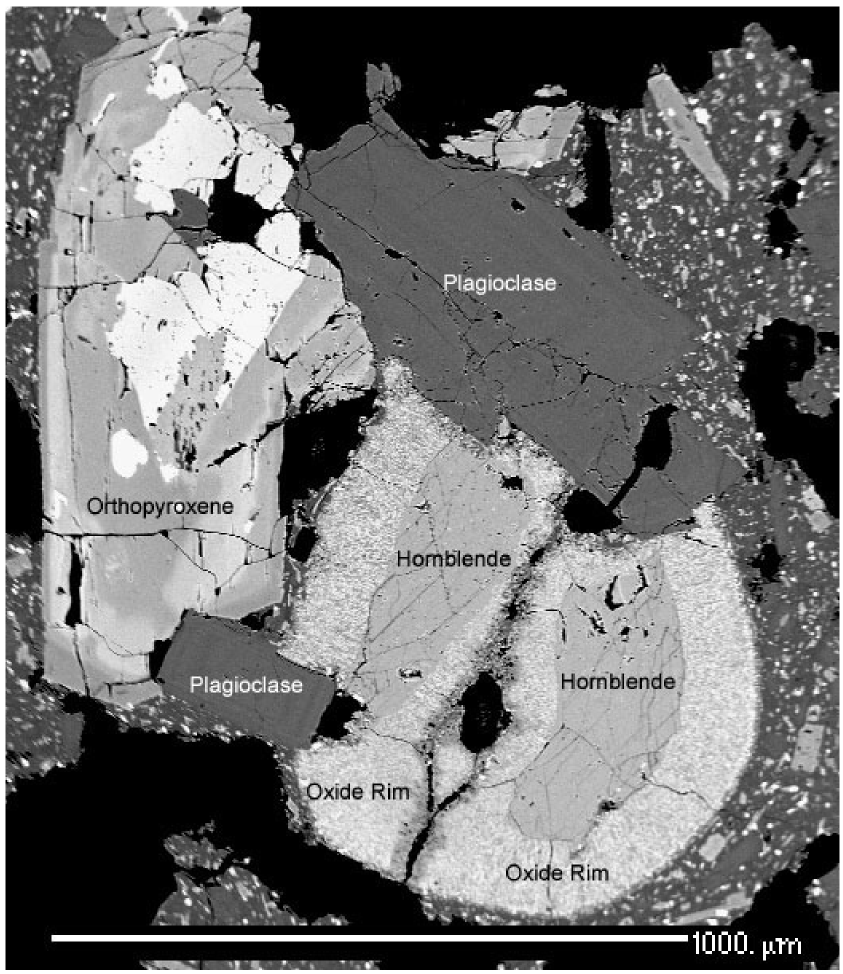

Figure 16: BSE image from PD-04-01 showing plagioclase, orthopyroxene, and hornblende crystals. Hornblende crystals have rims of oxides formed by rapid accent of magma leaving hornblende in disequilibrium.

Fe-Ti Oxides

Fe-Ti oxides are found in all of the samples from Mount Hood as both phenocrysts and in the groundmass. They comprise approximately 10% to 20% of the phenocryst populations. As phenocrysts they range from 0.5 mm in length to 1 mm in length and as part of the groundmass are typically less than 100 µm. Cribb and Barton (1997) performed a more extensive study on Fe-Ti oxides in Mount Hood lavas and were able to classify them as magnetite with a range of Usp_{23-39} and ilmenite with a range of Ilm_{76-92}.

Partition Coefficients

It has been observed that the partition coefficient of elements changes with changing anorthite in plagioclase (Bindeman, et al., 1998). Figure 17 shows how partition coefficients for several elements in plagioclase will vary with changing anorthite and temperature. Partition coefficients for all of the listed elements in plagioclase decrease as anorthite increases. Partition coefficients were calculated using the following equation from Bindeman, et al. (1998):

$$RT \ln (D_i) = a\, X_{An} + b \qquad (2)$$

where R is the gas constant in kJ/(mol·K), and a and b are listed in Bindeman, et al. (1998).

The elements Mg, Fe, Ti, and Ce have small partition coefficients with respect to plagioclase ($D < 1$) meaning that they are incompatible with plagioclase. Sr and Ba have larger partition coefficients ($D > 1$) meaning that they are compatible with plagioclase. As anorthite increases all of the listed elements have decreasing partition coefficients indicating that they are becoming more incompatible with plagioclase that has higher anorthite. Temperature has a much smaller and in some cases non-existent effect on the elements' partition coefficients than anorthite.

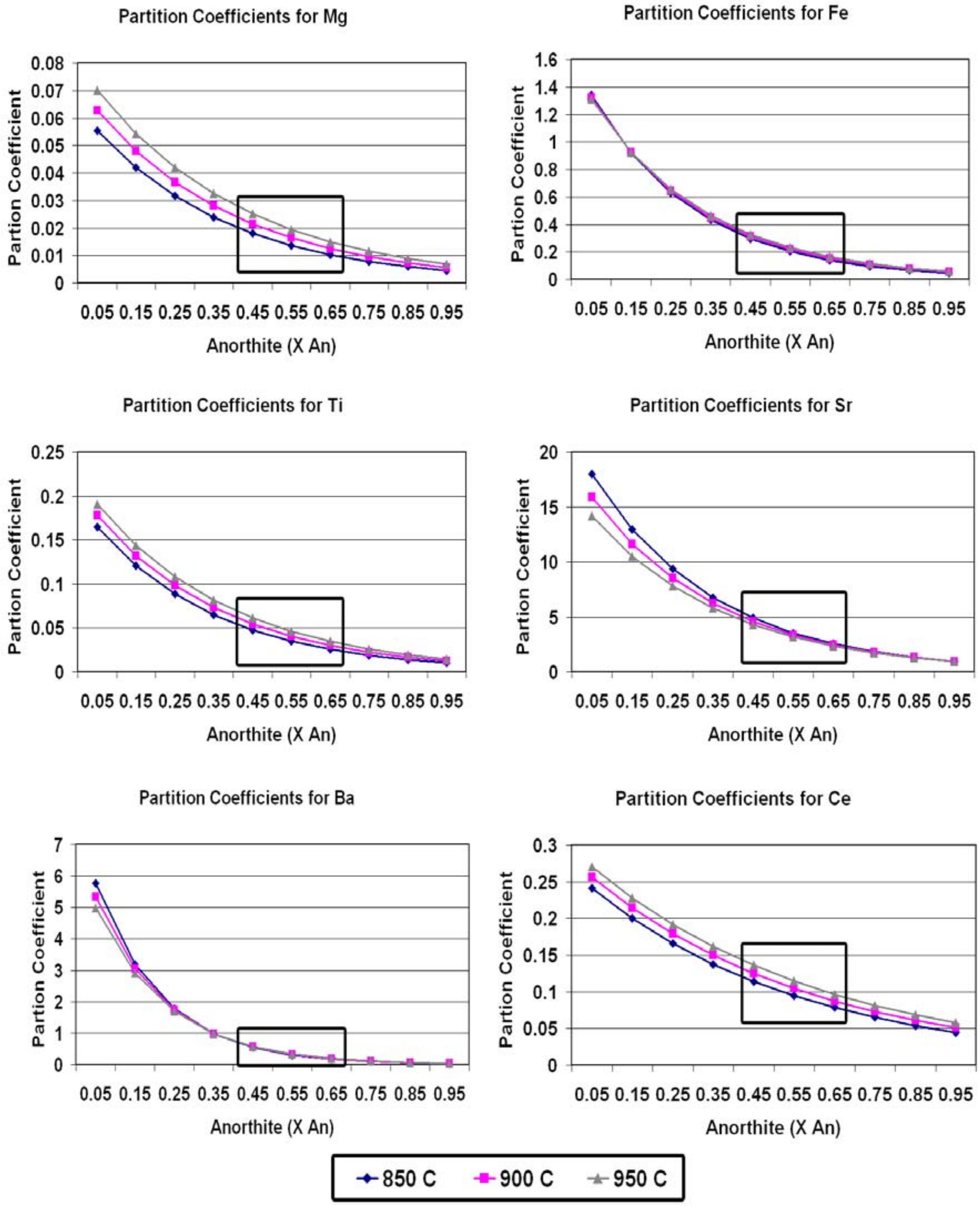

Figure 17: Calculated partition coefficients for Mg, Fe, Ti, Sr, Ba, and Ce with varying anorthite and temperatures. All elements listed show a decrease in compatibility with increasing anorthite. Anorthite values within box are the most common among plagioclase from lavas from Mount Hood.

Plagioclase Transects

Major Elements

Plagioclase transects from four different thin sections were measured using EMPA. Each transect was performed at 5 µm spacing starting at the core of the phenocryst and ending at the rim. Given the wide variety of textural types these transects do not fully represent all of the plagioclase in the samples, but provide a guide to the chemical variations present in plagioclase phenocrysts in each sample.

The transects (Figures 18 - 25) show changing anorthite, MgO, and FeO contents from the core of the phenocrysts to the rim. In each of the figures there is a BSE image of the whole crystal plus a blown up portion of the BSE image showing the location of the EMPA transect line. Lighter coloration in each of the pictures represents areas that contains elements with higher mean atomic number, in this case Ca, which are areas that are richer in anorthite.

CC-04-01 is the most primitive lava sample with a silica value of 55.7 weight percent. WR-05-01 is the most evolved sample with a silica value of 63.7 weight percent. This sample was part of the dacite dome known as Crater Rock that was deposited in the White River channel near highway 35 during a pyroclastic flow caused by the dome collapse approximately 215 years ago. PD-04-01 and PD-05-02 are both from the same flow with silica values of 58.8 weight percent. PD-04-01 comes from the end of the Parkdale flow, while PD-05-02 comes from the middle of the flow.

Transects from CC-04-01 have little variation in anorthite values from core to rim ranging from An_{60} to An_{70} (Figures 18 and 19). It is not until the end of transect, closest to the rim, that the anorthite values change significantly. Approximately 20 µm from the rim of both plagioclase crystals anorthite values begin to decrease to values below An_{50}. MgO and FeO plots for both correlate broadly with anorthite.

WR-05-01 transects have much more variation in anorthite from core to the rim, which forms a spiky pattern with An_{50} to An_{65} for one and An_{35} to An_{65} for the second (Figures 20 and 21). In the last 30 µm of both transects the anorthite value increases to its highest value in the whole phenocryst. This increased anorthite composition is also mimicked in the MgO and FeO transects, which show increased MgO and FeO in the plagioclase.

PD-04-01 transects, like WR-05-01, have variation in anorthite values leading to a spiky pattern from core to rim on both transects with an anorthite range from An_{43} to An_{70} (Figures 22 and 23). Both transects start off at a somewhat constant An_{50}, and approximately 240 µm out from the core, larger changes in anorthite begin. Approximately 40 µm from the rim both phenocrysts begin their largest increase in anorthite composition. The MgO and FeO transects show a similar increase at this same distance from the rim. In figure 22, this increase in anorthite, MgO, and FeO is correlated with the presence of a spongy dissolution texture.

PD-05-02 transects have a similar pattern to the other Parkdale flow sample. The range of anorthite for these two transects are An_{43} to An_{72} (Figures 24 and 25). Approximately 60 µm from the rim both transects show an increase in anorthite along with increases in both MgO and FeO. These increases in the various parameters also clearly correspond to a spongy texture around the rim in both transects, similar to the phenocryst transect from PD-04-01.

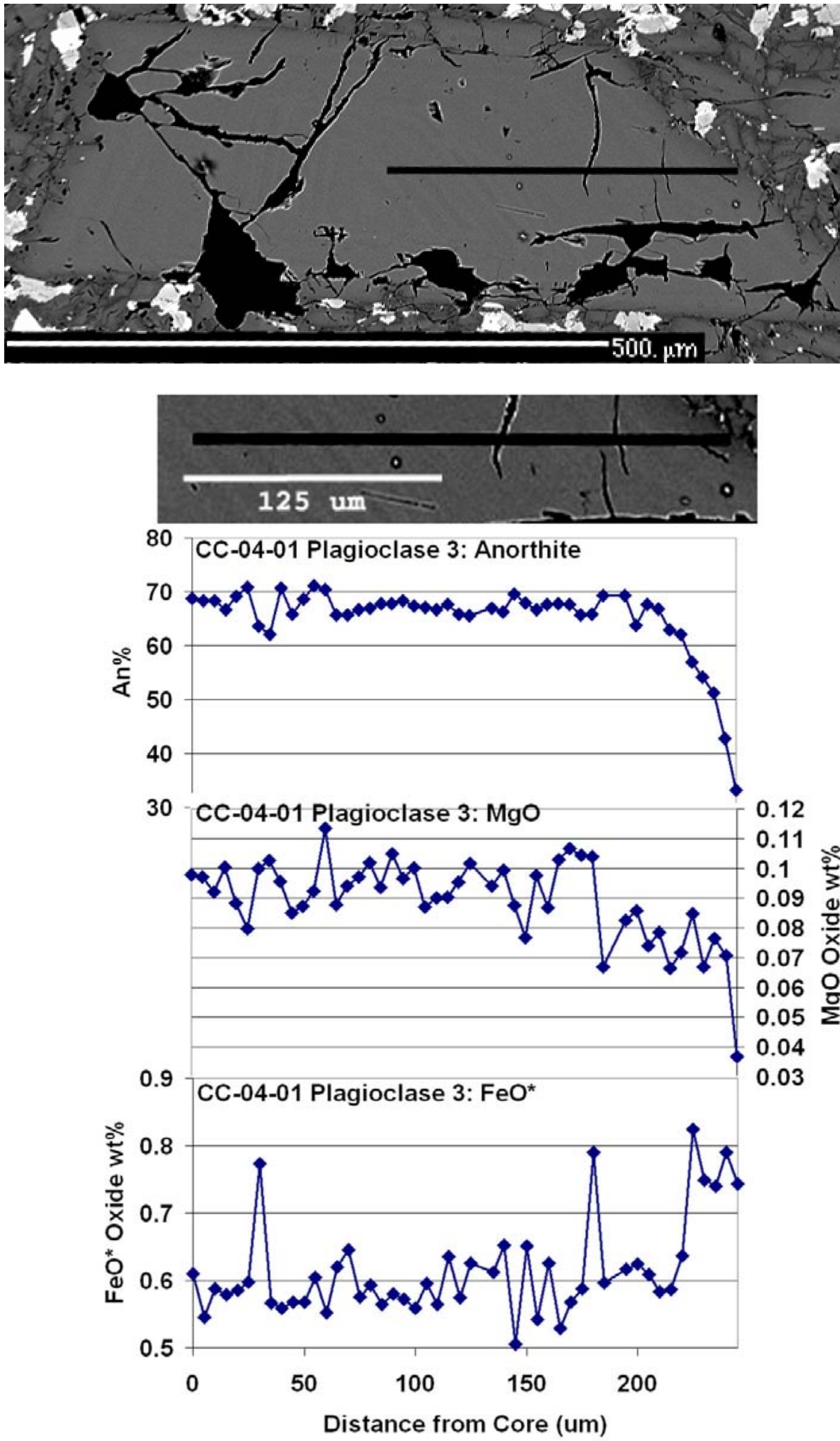

Figure 18: BSE image of plagioclase 3 from CC-04-01. Black line represents EMPA transect measured at 5 µm spacing (zoomed in section of transect in second picture). Dark bands represent areas that are anorthite poor, while light bands represent anorthite rich areas. Anorthite, MgO, and FeO all decrease at the rim of the plagioclase crystal.

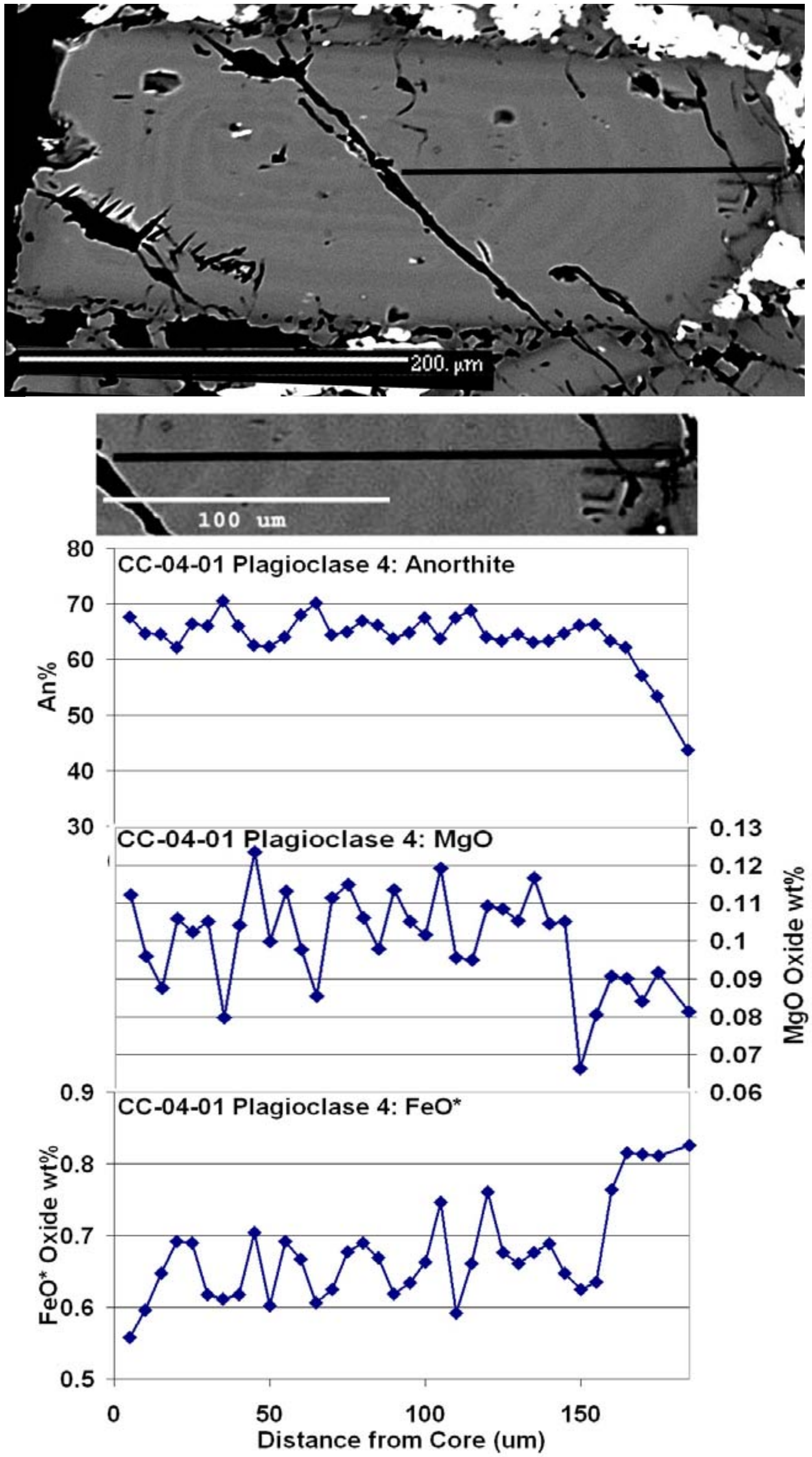

Figure 19: BSE image of plagioclase 4 from CC-04-01. Black line represents EMPA transect measured at 5 µm spacing (zoomed in section of transect in second picture). Dark bands represent areas that are anorthite poor, while light bands represent anorthite rich areas. Anorthite, MgO, and FeO all decrease at the rim of the plagioclase crystal.

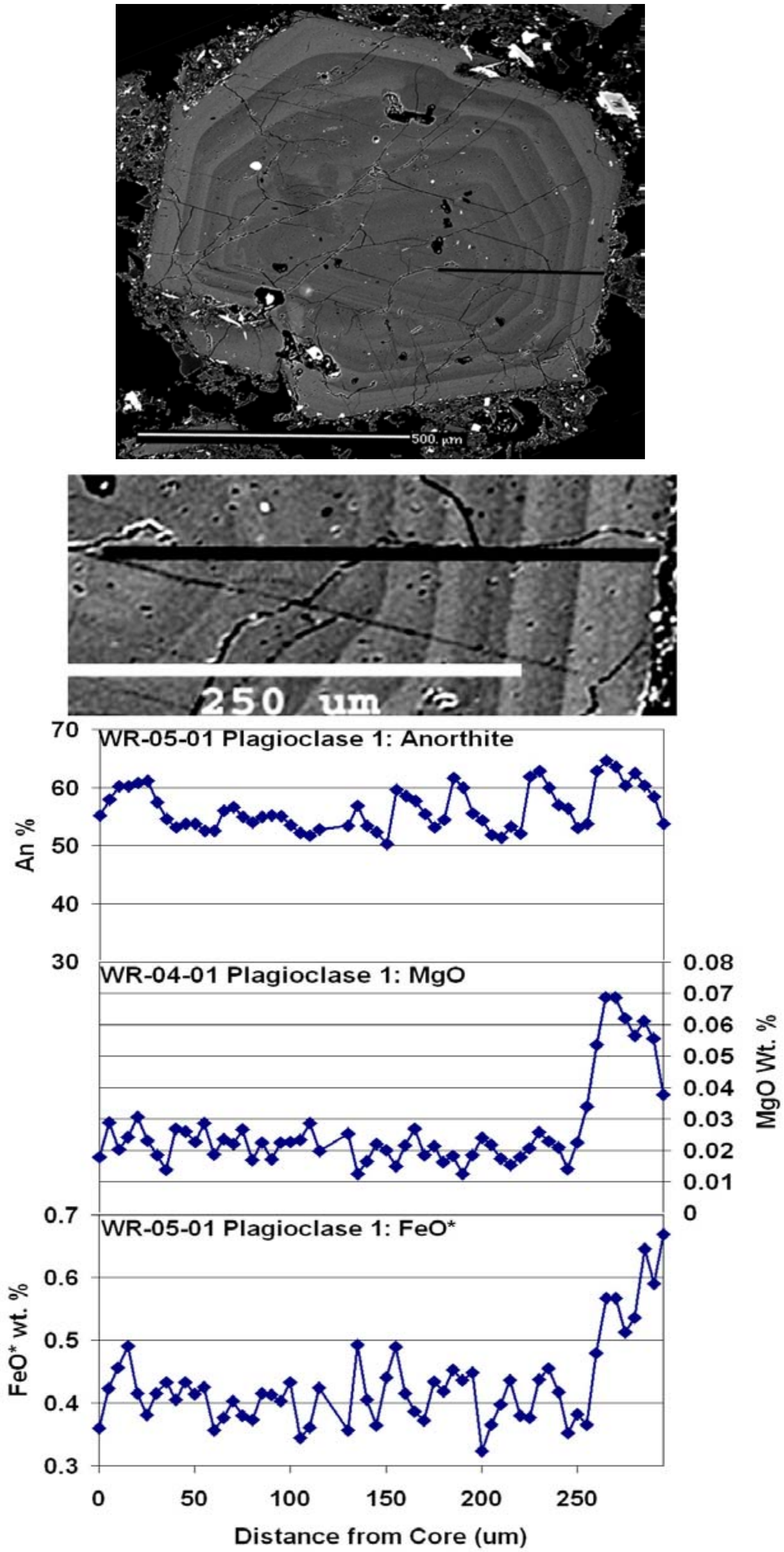

Figure 20: BSE image of plagioclase 1 from WR-05-01. Black line represents EMPA transect measured at 5 µm spacing (zoomed in section of transect in second picture). Dark bands represent areas that are anorthite poor, while light bands represent anorthite rich areas. Anorthite, MgO, and FeO all increase at the rim of the plagioclase crystal indicating a recharge event.

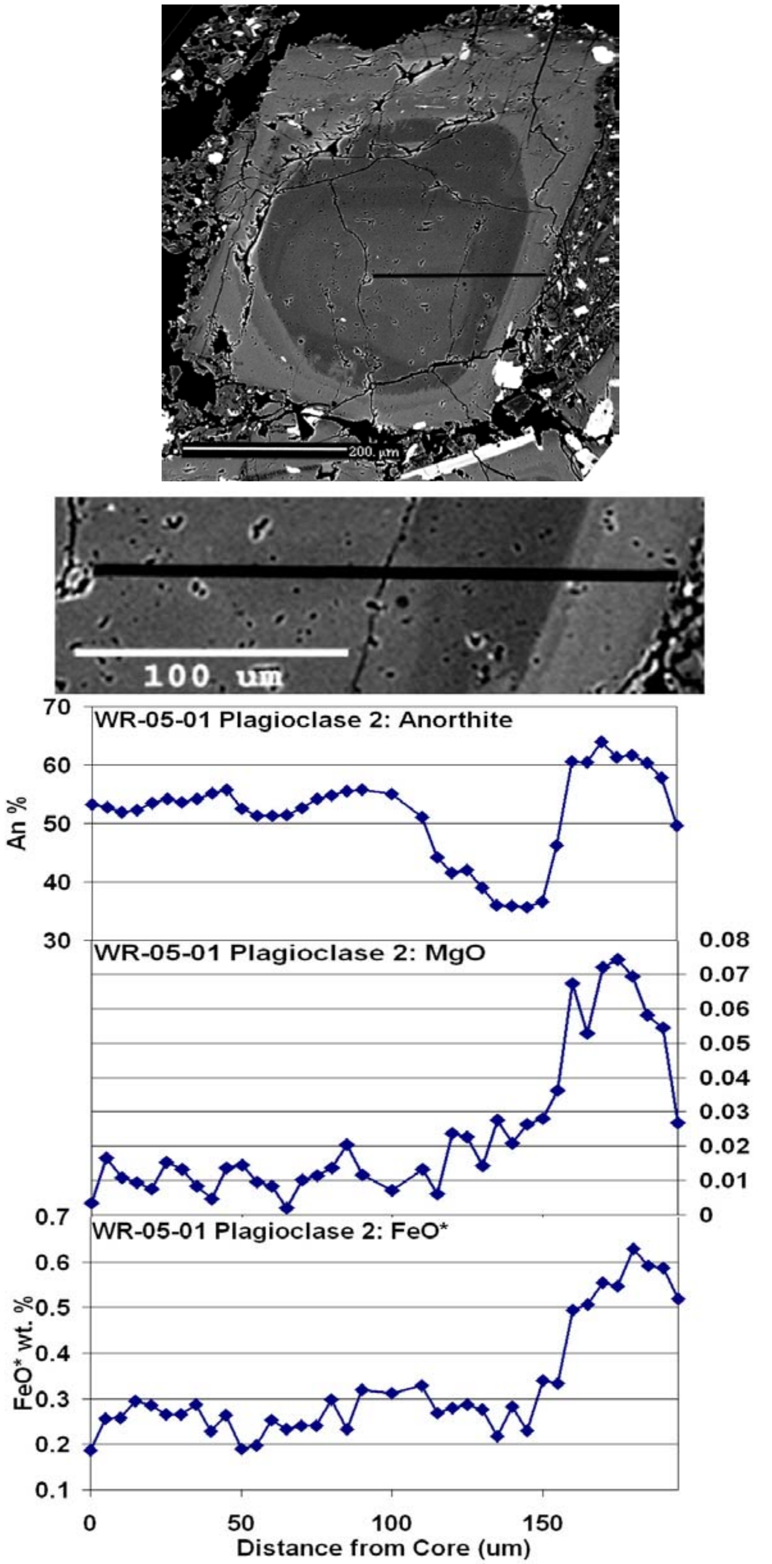

Figure 21: BSE image of plagioclase 2 from WR -05-01. Black line represents EMPA transect measured at 5 µm spacing (zoomed in section of transect in second picture). Dark bands represent areas that are anorthite poor, while light bands represent anorthite rich areas. Anorthite, MgO, and FeO all increase at the rim of the plagioclase crystal indicating a recharge event.

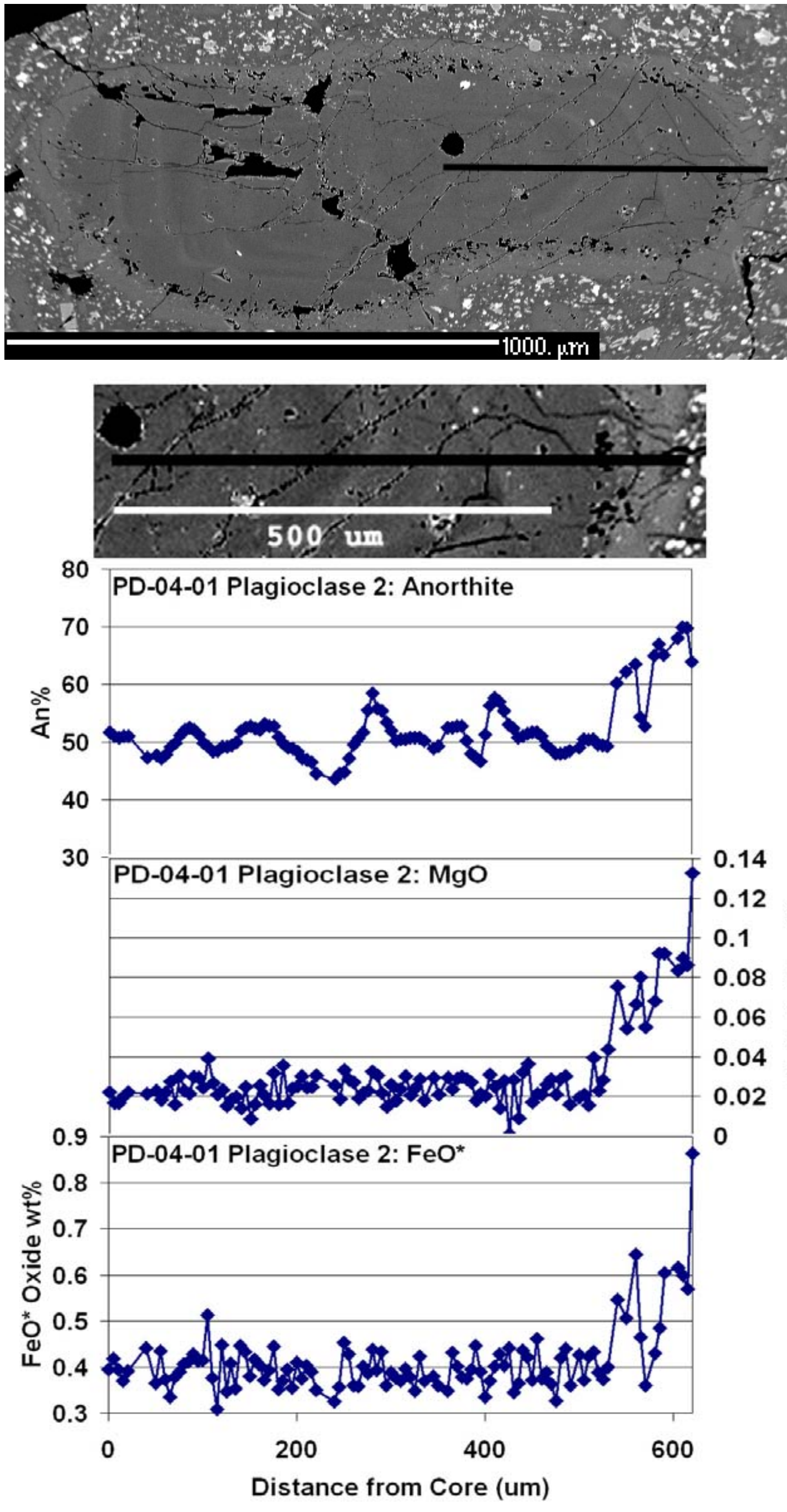

Figure 22: BSE image of plagioclase 2 from PD-04-01. Black line represents EMPA transect measured at 5 µm spacing (zoomed in section of transect in second picture). Dark bands represent areas that are anorthite poor, while light bands represent anorthite rich areas. Anorthite, MgO, and FeO all increase at the rim of the plagioclase crystal starting at the sieved rim indicating a recharge event.

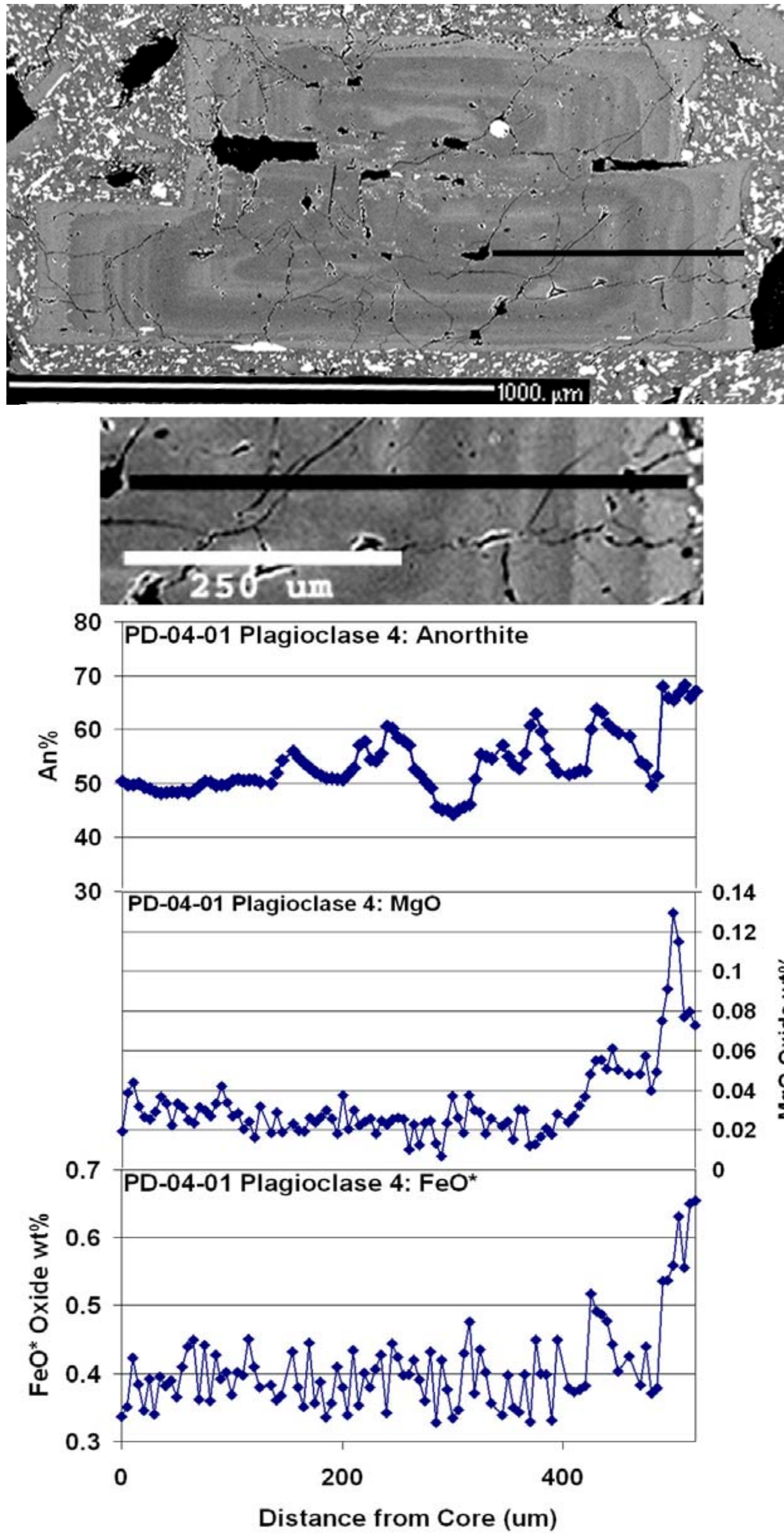

Figure 23: BSE image of plagioclase 4 from PD-04-01. Black line represents EMPA transect measured at 5 µm spacing (zoomed in section of transect in second picture). Dark bands represent areas that are anorthite poor, while light bands represent anorthite rich areas. Anorthite, MgO, and FeO all increase at the rim of the plagioclase crystal indicating a recharge event.

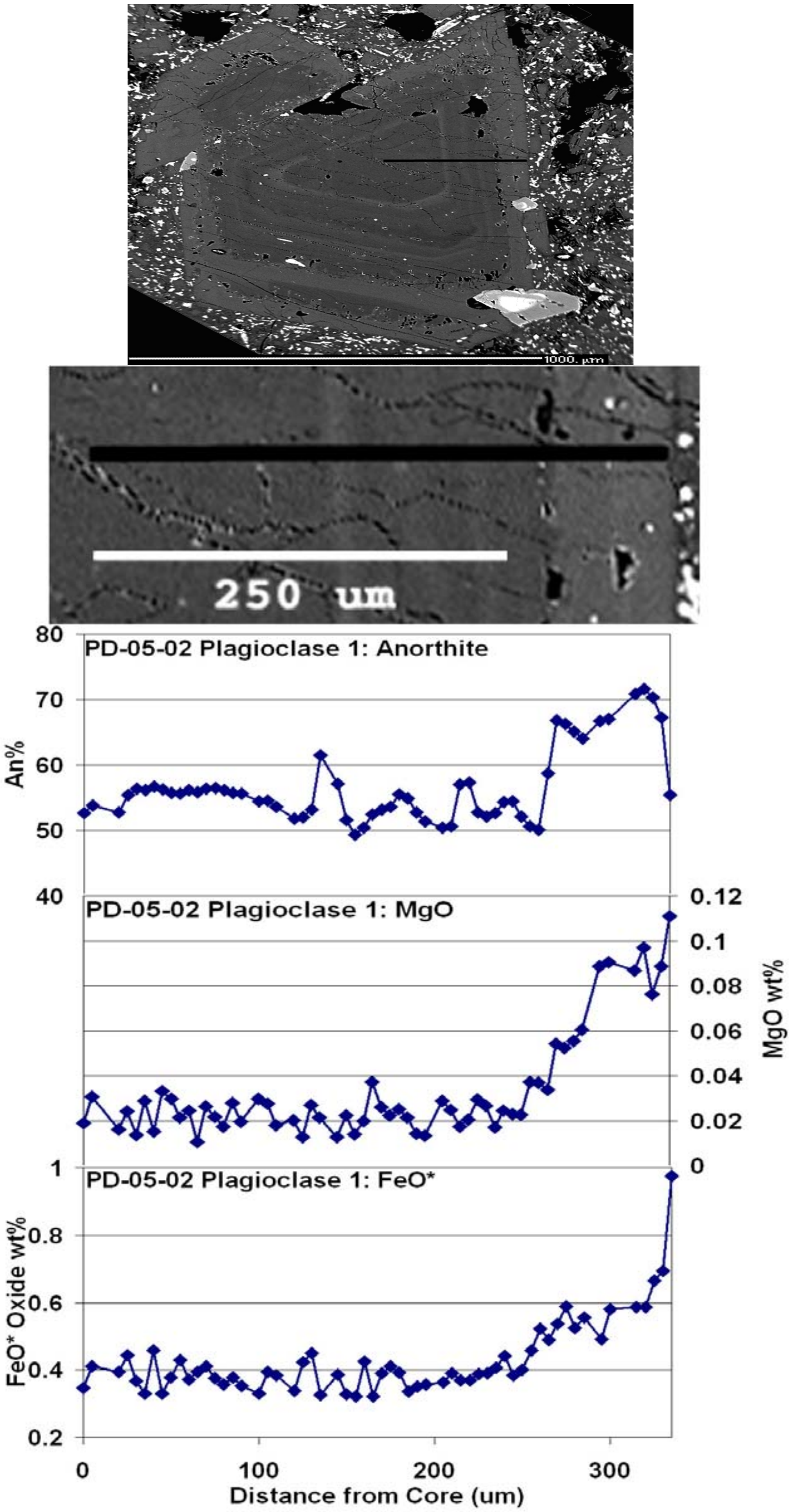

Figure 24: BSE image of plagioclase 1 from PD-05-02. Black line represents EMPA transect measured at 5 µm spacing (zoomed in section of transect in second picture). Dark bands represent areas that are anorthite poor, while light bands represent anorthite rich areas. Anorthite, MgO, and FeO all increase at the rim of the plagioclase crystal starting at the sieved rim indicating a recharge event.

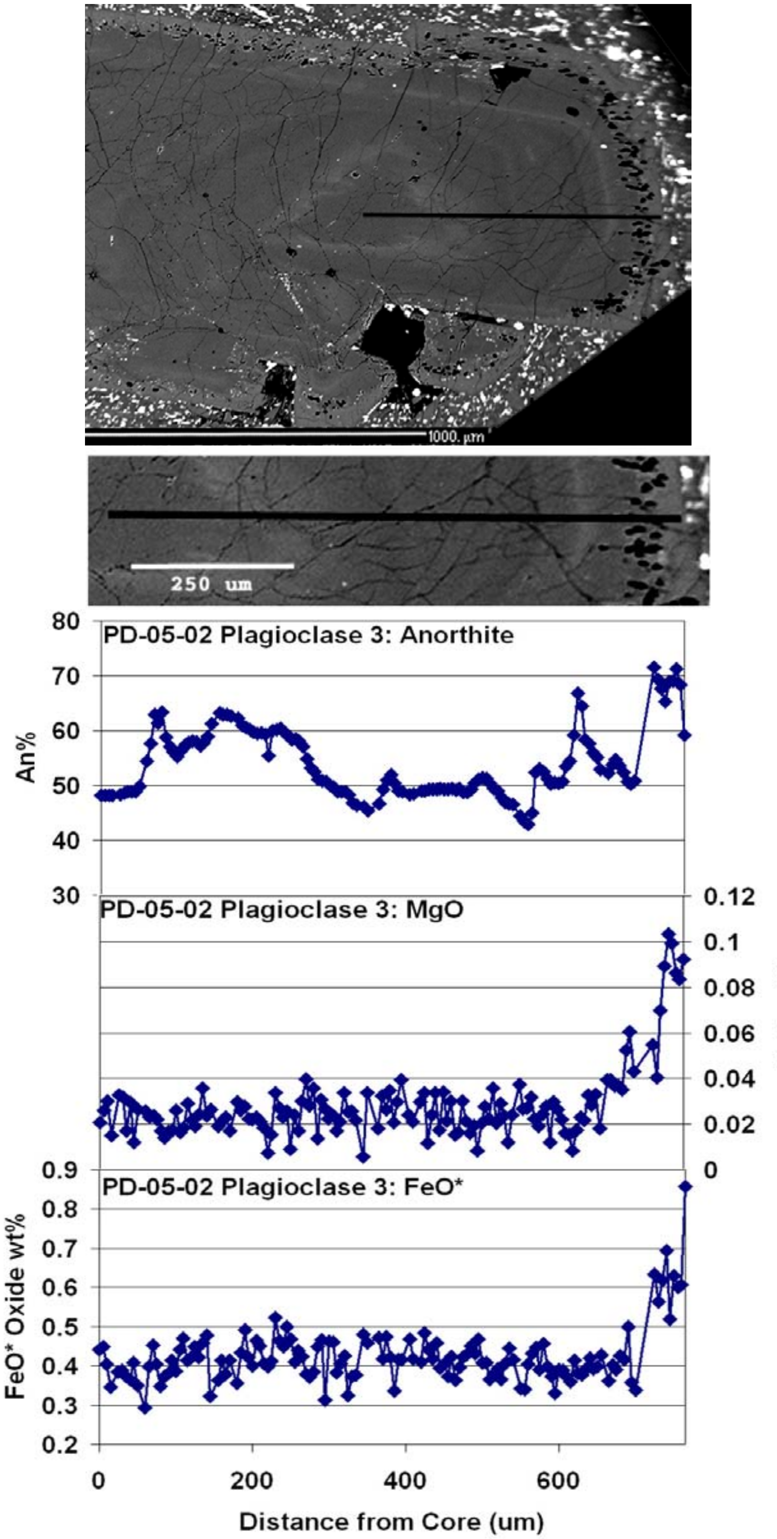

Figure 25: BSE image of plagioclase 3 from PD-05-02. Black line represents EMPA transect measured at 5 µm spacing (zoomed in section of transect in second picture). Dark bands represent areas that are anorthite poor, while light bands represent anorthite rich areas. Anorthite, MgO, and FeO all increase at the rim of the plagioclase crystal starting at the sieved rim indicating a recharge event.

Trace Elements

Plagioclase transects from the same four thin sections that were analyzed using EMPA were then analyzed for trace elements using LA-ICP-MS. Each analysis was performed using a 25 μm diameter beam along the same transect previously analyzed by EMPA for major elements. Due to the wider spacing needed to perform these analyses, less resolution is seen when compared to the anorthite plot created by EMPA. Figures 26 - 29 are plots of the changing anorthite, Ti, Sr, Ba, Ce, and the Sr/Ba ratio in the phenocrysts from the core to the rim. Certain trace elements were not used in the figures due to either low concentration levels that were below detection limits, as with most of the REE, or due to problems with degassing and rapid diffusion, such as Li. Although Li levels in the plagioclase were detectable, Li partitions into vapor relative to the melt at depth and rapidly equilibrates via diffusion (Berlo, et al., 2004) and therefore no discernable Li trend could be detected across the analyzed plagioclase transects.

Both plagioclase transects from CC-04-01 (Figure 26) have similar trace element trends from core to rim. Ti increases near the rim of the phenocryst as does Ba and Ce. Anorthite, Sr, and Sr/Ba have decreasing trends as the rim is approached.

Plagioclase transects from PD-04-01 (Figure 27) and PD-05-02 (Figure 29) also have similar trace element trends when compared to each other, although most of the trends are the reverse of what was seen in the previous sample. Anorthite, Ti, Sr, and Sr/Ba increase at the edge of the phenocrysts, while Ba and Ce mainly decrease. Plagioclase 4 from PD-04-01 and both plagioclase transects from PD-05-02 show these trends the clearest. All the increases and decreases at the rim of the phenocrysts correspond with an increase in anorthite. The same general trends seen in the Parkdale samples can be seen in both of the plagioclase from WR-05-01 (Figure 27).

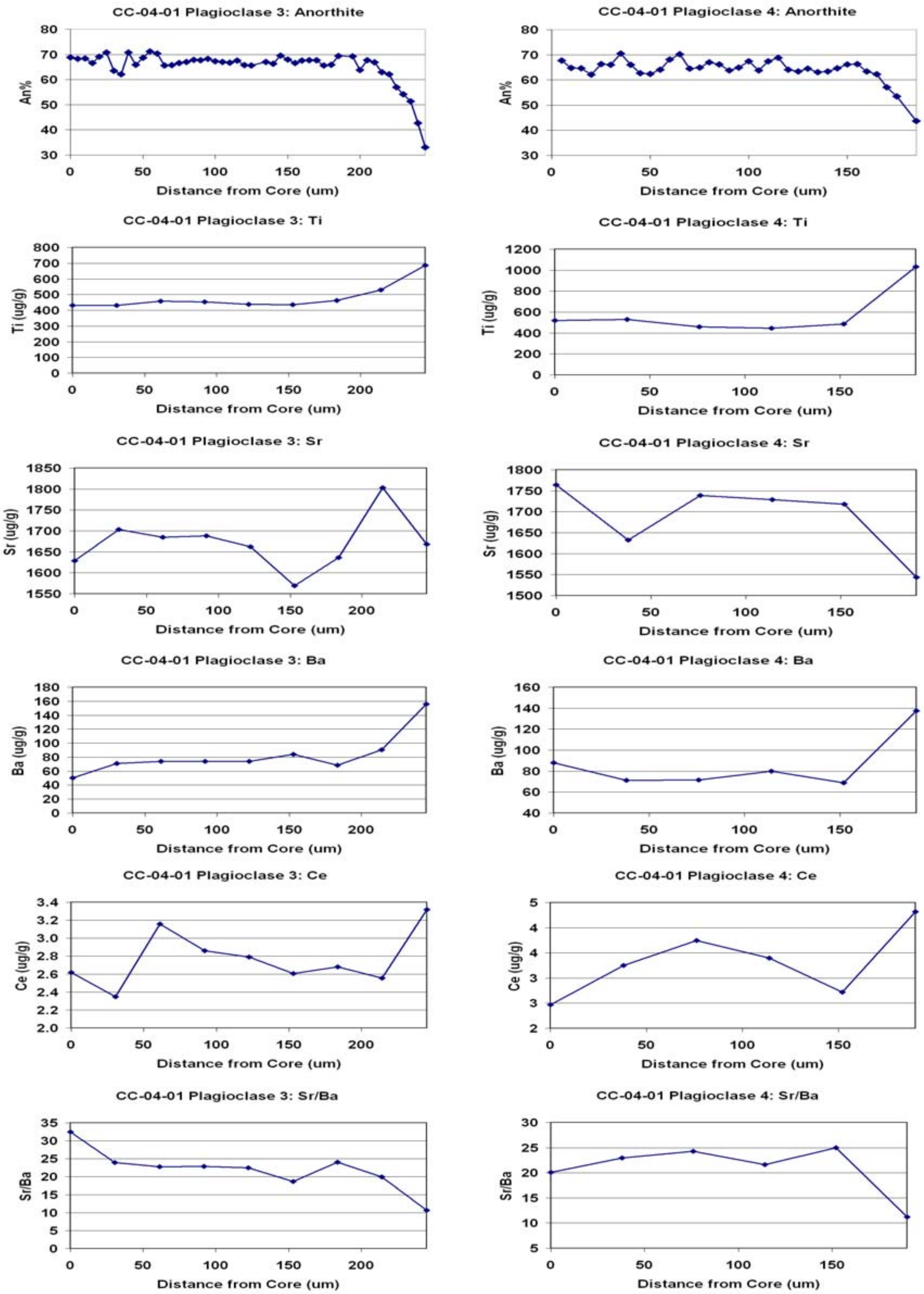

Figure 26: Plagioclase 3 (left) and 4 (right) from CC-04-01 trace elements (Ti, Sr, Ba, Ce, Sr/Ba) from core to rim analyzed by LA-ICP-MS, compared to anorthite transect. Increases in Ba and Ce and decreases in Sr, Sr/Ba, and anorthite at the rim indicates that there had been no recharge of magma into the system.

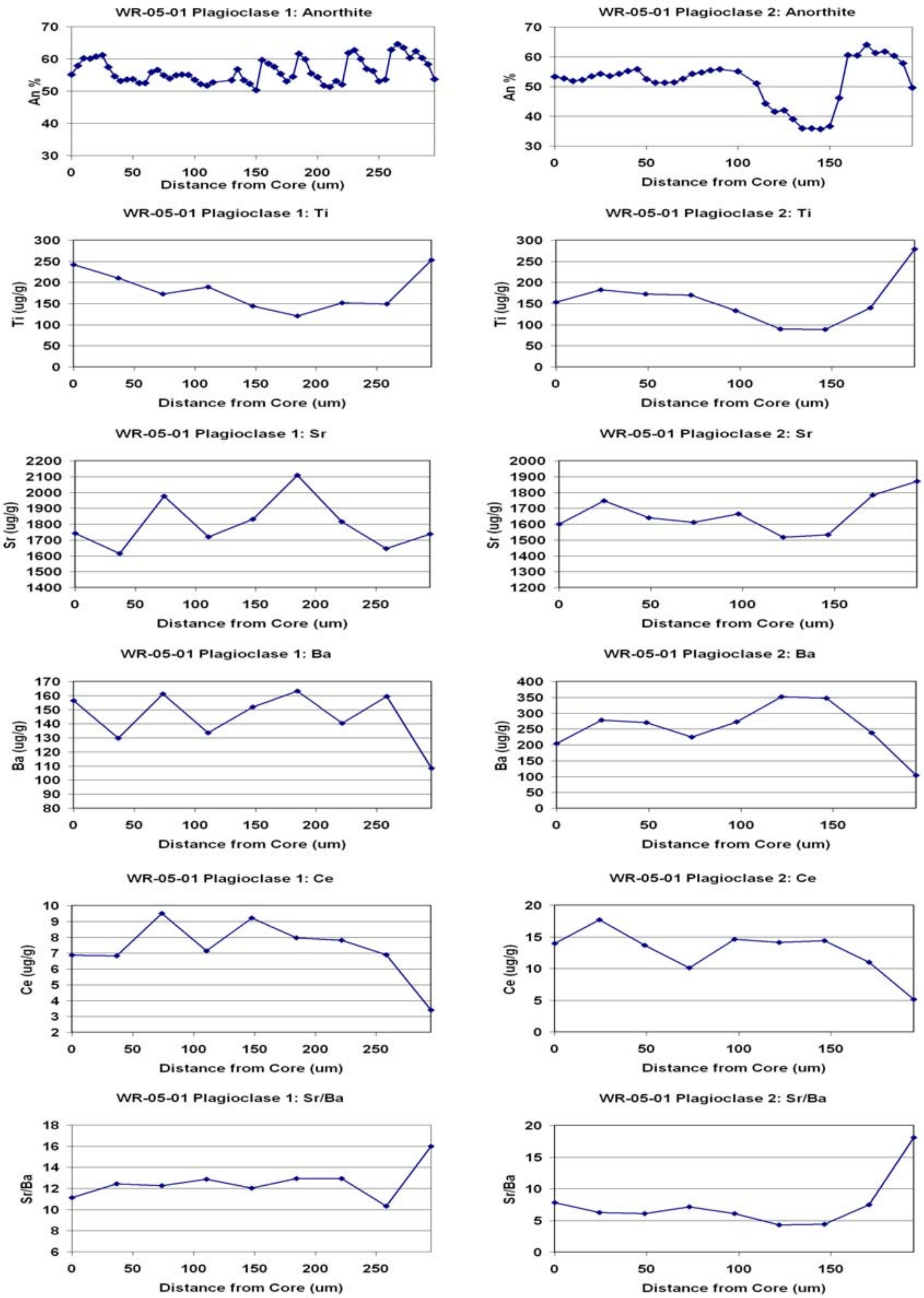

Figure 27: Plagioclase 1 (left) and 2 (right) from WR-04-01 trace elements (Ti, Sr, Ba, Ce, Sr/Ba) from core to rim analyzed by LA-ICP-MS, compared to anorthite transect. Increases in Ti, Sr, Sr/Ba, and anorthite and decreases in Ba and Ce at the rim indicate that there had been a mixing event during the last period of crystallization for these crystals.

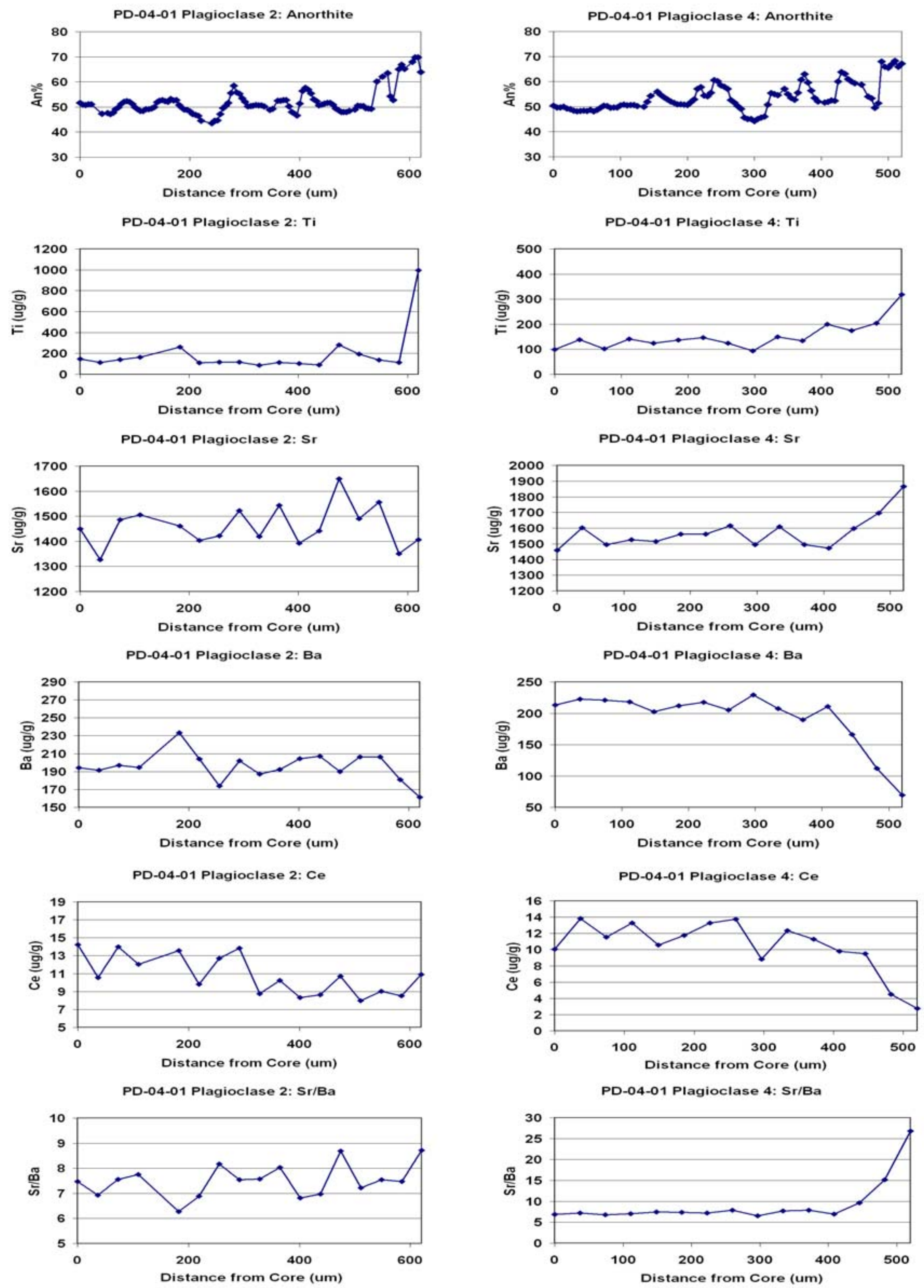

Figure 28: Plagioclase 2 (left) and 4 (right) from PD-04-01 trace elements (Ti, Sr, Ba, Ce, Sr/Ba) from core to rim analyzed by LA-ICP-MS compared to anorthite transect. Increases in Ti, Sr, Sr/Ba, and anorthite and decreased in Ba and Ce indicates that there had been a mixing event during the last period of crystallization for these crystals.

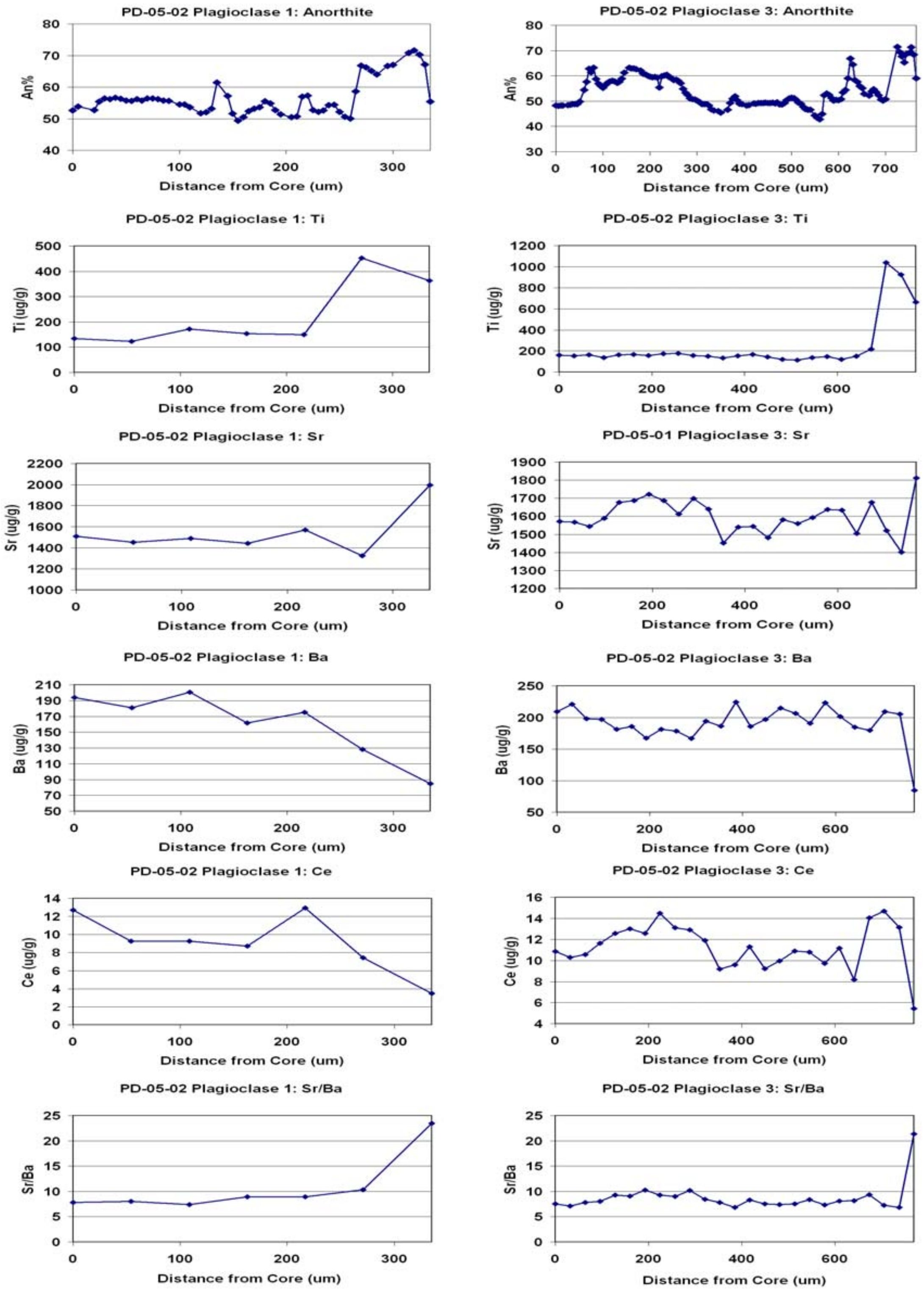

Figure 29: Plagioclase 1 (left) and 3 (right) from PD-05-02 trace elements (Ti, Sr, Ba, Ce, Sr/Ba) from core to rim analyzed by LA-ICP-MS compared to anorthite transect. Increases in Ti, Sr, Sr/Ba, and anorthite and decreases in Ba, and Ce at the rim indicates that there had been a mixing event during the last period of crystallization for these crystals.

Along with trace element data from plagioclase phenocrysts, trace element data was also gathered from plagioclase microlites (less than 1 mm in length). Since the microlites were so small only one point in the center was used for the analysis. Figure 30 is a plot of all the phenocryst and microlite data using Ti, Ba, Ce, and Sr/Ba versus anorthite compositions. The plots show that the points can be roughly divided into two groups. The first grouping consists of transect points from PD-04-01 phenocrysts, PD-05-02 phenocrysts, and WR-05-01 phenocrysts. This grouping is defined by higher concentrations of Ce and Ba and lower concentrations of Ti and Sr/Ba. The second grouping consists of the microlites from PD-04-01, microlites from HM-04-01, and the transect points from CC-04-01 plagioclase. This grouping is defined by lower concentrations of Ce, and Ba and higher concentrations of Ti and Sr/Ba. Data points from the rims of the larger phenocrysts from the first population have similar compositions to that of the second population and even plot within the area contained by the circle.

Using the calculated partition coefficients from figure 17, and the high and low compositions of the two groups of plagioclase from figure 30 and the following equation:

$$X_{melt} = \frac{X_{crystal}}{K_d} \tag{3}$$

where $X_{crystal}$ is the concentration of a certain element in plagioclase, K_d is the partition coefficient; the concentration of the element in the melt (X_{melt}) that is in equilibrium with the plagioclase can be calculated. Table 8 shows the results of these calculations.

Table 8: Range of calculated melt compositions that would be in equilibrium with plagioclase crystals from the two populations from figure 30. This shows that the melt in equilibrium with the more mafic plagioclase crystals is similar to the whole rock composition for CC-04-01, while the silicic melt is very different than the whole rock composition for WR-05-01.

	Circled Population					
	High Composition (µg/g)	**Calculated Mafic Melt (µg/g)**	**Low Composition (µg/g)**	**Calculated Mafic Melt (µg/g)**		**CC-04-01**
Ti	590	16837	300	8561		12300
Ba	100	330	50	165		252
Ce	5	53	2	21		29
	Not Circled Population					
	High Composition (µg/g)	**Calculated Silicic Melt (µg/g)**	**Low Composition (µg/g)**	**Calculated Silicic Melt (µg/g)**		**WR-05-01**
Ti	200	5707	100	2854		7700
Ba	275	908	150	495		344
Ce	15	159	8	85		39

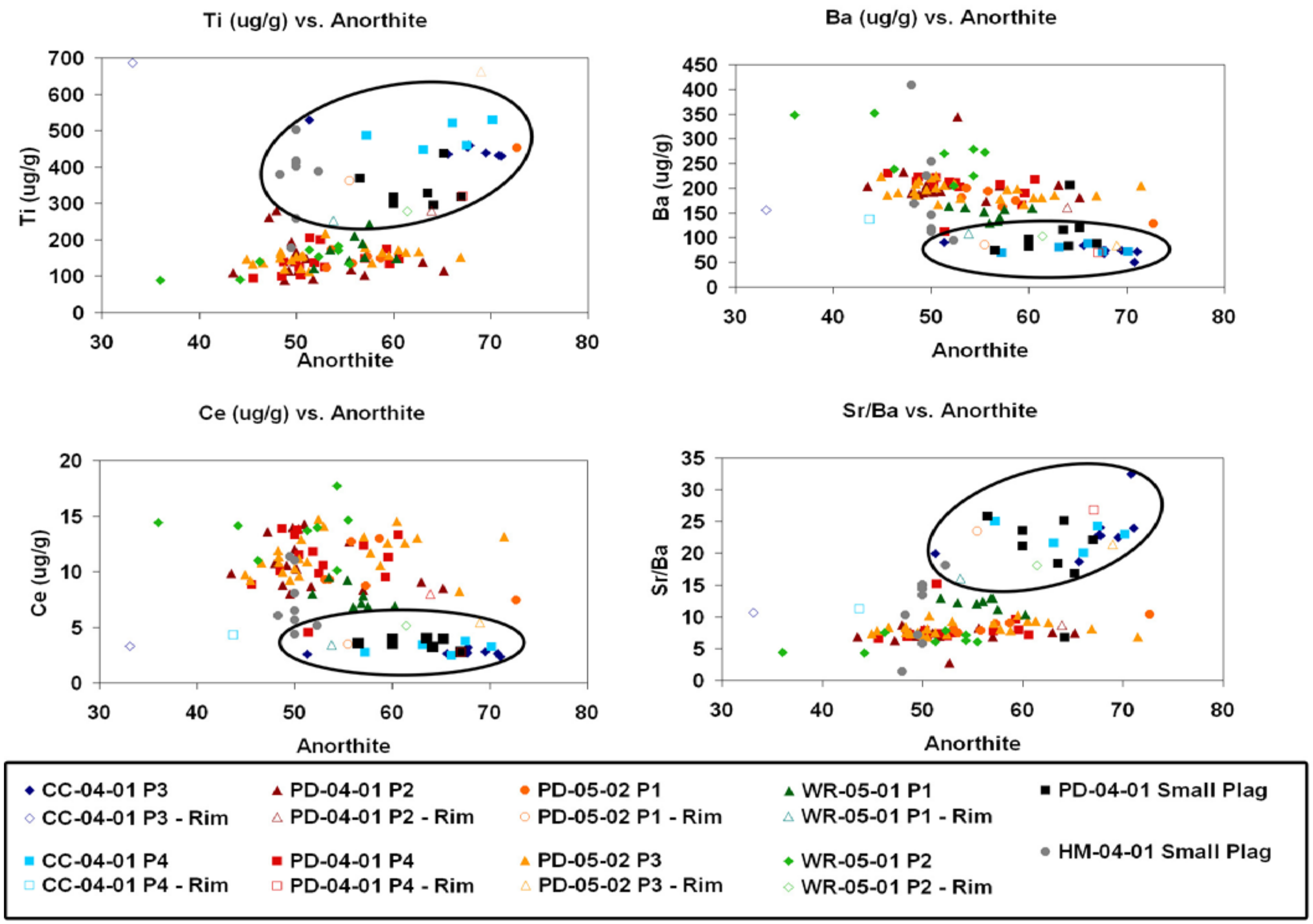

Figure 30: Plots of Ti, Ba, Ce and Sr/Ba versus anorthite of all LA-ICP-MS data points. Two distinct crystal populations exist. The circled population contains data points from CC-04-01, small plagioclase (< 1 mm in length) PD-04-01 and small plagioclase from HM-04-01. The population outside the circled area mostly are from PD-04-01, PD-05-02, and WR-05-01 (> 1 mm in length). Open symbols represent the analyses on the rim of the plagioclase. The rim analyses of the larger plagioclase show a composition similar to that of the circled population.

Crystal Size Distribution

CSD was used to identify different crystal populations based on size. The different crystal populations are interpreted to represent crystals from different sources, such as two magmas mixing together. Other evidence for mixing that supports this includes linear correlations between major and minor elements and silica (see Major and Minor Element Trends section). Table 9 summarizes the CSD results from the following samples. All slopes listed in Table 9 and in Figures 31 through 36 are significant at 98% or greater. All of the CSD graphs in the following figures have been plotted on the same scale in order to distinguish similarities between the plagioclase populations through all of the samples.

Table 9: Summary of CSD data from 6 samples from Mount Hood. Shaded cell represent the likely average residence time for each of the different sequences.

Sample	SiO_2 wt. %	Age	Different Crystal Population (Sequence #)	Slope	Slope Error	R2	Average Crystal Residence Time (years) G = 10^-9 mm/s	Average Crystal Residence Time (years) G = 10^-10 mm/s
CS-04-02	59.2	475 ka	1	-5.7883	0.331	0.9622	5.5 (± 0.3)	54.8 (± 0)
			2	-0.4747	0.005	0.9996	66.8 (± 0.7)	668.1 (± 7)
CD-04-01	60.0	225 ka	1	-8.0943	0.439	0.9770	3.9 (± 0.2)	39 (+2.2; - 2)
			2	-1.5029	0.141	0.8974	21.1 (+ 2.2; - 1.8)	211 (+22; - 18)
CC-04-01	55.7	55 ka	1	-6.5161	0.239	0.9828	4.9 (± 0.2)	48.7 (± 2)
HM-04-01	60.1	50 ka	1	-5.7635	0.278	0.9750	5.5 (± 0.3)	55 (± 2.6)
			2	-1.7918	0.165	0.9294	17.7 (+ 1.8; - 1.5)	177 (+ 18; - 15)
EB-04-01	61.9	35 ka	1	-6.8586	0.649	0.9255	4.6 (+ 0.5; - 0.4)	46 (+ 5; -4)
			2	-1.5801	0.297	0.7386	20.1 (+ 4.7; - 3.2)	201 (+ 47; - 32)
PD-04-01	58.8	7.5 ka	1	-8.1533	0.378	0.9831	3.9 (± 0.2)	39 (+ 1.9; - 1.7)
			2	-1.3957	0.218	0.8369	22.7 (+ 4.2; - 3.1)	227 (+ 42; - 31)

CS-04-02

Sample CS-04-02 is the oldest lava flow for this study; dated at 475 ka with a silica content of 59.2 weight percent. Plagioclase crystals in the sample range from less than 0.1 mm to 3 mm in length. They have a euhedral tabular shape and have minor lineation. Figure 31 is the CSD plot of the plagioclase crystals from this sample. The graph can be roughly divided into 2 sections that form a convex up pattern. The smaller sequence 1 of plagioclase crystals have an average residence time of 5.5 years, while the larger sequence 2 has an average residence time of 66.8 years, assuming a growth rate of 10^{-9} mm/s. Assuming a growth rate of 10^{-10} mm/s increases the average residence times to 54.8 years for sequence 1 and 668.1 years for sequence 2.

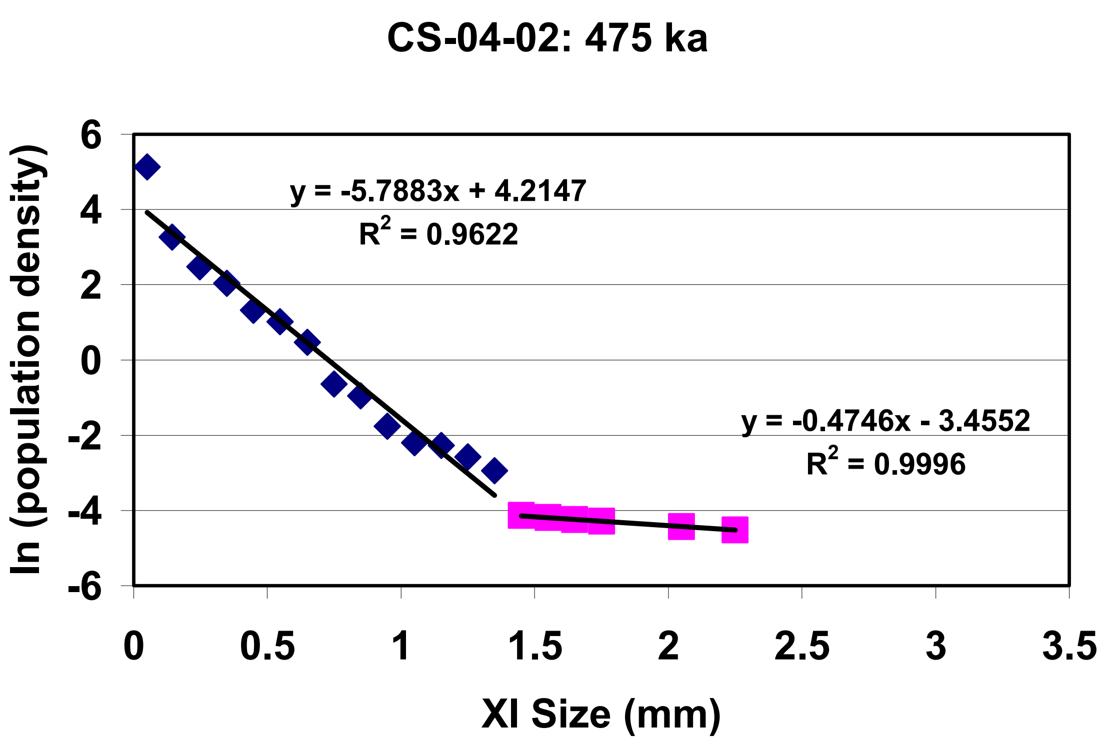

Figure 31: CS-04-02 CSD plot. Two distinct crystal populations exist in this sample distinguished by the convex shape the diagram produces. Sequence 1 has an average residence time of 5.5 years and sequence 2 that has and average residence time of 66.8 years (G = 10^{-9} mm/s), or 54.8 years for sequence 1 and 668.1 years for sequence 2 (G = 10^{-10} mm/s). The division between the two sequences is approximatly at 1.4 mm.

CD-04-01

Sample CD-04-01 is dated at 225 ka with a silica content of 60.0 weight percent. Plagioclase crystals in the sample range from less than 0.1 mm to 4 mm in length. They have a euhedral/subhedral tabular shape with no real lineation formed by the plagioclase crystals. Figure 32 is the CSD plot of the plagioclase crystals from this sample. The plot can be divided up into 2 distinct crystal populations that form a convex up pattern. The smaller sequence 1 of plagioclase crystals have an average residence time of 3.9 years, while the larger sequence 2 has an average residence time of 21.1 years, assuming a growth rate of 10^{-9} mm/s. Assuming a growth rate of 10^{-10} mm/s increases the average residence times to 39 years for sequence 1 and 211 years for sequence 2.

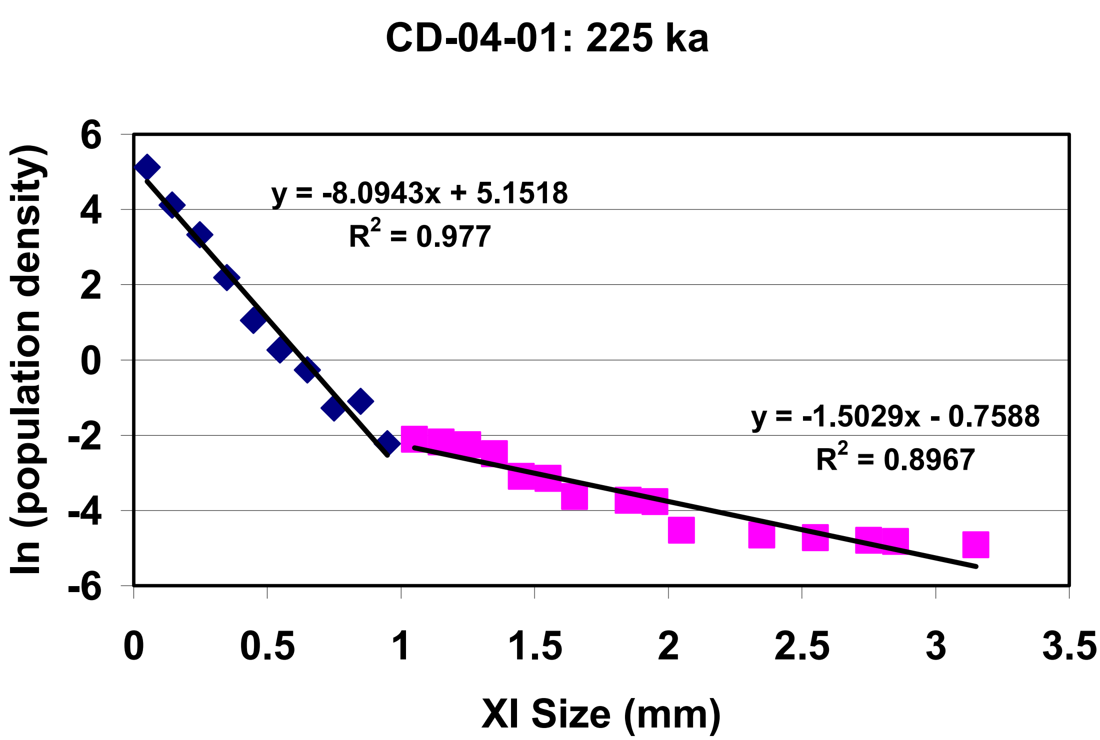

Figure 32: CD-04-01 CSD plot. Two distinct crystal populations exist in this sample distinguished by the convex shape the diagram produces. Sequence 1 has an average residence time of 3.9 years and sequence 2 that has and average residence time of 21.1 years (G = 10^{-9} mm/s), or 39 years for sequence 1 and 211 years for sequence 2 (G = 10^{-10} mm/s). The division between the two sequences is approximatly at 1 mm.

CC-04-01

Sample CC-04-01 is dated at 55 ka with a silica content of 55.7 weight percent making this the most mafic sample collected for this study. Plagioclase crystals in the sample range from less than 0.1 mm to 1.5 mm in length. They have a euhedral tabular shape with a distinct lineation pattern for both phenocrysts and the groundmass crystals. Figure 33 is the CSD plot of the plagioclase crystals from this sample. The plot shows only one clear population of crystals in this sample that has an average residence time of 4.9 years assuming a growth rate of 10^{-9} mm/s or 48.7 years assuming a growth rate of 10^{-10} mm/s.

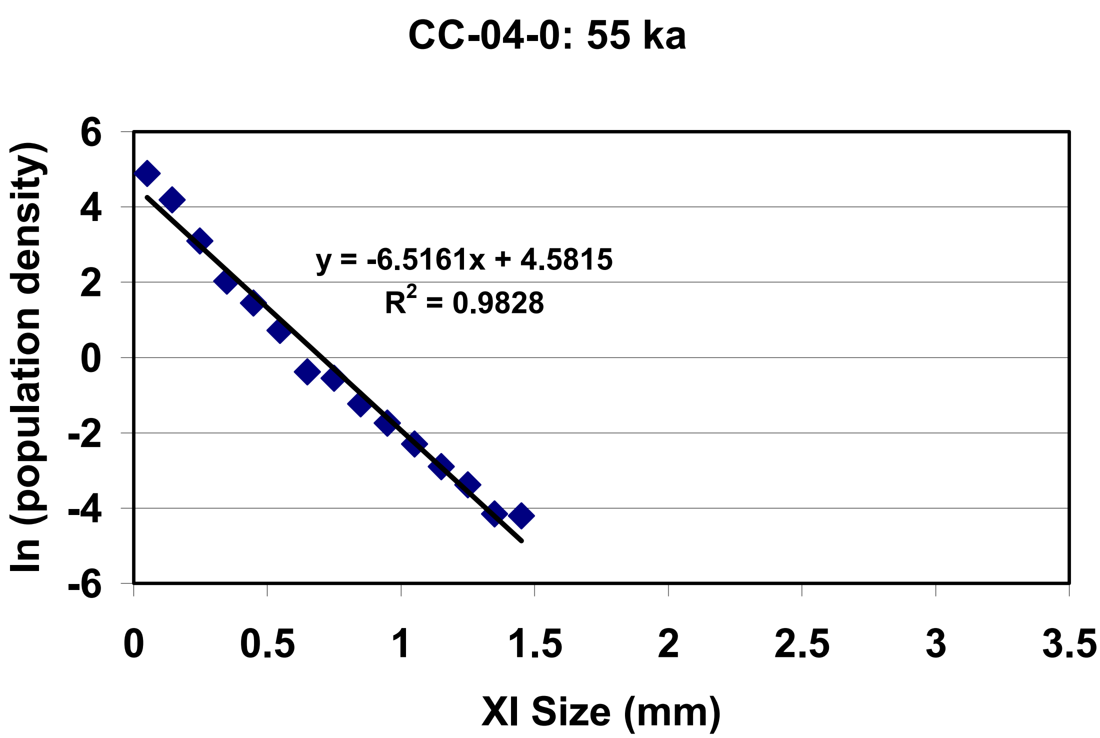

Figure 33: CC-04-01 CSD plot. Only one distinct crystal population exists in this sample. There is no convex shape produced in this diagram. Sequence 1 has an average residence time of 4.9 years (G = 10^{-9} mm/s) or 48.7 years (G = 10^{-10} mm/s), and the largest plagioclase crystals are less than 1.5 mm.

HM-04-01

Sample HM-04-01 is dated at 50 ka with a silica content of 60.1 weight percent. Plagioclase crystals in the sample range from less than 0.1 mm to 3 mm in length. They have a euhedral tabular shape with no real lineation formed by the phenocryst plagioclase, but the groundmass plagioclase crystals show a flow direction. Figure 34 is the CSD plot of the plagioclase crystals from this sample. The plot can be divided up into 2 distinct crystal populations that form a convex up pattern. The smaller sequence 1 of plagioclase crystals have an average residence time of 5.5 years, while the larger sequence 2 has an average residence time of 17.7 years, assuming a growth rate of 10^{-9} mm/s. Assuming a growth rate of 10^{-10} mm/s increases the average residence times to 55 years for sequence 1 and 177 years for sequence 2.

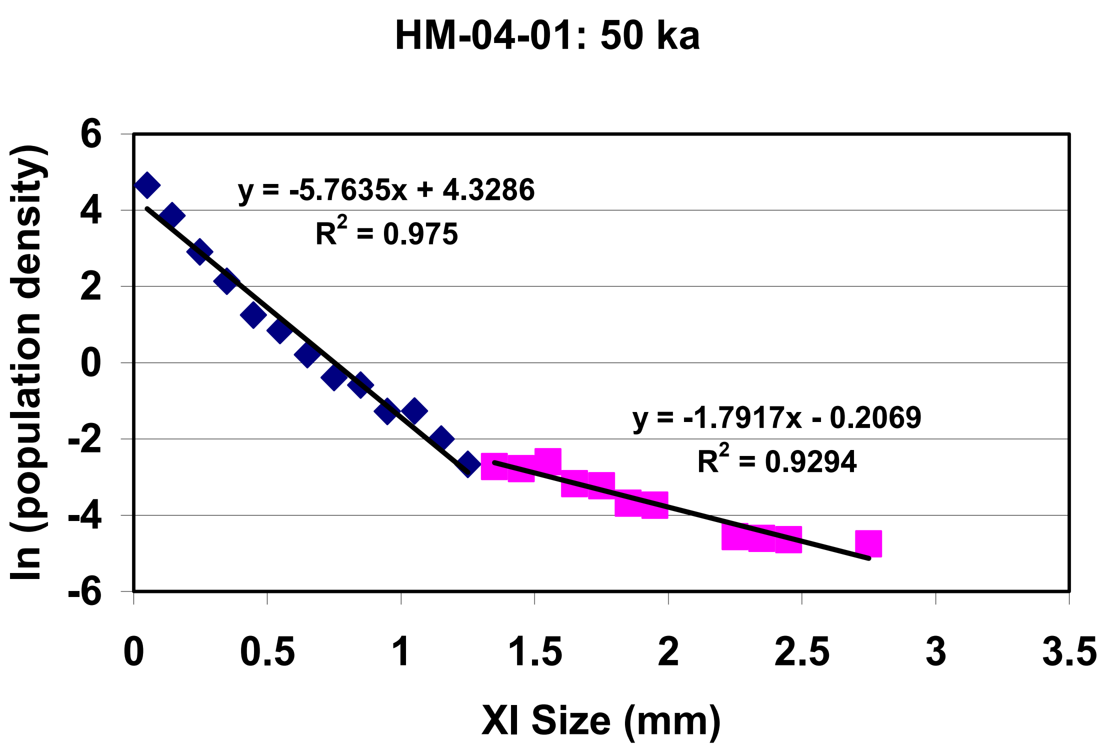

Figure 34: HM-04-01 CSD plot. Two distinct crystal populations exist in this sample distinguished by the convex shape the diagram produces. Sequence 1 has an average residence time of 5.5 years and sequence 2 that has and average residence time of 17.7 years (G = 10^{-9} mm/s), or 55 years for sequence 1 and 177 years for sequence 2 (G = 10^{-10} mm/s). The division between the two sequences is approximatly at 1.3 mm.

EB-04-01

Sample EB-04-01 is dated at 30 - 40 ka with a silica content of 61.9 weight percent making this the most silicic sample CSD was preformed on for this study. Plagioclase crystals in the sample range from less than 0.1 mm to 3 mm in length. They have a euhedral tabular shape with slight lineation evident in the groundmass plagioclase and none for the plagioclase phenocrysts. Figure 35 is the CSD plot of the plagioclase crystals from this sample. The plot can be divided up into 2 distinct crystal populations that form a convex up pattern. The smaller sequence 1 of plagioclase crystals have an average residence time of 4.6 years while the larger sequence 2 has an average residence time of 20.1 years, assuming a growth rate of 10^{-9} mm/s. Assuming a growth rate of 10^{-10} mm/s increases the average residence times to 46 years for sequence 1 and 201 years for sequence 2.

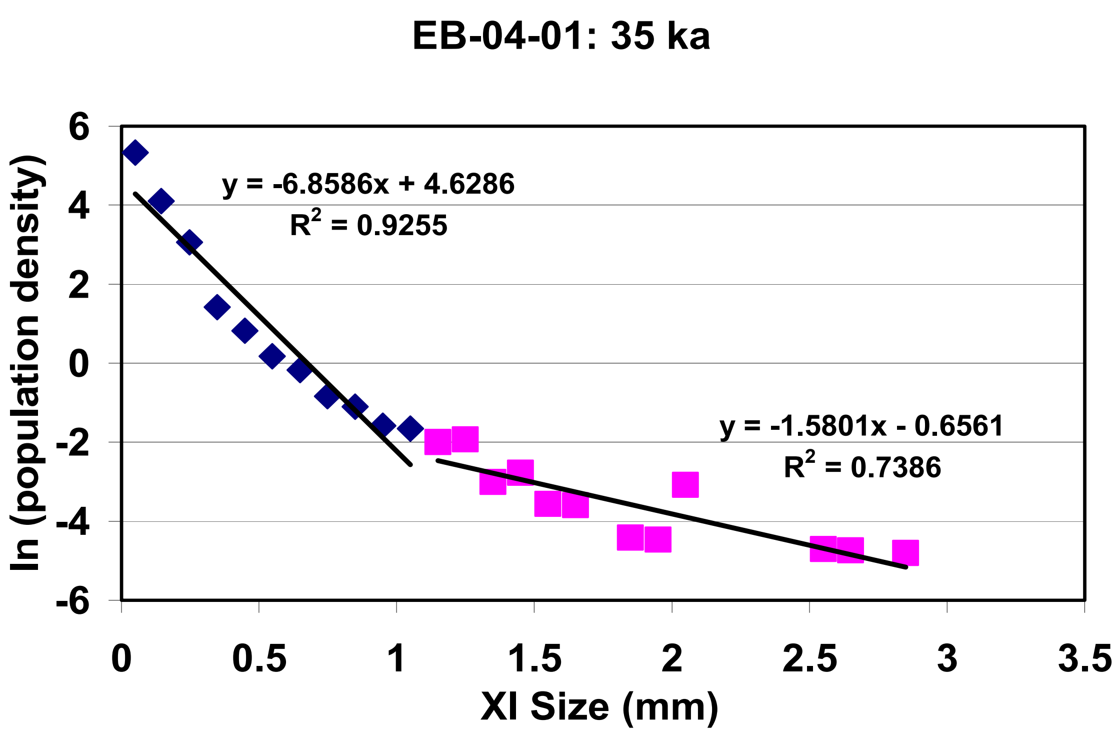

Figure 35: EB-04-01 CSD plot. Two distinct crystal populations exist in this sample distinguished by the convex shape the diagram produces. Sequence 1 has an average residence time of 4.6 years and sequence 2 that has and average residence time of 20.1 years (G = 10^{-9} mm/s), or 46 years for sequence 1 and 201 years for sequence 2 (G = 10^{-10} mm/s). The division between the two sequences is approxmately 1 mm.

PD-04-01

Sample PD-04-01 is dated at 7.5 ka with a silica content of 58.8 weight percent. This sample is from the middle section of the Parkdale lava flow. Plagioclase crystals in the sample range from less than 0.1 mm to 2 mm in length. They have a euhedral tabular shape with no distinct lineation formed by the plagioclase crystals. Figure 36 is the CSD plot of the plagioclase crystals from this sample. The plot can be divided up into 2 distinct crystal populations that form a convex up pattern. The smaller sequence 1 of plagioclase crystals have an average residence time of 3.9 years, while the larger sequence 2 has an average residence time of 22.7 years, assuming a growth rate of 10^{-9} mm/s. Assuming a growth rate of 10^{-10} mm/s increases the average residence times to 39 years for sequence 1 and 227 years for sequence 2.

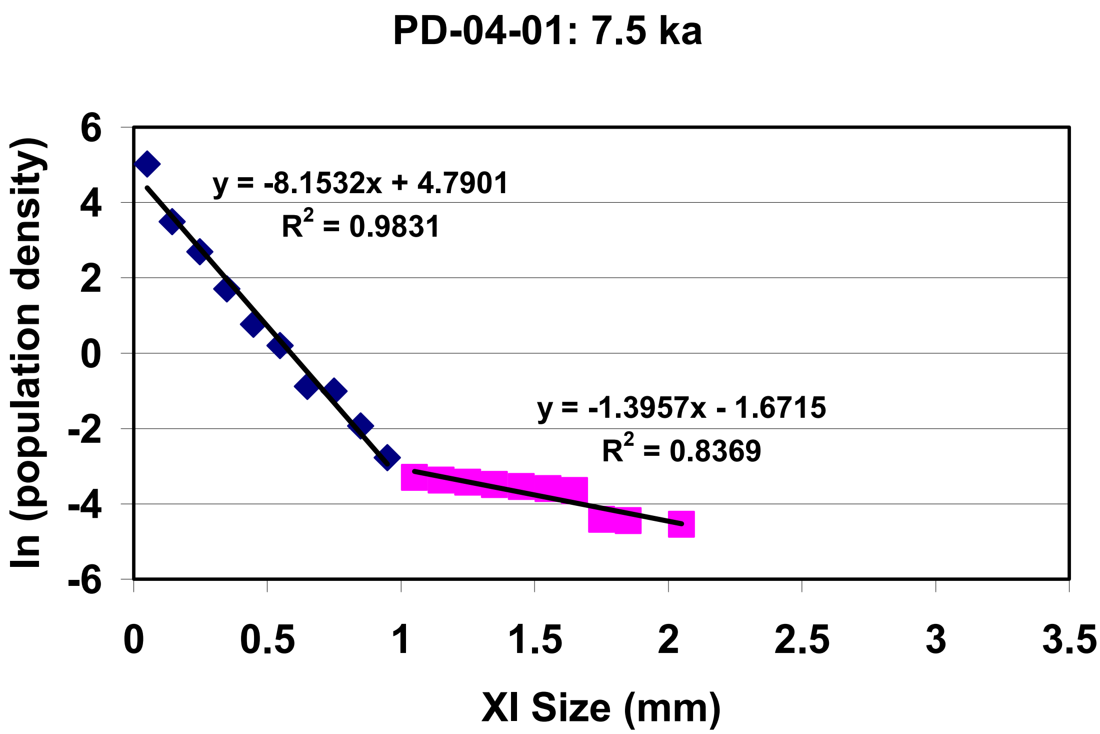

Figure 36: PD-04-02 CSD plot. Two distinct crystal populations exist in this sample distinguished by the convex shape the diagram produces. Sequence 1 has an average residence time of 3.9 years and sequence 2 that has and average residence time of 22.7 years (G = 10^{-9} mm/s), or 39 years for sequence 1 and 227 years for sequence 2 (G = 10^{-10} mm/s). The division between the two sequences is approximately at 1 mm.

Crystal Fractionation

Removal of crystallized phases can result in changes to magmatic compositions via a process known as crystal fractionation and can produce an evolution from mafic compositions to more silicic compositions. Fractionation of plagioclase, orthopyroxene, and a Fe-Ti oxide, all common abundant minerals found in the lavas of Mount Hood, would account for the trends observed in the Harker diagrams of Figure 11. These crystallizing assemblages would remove Al_2O_3, MgO, FeO*, CaO, TiO_2, while K_2O would become enriched in the residual melt. If this is the case, then if the mineral, starting, and ending compositions are known their mineral proportions removed can be modeled using a least-squares fitting procedure (Stormer and Nicholls, 1978). For this study, this was done using the XLFRAC spreadsheet. The program allows for a mass balance calculation to be performed between two magma compositions and several phase compositions. This calculation determines the proportion of the given phases that needs to be added or subtracted to produce the differences seen between the daughter and parent melts.

The initial magma for this study is taken to be the most mafic of the samples (CC-04-01; 55.7 weigh percent silica), while the final magma is taken to be the most evolved (WR-05-01; 63.8 weight percent silica). Five phase compositions were used in calculating the mass balance between the two magmas. Two plagioclase compositions, one at An_{65} and one at An_{32}, two orthopyroxene compositions, one at En_{70} and one at En_{53}, and lastly an ilmenite composition. Since XLFRAC cannot model mineral zonation changes in mineral with solid solutions such as plagioclase and orthopyroxene, two different plagioclase and orthopyroxene compositions were used as a way to approximate changes in mineral compositions during progressive fractionation. Mineral compositions are from EMPA analyses and are all from various flows from Mount Hood except the ilmenite composition which was taken from Deer, et al. (1992). Table 10 contains the mass balance results from the XLFRAC program. These proportions are 23.9% of plagioclase (An_{65}), 29.51% of plagioclase (An_{45}), 0.09% of orthopyroxene (En_{70}), 20.01% of orthopyroxene (En_{53}), and 2.06% of ilmenite. The composition of the total amount removed from the system is listed under the column labeled Bulk Composition

Added of Subtracted Material. Approximately 75.6% of the initial magma must crystallize and be removed from the system to produce a composition similar to the final magma. The sum of the squares of the residuals values that are less than 1 are deemed to be a good fit, and for this mass balance calculation the sum of the squares is 0.1151. Also, that the most primitive magma is not the oldest magma making it unlikely that the samples shown here represent the progressive products of crystal fractionation of a single batch of magmas, however, if these magma represent the range of magmas produced or present in the system, then crystal fractionation could still be used in the erupted products production.

Figure 37 shows the effect of crystal fractionation of the calculated proportions from the most primitive magma. Each point represents the removal of 10% crystals from the initial magma, and increased from left to right. Crystal fractionation can produce similar trends to those seen at Mount Hood; however, there are some notable differences. The fractionation model shows an ending composition with lower concentrations of Al_2O3, MgO, FeO*, CaO, and TiO_2, and higher concentrations of Na_2O and K_2O when compared to the known whole rock compositions. The observed trend in the whole rock data from lavas from Mount Hood cannot be reproduced through crystal fractionation. It is most likely that this trend can be reproduced via magma mixing.

Table 10: Results from XL FRAC program designed by Stomer and Nicholls, 1978. Composition removed from the system is listed under Bulk Composition of added of Subtracted Material.

Oxides	Initial Magma	Final Magma	Plag An65	Plag An32	OPX En 70	OPX En 53	Ilmenite
SiO2	56.035	64.014	51.72	59.81	54.51	52.07	0.11
TiO2	1.239	0.773	0.06	0	0.3	0.37	49.3
Al2O3	18.852	16.890	30.4	25.46	1.31	0.5	0.54
FeOtot	7.385	4.841	0.57	0.28	17.4	25.28	48.84
MgO	4.404	2.487	0.09	0.01	25.12	18.86	0.56
CaO	7.089	5.154	13.26	6.63	1.36	2.86	0.65
Na2O	4.296	4.384	3.84	7.24	0.01	0.05	0
K2O	0.699	1.457	0.06	0.55	0	0	0
Total	100	100	100	100	100	100	100

Results

Oxides	Bulk Composition of Added or Subtracted Material	Observed Differences Between Magmas	Calculated Differences Between Magmas	Observed - Calculated Residuals
SiO2	53.57	7.979	7.892	0.087
TiO2	1.463	-0.466	-0.521	0.055
Al2O3	19.706	-1.963	-2.128	0.166
FeOtot	8.335	-2.544	-2.64	0.096
MgO	5.073	-1.917	-1.954	0.037
CaO	7.561	-1.935	-1.819	-0.116
Na2O	4.056	0.088	0.248	-0.16
K2O	0.235	0.758	0.923	-0.165

Sum of the Squares of the Residuals 0.1151

Phase	Amount as Wt. % of Initial Magma	Amount as Wt. % of All Phases	Amount as Wt. % of Added Phases	Amount as Wt. % of Subtracted Phases
Plag An65	-23.9	31.62	0	31.62
Plag An32	-29.51	39.06	0	39.06
Opx En 70	-0.09	0.12	0	0.12
Opx En 53	-20.01	26.48	0	26.48
ilm	-2.06	2.73	0	2.73

Total Relative to Initial Magma 75.56

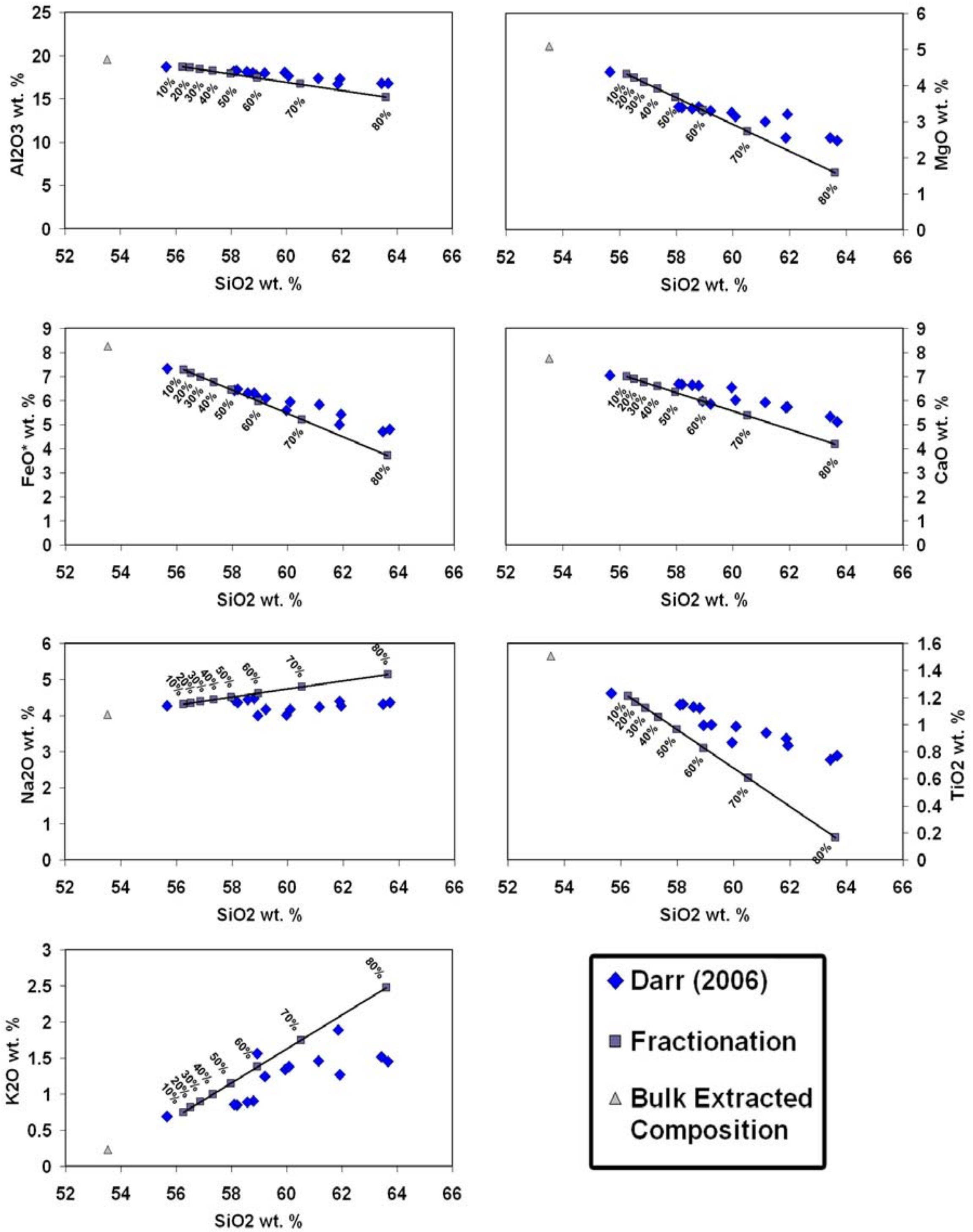

Figure 37: Effect of crystal fractionation (squares) of calculated bulk extracted composition (triangle) subtracted from CC-04-01. Each gray square represents the residual composition after an increase of 10% of crystals removed from the system from left to right. Blue diamonds represent actual whole rock data from Mount Hood. The XL FRAC calculation underestimates final compositions in Al_2O_3, MgO, FeO*, CaO, and greatly in TiO_2, and overestimates final compositions in Na_2O and K_2O.

Discussion

The results listed in the previous section have all recorded evidence that a process has occurred within the magma chamber to produce compositionally similar magmas over the eruptive history of Mount Hood. Magma mixing is the most viable processes that would lead to the compositions seen at the surface.

Whole rock geochemistry presented in figure 11 suggests that the sampled lavas are genetically related to each other and the patterns are consistent mixing between two end member magmas.

CSD of several lava samples shows that each of the lavas from Mount Hood are comprised of two significantly different crystal populations except for one sample (CC-04-01), which is the most mafic sample of this study. LA-ICP-MS results of each of the crystal populations have determined that each of the populations have different trace element chemical compositions, and derive from different composition magmas.

Plagioclase textures and chemistry show correlations between disequilibrium textures and increases in anorthite, MgO, FeO, and other trace element consistent with a mixing event with a mafic magma that has yet to be depleted in compatible elements from crystallization of plagioclase, pyroxenes, amphibole, and Fe-Ti oxides. These textural and chemical trends both occur near the rim of plagioclase phenocrysts and may correspond to an event that triggered an eruption.

The following is a more detailed explanation of these concepts and the evidence that supports that the homogeneous compositions seen at Mount Hood are created through magma mixing of a mafic undepleted magma with a slightly more evolved host magma that has undergone some crystal fractionation prior to mixing.

Magma Mixing

Major Elements in the Whole Rock

The linear trend in the Harker diagrams in Figure 11 indicates a mixing between the most primitive composition and the most evolved composition. Products of mixed magmas will lie on a line between the two end member compositions. As stated in the introduction, Woods (2004) was able to use the hypothetical end member compositions of Mount Hood magmas to produce the range of lava compositions seen at Mount Hood. Woods calculated two hypothetical mafic end members; one basaltic (49 weight percent SiO_2) and one basaltic andesite (54 weight percent SiO_2), and a hypothetical silicic end member (66.4 weight percent SiO_2). Both host rocks and the inclusions generally fell along the mixing line formed by the hypothetical end members.

In the Harker diagrams in Figure 11, the mafic end member is CC-04-01 (55.7 weight percent SiO_2); the silicic end member is WR-05-01 (63.8 weight percent SiO_2). These form a linear trend in which the remaining samples lie. One of the hypothetical mafic end members that Woods developed was a basaltic andesite which closely resembles the composition of CC-04-01 (Table 11). This observation could mean that the CC-04-01 represents the mafic end member in the Mount Hood system. Figure 38 shows the major element data from Mount Hood lavas with a mixing trend line formed by mixing CC-04-01 with WR-05-01. Also included are the hypothetical end members calculated by Woods (2004). Each point represents a 10% increase in the WR-05-01 component when moving from left to right on the diagram. These figures show that mixing between the most mafic sample and most silicic sample from this study present a reasonable process to create the range of lavas erupted from Mount Hood for most of the major elements.

Pyroxenes

Figure 15 shows the analyses of coexisting orthopyroxene and clinopyroxene phenocrysts in lavas from Mount Hood connected by tie lines. As melt compositions evolve, Mg would be removed from the system and more Fe-rich orthopyroxene and clinopyroxene phenocrysts would begin to form with each other in the melt, however, lavas from Mount Hood have Fe-rich orthopyroxene phenocrysts coexisting with Fe-poor clinopyroxene phenocrysts and visa-versa. Pyroxene compositions such as these would not normally by in equilibrium with each other in a melt. To have these compositions existing with each other in one sample can be achieved by mixing between two end member magmas, where one is relatively more mafic and is crystallizing Fe-poor pyroxenes and the other is more evolved (silicic) and is crystallizing Fe-rich pyroxenes.

Table 11: Comparison between CC-04-01(this study) and a hypothetical basaltic andesite end member calculated in Woods, 2004.

	CC-04-01	Woods Hypothetical Basaltic Andesite End Member
Major Element (Weight %)		
SiO2	55.66	54.02
TiO2	1.23	1.36
Al2O3	18.73	18.53
FeO*	7.34	7.77
MnO	0.12	0.13
MgO	4.37	4.72
CaO	7.04	8.57
Na2O	4.27	3.99
K2O	0.69	1.25
P2O5	0.24	0.34
Sum	99.69	100.68
Trace Elements (ppm)		
Cr	79	47.43
Sc	18	20.62
Ba	252	446.8
Rb	7	12.03
Sr	629	659.5
Zr	119	172.33
Y	18	17.88
Nb	7	12.89
La	11	30.9
Ce	29	58.23
Th	1	3.38

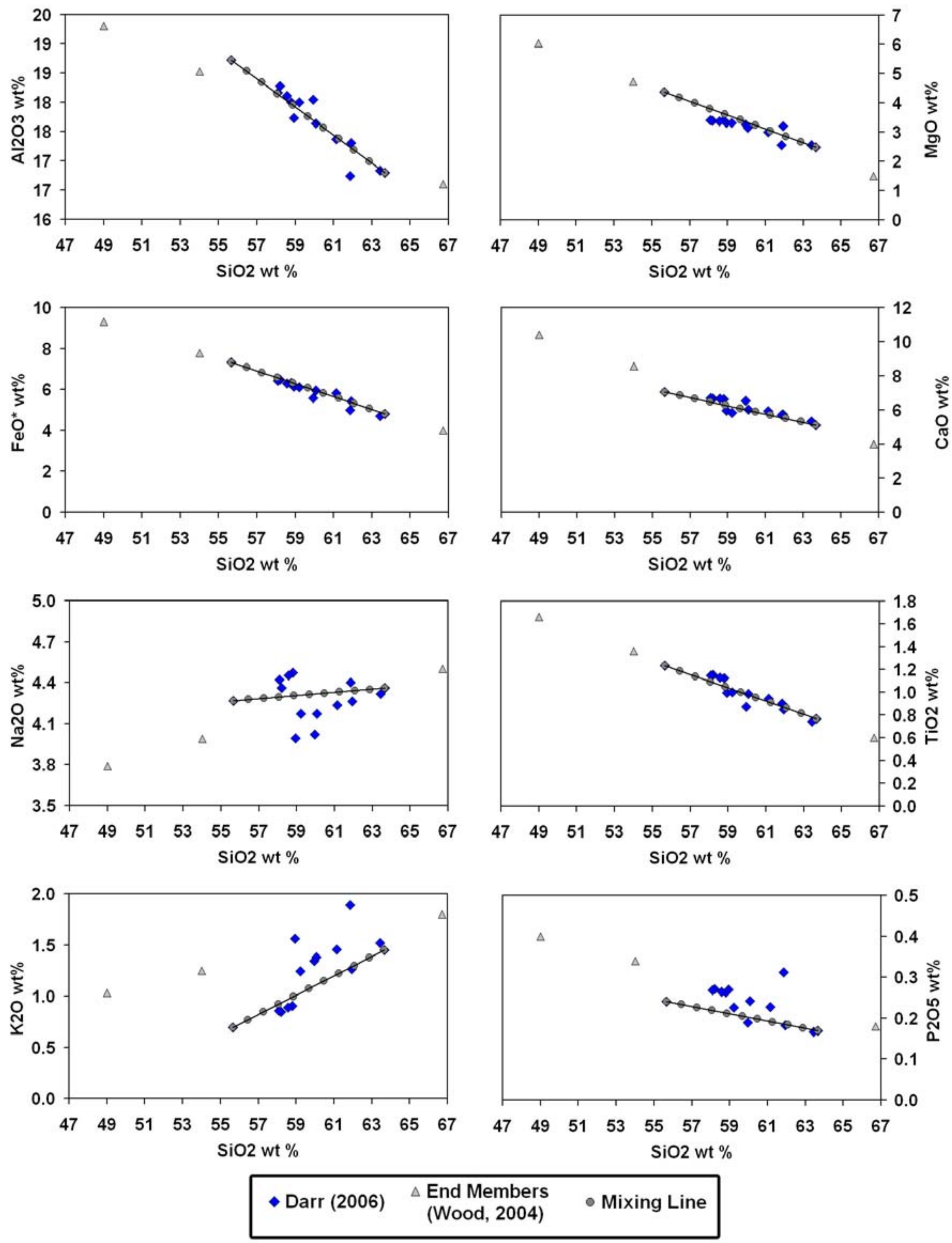

Figure 38: Effect of magma mixing between CC-04-01 and WR-05-01. Gray circles represent the mixing line between the two end members. Each gray dot represents an increase of 10% WR-05-01 component when moving from left to right. Blue diamonds represent actual whole rock data from Mount Hood. Most of the whole rock compositions are explained by mixing between these two end members.

CSD

Figures 31 through 36 are the CSD plots of six different thin sections. Five out of six of the plots that range in ages from 475 ka to 7.5 ka show that the samples are made of two distinct crystal populations. This is shown by the distinctive kink in the data forming a convex up pattern. The most likely way to create these two populations is by the mixing of two magmas with crystals of different sizes. This same pattern and interpretation has been seen in several other studies in the Aleutian Islands (Marsh, 1988), Makaopuhi lava lake, Hawaii (Cashman and Marsh, 1988), and Kameni Islands, Greece (Higgins, 1996). The division between these two populations ranges from 1 mm to 1.5 mm long axis crystal lengths. These plots indicate that regardless of age, there are two distinct populations of crystals in each of the magmas erupted from Mount Hood. This observation is similar to that seen in the CSD study from the Kameni Islands, Greece (Higgins, 1996).

The smaller crystal populations, named sequence 1 in Table 9, from the five samples with multiple crystal populations have average residence times that range from 5.5 years to 3.9 years with a crystal growth rate of 10^{-9} mm/sec or 54.8 years to 39 years with a crystal growth rate of 10^{-10} mm/s. The larger crystal populations, sequence 2, have average residence times varying from 22.7 to 17.7 year with a crystal growth rate of 10^{-9} mm/sec or 227 years to 177 years with a crystal growth rate of 10^{-10} mm/s. The oldest sample (CS-04-02) has an average residence time of 66.8 years (10^{-9} mm/s) or 668 (10^{-10} mm/s). Once again there is consistency through the samples with respect to the average residence times of the crystals. The narrow residence time range created by the samples for both sequence 1 and sequence 2 populations, regardless of what growth rate is used, shows that over the eruptive history of Mount Hood two magmas have been mixed together to form the lavas exposed at the surface, and each of these end member magmas have had a similar residence time (Figure 39).

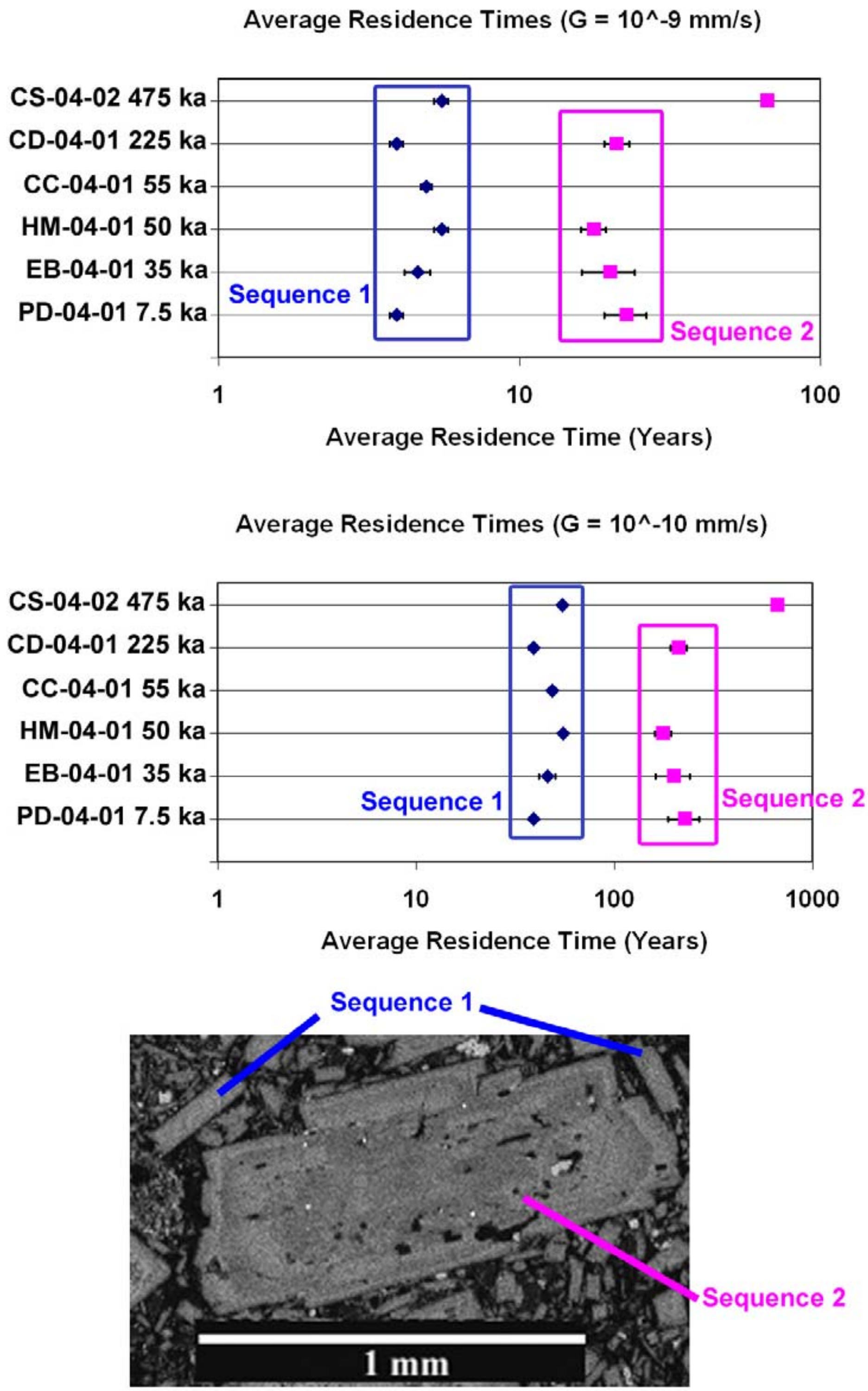

Figure 39: Calculated average residence times for sequence 1 and sequence 2 plagioclase crystal populations. First graph is for a growth rate of 10-9 mm/s and the second graph is for a growth rate of 10-10 mm/s. The two populations are distinct in each of the graphs. The similar residence time has persisted for the past 475 ka. Picture shows sequence 1 and sequence 2 crystals based on size.

Sample CC-04-01 is the only sample in which the CSD plot shows no indication of multiple crystal populations. This is also the most mafic sample studied. This suggests that this sample is not the result of mixing of magmas with different size populations. The single crystal population had no crystals that were over 1.5 mm in length and had an average residence time of 4.9 years (10^{-9} mm/s) or 48.7 years (10^{-10} mm/s). These observations of the crystal population are consistent with those of the sequence 1 populations from the other five samples.

This indicates that CC-04-01 may represent the host magma for sequence 1 crystals, and that somehow was able to erupt to the surface without mixing with the host magma for sequence 2 crystals. This, along with the whole rock data cited earlier, further indicates that this sample is a good estimate for a mafic end member of the Mount Hood magma system.

Textures, Major and Trace Elements in Plagioclase

Crystal textures can be used to interpret what is occurring in a magma chamber as the crystals are being formed. There are two main textures found in plagioclase phenocrysts from Mount Hood that can be used for these interpretations; oscillatory zonation and sieved rims.

Oscillatory zoning is formed by changes in the conditions of the chamber (P, T, P_{H2O}). Changes such as these have the ability to change the anorthite composition of crystallizing plagioclase. At higher temperatures, a more anorthite rich plagioclase will crystallize and as temperatures begin to decrease more, albitic plagioclase will form (Bowen, 1913). Gradual oscillations are typically formed by diffusion dependent depletion and re-enrichment of the melt next to the growing crystal (Pearce and Kolisnik, 1990). Addition and depletion of volatiles in the magma can have the same result by either decreasing or increasing the melting point which in turn shifts the equilibrium in the system (Pearce and Kolisnik, 1990).

Larger abrupt perturbations in a magma chamber (i.e. magma mixing) can lead to abrupt compositional changes (Couch, et al., 2001; Davidson and Tepley, 1997; Landi, et al., 2004; Pearce and Kolisnik, 1990; Tepley, et al., 1999, 2000; Triebold, et al., 2006). Larger complex oscillatory zonation, which is shown as significant increases in anorthite followed by a gradual return to equilibrium, is formed by self-mixing of a magma chamber (Couch, et al., 2001). Self-mixing is described by Couch, et al. (2001) as a convecting magma body of a single composition that is heated from below and cooled from the top. The hotter material would begin to rise to the top of the chamber and cooler material would take its place. This mixing would allow for large scale oscillatory zonation to form without the overall composition of the plagioclase to be changed dramatically. Complex oscillatory pattern as describe above are seen in all plagioclase transects (Figures 18 – 25) except those from CC-04-01. Magma mixing with a different composition magma can also form oscillatory patterns, but this would also change the composition of trace elements within the plagioclase structure.

Magma mixing can also create sieved features in plagioclase by putting the crystal into a state of disequilibrium. This allows for either dissolution of plagioclase forming embayments or rapid crystal growth forming a skeletal texture. These sieved cores and sieved rims characteristic of type 2 zoning are less abundant in the samples, and are typically only seen in plagioclase phenocrysts.

Crystallization of minerals will preferentially remove compatible elements from the magma system. Crystallization of plagioclase, pyroxenes, and oxides would remove elements (Mg, Fe, Ti and Sr) while others (Ba and Ce) would become more enriched in the melt since they will be less likely to be incorporated into the crystals structure.

Anorthite, Mg, and Fe are also all some what dependent on the degree of differentiation, P, T, and P_{H2O} of the magmas (Bindeman, et al., 1998; Triebold, et al., 2006). Less differentiated magmas have melts with higher concentrations of Mg and Fe and plagioclase with higher anorthite, while differentiated magmas have lower concentrations of Mg and Fe and crystallize plagioclase at lower anorthite. Since Mg and Fe are incompatible with plagioclase they can reflect the magma composition from which the plagioclase is crystallizing from (Triebold, et al., 2006). The partition coefficient Mg in particular does not have a large change with anorthite and will reflect the composition of the source in the plagioclase. If changes in anorthite across a phenocryst were due to just pressure and temperature changes in the chamber, anorthite would change but Mg and Fe should remain the same. However, if changes in the magma composition are due to recharge, mixing, or fractionation all parameters would show a significant difference and type 2 zonation patterns would be seen.

Ti is removed from the melt via ilmenite crystallization, while Sr is readily incorporated into plagioclase as it crystallizes, and these elements will decrease in concentration in the melt during progressive crystallization. As plagioclase continues to crystallize, trace elements such as Ba and Ce that are incompatible in the crystallizing assemblage will be progressively more enriched in the melt (although they become slightly more compatible due to plagioclase becoming less anorthite rich). If mixing between this evolved melt and a melt that has not experienced this fractionation occurs the depleted magma is re-enriched in the depleted elements and this will be recorded by the composition of crystallizing plagioclase. Elements that are enriched in the melt will have reduced concentrations after mixing/recharge and thus a recharge or mixing event recorded in a plagioclase will be shown as an increase in Ti and Sr, and decreases in Ba and Ce. The same would be true for anorthite, Mg and Fe. A re-enrichment of Mg and Fe will be recorded in plagioclase and an increase in temperature will induce the formation of a more anorthite rich plagioclase.

Plagioclase 3 and 4 from CC-04-01 (Figures 18 and 19) are both dominated by type 1 zoning. Anorthite varies by only 10 An % across the entire crystal. It is not until the edge of the crystal is reached and anorthite begins to decrease significantly, decreasing by greater than 20 An %. This significant decrease is most likely due to a drop in the system's pressure as it is being erupted. Decreasing a system's pressure forces the system to become saturated in volatiles, such as water, and as this occurs the plagioclase liquidus is depressed forcing more anorthite rich compositions to be crystallized (Johannes, 1978). Both MgO and FeO follow the same pattern as anorthite with no significant changes in the incorporation of these elements into the plagioclase phenocrysts. Figure 26 shows increasing Ba and Ce and the rim, while Sr is decreasing. This indicates that very few large events (if any) occurred within the chamber during the time that the magma that produced this flow was in residence in the chamber. There is no evidence of mixing with a significantly different composition magma.

Plagioclase 1 and 2 from WR-05-01 (Figure 20, 21, and 27) have an oscillatory zonation pattern that mainly varies under 10 An %, but at times the variation is greater (>30 An %) and is more representative of type 2 zonation. The frequency of the oscillation is much greater than those found in CC-04-01 suggesting more frequent condition changes occurring during crystallization. The larger scale zonation is likely to be resulting from self-mixing of the magma chamber being that these oscillations to not correspond to any large compositional changes in the trace elements. The last large variation near the rim of both plagioclase phenocryst do correspond to changes in the trace element compositions (increases in anorthite, MgO, FeO, Ti, Sr, and Sr/Ba, and decreases in Ba and Ce). The increase in the parameters at this point suggests a mixing event prior to the eruption of these crystals. This mixing event is likely an introduction of a hotter, more mafic magma. This is because to increase anorthite there must be either an increase in temperature or an increase in volatiles (Bowen, 1913; Johannes, 1978), or mixing with a more mafic (higher Ca/Na) magma. Since the partition coefficients for Mg and Fe decrease with increasing anorthite, there has to be an overall increase in the concentration of Mg and Fe in the melt to have an increase in the plagioclase along with an increase in anorthite. The increase in Ti and Sr is again considerably greater than could be attributed to changes in the partition coefficient but, is consistent with the Sr contents expected for plagioclase in equilibrium with mafic melt with higher Sr. Ba and Ce also decrease consistent with mixing of a more mafic magma where their abundances have not been concentrated by plagioclase crystallization. These patterns could be accomplished by mixing with a mafic recharge magma where the concentration of Mg, Fe, Ti and Sr are higher and incompatible elements such as Ba and Ce would be diluted.

Plagioclase 2 and 4 from PD-04-01 (Figure 22, 23, and 28) and over the course of the transect there are several large decreases in anorthite (>10 An %) followed by large increases in anorthite (>15 An %) that do not correspond to decreases or increases in trace elements. This can again be created via self-mixing as seen in the WR-05-01 plagioclase. Around the last 30 μm of each of the transects there is a significant increase in anorthite, MgO, FeO, Ti, Sr, and Sr/Ba and decreases in Ba and Ce. These compositional changes are similar to what is seen in the plagioclase from WR-05-01 and therefore, there was a mixing event with a hotter mafic magma prior to eruption for these plagioclase as well.

Plagioclase 1 and 3 from PD-05-02 (Figures 24, 25, and 29) are from the same lava flow as PD-04-01, but are found closer to the end of the flow. Both have a similar pattern of the plagioclase from PD-04-01 where there are significant increases (10 – 20 An %) and decreases (10 – 15 An %) in anorthite that do not correspond to significant compositional changes (self-mixing of the magma chamber). It is not until the last 100 μm of the transect where a significant change in anorthite and trace elements occur together (increasing anorthite, MgO, FeO, Ti, Sr, Sr/Ba, and decreasing Ba and Ce. Plagioclases 1 and 3 from PD-05-02 also have sieved rims, with a more prominent rim in plagioclase 3. Sieved rims such as these are typically formed by a shift to disequilibrium. The sieved rim corresponds to the increase in anorthite, MgO, FeO, Ti, and Sr. This further suggests that the magma that erupted to form the Parkdale lava flow underwent a mixing event prior to eruption.

The length along all of the transects that show the significant compositional change near the rim is approximately 50 μm to 100 μm long. Once again assuming a growth rate (10^{-10} mm/sec and 10^{-9} mm/sec) the length of time in which the two magmas had been together prior to eruption can be calculated (Table 12). Depending on the growth rate, the two magmas would be in contact with each other from approximately 3.2 years to 0.2 years prior to eruption.

In summary three, out of the four lava flows studied have plagioclase phenocrysts that show evidence of mixing with a more mafic magma immediately prior to their eruption. The phenocrysts from the lava flow that shows no sign of mixing are also the most mafic sample. As stated earlier, this sample has a composition similar to that of the hypothetical mafic end member determined by Woods (2004), and is also dominated by a single crystal population (Figure 33). The textural evidence gathered and described in this section further lends support that CC-04-01 is an end member composition that has not undergone mixing with a more silicic magma prior to eruption.

Table 12: Calculated time in which the two magmas were in contact with each other. Range of time determined using the same growth rates used to calculate the average residence times for CSD.

	Growth Rate	
Affected Distance	10^{-9} mm/sec	10^{-10} mm/sec
50 µm	1.6 years	0.2 years
100 µm	3.2 years	0.3 years

Plagioclase Crystal Populations

According to CSD, five out of six sample lava flows show two distinct crystal populations, while one (CC-04-01) showed only one population in the CSD plot. To determine if the crystals from each of the different sequences are truly from separate sources, trace element data was obtained from plagioclase crystals larger than 1 mm from PD-04-01, PD-05-01, and WR-05-01 and plagioclase crystals smaller than 1 mm from samples CC-04-01, PD-04-01, and HM-04-01. Plagioclase larger than 1 mm represents sequence 2 populations defined by CSD, while plagioclase smaller than 1 mm represents sequence 1 populations.

Figure 30 shows roughly two separate populations of crystals based on their trace element data. The circled population in the figure are comprised of data points from plagioclase crystals that are less than 1 mm in length (sequence 1 population), while the rest of the data points outside of the circle are crystals greater than 1 mm in length (sequence 2 population). Although some scatter exists in the data and not all sequence 1 crystals reside in the circle, the majority of the data does fit.

Sequence 1 crystals have higher concentrations of Ti and Sr and lower concentrations of Ba and Ce than sequence 2 crystals. These trace element levels indicate that the sequence 1 crystals are chemically different than sequence 2 even with similar anorthite values. As stated before, undifferentiated magmas have higher concentrations of Ti and Sr because plagioclase and ilmenite have yet to incorporate them into their structure as they crystallize. With the removal of Ti and Sr and other components incorporated into crystals, Ba and Ce become enriched where before they had lower concentrations with respect to the rest of the magma. High concentrations of

Ti and Sr and low concentrations of Ba and Ce represent a relatively undifferentiated magma (sequence 1), while low concentrations of Ti and Sr and high concentrations of Ba and Ce represent a more differentiated magma (sequence 2).

Table 8 contains the calculated melts in which the two different sequences of plagioclase crystals would be in equilibrium with and shows that they are different from each other. Sequence 1 crystals, represented by the circled population, would be in equilibrium with a more mafic melt, whereas sequence 2 crystals, represented by the un-circled portion, would be in equilibrium with a more silicic melt. The calculated mafic melt is similar to the whole rock composition of CC-04-01. This indicates that the plagioclase in the circled population in figure 30 would be in equilibrium with melt similar to a relatively mafic composition such as CC-04-01. The calculated silicic melt is very different than the whole rock composition of WR-05-01. This calculated value reflects the composition of the silicic end member melt that sequence 2 plagioclase are in equilibrium with, while WR-05-01 is the product of mixing two end members. The melt associated with sequence 1 is the mafic mixing end member and the melt associated with sequence 2 is the silicic mixing end member.

Conclusion

Mount Hood lavas have remained in a compositionally narrow range (SiO_2 53% to 63%) for approximately 475,000. Only in the past 15 ka years were slightly more dacitic compositions erupted. What caused this compositional homogeneity at Mount Hood while other Cascade volcanoes had a much broader range of eruptive products was the focus of this study. Whole rock geochemistry, CSD studies on plagioclase, and major and trace elements analyses of plagioclase were performed on several lava samples of varying ages from Mount Hood to determine what processes had occurred to produce these lava compositions. Specifically, textural and compositional studies were aimed at determining the relative role and timing of mixing, crystal fractionation, and crystal growth.

Whole rock geochemistry showed that the sampled lavas lie on linear trends that are consistent with mixing between two end member magmas. Crystal fractionation, although likely to contribute in removing elements from the magma bodies via crystallization of minerals, is not a major control of the range of magma compositions seen at Mount Hood, but is probably an important factor in the creation of the mixing end member compositions. Mixing between the most mafic sample (CC-04-01) and the most silicic sample (WR-05-02) from this study showed that the broad range of lava compositions can be explained by this processes and therefore is probably a major control on the compositions seen at Mount Hood.

Mixing is further supported by CSD studies that show the presence of two different crystal populations in all but the most mafic sampled lavas. Smaller sequence 1 crystals had an average residence time of 5.5 years to 3.9 years for a growth rate of 10^{-9} mm/sec or 54.8 – 39 years for a growth rate of 10^{-10} mm/sec. Sequence 2 crystals had an average residence time of 22.7 years to 17.7 years a growth rate of 10^{-9} mm/sec or 227 – 117 years for a growth rate of 10^{-10} mm/sec. The narrow residence time range created by the samples for both sequence 1 and sequence 2 populations (regardless of growth rate) again suggests that over the eruptive history of Mount Hood two magmas have been mixed to generate the lavas erupted at the surface, and for each of these magmas crystals have had a similar residence times and an implied similar time scale for mixing and eruption. The longer residence time for sequence 2 crystals also allows for the melt itself to become more evolved than the melt that sequence 1 has crystallized from through crystallization of minerals that would remove compatible elements.

Further, not only do the crystal populations have different average residence times, but they also show differences in trace element compositions, which reflect differences in melt from which they have crystallized. Sequence 1 crystals have higher concentrations of Ti and Sr/Ba ratios and lower concentrations of Ba and Ce when compared to sequence 2 crystals. Crystallization of plagioclase + ilmenite + orthopyroxene + clinopyroxene ± hornblende (the observed phenocryst phases) would result in decreased Sr, Ti, and Sr/Ba ratios and increased Ba and Ce. Therefore, sequence 1 crystals are from a relatively mafic un-evolved magma, while sequence 2 crystals are from a more evolved magma. Trace element analyses from the rim of plagioclase phenocrysts from sequence 2 crystals have compositions that are similar to sequence 1 crystals, this indicates that the mixing event occurred during the later stages of crystallization of the plagioclase in sequence 2. The area affected by the mixing of the magmas shows that the two magmas have been in contact with each other for 3 – 0.2 years prior to eruption.

The late stage of mixing between the two magmas is also shown in the textures of the plagioclase. Disequilibrium textures at the edge of plagioclase phenocrysts correlate to increases in anorthite, MgO, FeO, Ti, and Sr and decreases in Ba and Ce. Changes in anorthite content alone are unlikely to cause the observed differences in plagioclase composition. As anorthite increases, partition coefficients for the listed elements decrease and thus require changes in melt composition. Although speculative, this late stage mixing event might cause the original magma chamber to become over-pressured, due to the increased volume of magma and volatile saturation, resulting in an eruption of the mixed magma to occur.

The most mafic samples analyzed CC-04-01, shows only one crystal population, the length of the plagioclase crystals are all smaller than 1.5 mm in length, the average residence time for this crystal population is 3.9 years ($G = 10^{-9}$ mm/s), putting them in the size category for sequence 1 crystals, trace element data for plagioclase groups them with the sequence 1 crystals, and phenocrysts analyzed from this sample do not show disequilibrium textures or increases in anorthite, MgO, FeO, Ti, and Sr at the rim. This suggest that this lava may be the mafic end member that mixes with the more silicic melt to produce erupted compositions

In conclusion evidence shows that lavas produced at Mount Hood are the products of a late stage mixing event between two magmas. The first is a relatively undepleted mafic magma, while the second is more silicic magma. The degree in which the magmas have been depleted is controlled by the length of time it has been crystallizing minerals that would remove compatible elements from the system. These times have been constrained by CSD. The undepleted mafic end member of this system is represented by mafic sample CC-04-01. Although the link between mixing and eruption is more speculative, similar crystal residence times suggest that mixing immediately precede eruption.

Model for magma genesis at Mount Hood over the last 475,000 years

The following is a model based on the evidence presented in this paper. Figure 40 is a graphical model of showing magma genesis at Mount Hood.

The homogeneous lavas have been produced by mixing between two end member magmas. These two end members exist in two separated chambers, which allow them to evolve along their own path prior to mixing.

The top chamber hosts crystals representative of sequence 2. The more silicic composition is reached by the longer time in which the minerals have had to crystallize. Crystals will grow at a slower rate in a cooler silicic chamber, therefore, a growth rate of 10^{-10} mm/sec is assumed. With this growth rate an average residence time of 227 – 117 years is determined for the plagioclase crystals within the chamber. As plagioclase is crystallizing from this chamber, the chamber is convectively mixing itself. This self-mixing of the chamber mixes hotter portions of the melt with cooler portions and is recorded in plagioclase as sharp increases in anorthite followed by gradual decreases (see-saw pattern).

The second chamber hosts sequence 1 crystals. This has a relatively un-evolved mafic composition in which crystals would crystallize faster and a growth rate of 10^{-9}

mm/sec would be appropriate to use. The average residence time for plagioclase in this chamber is 5.5 – 3.9 years.

At some point the two magmas mix together. The un-evolved magma replenishes compatible elements in the first chamber. The effect of the mixing is seen in the larger plagioclase from the first chamber as increases in anorthite, Mg, Fe, Ti, and Sr. These two end member magmas continue to mix and grow together for 3 – 0.2 years before the mixed magma is erupted to the surface.

The process of mixing has occurred for at least the past 475,000 years at Mount Hood nearly unchanged. Variation arise from the time that each of the end members are allowed to evolve via crystal fractionation. These variations are seen at the surface as the restricted range of lava compositions. Whether the mixing actually leads to (triggers) eruptions is still only speculative, however, the mixing event does take place near the end of the plagioclase crystallization.

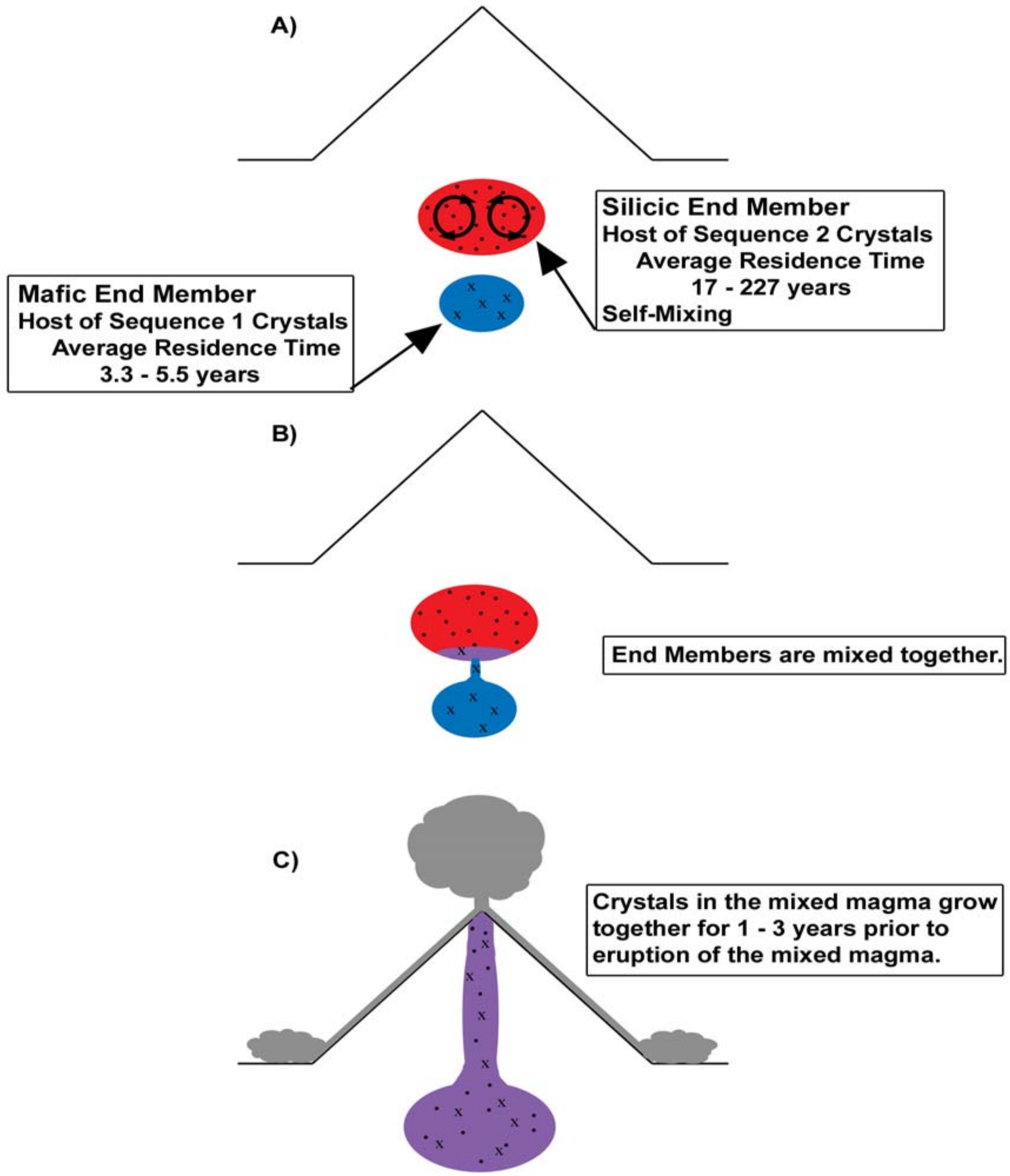

Figure 40: Simplified model of magma genesis at Mount Hood, Oregon. A) Two end member magmas exist; one silicic in composition that has been crystallizing for a longer period and is convectively mixing itself, and one relatively more mafic in composition that has been crystallizing for a shorter period. B) The end members are mixed together and plagioclase phenocrysts from the silicic composition record this period of mixing near the edges. C) After the magmas have been coexisting with each other for 3 – 0.2 years based on the thickness of the mixing affected rims, an eruption occurs. This process is nearly the same for the past 475,000 years.

REFERENCES

Berlo, K., Blundy, J., Turner, S., Cashman, K., Hawkesworth, C., Black, S., 2004, Geochemical Precursors to Volcanic Activity at Mount St. Helens, USA: Science, Vol. 306, p. 1,167 – 1,169.

Bindeman, I.N., 1993, A Practical Method for the Determination of Volume Proportions of Magma Chamber Refilling: Journal of Volcanology and Geothermal Research, Vol. 56, p. 133 – 144.

Bindeman, I.N., Davis, A.M., Drake, M.J., 1998, Ion Microprobe Study of Plagioclase-Basalt Partition Experiments at Natural Concentration Levels of Trace Elements: Geochimica et Cosmochimica Acta, Vol. 62, p. 1,175 – 1,193.

Blakely R.J., Jachens R.C., 1990, Volcanism, Isostatic Residual Gravity, and Regional Tectonic Setting of the Cascade Volcanic Province: Journal of Geophysical Research, Vol. 95, p. 19,439 – 19,451.

Bowen, N.L., 1913, Melting Phenomena in the Plagioclase Feldspars: American Journal of Science, Vol. 35, p. 577 – 599.

Browne, B.L., Eichelberger, J.C., Patino, L.C., Vogel, T.A., Uto, K., Hoshizumi, H., 2006, Magma Mingling as Indicated by Texture and Sr/Ba Ratios of Plagioclase Phenocrysts from Unzen Volcano, SW Japan: Journal of Volcanology and Geothermal Research, Vol. 154, p. 103 – 116.

Cameron, K.A., Pringle, P.T., 1986, Post-Glacial lahars of the Sandy River Basin, Mount Hood, Oregon: Northwest Science, Vol. 60, p. 225 – 237.

Cameron, K.A., Pringle, P.T., 1987, A Detailed Chronology of the Most Recent Major Eruptive Period at Mount Hood, Oregon: Geological Society of American bulletin, V. 99, p. 845 – 851.

Cashman, K.V., Marsh, B.D., 1988, Crystal Size Distribution (CSD) in Rocks and the Kinetics and Dynamics of Crystallization II Makaopuhi Lava Lake: Contributions to Mineralogy and Petrology, Vol. 99, p. 292 – 305.

Conrey, R.M., Sherrod, D.R., Uto, K., Uchiumi, S., 1996, Potassium-Argon Ages from Mount Hood Area of Cascade Range, Northern Oregon: Isochron/West, Vol. 63, p. 10 – 20.

Conrey R.M., Hooper, P.R., Larson, P.B., Chesley, J., Ruiz, J., 2001, Trace Element and Isotopic Evidence for Two Types of Crustal Melting Beneath a High Cascade Volcanic Center, Mt. Jefferson, Oregon: Contributions to Mineralogy and Petrology, Vol. 141. p. 710 – 732.

Couch, S., Sparks, R.S.J., Carroll, M.R., 2001, Mineral Disequilibrium in Lavas Explained by Convective Self-Mixing in Open Magma Chambers: Nature, Vol. 411, p. 1037 – 1039.

Crandell, D.R., 1980, Recent Eruptive History of Mount Hood, Oregon, and Potential Hazards from Future Eruptions: Geological survey Bulletin 1492.

Cribb, J.W., Barton, M., 1996, Geochemical Effects of Decoupled Fractional Crystallization and Crustal Assimilation: Lithos, Vol. 37, p. 293 – 307.

Cribb, J.W., Barton, M., 1997, Significance of Crustal and Source Region Processes on the Evolution of Compositionally Similar Calc-Alkaline lavas, Mt. Hood, Oregon: Journal of Volcanology and Geothermal Research, Vol. 76, p. 229 – 249.

Davidson, J.P., Tepley III, F.J., 1997, Recharge in Volcanic Systems: Evidence from Isotope Profiles of Phenocrysts: Science, Vol. 275, p. 826 – 829.

Deer, W.A., Howie, R.A., Zussman J., 1992, An Introduction to the Rock Forming Minerals: Edinburgh, Pearson Education Limited, pgs. 696.

Eichelberger, J.C., 1995, Silicic Volcanism: Ascent of Viscous Magmas From Crustal Reservoirs: Annual Review of Earth and Planetary Science, Vol. 23, p. 41 – 63.

Ewart, A., Griffin, W.L., 1994, Application of Proton-Microprobe Data to Trace-Element Partitioning in Volcanic Rocks: Chemical Geology, Vol. 117, p. 251 – 284.

Gardner, C.A, Scott, W.E., Major, J.J., Pierson, T.C., 2000, Mount Hood – History and Hazards of Oregon's Most Recently Active Volcano: United States Geological Survey Fact Sheet 060-00, p. 1 – 4.

Gray, L.B., Sherrod, D.R., Conrey, R.M., 1996, Potassium-Argon ages from the Northern Oregon Cascade Range: Isochron/West, Vol. 63, p. 21 – 28.

Guffanti, M, Weaver, C.S., 1988, Distribution of Late Cenozoic Volcanic Vents in the Cascade Range: Volcanic Arc Segmentation and Regional Tectonic Considerations: Journal of Geophysical Research, Vol. 93, p. 6,513 – 6,529.

Halliday, A.N., Fallick, A.E., Dickin, A.P., Mackenzie, A.B., Stephens, W.E., Hildreth, W., 1983, The Isotopic and Chemical Evolution of Mount St. Helens: Earth Plantary Science Letters, Vol. 63, p. 241 – 256.

Heliker, C.C., 1995, Inclusion in Mount St. Helens Dacite Erupted from 1980 to 1983: Journal of Volcanology and Geothermal Research, Vol. 66, p. 115 – 135.

Higgins, M.D., 1994, Numerical Modeling of Crystal Shapes in Thin Sections: Estimations of Crystal Habit and True Size: American Mineralogist, Vol. 79, p. 113 – 119.

Higgins, M.D., 1996, Magma Dynamics Beneath Kameni Volcano, Greece, as Revealed by Crystal Size and Shape Measurements: Journal of Volcanology and Geothermal Research, Vol. 70, p. 37 – 48.

Higgins, M.D., 1998, Origin of Anorthosite by Textural Coarsening: Quantitative Measurements of a Natural Sequence of Textural Development: Journal of Petrology, Vol. 39, p. 1307 – 1323.

Higgins, M.D., 2000, Measurement of crystal size distributions: American Mineralogist, Vol. 85, p. 1105 – 1116.

Higgins, M.D., 2002, Closure in Crystal Size Distributions (CSD), Verification of CSD Calculations and the Significance of CSD Fans: American Mineralogist, Vol. 87, p. 171 – 175.

Higgins, M.D., Roberge, J., 2006, Three Magmatic Components in the 1973 Eruption of Eldfell Volcano, Iceland: Evidence From Plagioclase Crystal Size Distribution (CSD) and Geochemistry: EOS Tras. AGU, Vol. 87, Fall Meeting Supplement, Abstract V23C-0640.

Hoblitt, R.P., Crandell, D.R., Mullineaux, D.R., 1980, Mount St. Helens Eruptive Behavior During the Past 1,500 yr: Geology, Vol. 8, p. 555 – 559.

Hoblitt, R.P., Miller, C.D., Scott, W.E., 1987, Volcanic Hazards with Regard to Siting Nuclear-Power Plants in the Pacific Northwest: United States Geological Survey Open File Report 87-297.

Izbekov, P.E., Eichelberger, J.C., Ivanov, B.V., 2004, The 1996 Eruption of Karymsky Volcano, Kamchatka: Historical Record of Basaltic Replenishment of an Andesite Reservoir: Journal of Petrology, Vol. 45, p. 2325 – 2345.

Johannes W., 1978, Melting of Plagioclase in the System Ab-An-H2O and Qz-Ab-An-H2O at PH2O = 5 kbars, an Equilibrium Problem: Contributions to Mineralogy and Petrology, Vol. 66, p. 295 – 303.

Johnson, D.M., Hooper, P.R., Conrey, R.M., 1999, XRF Analysis of Rocks and Minerals for Major and Trace Elements on a Single Low Dilution Li-tertraborate Fused Bead; JCPDS – International Centre for Diffraction Data.

Kent, Adam J.R., Jacobsen, B, Peate, D.W., Waight, T.E., Baker, J.A, 2004, Isotope Dilution MC-ICP-MS Rare Earth Element analysis of Geochemical Reference Material NIST SRM 610, NIST SRM 612, NIST SRM 614, BHVO-2G, BVHO-2, BCR-2G,JB-2, WS-E, W-2, AGV-1, and AGV-2: Geostandards and Geoanalytical Research, Vol. 28, p. 417 – 429.

Landi, P., Métrich, N., Betragnini, A., Rosi, M., 2004, Dynamics of Magma Mixing and Degassing Recorded in Plagioclase at Stromboli (Aeolian Archipelago, Italy): Contributions to Mineralogy and Petrology, Vol. 147, p. 213 – 227.

Larsen, J.F., 2005, Experimental Study of Plagioclase Rim Growth Around Anorthite Seed Crystals in Rhyodacitic Melt: American Mineralogist, Vol. 90, p. 407 – 427.

Le Bas, M.J., LeMaitre, R.W., Streckeisen, A.L., Zanettin, B., 1986, A Chemical Classification of Volcanic Rocks Based on the Total Alkali-Silica Diagram: Journal of Petrology, Vol., 27, p. 745 – 750.

Leeman, W.P., Smith, D.R., Hildreth, W., Palacz, Z.A., Rogers, N.W., 1990, Compositional Diversity of Late Cenozoic Basalts in a Transect Across the Southern Washington Cascades: Implications for Subduction Zone Magmatism: Journal of Geophysical Research, Vol. 95, p. 19,561 – 19,582.

Marsh, B.D., 1988, Crystal size distribution (CSD) in rocks and the kinetics and dynamics of crystallization I. Theory: Contributions to Mineralogy and Petrology, Vol. 99, p. 277 – 291.

Marsh, B.D., 1998, On the Interpretation of Crystal Size Distributions in Magmatic Systems: Journal of Petrology, Vol. 39, p. 553 – 599.

McBirney, A.R., 1978, Volcanic Evolution of the Cascade Range: Annual Reviews in Earth and Planetary Science Letters, Vol. 6, p. 437 – 456.

Melson, W.G., 1983, Monitoring the 1980-1982 Eruptions of Mount St. Helens: Compositions and Abundace of Glass: Science, Vol. 221, p. 1,387 – 1,391.

Miyashiro, A., 1974, Volcanic Rock Series in Island Arcs and Active Continental Margins: American Journal of Science, Vol. 274, p. 321 – 355.

Morgan, D.L., Blake, S., Rogers, N.W., DeVivo, B., Rolandi, G., Macdonald, R., Hawkesworth, C.J., 2004, Time Scales of Crystal Residence and Magma Chamber Volume from Modeling of Diffusion Profiles in Phenocrysts: Vesuvius 1944: Earth and Planetary Science Letters, Vol. 222, p. 933 – 946.

Murphy, M.D., Sparks, R.S.J., Barclay, J., Carroll, M.R., Lejeune, A-M, Brewer, T.S., Madonald, R., Black, S., Young, S., 1998, The Role of Magma Mixing in Triggering the Current Eruption at the Soufriere Hills Volcano, Montserrat, West Indies: Geophysical Research Letters, Vol. 25, p. 3433 – 3436.

Pearce, T.H., Kolisnik, A.M., 1990, Observations of Plagioclase Zoning Using Interference Imaging: Earth – Science Reviews, Vol. 29, p. 9 – 26.

Priest, G.R., 1982, Overview of the Geology and Geothermal Resources of the Mount Hood Area, Oregon: Oregon Department of Geology and Mineral Industries Special Paper, Vol. 14, p. 6 – 15.

Priest, G.R., 1990, Volcanic and Tectonic Evolution of the Cascade volcanic Arc, Central Oregon: Journal of Geophysical Research, Vol. 95, p. 19,583 – 19,599.

Rogers, G.C., 1985, Variation in Cascade Volcanism with Margin Orientation: Geology, Vol. 13, p. 495 – 498.

Rutherford, M.J., Hill, P.M., 1993, Magma Ascent Rates From Amphibole Breakdown: An Experimental Study Applied to the 1980 – 1986 Mount St. Helens Eruptions: Journal of Geophysical Research, Vol. 98, p. 19,667 – 19,685.

Scott, W.E., Pierson, T.C., Schilling, S.P., Costa, J.E., Gardner, C.A., Vallance, J.W., Major, J.J., 1997, Volcano Hazards in the Mount Hood Region, Oregon: United States Geological Survey Open File Report 97 – 89, p. 1 – 14.

Scott, W.E., Gardner, C.A., Tilling, R.I., Lanphere, M.A., 2003, Geologic History of Mount Hood Volcano, Oregon – A Field Trip Guidebook: State of the Arc Meeting, Timberline Lodge, Oregon, p. 1 – 39.

Sherrod, D.R., Smith, J.G., 1990, Quaternary Extrusion Rates of the Cascade Range, Northwestern United States and Southern British Columbia: Journal of Geophysical Research, Vol. 95, p. 19,465 – 19, 474.

Smith, D.R., Leeman, W.P., 1987, Petrogenesis of Mount St. Helens Dacitic Magmas: Journal of Geophysical Research, Vol. 92, p. 10,313 – 10,334.

Smith, D.R., Leeman, W.P., 1993, The origin of Mount St. Helens Andesites: Journal of Volcanology and Geothermal Research, Vol. 55, p. 271 – 303.

Sparks, S.R.J, Sigurdsson, H., Wilson, L., 1977, Magma Mixing: a Mechanism for Triggering Acid Explosive Eruptions: Nature, Vol. 267, p. 315 – 318.

Stormer, J.C., Nicholls, J., 1978, XLFRAC: A Program for the Interactive Testing of Magmatic Differentiation Models: Computers and Geosciences, Vol. 4, p. 143 – 159.

Taylor, E.M., 1990, Volcanic History and Tectonic Development of the Central High Cascade Range, Oregon: Journal of Geophysical Research, Vol. 95, p. 19,611 – 19,622.

Taylor, T.R., 1982, An Introduction to Error Analysis: The Study of Uncertainties to Physical Measurements: Oxford University Press, Mill Valley, CA, pgs. 270.

Tepley III, F.J., Davidson, J.P., Clynne, M.A., 1999, Magmatic Interactions as Recorded in Plagioclase Phenocrysts of Chaos Crags, Lassen Volcanic Center, California: Journal of Petrology, Vol. 40, p. 787 – 806.

Tepley III, F.J., Davidson, J.P., Tilling, R.I., Arth, J.G., 2000, Magma Mixing, Recharge and Eruptions Histories Recorded in Plagioclase Phenocrysts from El Chichón Volcano, Mexico: Journal of Petrology, Vol. 41, p. 1397 – 1411.

Triebold, S., Kronz, A., Wörner, G., 2006, Anorthite-calibrated Backscattered Electron Profiles, Trace Elements, and Growth Textures in Feldspars from the Teide-Pico Viejo volcanic Complex (Tenerife): Journal of Volcanology and Geothermal Research, Vol. 154, p. 117 – 130.

Watts, R.B., de Silva, S.L., Jimenez de Rios, G., Croudace, I., 1999, Effusive Eruptions of Viscous Silicic Magma Triggered and Driven by Recharge: A Case Study of the Cerro Chascon-Runtu Jarita Dome Complex in Southwest Bolivia: Bulletin of Volcanology, Vol. 60, p. 241 – 264.

White, C., 1980, Geology and Geochemistry of Mt. Hood Volcano: Oregon Department of Geology and Mineral Industries Special Paper, Vol. 8, p. 1 – 29.

Wise, W.S., 1969, Geology and Petrology of the Mt. Hood area: a study of High Cascade Volcanism: Geological Society of America Bulletin, Vol. 80, p. 969 – 1006.

Wood, C.A., Kienle, J., 1990, Volcanoes of North America: United States and Canada: Cambridge University Press, p. 173 – 175.

Woods, M.M., 2004, Compositional and Mineralogical Relationships Between Mafic Inclusions and Host Lavas as Key to Andesite Petrogenesis at Mount Hood Volcano, Oregon: Masters Thesis, Portland State University.

APPENDICES

Appendix A - EMPA Data

CC-04-01 Plagioclase (1 = Core; 2 = Rim)

	Oxides Weight %							
Plagioclase	**Na2O**	**MgO**	**SiO2**	**Al2O3**	**K2O**	**FeO**	**CaO**	**Total**
1/1.	6.087	0.0828	26.5286	56.508	0.3096	0.9423	9.0026	99.5642
1/2.	4.2362	0.0651	29.7832	52.1591	0.0997	0.6975	12.3865	99.5073
2/1.	3.5578	0.0904	30.6536	50.436	0.063	0.5604	13.6766	99.1051
3/1.	3.6556	0.0876	30.6474	51.0553	0.0585	0.655	13.5185	99.7337
3/2.	5.2637	0.0837	28.012	54.4346	0.1804	0.8345	10.7563	99.6537
4/1.	4.2462	0.1177	29.3867	52.3728	0.0801	0.6736	12.3903	99.3323
4/2.	3.829	0.0806	30.4041	51.1428	0.078	0.7875	13.0915	99.4631
5/1.	4.1254	0.1069	29.5948	51.8244	0.0801	0.6051	12.6668	99.0685
5/2.	6.0238	0.097	27.0525	55.7298	0.2437	1.0008	9.5165	99.7763
6/1.	4.141	0.1255	29.311	52.2742	0.0599	0.6716	12.3809	99.0365
6/2.	4.3634	0.0885	29.5229	52.165	0.1251	0.6856	12.3616	99.3885
7/1.	3.8069	0.0848	30.1049	51.2194	0.0566	0.5672	13.1276	99.0295
7/2.	4.9908	0.0772	28.6098	53.7505	0.1619	0.8454	11.2102	99.7259
8/1.	3.9761	0.1259	29.8943	51.484	0.0722	0.7842	12.8735	99.2668
9/1.	4.047	0.1037	29.9345	51.6843	0.0599	0.64	12.7901	99.3271
9/2.	6.6779	0.2711	25.2571	57.5585	0.347	1.4006	7.8153	99.4964
10/1.	3.831	0.0897	30.3672	51.1356	0.0624	0.6616	13.2622	99.4564
10/2.	3.8536	0.0748	30.2387	51.2712	0.0748	0.7192	13.139	99.4338
11/1.	4.4055	0.1096	29.5323	52.4678	0.0749	0.6022	12.4057	99.6639
11/2.	4.7771	0.1034	28.7885	53.5509	0.1194	0.701	11.5877	99.7195
12/1.	4.0143	0.1035	30.1035	51.5852	0.0605	0.6366	13.0263	99.597
12/2.	4.5412	0.1012	29.3831	52.2693	0.0776	0.7008	12.138	99.2774
13/1.	3.6666	0.0891	30.6819	50.7739	0.0643	0.5866	13.5525	99.4734
13/2.	4.5374	0.1393	29.1436	52.6075	0.0841	0.8083	12.0837	99.4557
14/1.	3.6226	0.1342	30.7111	50.8023	0.0468	0.7202	13.6161	99.7042
14/2.	6.6415	0.071	26.0479	57.5329	0.3135	0.8861	8.3078	99.9281
15/1.	4.1011	0.1121	29.9168	51.9541	0.0645	0.6336	12.8019	99.6408
15/2.	5.5394	0.0971	28.0219	54.5555	0.1694	0.8443	10.4197	99.7372
16/1.	4.2516	0.113	29.5675	52.2035	0.0632	0.6509	12.5323	99.4437
16/2.	3.57	0.088	30.4094	50.827	0.0877	0.6973	13.4677	99.2032
17/1.	3.9277	0.1028	30.1119	51.5285	0.0585	0.6105	13.1069	99.5072
17/2.	4.7171	0.1026	28.8194	53.1666	0.1493	0.8507	11.7627	99.6621
18/1.	4.4593	0.1146	29.5844	52.767	0.0632	0.6813	12.4082	100.1523
18/2.	4.0887	0.066	29.9074	51.61	0.1126	0.7529	12.5805	99.2061
19/1.	4.2598	0.1188	29.9152	52.2921	0.0736	0.6759	12.8056	100.2075
19/2.	6.6079	0.0868	26.0768	57.7982	0.347	0.8178	8.3943	100.2401
20/1.	4.271	0.1071	29.4869	51.9182	0.0671	0.6574	12.636	99.2167
21/1.	4.3188	0.1608	29.5247	52.1349	0.0795	0.714	12.5622	99.5709
21/2.	4.0112	0.1068	29.8949	51.8268	0.0664	0.8245	12.8964	99.6869
22/1.	4.3823	0.1138	29.8729	52.7238	0.0638	0.753	12.6169	100.5886
22/2.	6.5567	0.0773	26.2803	57.3074	0.3258	0.8917	8.6518	100.2108
23/1.	3.4705	0.0769	31.3303	50.7293	0.0578	0.6387	14.2479	100.6019
23/2.	3.9991	0.092	30.2982	51.8577	0.0716	0.6334	13.0887	100.1139
24/1.	4.2566	0.1169	30.0358	52.6158	0.0762	0.6715	12.7582	100.599

24/2.	6.0714	0.0565	26.9527	56.2809	0.3193	0.9383	9.4323	100.1606
25/1.	4.0244	0.0971	30.2213	51.9772	0.0475	0.6085	13.1599	100.1965
25/2.	4.4578	0.0865	29.3911	52.6216	0.1153	0.767	12.3241	99.8402
26/1.	4.2622	0.104	30.0074	52.3673	0.0684	0.6237	12.8838	100.3793
26/2.	4.4656	0.0774	29.5717	52.8343	0.1408	0.7487	12.3335	100.248
27/1.	3.5479	0.0871	31.076	50.6092	0.0396	0.5453	14.0053	99.9531
27/2.	5.0509	0.0888	28.6893	53.8043	0.1626	0.7889	11.2482	99.9203

CC-04-01 Plagioclase 3 and 4 Transects

		Oxides Weight %							
Plagioclase	**Location (um)**	**Na2O**	**MgO**	**SiO2**	**Al2O3**	**K2O**	**FeO**	**CaO**	**Total**
3 / 1.	0	3.4158	0.0979	51.0369	30.731	0.0533	0.6102	13.7478	99.6929
3 / 2.	5	3.4469	0.0972	51.0661	30.697	0.0557	0.5452	13.5653	99.4733
3 / 3.	10	3.4295	0.0922	51.0162	30.64	0.0545	0.5875	13.5703	99.3902
3 / 4.	15	3.6379	0.1004	51.4068	30.2237	0.0603	0.5785	13.2861	99.2937
3 / 5.	20	3.363	0.0883	50.8514	30.8451	0.0593	0.586	13.7925	99.5856
3 / 6.	25	3.1706	0.0799	50.6597	30.9871	0.0587	0.5981	14.1124	99.6665
3 / 7.	30	3.9559	0.168	52.3492	29.7043	0.0693	0.7738	12.6255	99.646
3 / 8.	35	4.1255	0.1026	52.781	29.3963	0.0751	0.5666	12.3761	99.4231
3 / 9.	40	3.1851	0.0956	50.3808	30.9462	0.0563	0.5587	14.0961	99.3188
3 / 10.	45	3.7209	0.0851	51.6052	30.0931	0.0652	0.5679	13.1587	99.2961
3 / 11.	50	3.4193	0.0874	50.8867	30.6777	0.0487	0.5679	13.6739	99.3616
3 / 12.	55	3.1411	0.0923	50.382	31.1091	0.0538	0.6041	14.1709	99.5533
3 / 13.	60	3.2445	0.1134	50.4281	31.1583	0.0593	0.5527	14.1027	99.659
3 / 14.	65	3.7239	0.0879	51.5402	30.1308	0.064	0.6195	13.0196	99.1858
3 / 15.	70	3.7266	0.0942	51.3342	30.0841	0.0628	0.6451	13.0855	99.0324
3 / 16.	75	3.6173	0.0972	51.5638	30.087	0.068	0.5756	13.2191	99.2279
3 / 17.	80	3.5908	0.102	51.4793	30.1334	0.0545	0.5937	13.2966	99.2502
3 / 18.	85	3.5098	0.0937	50.9167	30.5278	0.0642	0.5649	13.5625	99.2397
3 / 19.	90	3.4938	0.105	51.3255	30.3998	0.0722	0.58	13.4553	99.4316
3 / 20.	95	3.4447	0.0966	51.0248	30.3937	0.0712	0.5725	13.6188	99.2224
3 / 21.	100	3.5679	0.1002	51.2712	30.357	0.0719	0.5588	13.4709	99.3978
3 / 22.	105	3.5603	0.0871	51.4673	30.4316	0.061	0.5953	13.2499	99.4525
3 / 23.	110	3.6092	0.0902	51.1895	30.1985	0.0725	0.5649	13.2509	98.9756
3 / 24.	115	3.5211	0.0904	51.218	30.5479	0.0618	0.636	13.4394	99.5145
3 / 25.	120	3.7279	0.0953	51.5287	30.2031	0.0786	0.574	13.155	99.3626
3 / 26.	125	3.7274	0.1016	51.034	29.7774	0.0765	0.6255	13.0447	98.3871
3 / 28.	135	3.5835	0.0941	51.3175	30.4151	0.0619	0.6119	13.319	99.403
3 / 29.	140	3.6423	0.0994	51.6409	30.1923	0.0698	0.6527	13.1411	99.4386
3 / 30.	145	3.2993	0.0876	50.623	30.794	0.073	0.5058	13.835	99.2177
3 / 31.	150	3.491	0.0767	50.9154	30.5216	0.0804	0.6511	13.5894	99.3255
3 / 32.	155	3.6335	0.0976	51.281	30.587	0.0661	0.5422	13.3009	99.5083
3 / 33.	160	3.5408	0.0867	50.9863	30.4367	0.0521	0.6254	13.5006	99.2286
3 / 34.	165	3.5155	0.103	51.269	30.5671	0.0685	0.5286	13.5385	99.5902
3 / 35.	170	3.5255	0.1068	51.2294	30.4969	0.0652	0.568	13.5157	99.5074
3 / 36.	175	3.7179	0.1043	51.5374	30.0568	0.0787	0.5877	13.031	99.1138
3 / 37.	180	3.6815	0.1483	51.394	30.2237	0.0838	0.7904	13.0496	99.3713
3 / 38.	185	3.335	0.0669	50.8759	30.6373	0.0694	0.5967	13.8513	99.4325
3 / 40.	195	3.3393	0.0826	50.9858	30.8559	0.0697	0.6164	13.7996	99.7493

3 / 41.	200	3.9132	0.0857	52.0691	29.94	0.0848	0.6241	12.6206	99.3375
3 / 42.	205	3.5037	0.0739	51.244	30.687	0.0868	0.6088	13.4762	99.6804
3 / 43.	210	3.5911	0.0785	51.3401	30.14	0.1021	0.5832	13.3292	99.1641
3 / 44.	215	3.9915	0.0665	52.1433	29.7832	0.116	0.5863	12.523	99.2098
3 / 45.	220	4.0532	0.0717	52.7173	29.3272	0.0993	0.6363	12.2245	99.1295
3 / 46.	225	4.6405	0.0848	53.5897	28.8445	0.1521	0.8242	11.3726	99.5084
3 / 47.	230	4.881	0.0669	54.4585	28.0895	0.2145	0.7487	10.7253	99.1843
3 / 48.	235	5.1831	0.0764	55.2857	27.459	0.2283	0.7397	10.1675	99.1396
3 / 49.	240	6.0039	0.0707	57.2426	26.0935	0.369	0.7901	8.4446	99.0145
3 / 50.	245	7.0265	0.0369	59.6852	24.6992	0.4297	0.7434	6.5525	99.1734
4 / 2.	5	3.4853	0.1123	51.1356	30.3831	0.0665	0.558	13.3538	99.0946
4 / 3.	10	3.7708	0.096	52.2381	29.8198	0.0752	0.596	12.691	99.287
4 / 4.	15	3.8185	0.0875	52.0268	29.9857	0.0916	0.6475	12.8028	99.4603
4 / 5.	20	4.0608	0.1059	52.9242	29.3909	0.093	0.6915	12.2301	99.4964
4 / 6.	25	3.6301	0.1025	51.8644	30.0692	0.0662	0.6899	13.1274	99.5497
4 / 7.	30	3.6622	0.1052	51.8582	30.1333	0.0616	0.6171	13.0661	99.5036
4 / 8.	35	3.1961	0.0798	50.5452	30.822	0.0545	0.6109	14.0199	99.3284
4 / 9.	40	3.6323	0.1041	51.6499	29.8891	0.0696	0.6171	12.9758	98.9378
4 / 10.	45	4.0193	0.1236	52.5916	29.1107	0.0673	0.7037	12.3291	98.9452
4 / 11.	50	4.0499	0.0999	52.5207	29.2838	0.0926	0.6021	12.3329	98.982
4 / 12.	55	3.8929	0.1132	52.1815	29.6209	0.0657	0.6915	12.6752	99.2408
4 / 13.	60	3.4458	0.0977	51.1381	30.5384	0.0631	0.667	13.4474	99.3975
4 / 14.	65	3.2415	0.0855	50.5469	30.9029	0.0554	0.6064	13.9609	99.3994
4 / 15.	70	3.8394	0.1115	51.9286	29.6467	0.0657	0.6248	12.7422	98.9589
4 / 16.	75	3.7842	0.115	52.2731	29.7095	0.0739	0.6778	12.8435	99.477
4 / 17.	80	3.5699	0.1062	51.3836	30.2042	0.0698	0.6898	13.2612	99.2848
4 / 18.	85	3.6551	0.098	51.9039	30.0415	0.065	0.6688	13.0624	99.4947
4 / 19.	90	3.9202	0.1136	52.4388	29.5655	0.0645	0.6188	12.6002	99.3215
4 / 20.	95	3.8201	0.1051	52.0317	30.002	0.062	0.6338	12.8945	99.5493
4 / 21.	100	3.5098	0.1016	51.3651	30.2634	0.0506	0.6627	13.2967	99.2501
4 / 22.	105	3.9239	0.1192	52.0912	29.7789	0.0745	0.7459	12.6507	99.3843
4 / 23.	110	3.5247	0.0955	51.2487	30.1058	0.0512	0.5913	13.3734	98.9907
4 / 24.	115	3.3691	0.095	50.9012	30.3064	0.0546	0.661	13.5972	98.9844
4 / 25.	120	3.8865	0.1093	51.9603	29.597	0.0797	0.7611	12.701	99.0951
4 / 26.	125	3.9487	0.1085	52.1763	29.3877	0.0727	0.6763	12.4807	98.8509
4 / 27.	130	3.8351	0.1053	52.2793	29.8623	0.0715	0.6613	12.7891	99.6039
4 / 28.	135	3.9302	0.1168	52.3502	29.5056	0.0905	0.6764	12.3317	99.0015
4 / 29.	140	3.926	0.1046	52.2655	29.4046	0.0825	0.6885	12.4788	98.9505
4 / 30.	145	3.8154	0.1052	51.788	29.6747	0.0739	0.6475	12.7972	98.9018
4 / 31.	150	3.6454	0.0663	51.4087	30.1161	0.0677	0.6248	13.0949	99.0239
4 / 32.	155	3.6245	0.0805	51.3049	30.055	0.0766	0.6353	13.1121	98.8889
4 / 33.	160	3.9193	0.0907	51.8724	29.643	0.0971	0.7642	12.493	98.8798
4 / 34.	165	4.0305	0.0902	52.1726	29.0242	0.1268	0.8157	12.2523	98.5124
4 / 35.	170	4.5889	0.0841	54.093	28.716	0.1456	0.8131	11.3119	99.7526
4 / 36.	175	4.9349	0.0917	54.6399	27.7224	0.162	0.8117	10.4794	98.842
4 / 38.	185	5.8736	0.0813	57.1511	26.1739	0.2981	0.8257	8.5099	98.9137

CD-04-01 Plagioclase (1 = Core; 2 = Rim)

				Oxides Weight %				
Plagioclase	Na2O	MgO	SiO2	Al2O3	K2O	FeO	CaO	Total
4 / 1 .	5.441	0.0241	27.9462	54.4912	0.2674	0.4606	10.0113	98.6418
4 / 2 .	4.6248	0.0237	29.0493	52.8939	0.286	0.628	11.2259	98.7315
5 / 1 .	5.2537	0.0357	28.654	53.791	0.2251	0.3485	10.4462	98.7542
5 / 2 .	4.4276	0.0176	29.3326	52.1693	0.3118	0.739	11.6692	98.6671
6 / 1 .	5.0562	0.0489	28.7102	54.1278	0.2429	0.5412	10.682	99.4093
6 / 2 .	4.1731	0.0516	30.0549	51.9484	0.1961	0.5442	12.2918	99.26
7 / 1 .	5.172	0.0248	28.6592	54.1338	0.2169	0.4114	10.5667	99.1848
7 / 2 .	4.6027	0.0295	29.1792	52.7261	0.3067	0.7117	11.5532	99.1092
8 / 1 .	4.983	0.0144	28.6935	53.4975	0.3407	0.4349	10.7038	98.6678
8 / 2 .	2.4671	0.0134	32.4868	48.0106	0.1153	0.6612	15.3733	99.1277
9 / 1 .	6.2013	0.0497	26.1658	57.5406	0.6897	0.7219	7.8845	99.2536
9 / 2 .	4.2708	0.0424	29.6629	51.5008	0.2518	0.688	12.1166	98.5333
10 / 2 .	5.3587	0.0176	28.2656	54.2651	0.3167	0.3649	9.9721	98.5607
11 / 1 .	5.959	0.0183	27.4137	56.0023	0.252	0.3687	9.0261	99.0401
11 / 2 .	4.4861	0.0216	29.4894	52.2106	0.2738	0.5457	11.9356	98.9628
12 / 2 .	4.1924	0.0238	29.9532	51.7603	0.2493	0.6936	12.1654	99.0381
13 / 1 .	5.5823	0.0264	27.4357	55.2419	0.3743	0.3262	9.672	98.6588
13 / 2 .	4.3332	0.0258	29.4192	52.467	0.2532	0.566	11.9239	98.9884
14 / 1 .	5.624	0.0368	27.8223	55.2148	0.2436	0.5021	9.7658	99.2094
14 / 2 .	5.0538	0.0578	28.6904	53.8754	0.2092	0.5252	10.7701	99.1819
14 / 3 .	3.9018	0.0226	30.7413	50.7847	0.1948	0.6177	12.8993	99.1622
15 / 1 .	4.0528	0.0842	30.2403	51.5384	0.2415	0.7482	12.5132	99.4185
15 / 2 .	5.1333	0.0377	28.3315	53.5249	0.3125	0.8089	10.6162	98.765
16 / 1 .	4.8594	0.0249	28.869	53.2218	0.1699	0.4309	11.226	98.802
16 / 2 .	4.7983	0.0277	29.1826	52.9852	0.1657	0.4572	11.2516	98.8683
16 / 3 .	5.8663	0.0292	27.21	55.816	0.2917	0.3719	9.1762	98.7614
16 / 4 .	3.5454	0.0262	30.9281	50.1977	0.198	0.7261	13.4426	99.0641
17 / 1 .	5.444	0.0242	28.3355	54.5247	0.2058	0.3678	10.084	98.986
18 / 1 .	4.9588	0.0306	29.0716	53.3118	0.2241	0.4306	11.0752	99.1028
18 / 2 .	4.3194	0.0332	29.7972	52.0388	0.2415	0.7881	11.9949	99.213
19 / 2 .	4.4387	0.0284	29.6072	52.0773	0.2539	0.7633	11.819	98.9878
20 / 1 .	3.3339	0.0287	31.5425	49.2525	0.0969	0.4569	13.8781	98.5894
20 / 2 .	5.0967	0.6545	27.3914	53.7624	0.4374	1.57	10.1941	99.1064
21 / 1 .	5.6822	0.0206	27.9391	54.8722	0.4451	0.3591	9.4191	98.7374
21 / 2 .	4.4548	0.0367	29.596	51.6619	0.2524	0.9012	11.7356	98.6386

CS-04-01 Plagioclase (1 = Rim; 2 = Core)

				Oxides Weight %				
Plagioclase	Na2O	MgO	SiO2	Al2O3	K2O	FeO	CaO	Total
1 / 1 .	2.9643	0.0759	32.1948	50.8898	0.1591	0.5715	14.6298	101.4853
1 / 2 .	4.0471	0.0375	29.072	54.9653	0.7314	0.6255	11.5147	100.9935
1 / 3 .	1.5698	0.0266	34.851	47.3847	0.0735	0.6345	17.3014	101.8414
1 / 4 .	3.2203	0.0567	30.3985	50.9117	0.4557	2.2182	13.4101	100.6712
3 / 1 .	3.7077	0.1058	31.0638	52.654	0.1794	0.6185	13.0887	101.4179
3 / 2 .	3.3629	0.0216	31.5715	51.835	0.2748	0.6352	13.8078	101.5087

3 / 3 .	3.1577	0.0388	32.0162	51.162	0.2314	0.5884	14.2522	101.4467
3 / 4 .	3.4809	0.0675	31.2124	51.864	0.1473	0.6118	13.6122	100.9959
5 / 1 .	4.6434	0.0441	29.1931	54.8048	0.3601	0.8894	11.302	101.2368
5 / 2 .	4.9971	0.0216	28.9529	56.0354	0.259	0.318	10.5904	101.1744
6 / 1 .	5.8797	0.0164	27.2206	57.9147	0.5168	0.3817	8.8963	100.8263
6 / 2 .	5.4305	0.0326	28.0137	57.2268	0.393	0.3281	9.6272	101.0521
7 / 1 .	5.3994	0.0237	28.2334	56.3715	0.4428	0.5623	9.8267	100.8598
7 / 2 .	2.5252	0.0261	33.2681	49.4002	0.0626	0.4545	15.4343	101.171
8 / 1 .	4.367	0.0454	29.5245	53.937	0.2941	0.6557	11.4966	100.3202
8 / 2 .	4.2198	0.0525	30.0417	53.8834	0.1686	0.5954	12.0364	100.9978
9 / 1 .	3.9214	0.0318	30.1314	52.7052	0.2482	0.6822	12.4436	100.1638
9 / 2 .	5.3354	0.0377	27.779	56.5337	0.2983	0.3617	9.6322	99.978
10 / 1 .	4.0271	0.0749	29.8206	53.0178	0.2021	0.7556	12.556	100.4541
10 / 2 .	3.7434	0.0634	30.743	52.8583	0.1278	0.495	12.9602	100.9911
11 / 1 .	4.8974	0.0486	28.9611	55.4249	0.2616	0.5254	10.693	100.812
11 / 2 .	6.2999	0.0332	26.1282	59.7905	0.3949	0.2748	7.6948	100.6163
11 / 3 .	5.7946	0.0237	27.355	58.2956	0.3132	0.2579	8.7713	100.8113
11 / 4 .	5.7978	0.0186	27.2762	58.1294	0.3339	0.3014	8.9357	100.793
12 / 1 .	5.0862	0.0398	28.9009	56.0174	0.3571	0.5654	10.4886	101.4553
12 / 2 .	4.9178	0.0184	29.3134	55.3822	0.203	0.2779	11.0106	101.1232
13 / 1 .	4.4592	0.0513	29.517	54.2083	0.3194	0.7591	11.583	100.8974
13 / 2 .	5.0029	0.0507	28.6746	56.105	0.2316	0.4217	10.3736	100.8602
14 / 1 .	4.2461	0.0596	30.1724	53.4664	0.1421	0.5184	12.1322	100.7372
14 / 2 .	4.806	0.0232	29.1382	55.1888	0.2436	0.3481	10.9673	100.715
15 / 1 .	5.136	0.0377	28.2058	55.8081	0.3234	0.569	10.1124	100.1924
15 / 2 .	4.8616	0.0257	28.8502	55.2278	0.2333	0.3347	10.6972	100.2306
16 / 1 .	3.5789	0.0774	31.134	52.1623	0.122	0.6353	13.3817	101.0916
16 / 2 .	5.0163	0.0478	29.0125	55.5672	0.2409	0.3916	10.7168	100.9932
17 / 1 .	3.8886	0.0419	30.694	52.5738	0.2322	0.6219	12.7173	100.7698
17 / 2 .	3.6037	0.0826	31.1423	52.0415	0.0704	0.5417	13.4767	100.9589
18 / 1 .	4.3664	0.0335	29.4978	54.0636	0.3053	0.6355	11.6671	100.5692
18 / 2 .	5.0676	0.034	28.3981	56.1305	0.2845	0.4552	10.4037	100.7736
19 / 1 .	5.3391	0.0328	27.8861	56.2681	0.5682	0.9701	9.84	100.9043
19 / 2 .	4.5287	0.0493	29.638	54.402	0.247	0.3614	11.7228	100.9491
20 / 2 .	4.0912	0.0851	29.8851	53.3162	0.1449	0.6154	12.3821	100.52
21 / 1 .	3.4712	0.0525	31.3971	51.3821	0.1604	0.6485	13.5259	100.6376
21 / 2 .	3.5176	0.0736	30.9156	51.6495	0.2168	0.4447	13.3716	100.1894
22 / 1 .	4.7036	0.0365	29.148	54.7543	0.2906	0.4618	11.1613	100.5561
22 / 2 .	4.2479	0.1038	29.4808	53.722	0.2335	0.6322	12.0183	100.4385
23 / 1 .	3.7281	0.064	30.6962	52.4621	0.1306	0.5385	12.9172	100.5368
23 / 2 .	2.3127	0.0369	32.4885	49.3097	0.2616	0.5881	15.401	100.3985
24 / 1 .	4.9681	0.0941	28.14	55.337	0.4394	0.8766	10.2215	100.0766
24 / 2 .	3.7529	0.0666	30.553	52.2262	0.1128	0.5586	12.855	100.125
25 / 1 .	4.6733	0.0344	28.9478	54.7551	0.3357	0.7392	11.2474	100.7328
25 / 2 .	4.7644	0.0198	29.3551	55.0135	0.2228	0.2979	11.1049	100.7783
26 / 1 .	4.1958	0.0393	30.534	53.7976	0.2409	0.5218	12.3429	101.6723
26 / 2 .	5.1043	0.0358	28.9479	55.9095	0.2684	0.3581	10.5962	101.2202
27 / 2 .	4.76	0.046	28.9211	55.5285	0.2154	0.4753	10.6254	100.5716

EB-04-01 Plagioclase (1 = Rim; 2 = Core)

Oxides Weight %

Plagioclase	Na2O	MgO	SiO2	Al2O3	K2O	FeO	CaO	Total
1 / 1 .	5.8139	0.0134	27.1174	58.34	0.8045	0.4498	8.5016	101.0405
1 / 2 .	5.2203	0.0242	27.9932	56.189	0.3252	0.4074	9.8354	99.9945
2 / 1 .	6.1307	0.0552	22.6511	64.0656	1.6439	0.6296	5.4631	100.6392
2 / 2 .	5.2283	0.02	28.463	56.5716	0.2745	0.3878	10.0432	100.9884
3 / 1 .	4.372	0.0377	29.5064	54.3481	0.4688	0.7487	11.3648	100.8466
3 / 2 .	3.9929	0.0169	30.6746	53.1956	0.1922	0.4981	12.7822	101.3526
4 / 1 .	5.0948	0.2784	27.9836	56.5281	0.5568	1.0322	9.8898	101.3636
4 / 2 .	5.144	0.0511	28.53	56.105	0.3074	0.4529	10.289	100.8794
5 / 1 .	4.7876	0.0424	28.7307	55.2988	0.5081	0.814	10.662	100.8435
5 / 2 .	5.141	0.0424	28.5893	56.2252	0.2706	0.4366	10.2871	100.9923
6 / 1 .	4.6295	0.0427	29.2341	54.8023	0.4609	0.5894	11.2028	100.9617
6 / 2 .	4.8297	0.0442	28.9209	55.3445	0.2482	0.4235	10.7863	100.5973
7 / 1 .	3.9238	0.0379	30.3822	53.1044	0.3505	0.7453	12.5594	101.1036
7 / 2 .	5.2907	0.0304	28.4962	56.8445	0.3021	0.404	10.0505	101.4183
7 / 3 .	4.9626	0.0337	28.7901	55.9567	0.2419	0.4008	10.6499	101.0358
8 / 1 .	4.9996	0.0541	28.5134	55.8595	0.5296	0.801	10.4339	101.1911
8 / 2 .	5.1835	0.0342	28.2121	56.4885	0.2965	0.4789	10.0705	100.7643
9 / 1 .	2.9679	0.0371	32.2136	50.4349	0.2114	0.7449	14.4995	101.1092
9 / 2 .	5.6355	0.0314	27.5303	57.2845	0.3902	0.4888	9.1823	100.543
10 / 1 .	4.8313	0.0611	28.6873	55.2183	0.4519	0.8139	10.759	100.8227
10 / 2 .	3.3812	0.0222	31.694	51.6054	0.1606	0.3482	13.9692	101.1809
11 / 1 .	5.1485	0.0375	28.0777	56.2602	0.5903	0.5994	9.8124	100.5261
11 / 2 .	5.1211	0.0102	28.6428	56.4057	0.2533	0.2771	10.1851	100.8952
12 / 1 .	5.0411	0.0297	28.2568	56.01	0.4666	0.6058	10.1008	100.5108
12 / 2 .	4.4962	0.0217	29.6754	54.6567	0.2544	0.3225	11.3659	100.7928
13 / 1 .	4.5586	0.065	27.6091	55.8959	0.7685	0.9213	10.2853	100.1038
13 / 2 .	5.2623	0.0178	28.382	56.4346	0.2883	0.3422	10.0837	100.8109
14 / 1 .	3.8788	0.0874	30.2936	52.9947	0.2223	0.7745	12.6229	100.8742
14 / 2 .	4.3769	0.022	30.035	54.5679	0.2063	0.4006	11.9563	101.5651
15 / 1 .	5.4421	0.0363	27.8578	57.5121	0.5882	0.4594	9.4801	101.376
15 / 2 .	5.8484	0.0189	27.2332	58.3434	0.5478	0.2413	8.7075	100.9406
16 / 1 .	5.099	0.03	28.2091	56.2647	0.5565	1.0092	10.1027	101.2711
17 / 1 .	4.9759	0.0429	28.2277	55.5206	0.4937	0.7879	10.266	100.3147
17 / 2 .	4.7224	0.0174	29.3601	55.2503	0.2572	0.3811	11.1862	101.1748
18 / 1 .	5.7464	0.0062	27.6576	57.851	0.7255	0.2607	8.8916	101.139
18 / 2 .	5.1437	0.0237	28.5828	56.2797	0.2981	0.4951	10.2739	101.0971
19 / 1 .	4.3425	0.0572	29.4352	54.5345	0.4037	0.7325	11.5099	101.0154
19 / 2 .	5.3216	0.037	28.5532	56.865	0.269	0.3356	9.9665	101.3479
20 / 2 .	5.6531	0.0247	27.2769	56.9005	0.4035	0.3423	8.7759	99.3768
21 / 1 .	4.5271	0.0458	29.0681	54.7041	0.469	1.0024	10.929	100.7456
21 / 2 .	5.3217	0.0209	28.3637	56.1505	0.3628	0.2574	10.0298	100.5067
22 / 1 .	4.7978	0.027	28.9158	55.3353	0.4833	0.3941	10.8635	100.8169
22 / 2 .	5.1152	0.0511	28.8258	55.8202	0.2659	0.3877	10.4623	100.9282
23 / 1 .	4.9517	0.0392	28.6711	55.859	0.56	0.6968	10.3277	101.1054
23 / 2 .	4.673	0.0316	29.3713	55.1741	0.2085	0.3909	11.1637	101.013

HM-04-01 Plagioclase (1 = Core; 2 = Rim)

Plagioclase	Oxides Weight %							
	Na2O	MgO	SiO2	Al2O3	K2O	FeO	CaO	Total
1 / 1 .	5.421	0.0537	28.0817	55.1652	0.2437	0.4378	10.2839	99.6869
1 / 2 .	6.0663	0.0398	26.8629	56.7233	0.3347	0.5563	8.9067	99.49
2 / 1 .	5.0224	0.0331	28.6624	54.2476	0.1916	0.388	11.0025	99.5476
2 / 2 .	6.0008	0.0395	27.0805	56.7659	0.3329	0.6348	9.0835	99.9377
3 / 1 .	4.8809	0.0663	28.6236	54.1593	0.204	0.4669	11.2853	99.6863
3 / 2 .	4.5141	0.0474	29.6582	53.1004	0.1589	0.4636	11.9463	99.8887
3 / 3 .	5.2254	0.0602	28.2844	55.2416	0.212	0.553	10.606	100.1826
3 / 4 .	4.4676	0.0719	29.7465	52.5474	0.2196	0.6551	12.1288	99.8369
4 / 1 .	6.5508	0.0921	24.9336	59.4101	0.4827	0.695	7.488	99.6523
4 / 2 .	5.4833	0.0431	27.9625	55.3517	0.336	0.5266	9.9511	99.6542
5 / 1 .	5.9788	0.0447	27.1071	56.7838	0.3006	0.5898	9.0722	99.8771
5 / 2 .	5.1647	0.0569	28.2865	54.1083	0.2875	0.5862	10.6567	99.1469
6 / 1 .	5.5119	0.0332	27.4311	55.9722	0.2489	0.5432	9.7358	99.4763
6 / 2 .	6.2353	0.0365	26.4854	57.172	0.3421	0.3326	8.5085	99.1124
7 / 1 .	5.584	0.0523	27.4252	55.8489	0.2308	0.6762	9.8648	99.6822
7 / 2 .	5.0126	0.0427	28.3603	54.1535	0.3187	0.6626	10.7122	99.2626
8 / 1 .	5.1445	0.0157	28.2636	54.7343	0.1892	0.4875	10.6064	99.4413
8 / 2 .	5.5092	0.019	27.934	55.4308	0.3223	0.4316	10.0011	99.6479
9 / 1 .	5.275	0.0655	28.0632	55.0915	0.2361	0.4444	10.2306	99.4063
9 / 2 .	6.1954	0.0678	26.6968	56.957	0.3644	0.4018	8.7608	99.444
10 / 1 .	6.1053	0.0247	26.607	56.9835	0.3155	0.4478	8.6289	99.1127
10 / 2 .	6.8276	0.0208	25.265	59.2269	0.4787	0.4048	7.2189	99.4427
11 / 1 .	5.5051	0.0533	27.6291	55.5655	0.2369	0.4379	9.9976	99.4255
11 / 2 .	5.0935	0.0531	27.9989	54.6786	0.2164	0.3226	10.4638	98.827
11 / 3 .	5.9228	0.1034	26.5874	56.5146	0.2934	0.4578	9.0695	98.9489
11 / 4 .	5.0708	0.0524	28.3541	54.2717	0.2441	0.6153	10.6772	99.2855
12 / 1 .	4.9222	0.0224	28.9348	53.9497	0.2377	0.3719	11.0367	99.4756
12 / 2 .	6.5467	0.0767	25.7959	57.7366	0.3958	0.4545	7.8537	98.8599
13 / 1 .	5.1609	0.0531	28.2763	54.4394	0.2441	0.5496	10.7214	99.4448
13 / 2 .	5.5296	0.0344	27.5587	55.1643	0.3707	0.9343	9.9114	99.5035
14 / 1 .	6.0686	0.0278	26.7325	57.192	0.2965	0.4942	8.652	99.4636
14 / 2 .	4.7521	0.072	28.7509	53.2886	0.2656	0.7849	11.3781	99.2923
15 / 1 .	6.082	0.0318	26.3859	57.6898	0.3194	0.4641	8.6183	99.5913
15 / 2 .	5.6427	0.0382	27.2352	55.7156	0.3207	0.5427	9.5646	99.0597
16 / 1 .	4.3407	0.0454	29.4729	52.8547	0.1377	0.4344	12.015	99.3007
16 / 2 .	5.1737	0.0694	28.2243	54.2902	0.2672	0.5495	10.419	98.9933
17 / 1 .	5.1662	0.0529	28.3417	54.8989	0.1823	0.4581	10.6328	99.733
17 / 2 .	4.7599	0.0614	28.9101	53.8758	0.221	0.5534	11.3041	99.6857
18 / 1 .	5.6338	0.0267	27.7006	55.7749	0.2534	0.3329	9.6838	99.4061
18 / 2 .	4.5638	0.0742	29.414	52.6153	0.2128	0.8616	11.6747	99.4163
19 / 1 .	5.4544	0.0397	28.0941	54.8727	0.2201	0.3622	10.1337	99.1769
19 / 2 .	6.3568	0.0389	26.5702	57.1635	0.4479	0.4906	8.4356	99.5037
20 / 1 .	5.6095	0.0519	27.6938	55.7109	0.29	0.4418	9.538	99.3359
20 / 2 .	5.2308	0.0432	28.2633	54.4875	0.2972	0.5318	10.384	99.2379
21 / 1 .	5.7447	0.0308	27.4743	55.8243	0.25	0.4054	9.3776	99.1073
21 / 2 .	5.9842	0.0153	27.3754	55.9472	0.328	0.3033	9.0428	98.9961

22 / 1 .	5.6168	0.0384	27.5654	55.6112	0.2543	0.4408	9.6975	99.2243
22 / 2 .	5.381	0.0401	28.2487	54.4544	0.2664	0.5294	10.2662	99.1862
23 / 1 .	4.3798	0.0498	29.906	52.3996	0.1797	0.5317	12.0013	99.4479
23 / 2 .	6.9058	0.0406	24.6905	58.7394	1.1736	0.7849	6.4591	98.7939
24 / 1 .	5.0735	0.0474	28.4937	54.0146	0.1693	0.458	10.7524	99.0089
24 / 2 .	5.4583	0.0497	27.8098	55.3143	0.3222	0.4247	10.0161	99.395
25 / 1 .	5.4338	0.0291	28.1962	54.9188	0.2144	0.3325	10.2012	99.326
25 / 2 .	5.5696	0.0172	27.9145	55.5773	0.425	0.5563	9.7972	99.8571
26 / 1 .	5.9701	0.0466	27.2565	56.3471	0.2766	0.4314	9.136	99.4644
26 / 2 .	5.3027	0.0476	28.0612	54.6282	0.268	0.5726	10.3635	99.2437
27 / 1 .	4.8391	0.0316	29.2616	53.7613	0.1784	0.3983	11.3053	99.7755
27 / 2 .	5.2935	0.0377	28.2631	55.2919	0.3169	0.6549	10.2749	100.133

HW-04-01 Plagioclase (1 = Core; 2 = Rim)

				Oxides Weight %				
Plagioclase	**Na2O**	**MgO**	**SiO2**	**Al2O3**	**K2O**	**FeO**	**CaO**	**Total**
1 / 2 .	6.0317	0.0248	27.1617	56.0772	0.4371	0.4444	8.6709	98.8478
2 / 3 .	5.7116	0.0406	27.6784	55.361	0.2434	0.2897	9.5395	98.8642
2 / 4 .	5.1694	0.0202	28.6695	54.0991	0.3195	0.5823	10.4061	99.2662
3 / 1 .	5.9425	0.0214	27.7085	55.9065	0.2689	0.3339	9.3277	99.5094
3 / 2 .	5.6084	0.0518	27.9085	55.1404	0.3745	0.7871	9.9079	99.7786
4 / 1 .	5.61	0.0324	28.2887	55.1818	0.2343	0.2885	10.1044	99.7401
4 / 2 .	6.1053	0.0379	27.4344	56.7359	0.268	0.3118	9.0591	99.9524
4 / 3 .	5.8008	0.0362	27.8709	56.2636	0.2429	0.3647	9.7733	100.3525
4 / 4 .	5.3018	0.0563	28.5954	54.9544	0.2446	0.2254	10.5504	99.9282
4 / 5 .	6.0245	0.041	27.2954	56.6295	0.4646	0.3912	9.0396	99.8859
5 / 1 .	4.1955	0.0476	30.403	52.0415	0.1945	0.3751	12.5932	99.8505
5 / 2 .	5.0479	0.0309	29.0491	54.2068	0.3038	0.6349	11.0522	100.3256
6 / 1 .	5.3416	0.0343	28.6722	55.354	0.1991	0.3756	10.6369	100.6137
6 / 2 .	5.4639	0.0155	28.6479	55.195	0.3321	0.4086	10.2659	100.3288
7 / 1 .	5.0028	0.0224	29.3452	54.0911	0.1705	0.3582	11.1628	100.153
7 / 2 .	5.6812	0.0391	28.2073	55.9277	0.2869	0.3584	9.7751	100.2758
8 / 1 .	5.268	0.037	28.9917	55.1241	0.2185	0.5104	10.6457	100.7954
8 / 2 .	2.8617	0.0174	32.7803	49.1356	0.0633	0.4005	15.2567	100.5154
8 / 3 .	7.2575	0.0149	25.5151	59.946	0.5544	0.282	6.6495	100.2195
9 / 1 .	6.1821	0.019	27.0871	57.1916	0.3254	0.2372	8.6103	99.6527
9 / 2 .	6.0625	0.0271	27.5837	56.8015	0.2921	0.2108	9.0575	100.0351
9 / 3 .	6.1402	0.0351	27.1506	56.939	0.5484	0.484	8.7578	100.0551
10 / 1 .	6.0327	0.0213	27.8886	56.7847	0.2878	0.4348	9.2875	100.7373
10 / 2 .	5.6948	0.0249	28.1413	55.9967	0.3888	0.3424	9.7659	100.3548
11 / 1 .	5.6366	0.0279	27.6929	55.678	0.236	0.3582	9.5711	99.2007
11 / 2 .	5.6961	0.0168	27.8869	55.8413	0.3767	0.4476	9.7036	99.9689
12 / 1 .	5.8962	0.0081	27.887	56.8965	0.4274	0.2802	9.4811	100.8764
12 / 2 .	6.3224	0.0179	27.0102	57.4721	0.2828	0.3297	8.6863	100.1213
12 / 3 .	6.2619	0.0285	27.2516	57.0167	0.4356	0.3659	8.8103	100.1704
13 / 1 .	5.8339	0.054	28.144	56.2357	0.1818	0.3951	9.7947	100.6393
13 / 2 .	5.4922	0.0259	28.3952	55.8332	0.3374	0.3622	10.2937	100.7398
1 / 1 .	5.2018	0.0154	28.8394	54.1104	0.1967	0.3983	10.8818	99.6438
1 / 2 .	5.2309	0.0126	29.1072	54.603	0.3041	0.372	10.8497	100.4795

2 / 1 .	5.3869	0.0266	28.5343	55.5932	0.2526	0.4014	10.3026	100.4977
2 / 2 .	5.7396	0.0226	28.0819	56.0716	0.2848	0.3981	9.8125	100.411
3 / 1 .	5.8491	0.0265	27.8519	56.5107	0.2388	0.4917	9.6494	100.618
3 / 2 .	5.6972	0.0339	27.8791	55.8681	0.1989	0.455	9.9521	100.0843
3 / 3 .	3.9737	0.0211	30.5685	52.0136	0.1368	0.4511	13.0737	100.2384
3 / 4 .	5.9881	0.0272	27.4351	56.7974	0.3834	0.4049	9.2552	100.2912
4 / 1 .	5.6171	0.0188	28.3783	55.9466	0.2293	0.3854	10.1009	100.6762
5 / 1 .	6.6724	0.0059	26.5591	58.5339	0.3184	0.2191	7.9057	100.2146
5 / 2 .	4.2964	0.0276	29.8923	52.6168	0.2113	0.7882	12.3525	100.1852
6 / 2 .	5.6274	0.0222	28.3618	55.5703	0.2839	0.4682	9.9985	100.3324
7 / 1 .	5.2747	0.0179	28.7648	54.8524	0.2406	0.2567	10.743	100.1501
7 / 2 .	5.8706	0.0361	27.7019	56.539	0.3999	0.3883	9.4686	100.4046
7 / 3 .	6.0155	0.0203	27.6631	56.5631	0.4618	0.4343	9.0938	100.252
7 / 4 .	5.6997	0.0155	27.8341	56.0614	0.3642	0.3324	9.5425	99.8498
7 / 5 .	6.2468	0.0193	25.772	59.3407	0.5026	0.4084	7.9154	100.2052
8 / 1 .	4.6758	0.0032	29.9142	53.7717	0.1734	0.2634	11.8195	100.6213
8 / 2 .	6.2593	0.013	27.553	57.2508	0.469	0.2207	8.7573	100.5231
9 / 1 .	5.9545	0.0244	27.9464	56.6675	0.2743	0.1449	9.4608	100.4728
9 / 2 .	5.9007	0.0034	27.6995	56.7717	0.4164	0.3325	9.2358	100.3601
10 / 1 .	5.57	0.017	28.2655	55.9603	0.2398	0.2932	10.0532	100.399
10 / 2 .	6.2906	0.0153	27.3266	57.0556	0.3777	0.2965	8.8992	100.2614
11 / 1 .	5.9849	0.0395	27.2337	56.707	0.2333	0.3978	9.0984	99.6947
11 / 2 .	3.2782	0.0329	31.7679	49.5672	0.1149	0.6518	14.2987	99.7116

PD-04-01 Plagioclase (1 = Core; 2 = Rim)

				Oxides Weight %				
Plagioclase	**Na2O**	**MgO**	**SiO2**	**Al2O3**	**K2O**	**FeO**	**CaO**	**Total**
1 / 1 .	4.5498	0.0341	29.8392	53.6856	0.0804	0.3234	11.9341	100.4466
1 / 2 .	5.0041	0.0106	29.5509	54.5793	0.0854	0.2101	11.3263	100.7668
1 / 3 .	4.8323	0.0439	29.3862	54.2483	0.1065	0.38	11.4957	100.4931
2 / 1 .	3.6439	0.1308	30.7244	52.007	0.0829	0.6329	13.407	100.6289
2 / 2 .	5.4866	0.1915	25.6953	56.6951	0.378	1.6918	9.1554	99.2936
2 / 3 .	4.7595	0.0889	29.3478	54.1993	0.1431	0.8263	11.5574	100.9223
4 / 1 .	5.9085	0.0107	27.1458	56.1901	0.2362	0.327	9.023	98.8413
4 / 2 .	3.7826	0.0774	30.409	51.5521	0.0872	0.5631	12.7797	99.2512
5 / 1 .	5.3185	0.0172	28.1478	55.3266	0.1919	0.3135	10.0089	99.3244
5 / 2 .	3.8773	0.0909	30.2169	51.6784	0.071	0.6163	12.7427	99.2935
6 / 1 .	4.6764	0.0294	29.5475	53.6897	0.1065	0.4101	11.7046	100.1642
6 / 2 .	4.1246	0.1015	29.922	52.7974	0.1119	0.6697	12.4853	100.2124
7 / 1 .	4.6251	0.1091	29.0701	53.9464	0.1361	0.8097	11.3641	100.0606
8 / 1 .	3.8474	0.0786	30.6386	52.2442	0.0738	0.5698	13.1421	100.5944
8 / 2 .	4.6625	0.0872	29.1274	54.2688	0.146	0.7898	11.6342	100.716
9 / 1 .	3.5428	0.0792	31.4561	51.2399	0.0611	0.3532	13.8356	100.5679
9 / 2 .	3.8248	0.0915	30.7288	51.9147	0.0906	0.6429	13.2825	100.5759
10 / 1 .	2.6793	0.0545	32.7322	49.502	0.0448	0.3997	15.4029	100.8154
10 / 2 .	4.9184	0.0885	28.9695	54.9138	0.1391	0.8265	11.1628	101.0186
11 / 1 .	4.8588	0.0431	29.2404	54.4085	0.0791	0.3634	11.3705	100.3638
11 / 2 .	4.2786	0.0952	29.992	53.533	0.1042	0.7598	12.2242	100.987
12 / 1 .	4.2315	0.0842	29.9891	52.9926	0.0922	0.5433	12.5469	100.4797

12 / 2 .	4.7297	0.0893	29.0865	53.9658	0.1601	0.8297	11.5343	100.3953
13 / 1 .	3.946	0.0906	30.3119	52.5133	0.0985	0.5333	12.8768	100.3704
13 / 2 .	3.905	0.0866	30.5808	52.4749	0.0977	0.5065	13.0222	100.6736
14 / 1 .	3.6627	1.4718	28.7575	51.7751	0.0933	1.2883	13.2743	100.323
14 / 2 .	4.2478	0.0995	29.7199	53.4892	0.0803	0.7597	12.3978	100.7941
15 / 1 .	4.131	0.0942	30.2712	53.5367	0.0634	0.5833	12.5938	101.2735
15 / 2 .	4.332	0.0992	29.8954	53.5284	0.1119	0.8129	12.3722	101.1521
16 / 1 .	3.9096	0.0741	30.7057	52.549	0.0724	0.5931	13.3237	101.2277
17 / 1 .	3.8836	0.0893	30.9655	52.0512	0.0766	0.7827	13.1916	101.0404
17 / 2 .	6.4627	0.0955	25.3595	58.8119	0.3535	1.0403	8.5157	100.6391
18 / 1 .	3.6132	0.0883	31.334	51.8755	0.0449	0.6696	13.8284	101.4539
18 / 2 .	4.5145	0.0972	29.544	53.9508	0.1451	0.9295	12.0329	101.2142
19 / 1 .	3.8869	0.1038	30.7178	52.6495	0.0886	0.6331	13.2567	101.3364
19 / 2 .	5.0373	0.0819	28.4855	55.0797	0.1836	0.9232	10.9638	100.7549
20 / 1 .	6.1088	0.0097	27.2607	58.0304	0.3045	0.3904	9.0149	101.1194
20 / 2 .	5.3094	0.0205	28.452	55.8388	0.2009	0.4569	10.4303	100.7087
20 / 3 .	4.7124	0.0189	29.5554	54.3084	0.1763	0.3834	11.7284	100.8833
20 / 4 .	5.7536	0.0543	27.7147	56.8103	0.221	0.4003	9.8063	100.7605
20 / 5 .	5.4303	0.1145	28.2165	55.9507	0.1951	0.9132	10.538	101.3583
21 / 1 .	4.4413	0.0928	29.594	53.9635	0.2143	0.6932	11.8867	100.8856
22 / 1 .	3.7666	0.0749	30.8239	52.1318	0.0752	0.6497	13.4975	101.0195
22 / 2 .	5.6462	0.0461	27.3127	56.7491	0.252	1.0634	9.7189	100.7883

PD-04-01 Plagioclase All less than 1 mm in length (1 = Core; 2 = Rim)

	Oxides Weight %							
Plagioclase	Na2O	MgO	SiO2	Al2O3	K2O	FeO	CaO	Total
1 / 1 .	4.0389	0.1076	52.5211	29.9921	0.0712	0.6514	12.8871	100.2693
1 / 2 .	5.3161	1.5741	56.4635	23.671	0.2594	2.6204	9.7577	99.6622
2 / 1 .	3.8326	0.0997	52.1862	30.3333	0.0766	0.7015	13.1713	100.4012
2 / 2 .	4.8871	0.0727	54.5294	28.8291	0.1581	0.7787	11.2768	100.5319
3 / 1 .	4.7731	0.0578	54.5711	28.8091	0.117	0.5684	11.4046	100.3012
3 / 2 .	4.4787	0.8103	54.8168	26.7301	0.3192	1.9193	10.7578	99.8322
4 / 1 .	4.3682	0.0993	53.2086	29.4542	0.0884	0.7079	12.1174	100.044
4 / 2 .	5.3605	0.9758	61.5509	20.771	0.8243	3.2749	6.4522	99.2096
5 / 1 .	3.7352	0.0886	51.7725	30.567	0.0692	0.7108	13.47	100.4133
5 / 2 .	5.0127	0.1953	55.0869	28.1446	0.1666	1.0736	10.8136	100.4933
6 / 1 .	3.9572	0.0895	52.267	30.4701	0.0802	0.6498	13.0225	100.5363
6 / 2 .	5.1276	0.2927	55.2281	27.8281	0.1739	1.0471	10.4624	100.1599
7 / 1 .	3.6601	0.0895	51.5329	30.8795	0.072	0.6419	13.6487	100.5248
8 / 1 .	4.6507	0.0659	54.1454	29.4034	0.1154	0.5402	11.6939	100.6147
8 / 2 .	5.4403	0.5541	57.1362	25.4503	0.3977	1.5867	9.209	99.7743
9 / 1 .	5.0149	0.0762	54.6952	28.2249	0.1773	0.8384	10.892	99.9189
9 / 2 .	5.0912	0.0782	55.1343	28.2079	0.1657	0.8808	10.6688	100.2268
10 / 1 .	4.2567	0.0843	52.8762	29.7842	0.0913	0.595	12.4423	100.1299
10 / 2 .	3.8286	0.0975	51.948	30.2536	0.0805	0.711	13.1639	100.083
11 / 1 .	4.1704	0.1001	52.7269	29.708	0.0986	0.6624	12.6259	100.0924
11 / 2 .	4.5941	0.0649	53.8925	29.1401	0.1486	0.7551	11.7495	100.3447
12 / 1 .	3.9433	0.1087	52.4255	30.3914	0.0812	0.6498	12.9162	100.516
12 / 2 .	5.0853	0.1206	55.0209	28.0383	0.1602	0.8181	10.7153	99.9586

13 / 1 .	3.5975	0.0888	51.6742	30.6554	0.0714	0.6607	13.5577	100.3057
13 / 2 .	4.4775	0.1005	53.618	29.3312	0.1133	0.7017	11.9744	100.3166
14 / 1 .	4.0866	0.0858	52.5746	30.0094	0.0996	0.7705	12.7103	100.3368
14 / 2 .	4.5969	0.0895	53.1589	28.7362	0.1344	0.7347	11.5183	98.9688
15 / 1 .	3.753	0.0787	51.9656	30.5512	0.0743	0.6325	13.4978	100.553
15 / 2 .	4.6576	0.0934	53.725	29.0774	0.1369	0.8053	11.7621	100.2577

PD-04-01 Plagioclase 2 and 4 Transects

		Oxides Weight %							
Plagioclase	Location (um)	Na2O	MgO	SiO2	Al2O3	K2O	FeO	CaO	Total
2 / 1 .	0	5.1522	0.022	55.1641	27.9216	0.205	0.394	10.2115	99.0704
2 / 2 .	5	5.2392	0.0166	55.4903	27.7723	0.205	0.4176	10.1179	99.2588
2 / 3 .	10	5.2769	0.0168	55.7359	27.5842	0.1794	0.3955	10.0646	99.2532
2 / 4 .	15	5.1755	0.0201	55.551	27.6498	0.2239	0.3702	10.0437	99.0343
2 / 5 .	20	5.2217	0.022	55.4648	27.7885	0.1887	0.3908	10.0837	99.1601
2 / 9 .	40	5.6276	0.0214	56.5494	27.1885	0.2172	0.4414	9.3875	99.4331
2 / 11 .	50	5.5534	0.023	56.5247	27.2457	0.2253	0.3655	9.3877	99.3253
2 / 12 .	55	5.6381	0.018	56.3311	27.0701	0.2172	0.4351	9.3197	99.0292
2 / 13 .	60	5.5619	0.0222	56.5978	27.1933	0.2435	0.3735	9.4699	99.462
2 / 14 .	65	5.4464	0.0274	55.7495	27.1933	0.2045	0.3354	9.7716	98.7283
2 / 15 .	70	5.3687	0.0159	55.7761	27.6484	0.2205	0.3781	9.9255	99.3332
2 / 16 .	75	5.2052	0.0304	55.5843	27.8888	0.1899	0.3891	10.1205	99.4083
2 / 17 .	80	5.1355	0.0228	55.1436	28.0398	0.186	0.4065	10.3541	99.2883
2 / 18 .	85	5.0789	0.0211	55.1678	27.8049	0.1886	0.4113	10.3699	99.0426
2 / 19 .	90	5.1237	0.0299	55.2861	28.1595	0.194	0.4286	10.3367	99.5585
2 / 20 .	95	5.2002	0.0294	55.2515	27.6623	0.1995	0.4128	10.1496	98.9055
2 / 21 .	100	5.3595	0.0245	55.7505	27.7119	0.2112	0.4145	9.8782	99.3502
2 / 22 .	105	5.409	0.0391	55.9898	27.4828	0.2106	0.5125	9.6867	99.3305
2 / 23 .	110	5.4991	0.0268	56.2084	27.3351	0.2293	0.3766	9.5908	99.266
2 / 24 .	115	5.4486	0.021	56.3768	27.3	0.2188	0.3086	9.5281	99.2018
2 / 25 .	120	5.3958	0.0232	56.1545	27.663	0.2078	0.4477	9.6883	99.5803
2 / 26 .	125	5.4519	0.0152	56.3826	27.4879	0.2087	0.3465	9.7874	99.6802
2 / 27 .	130	5.3894	0.0185	55.9835	27.6454	0.1994	0.4082	9.7739	99.4182
2 / 28 .	135	5.3516	0.0198	55.663	27.6156	0.2163	0.3528	9.941	99.1601
2 / 29 .	140	5.137	0.0139	55.21	27.8949	0.1841	0.446	10.2717	99.1576
2 / 30 .	145	5.1087	0.0249	54.6946	28.156	0.1747	0.4334	10.4559	99.0481
2 / 31 .	150	5.0608	0.0086	54.9798	28.0558	0.1949	0.3797	10.4675	99.1471
2 / 32 .	155	5.1296	0.0159	54.8851	27.9292	0.185	0.416	10.4105	98.9713
2 / 33 .	160	5.1191	0.0254	55.2874	28.0561	0.2059	0.405	10.3073	99.4062
2 / 34 .	165	5.0134	0.0206	54.8759	28.165	0.1815	0.3719	10.5256	99.1539
2 / 35 .	170	5.0635	0.0161	54.7335	27.9643	0.1978	0.3923	10.4648	98.8321
2 / 36 .	175	5.0375	0.0316	55.4929	28.1765	0.169	0.4445	10.4067	99.7587
2 / 37 .	180	5.2648	0.0157	55.6172	27.8621	0.2009	0.3512	10.102	99.4139
2 / 38 .	185	5.3521	0.0357	55.896	27.3852	0.2186	0.3702	9.8201	99.078
2 / 39 .	190	5.4398	0.0168	56.1356	27.5369	0.2152	0.3955	9.7046	99.4443
2 / 40 .	195	5.3992	0.0239	56.0551	27.1772	0.2255	0.3545	9.5797	98.815
2 / 41 .	200	5.4731	0.0251	56.161	27.1188	0.2184	0.4098	9.5014	98.9075
2 / 42 .	205	5.6237	0.03	56.5347	27.0002	0.2285	0.375	9.3294	99.1215
2 / 43 .	210	5.6269	0.0242	56.4251	27.1521	0.2394	0.4035	9.2546	99.1257
2 / 44 .	215	5.6637	0.0249	56.9322	26.853	0.2418	0.3893	9.1309	99.2357
2 / 45 .	220	5.8352	0.0307	57.9008	27.046	0.2665	0.3498	8.7335	100.162

2 / 49 .	240	5.9658	0.0256	57.6626	26.3347	0.2691	0.3245	8.5735	99.1559
2 / 50 .	245	5.8661	0.0187	57.6759	26.5422	0.2382	0.3561	8.7601	99.4573
2 / 51 .	250	5.9069	0.0333	57.2456	26.7599	0.2656	0.4526	8.9084	99.5724
2 / 52 .	255	5.627	0.0283	56.4163	27.0739	0.2362	0.4288	9.3287	99.1393
2 / 53 .	260	5.3465	0.0269	56.0012	27.5905	0.1905	0.3593	9.7349	99.2498
2 / 54 .	265	5.3043	0.0191	55.7814	27.6291	0.2159	0.3575	10.0776	99.385
2 / 55 .	270	5.198	0.0218	55.3346	27.825	0.1646	0.4018	10.2497	99.1955
2 / 56 .	275	4.7311	0.023	54.2239	28.447	0.1902	0.3859	10.9872	98.9882
2 / 57 .	280	4.4096	0.0324	53.6702	29.1345	0.1421	0.438	11.4818	99.3087
2 / 58 .	285	4.7437	0.0304	54.3314	28.6572	0.1662	0.3923	11.0971	99.4183
2 / 59 .	290	4.7727	0.0216	54.5795	28.6594	0.1663	0.4334	10.9442	99.577
2 / 60 .	295	5.0037	0.0147	54.9504	28.1696	0.1677	0.3606	10.6242	99.2909
2 / 61 .	300	5.1273	0.026	55.3454	27.8065	0.1896	0.3876	10.2985	99.1808
2 / 62 .	305	5.3204	0.0179	55.8205	27.7511	0.1987	0.3766	9.9724	99.4577
2 / 63 .	310	5.278	0.0234	55.7717	27.6282	0.1885	0.3703	9.9412	99.2012
2 / 64 .	315	5.3198	0.0303	55.7422	27.9517	0.2105	0.3971	10.089	99.7406
2 / 65 .	320	5.2483	0.0205	55.6989	27.8857	0.2115	0.3781	10.0637	99.5067
2 / 66 .	325	5.2421	0.0239	55.4859	27.5883	0.2083	0.3481	10.0172	98.9136
2 / 67 .	330	5.2477	0.0286	55.5562	27.7406	0.2076	0.4224	10.0355	99.2387
2 / 68 .	335	5.2982	0.0179	55.7724	27.7456	0.2038	0.3703	9.9402	99.3484
2 / 70 .	345	5.4477	0.0293	56.1546	27.36	0.194	0.3798	9.6317	99.197
2 / 71 .	350	5.4036	0.0208	56.0794	27.554	0.2117	0.3593	9.7445	99.3733
2 / 73 .	360	5.0793	0.0292	55.6478	28.1112	0.1825	0.3481	10.3985	99.7967
2 / 74 .	365	5.094	0.0235	55.2573	28.004	0.1937	0.4319	10.4529	99.4573
2 / 75 .	370	5.0585	0.0291	55.1273	28.2899	0.1898	0.4018	10.4816	99.578
2 / 76 .	375	5.0322	0.0299	55.1963	28.1057	0.1729	0.3781	10.4088	99.324
2 / 77 .	380	5.284	0.0288	55.5467	27.6593	0.209	0.375	9.8854	98.9882
2 / 78 .	385	5.5077	0.0269	56.3938	27.0737	0.2262	0.3941	9.4401	99.0626
2 / 79 .	390	5.5657	0.0176	57.0348	26.9991	0.2507	0.4463	9.3	99.6142
2 / 80 .	395	5.6735	0.0212	57.0419	26.9534	0.228	0.3893	9.1857	99.4931
2 / 81 .	400	5.1919	0.0201	55.4647	27.8794	0.189	0.3354	10.1487	99.2292
2 / 82 .	405	4.6582	0.031	54.3291	28.5716	0.1554	0.3702	11.1133	99.2286
2 / 83 .	410	4.5068	0.0249	53.9791	29.0955	0.1505	0.4017	11.3786	99.5371
2 / 84 .	415	4.6363	0.014	53.9224	29.0656	0.1514	0.4286	11.352	99.5703
2 / 85 .	420	4.7606	0.0278	54.5999	28.7179	0.1701	0.4033	10.9667	99.6464
2 / 86 .	425	5.0292	0.0008	54.9958	28.0848	0.1898	0.4413	10.5232	99.2649
2 / 87 .	430	5.0876	0.0281	55.3034	28.1056	0.1992	0.3449	10.3734	99.4422
2 / 88 .	435	5.2495	0.0088	55.5323	27.7802	0.1977	0.3655	10.0137	99.1477
2 / 89 .	440	5.1788	0.0321	55.7092	27.7768	0.1785	0.4367	9.975	99.2871
2 / 90 .	445	5.1774	0.0362	55.6882	27.8584	0.1909	0.4209	10.1544	99.5263
2 / 91 .	450	5.145	0.0171	55.5504	27.8143	0.2152	0.3718	10.2226	99.3364
2 / 92 .	455	5.1723	0.0212	55.5359	27.8442	0.187	0.4619	10.226	99.4485
2 / 93 .	460	5.2566	0.0207	55.4989	27.7619	0.1824	0.3752	10.1344	99.23
2 / 94 .	465	5.329	0.0261	55.9453	27.0947	0.2011	0.3877	9.6624	98.6463
2 / 95 .	470	5.4375	0.0288	56.5698	27.5975	0.2114	0.3624	9.6084	99.8158
2 / 96 .	475	5.5216	0.021	56.0896	27.0982	0.232	0.326	9.4647	98.7532
2 / 97 .	480	5.4863	0.0288	56.2433	27.1033	0.2394	0.4193	9.4284	98.9489
2 / 98 .	485	5.5284	0.0302	56.3543	27.4161	0.223	0.4399	9.4951	99.487
2 / 99 .	490	5.474	0.0158	56.3333	27.3359	0.2105	0.3593	9.5633	99.292
2 / 101 .	500	5.4252	0.0195	56.1338	27.3055	0.2171	0.4256	9.6681	99.1948
2 / 102 .	505	5.2278	0.021	55.8723	27.478	0.2099	0.3719	9.9235	99.1044
2 / 103 .	510	5.2792	0.0156	55.7979	27.7143	0.2058	0.4225	9.9571	99.3924
2 / 104 .	515	5.2494	0.0394	55.8284	27.6396	0.2099	0.4335	9.9171	99.3175

2 / 105 .	520	5.3473	0.0227	56.1756	27.3943	0.2088	0.3877	9.7308	99.2672
2 / 106 .	525	5.3243	0.0281	56.1108	27.4376	0.2271	0.3735	9.6697	99.1711
2 / 107 .	530	5.323	0.0437	56.3577	27.3795	0.2165	0.4004	9.6241	99.3449
2 / 109 .	540	4.1443	0.0754	53.3839	29.567	0.1663	0.5455	11.6341	99.5164
2 / 111 .	550	4.0606	0.0542	52.66	29.5302	0.1345	0.5059	12.3211	99.2665
2 / 113 .	560	3.9383	0.0665	52.6012	29.8911	0.1331	0.6433	12.6948	99.9684
2 / 114 .	565	4.8558	0.0802	54.8144	28.3973	0.1625	0.4651	10.6927	99.468
2 / 115 .	570	5.012	0.0549	54.8587	27.9474	0.186	0.3592	10.3583	98.7764
2 / 117 .	580	3.8188	0.0679	52.1424	30.346	0.0882	0.43	13.0272	99.9205
2 / 118 .	585	3.5846	0.0922	51.6463	30.426	0.0633	0.4853	13.2864	99.584
2 / 119 .	590	3.7442	0.0922	51.9046	30.2349	0.0789	0.6038	12.8466	99.5051
2 / 122 .	605	3.5031	0.0835	51.1442	30.6036	0.0524	0.6163	13.5885	99.5917
2 / 123 .	610	3.2687	0.0898	50.9503	30.901	0.0445	0.599	13.8311	99.6844
2 / 124 .	615	3.2807	0.0864	50.9574	31.0044	0.0575	0.5689	13.8528	99.8081
2 / 125 .	620	3.9049	0.1326	52.1456	29.6043	0.1047	0.8628	12.7301	99.485
4 / 1 .	0	5.4213	0.0195	55.6083	27.8763	0.1638	0.3371	10.1415	99.5678
4 / 2 .	5	5.4018	0.0386	55.8863	27.6977	0.1777	0.3514	9.8549	99.4083
4 / 3 .	10	5.3929	0.0442	55.8988	27.6317	0.2097	0.4226	9.9082	99.5083
4 / 4 .	15	5.3821	0.0317	55.7753	27.7612	0.1898	0.3847	9.945	99.4698
4 / 5 .	20	5.4265	0.0264	56.1869	27.6285	0.1998	0.345	9.7561	99.5693
4 / 6 .	25	5.4052	0.0254	56.0356	27.4435	0.1962	0.3923	9.622	99.1204
4 / 7 .	30	5.4878	0.0293	56.435	27.4019	0.2108	0.3403	9.5878	99.493
4 / 8 .	35	5.5571	0.0368	56.3191	27.2939	0.1986	0.3957	9.5372	99.3384
4 / 9 .	40	5.5281	0.0332	56.3047	27.3438	0.206	0.3815	9.5717	99.369
4 / 10 .	45	5.5003	0.0224	55.793	27.2421	0.2056	0.3894	9.5665	98.7193
4 / 11 .	50	5.5157	0.0332	56.3939	27.4083	0.1881	0.3658	9.5248	99.4297
4 / 12 .	55	5.455	0.0313	56.2364	27.328	0.1925	0.4099	9.5735	99.2268
4 / 13 .	60	5.5558	0.0249	56.0715	27.4272	0.2172	0.44	9.5707	99.3072
4 / 14 .	65	5.484	0.0237	56.5822	27.5818	0.1919	0.4495	9.6286	99.9416
4 / 15 .	70	5.3658	0.0315	56.0502	27.6507	0.1947	0.3625	9.7496	99.4051
4 / 16 .	75	5.3091	0.03	55.6908	27.843	0.2	0.4415	9.9884	99.5028
4 / 17 .	80	5.3163	0.0271	55.9261	27.8242	0.2017	0.3593	9.9524	99.607
4 / 18 .	85	5.3228	0.0332	55.5556	27.531	0.2219	0.4273	9.7378	98.8297
4 / 19 .	90	5.2832	0.042	55.7232	27.539	0.2476	0.3925	9.7192	98.9467
4 / 20 .	95	5.3218	0.0339	56.0171	27.6616	0.2332	0.402	9.8064	99.476
4 / 21 .	100	5.2592	0.0269	55.7097	27.7236	0.2096	0.3688	9.9641	99.2619
4 / 22 .	105	5.2648	0.0286	55.7577	27.8655	0.1798	0.402	10.0728	99.5711
4 / 23 .	110	5.3179	0.0203	55.6436	27.7762	0.1878	0.3973	10.0745	99.4177
4 / 24 .	115	5.2855	0.0244	55.5961	27.8277	0.1945	0.451	10.059	99.4383
4 / 25 .	120	5.2514	0.0163	55.6807	27.5244	0.2007	0.4099	10.012	99.0953
4 / 26 .	125	5.2629	0.0318	55.6199	27.4694	0.2046	0.3799	9.8431	98.8115
4 / 28 .	135	5.3892	0.0186	56.1892	27.6621	0.219	0.383	10.0025	99.8637
4 / 29 .	140	5.1471	0.0287	55.5028	28.3019	0.19	0.3608	10.3159	99.8473
4 / 30 .	145	4.8979	0.0188	55.0617	28.3415	0.1789	0.3671	10.7738	99.6396
4 / 32 .	155	4.74	0.0233	54.3094	28.8624	0.1708	0.432	11.1799	99.7178
4 / 33 .	160	4.8521	0.0196	54.5043	28.6149	0.1772	0.3798	10.8743	99.4222
4 / 34 .	165	4.9653	0.0193	55.0478	28.3714	0.1946	0.3513	10.7146	99.6643
4 / 35 .	170	5.0533	0.026	55.1317	28.2734	0.1854	0.4446	10.5231	99.6375
4 / 36 .	175	5.121	0.0238	55.3153	28.0231	0.2031	0.3561	10.3443	99.3868
4 / 37 .	180	5.2121	0.0266	55.5054	27.906	0.1894	0.3877	10.2377	99.4649
4 / 38 .	185	5.2424	0.0298	55.8463	27.9792	0.2032	0.3356	10.0872	99.7237
4 / 39 .	190	5.2455	0.0259	55.642	27.8115	0.2186	0.3561	10.1202	99.4198

4 / 40 .	195	5.2495	0.0184	55.8523	27.8494	0.2019	0.4099	10.0555	99.6369
4 / 41 .	200	5.2736	0.0376	55.9545	28.0273	0.1927	0.3799	10.0617	99.9272
4 / 42 .	205	5.1801	0.0206	55.6662	28.1143	0.1849	0.3387	10.3329	99.8377
4 / 43 .	210	5.0507	0.0299	55.3607	28.2808	0.1847	0.4336	10.5386	99.8791
4 / 44 .	215	4.6018	0.0223	54.3257	29.0597	0.1771	0.3528	11.3495	99.8888
4 / 45 .	220	4.5263	0.0241	53.9841	29.1121	0.1578	0.4003	11.4771	99.6819
4 / 46 .	225	4.8661	0.0258	55.062	28.5112	0.1837	0.3798	10.8037	99.8323
4 / 47 .	230	4.9332	0.0182	55.0135	28.5349	0.191	0.4066	10.8335	99.9309
4 / 48 .	235	4.7601	0.0247	54.4904	28.6961	0.1599	0.4272	11.0173	99.5757
4 / 49 .	240	4.2433	0.0227	53.1918	29.7253	0.1331	0.3417	12.0565	99.7144
4 / 50 .	245	4.2798	0.0256	53.2169	29.5409	0.1452	0.4445	11.9699	99.6229
4 / 51 .	250	4.472	0.026	53.7581	29.148	0.1386	0.424	11.6256	99.5921
4 / 52 .	255	4.5117	0.0256	54.1814	28.9151	0.1502	0.3971	11.5181	99.6992
4 / 53 .	260	4.6308	0.0101	54.2292	28.9136	0.1607	0.3987	11.4103	99.7534
4 / 54 .	265	5.0655	0.0228	55.1822	28.0687	0.1877	0.4194	10.4168	99.3631
4 / 55 .	270	5.2071	0.0125	55.5624	27.6817	0.2018	0.3909	10.3407	99.3972
4 / 56 .	275	5.3264	0.0234	56.0225	27.7557	0.2065	0.3593	9.9959	99.6896
4 / 57 .	280	5.4204	0.0246	56.4566	27.3319	0.2287	0.4322	9.7456	99.64
4 / 58 .	285	5.7892	0.0134	57.3571	26.8927	0.2497	0.3278	9.0686	99.6986
4 / 59 .	290	5.865	0.0068	57.5273	26.7374	0.2304	0.4196	8.9242	99.7107
4 / 60 .	295	5.8105	0.0234	57.6063	26.6602	0.2289	0.3769	8.8615	99.5677
4 / 61 .	300	5.817	0.0373	57.8868	26.4828	0.3248	0.3341	8.6408	99.5237
4 / 62 .	305	5.7902	0.0263	57.6896	26.6162	0.2415	0.3468	8.8437	99.5542
4 / 63 .	310	5.8046	0.0185	57.1675	26.6456	0.2403	0.4291	9.0536	99.3592
4 / 64 .	315	5.5943	0.0377	57.5934	26.4387	0.3564	0.4766	8.9828	99.4798
4 / 65 .	320	5.2199	0.0299	56.0625	28.0331	0.21	0.3704	10.0326	99.9586
4 / 66 .	325	4.7639	0.0289	54.4375	28.6534	0.181	0.4351	10.9613	99.4611
4 / 67 .	330	4.8317	0.0184	54.3441	28.7724	0.1689	0.4019	10.9136	99.4511
4 / 68 .	335	4.8721	0.0257	54.915	28.5289	0.1862	0.3561	10.8895	99.7735
4 / 70 .	345	4.5991	0.0221	53.933	28.7976	0.1493	0.3386	11.3232	99.1629
4 / 71 .	350	4.8297	0.0242	54.6133	28.4879	0.1622	0.3972	10.9212	99.4356
4/ 72 .	355	5.0124	0.0152	55.0534	28.2969	0.1754	0.3498	10.6666	99.5696
4 / 73 .	360	5.0326	0.0303	55.2673	28.1037	0.1845	0.3435	10.4114	99.3733
4 / 74 .	365	4.7649	0.0299	54.4178	28.8237	0.1717	0.3987	11.0291	99.6358
4 / 75 .	370	4.2598	0.0123	53.3297	29.4689	0.1209	0.3291	12.1135	99.6342
4 / 76 .	375	3.974	0.0128	52.4603	29.8763	0.1249	0.4491	12.5123	99.4098
4 / 77 .	380	4.3459	0.0167	53.3412	29.3325	0.1344	0.4002	11.8334	99.4043
4 / 78 .	385	4.6798	0.0209	54.7863	28.8918	0.1551	0.3988	11.186	100.119
4 / 79 .	390	5.0081	0.0177	55.38	28.1245	0.1524	0.3308	10.5905	99.6041
4 / 80 .	395	5.1236	0.0281	55.6056	28.0969	0.189	0.4495	10.3247	99.8174
4 / 82 .	405	5.1611	0.024	55.553	28.0201	0.1856	0.3783	10.2249	99.547
4 / 83 .	410	5.1462	0.0271	55.6694	27.9806	0.1775	0.3736	10.276	99.6503
4 / 84 .	415	5.0797	0.0323	55.5205	28.0206	0.1675	0.3767	10.4007	99.598
4 / 85 .	420	5.1078	0.0369	55.5459	28.075	0.1688	0.3815	10.3979	99.7138
4 / 86 .	425	4.3217	0.0481	53.4658	29.5698	0.1216	0.5172	11.9616	100.006
4 / 87 .	430	3.9354	0.0552	52.496	29.9899	0.0978	0.4919	12.723	99.7891
4 / 88 .	435	4.0008	0.0554	52.6523	29.9092	0.1004	0.4872	12.5769	99.7823
4 / 89 .	440	4.2283	0.0509	53.3451	29.632	0.1085	0.4777	12.202	100.044
4 / 90 .	445	4.3391	0.061	53.5146	29.425	0.1009	0.443	11.9524	99.8359
4 / 91 .	450	4.3727	0.0505	54.2101	29.6316	0.1109	0.4035	11.7382	100.517
4 / 93 .	460	4.4272	0.0481	53.8938	29.0438	0.1214	0.4257	11.6457	99.6057
4 / 95 .	470	4.858	0.0483	55.3345	28.6344	0.1374	0.383	10.5215	99.9171
4 / 96 .	475	4.7325	0.0574	55.2842	30.5028	0.1356	0.44	9.9624	101.115

4 / 97 .	480	5.4945	0.0398	56.4524	28.8574	0.1594	0.3704	9.9305	101.304
4 / 98 .	485	5.3287	0.0495	55.034	28.0092	0.1528	0.3783	10.399	99.3515
4 / 99 .	490	3.4833	0.0751	50.5782	30.5965	0.082	0.5359	13.5784	98.9294
4 / 100 .	495	3.7109	0.0911	51.8718	30.4452	0.0716	0.5376	13.1353	99.8636
4 / 101 .	500	3.7189	0.1295	51.7973	30.0666	0.064	0.5598	12.9237	99.2598
4 / 102 .	505	3.5918	0.1151	51.3731	30.2356	0.0547	0.6309	13.2183	99.2194
4 / 103 .	510	3.4504	0.0769	51.3365	30.6088	0.0601	0.5565	13.5797	99.6689
4 / 104 .	515	3.7095	0.0798	52.0041	30.1618	0.0792	0.6498	13.1779	99.8621
4 / 105 .	520	3.5805	0.0728	51.623	30.35	0.0639	0.6545	13.3984	99.7431

PD-05-02 Plagioclase (1 = Core; 2 = Rim)

Oxides Weight %

Plagioclase	Na2O	MgO	SiO2	Al2O3	K2O	FeO	CaO	Total
1 / 1 .	5.7386	0.0166	27.3937	55.5109	0.2291	0.3955	9.9242	99.2183
1 / 2 .	5.9232	0.0274	27.597	56.7402	0.2051	0.4683	9.6325	100.6231
2 / 1 .	5.8701	0.0271	27.5159	56.2876	0.1978	0.3868	9.7704	100.0737
2 / 2 .	5.6341	0.0273	27.822	55.9771	0.2082	0.3814	9.9374	100.0184
2 / 3 .	5.0241	0.0406	28.8426	53.8954	0.0979	0.3324	11.2044	99.4584
2 / 4 .	4.3741	0.0794	29.4595	52.2706	0.1119	0.7597	12.4289	99.5566
3 / 1 .	4.1867	0.0673	29.9334	51.678	0.0663	0.4841	12.9299	99.3915
4 / 1 .	5.5578	0.0249	27.5095	54.5874	0.176	0.4107	10.235	98.5171
4 / 2 .	4.0202	0.088	29.9427	51.5459	0.076	0.6219	12.9401	99.2811
5 / 1 .	3.3921	0.0529	30.8893	50.2411	0.0727	0.4168	13.9495	99.0546
5 / 2 .	3.8264	0.0995	30.1106	50.6269	0.0597	0.5883	13.2828	98.6391
6 / 1 .	5.3722	0.0904	27.7152	54.669	0.1333	0.6136	10.5444	99.2039
6 / 2 .	3.7812	0.0921	30.1796	51.2094	0.0805	0.6034	13.3535	99.3292
7 / 1 .	5.9105	0.017	27.3118	56.3305	0.2235	0.3652	9.6409	99.8052
7 / 2 .	5.9694	0.0154	27.0625	56.8381	0.2269	0.388	9.3309	99.8403
7 / 3 .	6.3013	0.0706	25.3307	59.6731	0.3614	0.6045	7.6105	99.9625
7 / 4 .	4.184	0.0733	29.7671	51.9259	0.0813	0.7412	12.6154	99.4428
8 / 1 .	5.8234	0.0272	27.4925	56.6728	0.2143	0.4086	9.6159	100.2728
8 / 2 .	5.8176	0.0326	27.688	56.3019	0.2011	0.4379	9.7989	100.3069
9 / 1 .	3.6435	0.0697	30.8941	50.8503	0.0487	0.5209	13.8578	99.9203
9 / 2 .	4.0728	0.0803	29.8771	51.1915	0.0825	0.7098	12.9942	99.0645
10 / 1 .	4.8518	0.0218	29.1958	53.7221	0.1448	0.3997	11.5325	99.8885
10 / 2 .	3.9996	0.1127	30.3365	51.7853	0.0676	0.7292	13.0286	100.0934
11 / 1 .	5.3013	0.027	28.5837	55.0058	0.1693	0.4378	10.7453	100.2968
11 / 2 .	5.6797	0.0191	27.9255	55.7251	0.2271	0.4085	10.2118	100.2278
11 / 3 .	5.7748	0.0285	27.4977	56.3731	0.1854	0.3424	9.9138	100.1597
11 / 4 .	5.4292	0.0172	28.4682	55.2892	0.1785	0.3889	10.6136	100.4009
11 / 5 .	5.6441	0.0299	28.0862	56.0742	0.1872	0.3847	10.2429	100.6786
11 / 6 .	4.4568	0.0718	29.8087	52.9488	0.0957	0.6123	12.4311	100.4656
11 / 7 .	4.0039	0.0705	30.3632	51.6463	0.0676	0.4711	13.1626	99.8239
11 / 8 .	4.0628	0.0729	30.3644	52.2565	0.0774	0.4831	12.8169	100.1668
11 / 9 .	4.5715	0.0669	29.7412	53.1057	0.1049	0.5287	12.221	100.3796
11 / 10 .	3.7337	0.09	30.7112	50.9546	0.0707	0.7487	13.6753	100.0346
12 / 1 .	4.2099	0.054	30.2674	51.9368	0.0806	0.4928	12.9727	100.0568
12 / 2 .	4.6924	0.0894	29.0941	53.3946	0.1159	0.815	12.0413	100.3104

13 / 1 .	5.8997	0.0202	27.4593	56.9867	0.2268	0.4152	9.5501	100.5728
13 / 2 .	3.592	0.0741	30.5898	50.8889	0.0883	0.7932	13.3277	99.4062
14 / 1 .	6.1427	0.0234	26.6	57.4771	0.2567	0.3653	8.8099	99.6925
14 / 2 .	3.9064	0.0773	30.1973	51.8433	0.108	0.6882	12.6243	99.4935
15 / 1 .	6.0252	0.0296	27.2176	57.3038	0.2151	0.4207	9.3909	100.6276
15 / 3 .	5.3273	0.031	28.4016	55.1348	0.1792	0.4693	10.5894	100.1453
15 / 4 .	3.8108	0.0945	30.3063	51.4642	0.0533	0.6024	13.3706	99.7555
16 / 1 .	4.1227	0.0217	28.0118	50.0131	0.1453	0.4149	11.626	94.3678
16 / 2 .	5.5188	0.0257	27.8616	56.1526	0.1722	0.4011	10.0289	100.1976
16 / 3 .	5.6477	0.0228	27.3612	56.1947	0.1985	0.4228	9.7431	99.6082
16 / 4 .	3.836	0.0897	30.5572	51.3829	0.0792	0.597	13.4792	100.0682
17 / 1 .	5.6591	0.0184	27.7536	55.8104	0.1944	0.3879	10.2004	100.0503
17 / 2 .	3.5999	0.0723	30.9586	50.6144	0.0642	0.6208	13.8126	99.7788
18 / 1 .	6.2483	0.0133	26.6135	58.1856	0.2746	0.348	8.766	100.4532
19 / 1 .	5.8499	0.0271	27.4151	56.5659	0.2105	0.3772	9.4754	99.9235
19 / 2 .	4.3248	0.0803	29.8556	52.2608	0.1093	0.774	12.5945	100.0523
20 / 1 .	5.3778	0.0197	28.6332	55.221	0.166	0.4194	10.7634	100.6207
20 / 2 .	3.6061	0.0877	31.0048	51.1978	0.0649	0.7075	13.9712	100.6818
21 / 1 .	5.6577	0.017	28.2072	55.8385	0.2003	0.3489	10.1678	100.4506
22 / 1 .	5.4477	0.0179	28.3234	55.195	0.1674	0.427	10.6396	100.244
22 / 2 .	3.7562	0.0737	30.778	51.0944	0.0682	0.5774	13.5666	99.9596
23 / 1 .	3.7012	0.0296	30.8606	50.8457	0.0805	0.4495	13.4517	99.435
23 / 2 .	4.0449	0.1065	30.1011	51.8062	0.0884	0.6339	12.9447	99.7811
24 / 1 .	5.3626	0.0312	28.0824	54.9611	0.155	0.3978	10.5011	99.5217
24 / 2 .	3.8638	0.0932	30.0964	51.1093	0.089	0.7131	13.1829	99.1869
25 / 1 .	5.4822	0.0177	28.5932	56.0271	0.1689	0.3423	10.3335	100.9839
25 / 2 .	5.072	0.1038	28.619	54.3357	0.1494	1.003	11.2106	100.5704
26 / 1 .	3.8265	0.0592	30.9627	51.375	0.0526	0.4462	13.5595	100.3538
26 / 2 .	4.154	0.0883	30.4464	52.1488	0.1086	0.6524	13.1904	100.828
27 / 1 .	4.1839	0.0317	29.9092	52.6788	0.1237	0.5376	12.6797	100.172
27 / 2 .	4.2917	0.1023	29.8836	52.2996	0.0918	0.7393	12.4408	99.9103

PD-05-02 Plagioclase 1 and 3 Transects

		Oxides Weight %							
Plagioclase	**Location (um)**	**Na2O**	**MgO**	**SiO2**	**Al2O3**	**K2O**	**FeO**	**CaO**	**Total**
1 / 1 .	0	4.983	0.0189	54.9199	27.8302	0.2038	0.3468	10.2957	98.5983
1 / 2 .	5	4.894	0.0306	54.7798	28.2097	0.1899	0.4116	10.5809	99.0965
1 / 5 .	20	4.9864	0.0162	55.0258	28.0546	0.1983	0.3942	10.3305	99.0059
1 / 6 .	25	4.7168	0.0243	54.3466	28.585	0.1702	0.4431	10.8608	99.1469
1 / 7 .	30	4.5835	0.0135	54.4219	28.4807	0.1712	0.3672	10.9798	99.0178
1 / 8 .	35	4.6628	0.0289	54.4012	28.7356	0.1612	0.3308	11.0769	99.3973
1 / 9 .	40	4.5906	0.0152	54.1844	28.7694	0.1615	0.4589	11.1239	99.3038
1 / 10 .	45	4.6056	0.0332	53.9722	28.6642	0.1692	0.3308	11.0021	98.7774
1 / 11 .	50	4.7059	0.0297	53.882	28.3384	0.1693	0.3785	10.9972	98.5009
1 / 12 .	55	4.7041	0.0213	54.3324	28.4638	0.1632	0.4289	10.9202	99.0338
1 / 13 .	60	4.6112	0.0245	54.3609	28.2827	0.1581	0.372	10.9516	98.7609
1 / 14 .	65	4.648	0.0105	54.391	28.445	0.1565	0.3941	10.8572	98.9022
1 / 15 .	70	4.6758	0.0265	53.928	28.8307	0.1592	0.4114	11.1788	99.2105
1 / 16 .	75	4.5961	0.0216	54.0816	28.734	0.1743	0.3767	11.0615	99.0458

1 / 17 .	80	4.6239	0.0174	54.2689	28.7019	0.1587	0.3577	10.9657	99.0941
1 / 18 .	85	4.7067	0.028	54.1777	28.6295	0.1743	0.3783	11.0113	99.1059
1 / 19 .	90	4.6803	0.0196	54.455	28.4144	0.1776	0.353	10.8855	98.9854
1 / 21 .	100	4.7808	0.0297	54.4644	28.4207	0.1828	0.3309	10.6175	98.8268
1 / 22 .	105	4.7763	0.0275	54.3346	28.2083	0.1854	0.3941	10.6436	98.5697
1 / 23 .	110	4.8992	0.0179	54.8768	27.9967	0.1672	0.3847	10.4702	98.8127
1 / 25 .	120	5.1025	0.0203	55.1331	27.8907	0.185	0.3388	10.1427	98.813
1 / 26 .	125	5.0079	0.0127	55.2892	27.6803	0.1805	0.4227	10.0672	98.6606
1 / 27 .	130	4.9178	0.0269	54.6518	28.1414	0.1868	0.4511	10.3442	98.72
1 / 28 .	135	4.0947	0.0214	52.7301	29.5112	0.1257	0.326	12.0543	98.8634
1 / 30 .	145	4.5135	0.0128	53.8958	28.864	0.1446	0.3862	11.1307	98.9476
1 / 31 .	150	5.0992	0.0222	55.4032	27.662	0.2036	0.3278	10.1008	98.8188
1 / 32 .	155	5.3061	0.014	55.898	27.6819	0.209	0.3215	9.5986	99.0291
1 / 33 .	160	5.1608	0.02	55.4447	27.5016	0.2108	0.4259	9.7653	98.5289
1 / 34 .	165	4.9608	0.0372	55.2168	27.8137	0.1837	0.3214	10.1309	98.6644
1 / 35 .	170	4.9693	0.0259	54.9206	28.0554	0.1915	0.3895	10.4855	99.0377
1 / 36 .	175	4.9965	0.0223	55.6213	28.7161	0.1928	0.41	10.7307	100.69
1 / 37 .	180	4.7043	0.025	54.1813	28.6534	0.1702	0.3926	10.906	99.0328
1 / 38 .	185	4.7576	0.0213	54.6149	28.3543	0.1687	0.3372	10.7301	98.9841
1 / 39 .	190	4.9676	0.0142	54.983	27.7298	0.1561	0.3515	10.2492	98.4514
1 / 40 .	195	5.1028	0.0134	55.7925	27.784	0.177	0.3563	9.9987	99.2246
1 / 42 .	205	5.2112	0.0289	55.6016	27.5153	0.2053	0.3626	9.8601	98.785
1 / 43 .	210	5.1856	0.0249	55.6751	27.6572	0.2088	0.3895	9.9017	99.0427
1 / 44 .	215	4.5502	0.0174	53.728	28.8761	0.1695	0.3704	11.1882	98.8997
1 / 45 .	220	4.4983	0.0206	53.6683	28.7983	0.1583	0.3704	11.1834	98.6977
1 / 46 .	225	4.9839	0.0296	54.8	28.0314	0.1705	0.3879	10.3009	98.7042
1 / 47 .	230	5.0517	0.0266	55.1503	27.984	0.1721	0.3911	10.1843	98.96
1 / 48 .	235	4.989	0.0171	55.0144	27.9291	0.1775	0.4069	10.2651	98.7992
1 / 49 .	240	4.7437	0.0245	54.2454	27.9657	0.1512	0.4417	10.4198	97.9919
1 / 50 .	245	4.894	0.023	55.2399	28.6192	0.1636	0.3831	10.8066	100.129
1 / 51 .	250	5.0326	0.0227	55.1464	27.8043	0.1795	0.4006	10.1596	98.7458
1 / 52 .	255	5.1923	0.0373	55.3694	27.626	0.1992	0.4591	9.8925	98.7757
1 / 53 .	260	5.1923	0.0369	55.8161	27.5098	0.1835	0.5224	9.6483	98.9094
1 / 54 .	265	4.3375	0.0339	53.9302	28.9841	0.1375	0.4891	11.3813	99.2934
1 / 55 .	270	3.5827	0.0543	51.6439	30.4179	0.0812	0.5378	13.2318	99.5495
1 / 56 .	275	3.6184	0.0523	51.331	30.1767	0.0799	0.5884	13.0493	98.896
1 / 57 .	280	3.7337	0.0555	51.4451	29.9645	0.0844	0.5252	12.8125	98.6209
1 / 58 .	285	3.8234	0.0604	51.9799	29.6741	0.0685	0.5553	12.441	98.6026
1 / 60 .	295	3.5544	0.0886	51.4511	30.1787	0.0761	0.492	13.0837	98.9245
1 / 61 .	300	3.5372	0.0905	51.2419	30.1935	0.0617	0.5805	13.1795	98.8848
1 / 63 .	*310*	*3.0021*	*0.0847*	*50.0538*	*31.283*	*0.0457*	*0.585*	*14.2734*	*99.3278*
1 / 64 .	315	3.1471	0.0868	50.5241	30.9518	0.0623	0.5866	14.0135	99.3721
1 / 65 .	320	3.0481	0.097	50.0541	30.9455	0.0537	0.5866	14.0746	98.8597
1 / 66 .	325	3.2075	0.0763	50.6221	30.7158	0.068	0.6657	13.919	99.2743
1 / 67 .	330	3.5029	0.0887	51.1137	30.2821	0.0875	0.6942	13.2002	98.9693
1 / 68 .	335	4.6941	0.1111	54.102	27.9097	0.1497	0.9761	10.7723	98.7149
3 / 1 .	0	5.372	0.0207	56.0352	27.3754	0.2399	0.4419	9.3267	98.8117
3 / 2 .	5	5.4258	0.0261	56.2712	27.2713	0.2274	0.4498	9.3935	99.065

3 / 3 .	10	5.4174	0.0302	56.6359	27.1476	0.2207	0.4039	9.3785	99.2342
3 / 4 .	15	5.4143	0.0151	56.2099	27.3009	0.23	0.3453	9.3818	98.8974
3 / 6 .	25	5.409	0.0329	56.3653	27.2788	0.2126	0.3849	9.4153	99.0987
3 / 7 .	30	5.462	0.0319	55.9863	27.1754	0.2215	0.3881	9.5746	98.8397
3 / 8 .	35	5.3578	0.0169	55.9604	27.268	0.2241	0.3722	9.5173	98.7167
3 / 9 .	40	5.3683	0.0295	56.1066	27.512	0.2151	0.3659	9.5467	99.1441
3 / 10 .	45	5.3587	0.0119	55.7716	27.3861	0.2209	0.4086	9.5286	98.6865
3 / 11 .	50	5.2443	0.0264	55.8549	27.4686	0.2218	0.3501	9.6897	98.8558
3 / 13 .	60	4.7914	0.0258	54.5162	28.2727	0.1631	0.293	10.5732	98.6354
3 / 14 .	65	4.4716	0.0229	53.7534	28.7487	0.1615	0.3974	11.2805	98.836
3 / 15 .	70	3.9674	0.0236	52.3872	29.9044	0.1295	0.4526	12.4249	99.2896
3 / 16 .	75	4.1318	0.0222	52.8065	29.5323	0.1363	0.4036	12.1397	99.1724
3 / 17 .	80	3.9226	0.017	51.9756	29.8888	0.1247	0.3482	12.4865	98.7633
3 / 18 .	85	4.3786	0.014	53.1484	29.1195	0.1473	0.3736	11.5425	98.7239
3 / 19 .	90	4.5346	0.0167	53.9472	28.8261	0.1712	0.3816	11.1553	99.0326
3 / 20 .	95	4.6358	0.0174	53.8794	28.6576	0.1776	0.4148	11.0193	98.802
3 / 21 .	100	4.7481	0.0262	54.3861	28.4556	0.1629	0.3863	10.8683	99.0336
3 / 22 .	105	4.6515	0.0164	54.1337	28.7133	0.1558	0.4417	11.1526	99.265
3 / 23 .	110	4.5319	0.0184	53.5462	28.686	0.1659	0.4702	11.2931	98.7118
3 / 24 .	115	4.461	0.0292	53.6165	28.8107	0.1618	0.4148	11.3363	98.8304
3 / 25 .	120	4.4453	0.0218	53.5789	29.1223	0.1352	0.4226	11.3552	99.0812
3 / 26 .	125	4.478	0.0192	53.4695	28.9043	0.18	0.4496	11.4198	98.9204
3 / 27 .	130	4.5409	0.0243	53.8149	28.6897	0.1705	0.4211	11.2395	98.9009
3 / 28 .	135	4.482	0.0358	53.5294	28.972	0.1589	0.4591	11.3321	98.9693
3 / 29 .	140	4.3661	0.0236	53.2539	29.3139	0.1339	0.478	11.5702	99.1395
3 / 30 .	145	4.1002	0.0263	52.8559	29.3656	0.1421	0.323	12.0226	98.8356
3 / 32 .	155	3.9184	0.019	52.3852	29.8312	0.1171	0.3625	12.4477	99.081
3 / 33 .	160	3.959	0.0212	51.9331	29.6284	0.1269	0.4146	12.4416	98.5248
3 / 34 .	165	3.931	0.0232	52.207	29.5499	0.1369	0.3783	12.3423	98.5686
3 / 35 .	170	3.9754	0.0172	52.1139	29.6286	0.1295	0.4146	12.3161	98.5953
3 / 37 .	180	4.0238	0.0298	52.6269	29.8643	0.1203	0.3546	12.1979	99.2175
3 / 38 .	185	4.1372	0.0261	52.9811	29.64	0.1367	0.4337	11.9281	99.2829
3 / 39 .	190	4.2089	0.0277	52.9243	29.3489	0.1376	0.4922	11.9255	99.065
3 / 40 .	195	4.2698	0.0223	53.1506	29.3482	0.1325	0.4226	11.8659	99.2119
3 / 41 .	200	4.2665	0.0219	53.145	29.2706	0.1339	0.4005	11.717	98.9554
3 / 42 .	205	4.3071	0.0229	53.3018	29.2694	0.1511	0.4654	11.6934	99.2112
3 / 43 .	210	4.3167	0.0211	53.583	29.426	0.1345	0.4511	11.7607	99.6931
3 / 44 .	215	4.3372	0.0185	53.2722	29.2784	0.1502	0.4052	11.7234	99.1851
3 / 45 .	220	5.4839	0.0075	53.3176	28.4217	0.1632	0.3974	10.7293	98.5207
3 / 46 .	225	4.2383	0.0155	53.2522	29.3868	0.1409	0.4116	11.7238	99.1691
3 / 47 .	230	4.2088	0.0337	53.0783	29.3958	0.1562	0.5224	11.774	99.1691
3 / 48 .	235	4.184	0.027	52.9596	29.1792	0.1306	0.4654	11.8266	98.7723
3 / 49 .	240	4.2961	0.0231	53.258	29.3259	0.1469	0.448	11.7652	99.2632
3 / 50 .	245	4.3231	0.0256	53.5492	29.0909	0.1272	0.5002	11.574	99.1903
3 / 51 .	250	4.3928	0.0089	53.4153	28.9812	0.1499	0.4686	11.3949	98.8118
3 / 52 .	255	4.4106	0.0241	53.3954	28.9654	0.1477	0.4101	11.5057	98.859
3 / 53 .	260	4.4516	0.017	54.1929	29.0025	0.1599	0.4401	11.3972	99.6613
3 / 54 .	265	4.5882	0.0301	54.0534	28.7497	0.1605	0.4227	11.2942	99.2987
3 / 55 .	270	4.7252	0.0397	54.367	28.4653	0.1951	0.3785	10.6806	98.8514

3 / 56 .	275	4.935	0.0282	55.0539	27.8716	0.1766	0.3706	10.4173	98.8533
3 / 57 .	280	5.0048	0.0357	55.2131	28.103	0.1991	0.3849	10.2603	99.2009
3 / 58 .	285	5.1752	0.0137	55.5787	27.7351	0.1925	0.4483	10.0373	99.1808
3 / 59 .	290	5.1378	0.0307	55.6153	27.601	0.2044	0.4673	9.8707	98.927
3 / 60 .	295	5.18	0.0269	55.6929	27.6119	0.1935	0.3121	9.8685	98.8859
3 / 61 .	300	5.2482	0.0224	55.5804	27.6167	0.2147	0.4625	9.833	98.9778
3 / 62 .	305	5.2892	0.0239	55.894	27.4592	0.2218	0.461	9.7118	99.0609
3 / 63 .	310	5.4016	0.017	56.055	27.393	0.229	0.3834	9.5973	99.0762
3 / 64 .	315	5.3807	0.0212	56.2278	27.3935	0.229	0.4056	9.5566	99.2143
3 / 65 .	320	5.3712	0.0336	56.0429	27.2673	0.2168	0.4262	9.527	98.8849
3 / 66 .	325	5.3919	0.0254	55.9852	27.2729	0.2307	0.3248	9.3897	98.6206
3 / 67 .	330	5.5535	0.0259	56.565	27.036	0.2331	0.3724	9.0875	98.8733
3 / 68 .	335	5.6091	0.0216	56.7171	26.7272	0.2479	0.3771	9.023	98.7231
3 / 69 .	340	5.5329	0.0659	64.9629	21.5768	1.0305	0.6886	5.2324	99.0901
3 / 70 .	345	5.5949	0.0056	57.0173	26.8532	0.2371	0.4801	8.903	99.0911
3 / 71 .	350	5.6528	0.0338	57.1984	26.6653	0.2706	0.458	8.7991	99.0779
3 / 74 .	365	5.5567	0.0182	56.6428	27.0639	0.2392	0.4722	9.0313	99.0241
3 / 75 .	370	5.3514	0.0324	56.1897	27.5535	0.2206	0.4182	9.6614	99.4272
3 / 76 .	375	5.1605	0.0263	55.6172	27.6272	0.2031	0.4736	9.9784	99.0863
3 / 77 .	380	5.0629	0.0349	55.5013	27.9782	0.1892	0.4214	10.1303	99.3181
3 / 78 .	385	5.237	0.0207	55.6603	27.4243	0.1935	0.3359	9.8866	98.7583
3 / 79 .	390	5.3891	0.0297	56.0264	27.5228	0.2017	0.4167	9.613	99.1993
3 / 80 .	395	5.358	0.0395	56.1708	27.258	0.2245	0.4151	9.5231	98.9889
3 / 82 .	405	5.4253	0.0241	56.6949	27.3783	0.2249	0.4674	9.4209	99.6357
3 / 83 .	410	5.449	0.021	56.3053	27.3813	0.2059	0.4183	9.4943	99.2752
3 / 85 .	420	5.346	0.0297	55.9997	27.4919	0.2181	0.4103	9.5791	99.0747
3 / 86 .	425	5.3161	0.0336	55.7458	27.421	0.2068	0.4832	9.4852	98.6917
3 / 87 .	430	5.3223	0.0117	56.0087	27.2563	0.2068	0.442	9.5825	98.8303
3 / 88 .	435	5.3152	0.0242	55.7433	27.4266	0.201	0.4183	9.5766	98.7052
3 / 89 .	440	5.3615	0.0337	55.9444	27.5688	0.2257	0.4594	9.6748	99.2683
3 / 90 .	445	5.2991	0.0173	56.1132	27.476	0.2171	0.3945	9.6464	99.1636
3 / 91 .	450	5.3092	0.0342	55.7845	27.4006	0.2171	0.404	9.5817	98.7314
3 / 92 .	455	5.3706	0.0214	56.2423	27.3724	0.2145	0.3724	9.6873	99.2808
3 / 93 .	460	5.304	0.03	56.4081	27.6818	0.2177	0.423	9.6499	99.7145
3 / 94 .	465	5.3617	0.0154	56.1915	27.2962	0.2389	0.3629	9.6489	99.1155
3 / 95 .	470	5.3254	0.0163	56.1079	27.5325	0.1991	0.3961	9.6798	99.257
3 / 96 .	475	5.388	0.03	56.1908	27.1963	0.2268	0.4215	9.5366	98.9901
3 / 97 .	480	5.3807	0.0215	56.2779	27.0286	0.2136	0.4294	9.4776	98.8294
3 / 98 .	485	5.3146	0.0159	55.8929	27.2644	0.2149	0.4516	9.607	98.7613
3 / 99 .	490	5.216	0.0195	55.9254	27.4173	0.2057	0.431	9.8576	99.0724
3 / 100 .	495	5.1129	0.0083	55.4672	27.668	0.2214	0.4689	9.9296	98.8764
3 / 101 .	500	5.1461	0.0203	55.6519	27.9344	0.1883	0.4088	10.0829	99.4327
3 / 102 .	505	5.0967	0.0279	55.562	27.7328	0.2067	0.4072	9.9735	99.0067
3 / 103 .	510	5.226	0.0225	55.8165	27.6167	0.1907	0.366	9.8712	99.1096
3 / 104 .	515	5.3141	0.0356	55.9948	27.2809	0.1908	0.3787	9.6116	98.8065
3 / 105 .	520	5.3501	0.0203	56.1982	27.4847	0.194	0.393	9.5186	99.1588
3 / 106 .	525	5.5091	0.029	56.7272	27.0888	0.225	0.3645	9.3548	99.2984
3 / 107 .	530	5.5883	0.0236	56.6473	26.8846	0.2305	0.4057	9.1657	98.9458
3 / 108 .	535	5.5952	0.0122	56.7327	27.1467	0.2334	0.4453	9.0933	99.2587

3 / 109 .	540	5.5904	0.0239	56.4802	26.9476	0.2473	0.4153	9.0823	98.787
3 / 111 .	550	5.8192	0.0374	57.5372	26.6545	0.2598	0.3424	8.6638	99.3142
3 / 112 .	555	5.8685	0.0267	57.7678	26.6247	0.2593	0.3392	8.3958	99.282
3 / 113 .	560	5.9233	0.027	57.9239	26.155	0.3035	0.4042	8.3186	99.0555
3 / 114 .	565	5.744	0.0316	57.1896	26.7769	0.2816	0.4311	8.7551	99.2099
3 / 115 .	570	5.0103	0.0223	55.4365	28.0723	0.1873	0.4468	10.2183	99.3938
3 / 116 .	575	4.9646	0.0189	55.1949	28.0529	0.1917	0.3913	10.3932	99.2077
3 / 117 .	580	4.999	0.0244	55.4327	27.8825	0.1857	0.4563	10.2565	99.237
3 / 118 .	585	5.1445	0.0276	55.6611	27.8013	0.2198	0.3993	10.058	99.3115
3 / 119 .	590	5.245	0.0122	55.6841	27.4849	0.1971	0.374	9.8512	98.8485
3 / 120 .	595	5.1801	0.0296	56.0135	27.6766	0.1978	0.3297	9.8023	99.2295
3 / 121 .	600	5.204	0.0263	56.0968	27.52	0.2103	0.3914	9.8127	99.2615
3 / 122 .	605	5.148	0.022	55.6818	27.8834	0.2183	0.3882	9.8676	99.2093
3 / 123 .	610	4.9084	0.0159	55.3202	28.223	0.1917	0.3739	10.4712	99.5043
3 / 124 .	615	4.8043	0.0154	55.002	28.3846	0.1996	0.3596	10.6785	99.4441
3 / 125 .	620	4.3415	0.0083	53.4557	29.3238	0.1464	0.4133	11.6041	99.2931
3 / 126 .	625	3.5271	0.0173	51.8371	30.506	0.1134	0.38	13.15	99.5309
3 / 127 .	630	3.784	0.023	52.6183	30.0885	0.1104	0.3768	12.6801	99.6812
3 / 128 .	635	4.4231	0.0218	53.683	29.1269	0.1407	0.3928	11.4636	99.2519
3 / 129 .	640	4.5115	0.0329	53.9167	28.918	0.1625	0.4197	11.3989	99.3603
3 / 130 .	645	4.6702	0.0284	53.941	28.5367	0.1774	0.3928	10.9987	98.7451
3 / 131 .	650	4.7576	0.033	54.8398	28.4199	0.1829	0.3992	10.8357	99.4681
3 / 132 .	655	4.9876	0.0181	55.5311	27.9577	0.178	0.4278	10.4016	99.5019
3 / 134 .	665	5.0272	0.0396	55.332	27.8387	0.1822	0.3613	10.1964	98.9775
3 / 135 .	670	4.8879	0.0394	55.4949	28.1989	0.1786	0.4024	10.5542	99.7562
3 / 136 .	675	4.8019	0.0367	54.8948	28.3242	0.1509	0.3897	10.7383	99.3365
3 / 137 .	680	4.93	0.0367	55.0492	28.0543	0.1741	0.4262	10.5279	99.1984
3 / 138 .	685	5.0027	0.035	55.4394	27.6181	0.186	0.4151	10.2118	98.9082
3 / 139 .	690	5.2259	0.0525	56.1687	27.5975	0.1842	0.4991	9.9294	99.6574
3 / 140 .	695	5.2294	0.0605	55.848	27.4672	0.1981	0.3566	9.8124	98.9722
3 / 141 .	700	5.2021	0.0432	55.9178	27.6333	0.1942	0.3376	9.9535	99.2817
3 / 146 .	725	3.0623	0.0549	50.6331	31.305	0.0861	0.6345	14.1579	99.9337
3 / 147 .	730	3.2688	0.0406	50.9705	31.174	0.1123	0.5634	13.6731	99.8027
3 / 148 .	735	3.4987	0.0697	51.1326	30.5378	0.0904	0.6188	13.4807	99.4287
3 / 149 .	740	3.7303	0.0893	52.2087	30.0672	0.1042	0.6933	12.9412	99.8343
3 / 150 .	745	3.3301	0.1033	51.3739	30.6788	0.0713	0.5192	13.5111	99.5878
3 / 151 .	750	3.3468	0.0994	50.9867	30.7511	0.0678	0.6298	13.6867	99.5682
3 / 152 .	755	3.0934	0.0861	50.3364	31.2654	0.0629	0.6013	14.0932	99.5388
3 / 153 .	760	3.409	0.0835	50.9433	30.2695	0.0824	0.6061	13.536	98.9298
3 / 154 .	765	4.3735	0.0923	53.3955	28.7454	0.1214	0.8564	11.6465	99.231

PD-05-03 Plagioclase (1 = Core; 2 = Rim)

Plagioclase	Oxides Weight %							
	Na2O	MgO	SiO2	Al2O3	K2O	FeO	CaO	Total
1 / 1 .	5.7408	-0.0012	27.4995	55.968	0.1659	0.1783	9.4745	99.0394
1 / 2 .	5.413	-0.0044	28.4292	55.6379	0.1741	0.2	10.368	100.2222
1 / 3 .	5.4138	0.0047	28.2508	55.2268	0.152	0.0946	10.186	99.3524
1 / 5 .	5.2994	0.0044	28.6234	55.7195	0.1604	0.1511	10.4231	100.3937
1 / 6 .	5.4018	0.0016	28.7828	55.1763	0.1453	0.1511	10.5346	100.1992
1 / 7 .	5.8579	-0.0033	27.2683	56.4721	0.1909	0.1816	9.3872	99.3799
1 / 8 .	6.2791	-0.0014	26.9291	57.1066	0.1819	0.1468	8.8997	99.5724
1 / 9 .	6.4579	-0.0018	26.8542	57.9335	0.2557	0.1197	8.622	100.2575
1 / 10 .	5.6736	0.0048	28.1477	55.9372	0.1966	0.1642	9.9015	100.0438
1 / 11 .	6.0721	0.0036	27.3108	57.1586	0.2101	0.1284	9.1999	100.1085
1 / 12 .	5.8945	0.0081	27.6813	56.638	0.1889	0.1501	9.7249	100.3046
1 / 13 .	4.9731	0.0576	28.7061	54.1595	0.1235	0.2315	10.9573	99.246
1 / 14 .	3.5758	0.7097	27.9831	54.3307	0.2513	1.2145	12.1926	100.4896
1 / 15 .	3.7355	0.1068	30.5214	51.4416	0.0702	0.6307	13.2466	99.8021
2 / 1 .	3.6875	0.0871	29.7808	50.823	0.054	0.5375	13.0436	98.0518
2 / 2 .	2.4011	0.0486	33.028	48.0125	0.0252	0.5381	15.9656	100.0452
3 / 1 .	5.4164	0.0132	28.0639	55.448	0.2036	0.4174	10.2748	99.8516
3 / 2 .	3.8545	0.1136	30.3021	51.6746	0.0397	0.569	13.2014	99.7926
4 / 1 .	3.4604	0.086	31.2027	50.5098	0.0539	0.5146	13.9665	99.8342
4 / 2 .	3.4811	0.0955	30.8943	50.6905	0.0325	0.6188	13.7584	99.6081
5 / 1 .	6.035	0.0186	27.0453	57.7994	0.2298	0.2947	9.0845	100.5301
5 / 2 .	5.9651	0.0131	27.3424	57.4181	0.2422	0.2447	9.2815	100.5288
5 / 3 .	3.246	0.0901	31.4937	50.4504	0.0493	0.5873	14.3596	100.317
5 / 4 .	2.8656	0.0866	31.8528	49.5401	0.0498	0.5969	15.1839	100.2105
6 / 1 .	5.5641	0.026	27.4195	55.9878	0.2038	0.4305	9.726	99.3715
7 / 1 .	5.5177	0.0241	28.1155	56.1841	0.1676	0.3522	10.3453	100.7269
7 / 2 .	3.7576	0.0892	30.9209	51.4645	0.05	0.5082	13.6471	100.472
8 / 1 .	5.4647	0.0565	28.0404	55.739	0.1277	0.3838	10.1959	100.0311
8 / 2 .	4.1964	0.1113	30.0579	52.5772	0.0533	0.7416	12.8893	100.6939
9 / 1 .	3.5478	0.0607	30.9802	50.6155	0.072	0.494	13.9357	99.7457
9 / 2 .	4.7222	0.1222	28.5891	53.9004	0.1109	0.781	11.5913	99.8773
10 / 1 .	3.3975	0.1328	30.8207	50.2232	0.0902	0.5842	13.9807	99.2736
10 / 2 .	3.5668	0.0974	30.9924	50.9732	0.0675	0.5679	13.8733	100.1854
11 / 1 .	4.7148	0.0488	29.4219	53.9204	0.0496	0.5866	11.7993	100.5858
11 / 2 .	4.0228	0.1143	30.0382	51.8611	0.0813	0.6766	12.8569	99.7082
12 / 1 .	3.852	0.1005	30.5868	51.1446	0.0721	0.6959	13.6104	100.1109
12 / 2 .	5.4499	0.198	27.4925	55.4021	0.1687	0.8712	10.3668	100.059
13 / 1 .	5.1496	0.0516	28.5592	55.4202	0.1046	0.4337	10.8632	100.6021
13 / 2 .	3.8446	0.0794	30.8384	51.4686	0.0559	0.5407	13.4568	100.3293
13 / 3 .	3.8582	0.0919	30.622	51.7024	0.0546	0.618	13.331	100.3248
14 / 1 .	3.7748	0.0882	31.0235	51.2005	0.0383	0.5527	13.5538	100.2778
14 / 2 .	3.6849	0.1062	31.0562	51.2802	0.0578	0.6384	13.7586	100.6249

15 / 1 .	3.5715	0.9462	30.1434	51.3905	0.0766	1.056	13.3089	100.5385
15 / 2 .	3.3542	0.0922	31.8611	50.7414	0.0597	0.57	14.2423	100.9583
16 / 1 .	3.3402	0.0754	31.6798	50.0413	0.0564	0.5624	14.4317	100.2221
16 / 2 .	3.2462	0.1004	31.5707	49.9966	0.0382	0.6578	14.5631	100.203
17 / 1 .	3.5772	1.0421	27.2323	52.165	0.2015	2.7526	12.9404	100.3883
17 / 2 .	3.3037	0.0813	31.4313	50.5299	0.0409	0.5656	14.1404	100.1247
18 / 1 .	4.6194	0.0505	29.9581	53.6171	0.0809	0.4541	12.1325	100.9471
18 / 2 .	3.8751	0.1091	30.7718	51.5393	0.0396	0.6384	13.3696	100.3805

PD-05-04 Plagioclase (1 = Core; 2 = Rim)

	Oxides Weight %							
Plagioclase	Na2O	MgO	SiO2	Al2O3	K2O	FeO	CaO	Total
1 / 1 .	3.2964	0.0867	31.031	50.1387	0.0292	0.5723	14.2034	99.4005
1 / 6 .	5.9231	0.468	24.7648	58.1619	0.2679	1.227	8.4706	99.4374
1 / 8 .	6.1545	0.0945	25.8389	59.0079	0.2582	1.0304	8.4846	101.0066
2 / 1 .	3.7321	0.0896	30.6998	51.2305	0.0611	0.607	13.5373	100.0068
2 / 2 .	4.6629	0.1102	28.7295	53.7738	0.105	0.8549	11.6714	99.9826
3 / 1 .	4.106	0.1158	30.1054	52.2722	0.0651	0.6604	12.9113	100.3021
3 / 2 .	4.9299	0.1007	28.2454	55.199	0.1189	0.778	11.0634	100.4994
4 / 1 .	5.4902	0.0164	27.9677	56.1486	0.2694	0.348	9.9217	100.1926
4 / 2 .	5.7222	0.0137	27.4705	56.6688	0.2407	0.3121	9.5519	100.0017
4 / 3 .	6.3412	0.015	26.4089	58.2046	0.2966	0.3449	8.3899	100.0134
4 / 4 .	3.5576	0.1007	30.5079	50.8791	0.0701	0.6363	13.5736	99.3776
5 / 1 .	3.5895	0.0967	30.6189	51.0787	0.0585	0.6038	13.5695	99.6558
5 / 2 .	4.1321	0.1104	29.7563	52.2718	0.0657	0.7071	12.5832	99.7022
6 / 1 .	3.4537	0.0906	31.0911	50.4962	0.0513	0.5191	13.9997	99.7411
6 / 2 .	4.3681	0.1009	29.7817	52.8467	0.0677	0.7451	12.5083	100.4838
7 / 2 .	4.4262	0.1208	29.3499	53.0287	0.0704	0.7462	12.3075	100.1213
8 / 1 .	4.3134	0.0489	30.0755	52.4149	0.0664	0.414	12.672	100.0317
8 / 2 .	4.3884	0.0329	29.9631	52.4025	0.0593	0.3521	12.4425	99.6746
9 / 1 .	3.754	0.0944	30.7623	51.1625	0.0877	0.6277	13.6652	100.2046
9 / 2 .	3.7996	0.0972	30.6562	51.7911	0.0748	0.6344	13.4417	100.5402
10 / 1 .	3.5425	0.1068	30.4505	50.4164	0.052	0.6115	13.4363	98.6721
10 / 2 .	5.1638	0.1051	27.9265	54.5483	0.1568	0.8484	10.8554	99.6937
11 / 1 .	3.8938	0.1063	31.0822	52.166	0.0501	0.5691	13.4545	101.3678
11 / 2 .	4.1703	0.1091	29.5981	52.9084	0.0768	0.7095	12.6627	100.297
12 / 1 .	3.7721	0.0815	30.6882	51.2391	0.0643	0.4888	13.4023	99.7712
12 / 2 .	3.5475	0.0971	30.6804	50.6263	0.0344	0.6277	13.7115	99.3616
13 / 1 .	3.6711	0.0382	30.8718	50.8219	0.0312	0.5235	13.6361	99.6367
13 / 2 .	4.7498	0.1156	28.5944	53.5259	0.09	0.8201	11.7322	99.7052
14 / 1 .	3.7535	0.1015	30.6367	51.1973	0.0669	0.5279	13.4564	99.7801
14 / 2 .	4.3884	0.1039	29.246	52.5363	0.0886	0.6931	12.1354	99.2385
15 / 1 .	3.9684	0.094	30.3258	51.7332	0.0637	0.5355	13.296	100.0714
15 / 2 .	5.4759	0.8663	26.0986	56.4027	0.1958	1.2604	9.7058	100.1475
16 / 1 .	3.9063	0.0563	30.5659	51.9682	0.0533	0.5106	13.1996	100.302
16 / 2 .	3.5092	0.1036	30.6158	50.9339	0.0468	0.6365	13.8293	99.7096
17 / 1 .	5.2226	0.0205	28.2392	55.5265	0.1669	0.3545	10.5989	100.1496
18 / 2 .	3.7483	0.094	30.7107	51.1936	0.052	0.6494	13.4587	99.9592
19 / 1 .	5.5864	0.0277	27.7003	56.3874	0.2097	0.4285	10.053	100.4119

19 / 2 .	3.253	0.0927	31.3259	49.8756	0.048	0.5212	14.5065	99.6745
20 / 1 .	3.0769	0.0909	31.3911	50.2189	0.0745	0.6341	14.7414	100.2749
20 / 2 .	5.2238	2.0614	18.8042	56.3407	0.4697	9.4961	7.6566	101.5975
21 / 1 .	3.6172	0.086	30.9496	50.9649	0.0708	0.5833	13.891	100.2
21 / 2 .	3.9646	0.1163	30.4169	51.4618	0.065	0.9878	13.227	100.2756
22 / 1 .	4.0171	0.1031	30.5052	51.8393	0.0358	0.5541	13.166	100.2542
22 / 2 .	3.6703	0.0984	30.7105	51.1488	0.0552	0.5519	13.6001	99.8767
23 / 1 .	3.9914	0.003	30.5396	51.7183	0.0943	0.4096	13.0626	99.8267
23 / 2 .	4.9372	0.1128	28.4556	53.7528	0.1318	0.933	11.4213	99.8249

WR-05-01 Plagioclase (1 = Core; 2 = Rim)

	Oxides Weight %							
Plagioclase	**Na2O**	**MgO**	**SiO2**	**Al2O3**	**K2O**	**FeO**	**CaO**	**Total**
1 / 1 .	5.3827	0.0191	56.0372	27.929	0.2137	0.2707	9.7919	99.6443
1 / 2 .	5.9651	0.0059	57.8282	27.0555	0.4262	0.2628	8.4767	100.0204
2 / 1 .	4.5918	0.0057	53.7008	29.1222	0.145	0.3559	11.4479	99.3693
2 / 2 .	6.1055	0.01	57.777	26.5506	0.3101	0.2565	7.8846	98.8943
4 / 1 .	6.1892	0.0221	57.4716	26.922	0.2641	0.3213	8.2307	99.4211
4 / 2 .	5.6882	0.0217	57.0695	27.7223	0.3371	0.402	9.2288	100.4697
5 / 1 .	5.1699	0.0204	55.5995	28.775	0.1669	0.3006	10.3815	100.4138
5 / 2 .	5.8365	0.0171	56.659	27.4939	0.261	0.3767	9.1985	99.8428
6 / 1 .	5.8084	0.0066	56.9274	27.6608	0.2402	0.3292	9.0727	100.0453
6 / 2 .	4.0343	0.0796	52.0436	30.9546	0.1576	0.5642	12.8771	100.711
7 / 1 .	5.5771	0.0151	57.4312	27.9412	0.2223	0.2375	9.3099	100.7343
7 / 2 .	5.864	0.0136	58.168	27.6016	0.4042	0.3515	8.694	101.0968
8 / 2 .	6.0357	0.0088	58.0974	27.5874	0.3444	0.3485	8.8941	101.3163
9 / 1 .	4.029	0.0084	53.3932	30.14	0.1917	0.3432	12.1417	100.2471
9 / 2 .	4.538	0.0214	54.117	29.6142	0.1361	0.3386	11.6253	100.3907
10 / 1 .	5.561	0.0149	56.7692	28.2404	0.1861	0.2564	9.7234	100.7514
10 / 2 .	5.3259	0.0156	56.7733	28.5781	0.2014	0.3845	9.8297	101.1084
11 / 1 .	5.5996	0.0237	57.4924	28.2942	0.2097	0.2327	9.4246	101.2769
11 / 2 .	6.0959	0.018	58.3171	27.3296	0.2258	0.2676	8.5687	100.8227
12 / 1 .	5.895	0.0203	57.329	27.1822	0.2138	0.3119	8.7639	99.7161
12 / 2 .	5.5001	0.0154	57.0221	27.8242	0.3462	0.2865	9.2808	100.2751
13 / 2 .	6.4243	0.01	58.8576	27.3988	0.2595	0.2787	8.2021	101.4309
14 / 1 .	5.0313	0.0153	53.9364	30.1228	0.1918	0.4382	9.3381	99.074
14 / 2 .	5.0452	0.0132	55.0137	28.9343	0.1688	0.4003	10.3019	99.8771
15 / 1 .	5.5175	0.0164	56.3428	28.3607	0.2014	0.2342	9.826	100.4991
15 / 2 .	6.0016	0.0192	57.5207	27.0281	0.2843	0.3848	7.4419	98.6806
16 / 1 .	5.9691	0.0134	57.9243	27.4877	0.2332	0.2945	8.5694	100.4916
17 / 1 .	5.3908	0.0355	56.535	28.4539	0.1958	0.2976	9.4751	100.3838
17 / 2 .	5.1743	0.0007	55.6152	27.9957	0.2338	0.4305	9.6437	99.0939
18 / 1 .	5.1948	0.0179	55.0949	28.4037	0.1781	0.4019	10.2149	99.5063
18 / 2 .	4.7883	0.0326	54.1292	29.2657	0.1661	0.4366	10.5535	99.3721
19 / 1 .	5.1386	0.021	55.3379	28.8881	0.1723	0.3291	10.4418	100.3287
19 / 2 .	5.0037	0.014	55.3476	28.7347	0.1781	0.3576	10.272	99.9077
20 / 1 .	5.1983	0.0279	55.6308	28.2546	0.168	0.2453	9.9571	99.482
20 / 2 .	5.7106	0.0141	56.2635	27.7702	0.3372	0.4194	9.0144	99.5294

WR-05-01 Plagioclase 1 and 2 Transects

Plagioclase	Location (um)	Oxides Weight % Na2O	MgO	SiO2	Al2O3	K2O	FeO	CaO	Total
1 / 1 .	0	4.9119	0.0178	53.376	28.7875	0.14	0.3595	11.1412	98.7339
1 / 2 .	5	4.6266	0.0288	53.8236	29.3651	0.1283	0.4235	11.7053	100.1011
1 / 3 .	10	4.352	0.0201	53.5358	29.6804	0.1323	0.4562	12.1407	100.3174
1 / 4 .	15	4.3534	0.0242	53.2069	29.6608	0.1484	0.4906	12.1528	100.037
1 / 5 .	20	4.3	0.0306	53.1164	29.8516	0.1214	0.4156	12.2643	100.0999
1 / 6 .	25	4.2544	0.0231	52.9428	29.8385	0.1108	0.3812	12.3394	99.8901
1 / 7 .	30	4.637	0.0184	54.0403	29.1725	0.1312	0.4157	11.5555	99.9705
1 / 8 .	35	4.9616	0.0137	54.8145	28.963	0.1681	0.433	11.0423	100.3962
1 / 9 .	40	5.1105	0.0269	55.2755	28.605	0.1647	0.4049	10.7225	100.3099
1 / 10 .	45	5.0354	0.0259	54.6485	28.6039	0.1591	0.4329	10.78	99.6857
1 / 11 .	50	4.9649	0.0225	54.6811	28.4076	0.1721	0.4142	10.651	99.3133
1 / 12 .	55	5.1061	0.0285	54.6452	28.103	0.1608	0.4251	10.4426	98.9115
1 / 13 .	60	5.1169	0.0187	55.0715	28.1164	0.157	0.3565	10.4475	99.2845
1 / 14 .	65	4.7377	0.0235	54.0257	28.4977	0.1397	0.3767	11.1126	98.9135
1 / 15 .	70	4.7646	0.0219	54.1114	29.0318	0.1361	0.4032	11.4336	99.9024
1 / 16 .	75	4.9215	0.0267	54.5863	28.6755	0.1465	0.3798	11.0572	99.7935
1 / 17 .	80	4.9863	0.0169	54.4999	28.5597	0.1704	0.3736	10.8045	99.4113
1 / 18 .	85	4.9313	0.0223	54.407	28.7479	0.1452	0.4157	11.0713	99.7408
1 / 19 .	90	4.9137	0.017	54.5081	28.9324	0.1384	0.4126	11.1526	100.0748
1 / 20 .	95	4.8994	0.0223	54.5644	28.7639	0.1362	0.4032	11.0742	99.8635
1 / 21 .	100	5.0723	0.0225	54.9935	28.4648	0.163	0.433	10.777	99.9262
1 / 22 .	105	5.2471	0.0232	55.1171	28.3198	0.1612	0.344	10.5792	99.7915
1 / 23 .	110	5.3146	0.0286	55.6064	28.4251	0.197	0.3611	10.5498	100.4827
1 / 24 .	115	5.189	0.0197	55.2366	28.448	0.1647	0.4236	10.7045	100.1861
1 / 27 .	130	5.0718	0.0252	55.2443	28.5187	0.1734	0.3564	10.7488	100.1385
1 / 28 .	135	4.7612	0.0123	54.0812	29.2259	0.1097	0.4923	11.4994	100.1819
1 / 29 .	140	5.1251	0.0165	55.1336	28.6155	0.1553	0.4048	10.8433	100.2941
1 / 30 .	145	5.1847	0.0219	55.4578	28.1639	0.157	0.3643	10.4993	99.849
1 / 31 .	150	5.3952	0.0199	55.9645	28.0311	0.1914	0.4409	10.1018	100.1447
1 / 32 .	155	4.4214	0.0149	53.4897	29.6071	0.1446	0.4891	12.0687	100.2355
1 / 33 .	160	4.5215	0.0215	53.9057	29.418	0.1392	0.4157	11.7799	100.2016
1 / 34 .	165	4.6394	0.0269	53.8379	29.2926	0.1441	0.3861	11.6459	99.973
1 / 35 .	170	4.897	0.0183	54.4372	28.8844	0.1417	0.3722	11.2256	99.9765
1 / 36 .	175	5.1306	0.0212	55.0043	28.5807	0.1592	0.4346	10.7318	100.0625
1 / 37 .	180	4.9482	0.0161	55.0046	28.4839	0.1411	0.419	10.9154	99.9284
1 / 38 .	185	4.2119	0.0181	52.7857	30.1064	0.0982	0.4531	12.4299	100.1033
1 / 39 .	190	4.3662	0.0125	53.3901	29.7156	0.132	0.436	12.052	100.1044
1 / 40 .	195	4.88	0.0184	54.5863	28.9788	0.159	0.4486	11.271	100.3421
1 / 41 .	200	4.9804	0.024	54.8222	28.6525	0.1575	0.3236	10.9516	99.9119
1 / 42 .	205	5.2979	0.0217	55.164	28.1835	0.1599	0.3659	10.494	99.6868
1 / 43 .	210	5.3329	0.0173	55.3349	28.0806	0.1684	0.3971	10.4032	99.7343
1 / 44 .	215	5.1217	0.0154	54.9852	28.6654	0.1718	0.4362	10.7615	100.1572
1 / 45 .	220	5.2088	0.0177	55.1748	27.9934	0.1651	0.3799	10.4571	99.3968
1 / 46 .	225	4.1898	0.0205	53.0436	29.9776	0.113	0.3766	12.5265	100.2476
1 / 47 .	230	4.0673	0.0257	52.6093	30.2235	0.1315	0.4375	12.6736	100.1684
1 / 48 .	235	4.3643	0.0229	53.1419	29.4312	0.1089	0.4547	12.0244	99.5483
1 / 49 .	240	4.6852	0.0208	54.421	29.1226	0.1332	0.4173	11.438	100.2382
1 / 50 .	245	4.7616	0.0139	54.4117	29.1581	0.1442	0.3517	11.3178	100.159
1 / 51 .	250	5.1471	0.0224	55.1078	28.5983	0.1573	0.3815	10.7294	100.1438
1 / 52 .	255	5.0755	0.034	55.1026	28.6123	0.1366	0.3658	10.825	100.1519

1 / 53 .	260	4.1015	0.0537	52.5309	30.0415	0.1065	0.4795	12.7454	100.059
1 / 54 .	265	3.9	0.0687	52.0716	30.2594	0.0747	0.567	13.0324	99.9738
1 / 55 .	270	4.0339	0.0686	52.3894	29.9501	0.0904	0.5671	12.887	99.9866
1 / 56 .	275	4.3588	0.062	53.1676	29.4301	0.1159	0.5125	12.2119	99.8588
1 / 57 .	280	4.1254	0.0566	52.4911	29.709	0.0946	0.5359	12.6063	99.6189
1 / 58 .	285	4.3344	0.0612	52.9451	29.4056	0.1259	0.6452	12.1456	99.6629
1 / 59 .	290	4.504	0.0556	53.3146	28.9248	0.187	0.5906	11.7535	99.3301
1 / 60 .	295	4.9919	0.0376	54.067	28.0217	0.2952	0.6688	10.9078	98.99
2 / 1 .	0	5.0699	0.0034	54.9823	28.5428	0.1574	0.1861	10.6838	99.6257
2 / 2 .	5	5.136	0.0166	55.1227	28.3752	0.1771	0.2565	10.6162	99.7003
2 / 3 .	10	5.2195	0.0109	55.5523	28.3339	0.1546	0.2581	10.416	99.9453
2 / 4 .	15	5.1744	0.0094	54.9865	28.2266	0.1712	0.2956	10.4956	99.3593
2 / 5 .	20	5.0442	0.0075	54.6032	28.4436	0.1644	0.2862	10.714	99.2631
2 / 6 .	25	4.9611	0.0153	54.7343	28.6923	0.1543	0.2658	10.871	99.6941
2 / 7 .	30	5.0385	0.0134	54.8778	28.4343	0.147	0.2659	10.7417	99.5185
2 / 8 .	35	4.9537	0.0084	54.4477	28.516	0.1518	0.2877	10.8529	99.2181
2 / 9 .	40	4.9131	0.0048	54.353	28.9758	0.1456	0.2283	11.1817	99.8022
2 / 10 .	45	4.8088	0.0137	54.2043	28.9873	0.1414	0.2643	11.2087	99.6284
2 / 11 .	50	5.1674	0.0146	55	28.2001	0.1635	0.1892	10.5491	99.284
2 / 12 .	55	5.2871	0.0096	55.4693	28.1261	0.1662	0.1971	10.2809	99.5363
2 / 13 .	60	5.3342	0.0084	55.5407	28.1797	0.1627	0.2534	10.3824	99.8615
2 / 14 .	65	5.2703	0.0021	55.4892	28.0192	0.1697	0.233	10.3323	99.5159
2 / 15 .	70	5.1565	0.0102	55.1344	28.3075	0.1822	0.2409	10.6079	99.6396
2 / 16 .	75	4.9714	0.0115	54.7895	28.7898	0.1354	0.2409	10.8619	99.8002
2 / 17 .	80	4.9421	0.0138	54.1424	28.8621	0.1498	0.2986	11.0545	99.4633
2 / 18 .	85	4.8419	0.0204	54.7224	28.9168	0.1459	0.233	11.1372	100.0177
2 / 19 .	90	4.7753	0.0117	54.376	28.7643	0.133	0.319	11.118	99.4972
2 / 21 .	100	4.8982	0.0072	55.2034	29.1028	0.1698	0.3111	11.1141	100.8066
2 / 23 .	110	5.298	0.0133	56.0166	28.0886	0.1676	0.3285	10.2072	100.1197
2 / 24 .	115	5.9817	0.0062	57.6239	26.8466	0.2018	0.2692	8.7823	99.7118
2 / 25 .	120	6.2913	0.0238	58.3675	26.4549	0.2425	0.2801	8.2884	99.9486
2 / 26 .	125	6.2046	0.0227	58.0888	26.4452	0.2376	0.2864	8.3592	99.6446
2 / 27 .	130	6.5687	0.0144	58.6313	25.996	0.2645	0.277	7.8016	99.5535
2 / 28 .	135	6.8213	0.0276	59.5674	25.4212	0.3241	0.2176	7.1582	99.5374
2 / 29 .	140	6.8015	0.0209	59.4304	25.164	0.3471	0.2818	7.1417	99.1873
2 / 30 .	145	6.817	0.0264	59.3923	25.2777	0.329	0.2302	7.0544	99.1268
2 / 31 .	150	6.7992	0.0281	59.2087	25.4178	0.2865	0.3397	7.3271	99.4071
2 / 32 .	155	5.8055	0.0363	56.5751	27.109	0.2161	0.3332	9.2559	99.331
2 / 33 .	160	4.2887	0.0673	52.738	29.2331	0.1221	0.4939	12.1881	99.1311
2 / 34 .	165	4.2989	0.0528	52.7436	29.2799	0.1054	0.5064	12.0803	99.0672
2 / 35 .	170	3.9404	0.0721	52.1326	29.9578	0.1113	0.5547	12.9136	99.6824
2 / 36 .	175	4.2242	0.0743	52.6973	29.5456	0.1111	0.5469	12.3481	99.5475
2 / 37 .	180	4.1808	0.0694	52.3659	29.609	0.1239	0.6296	12.4453	99.4239
2 / 38 .	185	4.2982	0.0582	52.8448	29.2616	0.1644	0.5922	12.1574	99.3767
2 / 39 .	190	4.555	0.0544	53.4269	28.7815	0.1887	0.5876	11.6395	99.2337
2 / 40 .	195	5.3402	0.0268	55.2197	27.3833	0.3766	0.5191	9.9807	98.8464

Appendix B – LA-ICP-MS Data

CC-04-01 Plagioclase 3

Distance (um)	245	214.2	183.6	153	122.4
Calculated values (ug/g)					
Li	BDL	BDL	BDL	BDL	BDL
Mg	535	666	483	2629	711
Si	596900	552900	512400	515400	506200
Ca	169282	201809	185816	174931	182151
Ti	687	530	462	436	439
Sr[1]	1647	1690	1644	1567	1638
Sr[2]	1668	1803	1636	1569	1662
Ba	156	90.6	68.1	84.2	73.8
La	2.29	1.92	1.79	1.34	1.49
Ce	3.32	2.56	2.68	2.60	2.79
Pr	BDL	BDL	BDL	BDL	0.40
Nd	BDL	BDL	BDL	BDL	BDL
Eu	0.79	BDL	0.71	BDL	0.90
Pb	2.10	1.01	BDL	2.21	0.52

CC-04-01 Plagioclase 3 (continued)

Distance (um)	91.8	61.2	30.6	0
Calculated values (ug/g)				
Li	BDL	10.3	BDL	17.4
Mg	722	539	610	633
Si	512200	509200	503800	505700
Ca	192076	187994	196890	181361
Ti	453	459	431	431
Sr[1]	1624	1655	1659	1744
Sr[2]	1689	1685	1703	1628
Ba	73.7	74.0	71.1	50.2
La	1.59	1.70	1.73	1.47
Ce	2.86	3.16	2.35	2.62
Pr	BDL	0.18	BDL	BDL
Nd	BDL	BDL	BDL	BDL
Eu	BDL	0.95	0.76	BDL
Pb	BDL	0.50	BDL	BDL

[1] Calculated 86Sr
[2] Calculated 88Sr

CC-04-01 Plagioclase 4

Distance (um)	190	152	114	76	38
Calculated values (ug/g)					
Li	18.6	14.7	BDL	10.3	BDL
Mg	508	581	673	661	731.1
Si	583700	540900	523500	513700	505500
Ca	158321	206949	182300	190652	175759
Ti	1033	487	447	459	529
Sr[1]	1519	1670	1644	1724	1591
Sr[2]	1544	1718	1729	1738	1633
Ba	137	68.8	79.9	71.6	71.2
La	2.07	1.65	2.02	2.05	1.79
Ce	4.32	2.72	3.40	3.74	3.25
Pr	0.75	BDL	0.63	BDL	0.42
Nd	BDL	BDL	BDL	BDL	BDL
Eu	BDL	0.80	BDL	BDL	0.81
Pb	BDL	BDL	BDL	BDL	BDL

CC-04-01 Plagioclase 4 (continued)

Distance (um)	0
Calculated values (ug/g)	
Li	BDL
Mg	654
Si	518600
Ca	194287
Ti	520
Sr[1]	1748
Sr[2]	1764
Ba	87.9
La	0.76
Ce	2.47
Pr	BDL
Nd	BDL
Eu	1.06
Pb	BDL

[1] Calculated 86Sr
[2] Calculated 88Sr

PD-04-01 Plagioclase 2

Distance (um)	620	584	547.5	511	474.5
Calculated values (ug/g)					
Li	13.7	16.8	14.3	13.5	17.9
Mg	1548	164	187	253	401
Si	521500	519000	591000	561800	563500
Ca	134767	114309	141054	133483	164024
Ti	994	114	138	194	280
Sr[1]	1401	1389	1587	1605	1609
Sr[2]	1407	1351	1556	1490	1650
Ba	161	181	207	206	190
La	5.65	4.66	5.80	4.97	6.70
Ce	10.9	8.50	9.03	7.97	10.7
Pr	1.71	0.65	1.05	0.71	1.25
Nd	4.76	2.46	2.24	2.69	BDL
Eu	1.69	1.03	2.02	1.56	1.94
Pb	3.06	2.11	3.19	3.87	4.28

PD-04-01 Plagioclase 2 (continued)

Distance (um)	438	401.5	365	328.5	292
Calculated values (ug/g)					
Li	10.3	13.5	12.7	24.1	19.9
Mg	215	162	159	311	281
Si	555500	539200	555500	561500	557700
Ca	121175	119437	138703	121983	132372
Ti	91.4	102	1134	88.8	118
Sr[1]	1458	1462	1589	1445	1547
Sr[2]	1442	1393	1543	1419	1522
Ba	207	204	192	187	202
La	4.22	4.93	5.28	5.97	6.89
Ce	8.64	8.32	10.2	8.74	13.9
Pr	0.56	0.69	0.97	0.61	1.62
Nd	3.18	3.75	2.69	2.57	5.60
Eu	1.49	1.10	0.95	1.57	1.28
Pb	2.80	2.94	3.29	3.14	2.57

[1] Calculated 86Sr
[2] Calculated 88Sr

PD-04-01 Plagioclase 2 (continued)

Distance (um)	255.5	219	182.5	146	109.5
Calculated values (ug/g)					
Li	12.9	15.6	20.6	15.0	24.8
Mg	142	157	235	653	303.7
Si	542200	576600	565300	547300	556600
Ca	133446	114361	128661	90466	133648
Ti	118	109	261	1617	165
Sr[1]	1448	1465	1455	969	1505
Sr[2]	1423	1404	1461	939	1506
Ba	174	204	233	345	194
La	6.88	5.19	7.10	12.2	6.54
Ce	12.7	9.83	13.6	27.7	12.0
Pr	1.17	0.77	1.57	3.52	0.96
Nd	3.28	3.86	4.63	15.2	5.82
Eu	1.55	1.16	1.94	1.59	1.57
Pb	3.25	3.13	4.84	3.91	3.06

PD-04-01 Plagioclase 2 (continued)

Distance (um)	73	36.5	0
Calculated values (ug/g)			
Li	17.9	18.6	10.7
Mg	116	117	112
Si	557500	5.7500	553500
Ca	134455	113877	131847
Ti	139	114	148
Sr[1]	1515	1285	1497
Sr[2]	1487	1327	1450
Ba	197	192	194
La	7.77	6.42	6.93
Ce	14.0	10.6	14.2
Pr	1.22	1.19	0.89
Nd	6.28	2.75	5.32
Eu	1.72	1.13	2.20
Pb	3.94	2.55	3.36

[1] Calculated 86Sr
[2] Calculated 88Sr

PD-04-01 Plagioclase 4

Distance (um)	520	482.3	445.2	408.1	371
Calculated values (ug/g)					
Li	16.5	18.1	18.1	17.2	14.7
Mg	432	324	219	1071	216
Si	516200	550300	542100	555200	533400
Ca	199373	167628	155548	151036	144232
Ti	319	204	175	200	134
Sr[1]	1828	1685	1609	1529	1512
Sr[2]	1865	1695	1597	1472	1494
Ba	69.7	112	166	211	190
La	1.69	2.71	6.86	6.20	7.27
Ce	2.76	4.50	9.52	9.82	11.3
Pr	0.55	0.91	1.31	1.03	1.03
Nd	BDL	BDL	3.22	3.35	4.39
Eu	BDL	1.28	1.58	1.62	1.97
Pb	BDL	1.50	3.21	2.83	3.01

PD-04-01 Plagioclase 4 (continued)

Distance (um)	333.9	296.8	259.7	222.6	185.5
Calculated values (ug/g)					
Li	19.6	21.0	16.2	21.2	15.5
Mg	136	177	158	140	349
Si	539300	571700	560200	531900	556700
Ca	154139	122082	149744	147256	140994
Ti	149	93.4	124	147	137
Sr[1]	1657	1582	1605	1585	1620
Sr[2]	1609	1496	1616	1563	1561
Ba	208	229	205	218	212
La	7.39	7.56	9.18	8.05	7.38
Ce	12.3	8.83	13.8	13.3	11.8
Pr	1.55	1.19	1.25	1.42	1.58
Nd	5.86	3.55	3.10	5.69	4.17
Eu	2.06	2.02	2.77	1.57	1.89
Pb	2.75	3.22	1.97	3.19	3.43

[1] Calculated 86Sr
[2] Calculated 88Sr

PD-04-01 Plagioclase 4 (continued)

Distance (um)	148.4	111.3	74.2	37.1	0
Calculated values (ug/g)					
Li	22.4	17.3	20.2	16.9	14.9
Mg	262	213	410	151	315
Si	551300	561900	557100	565800	564400
Ca	135628	142309	132254	157086	126266
Ti	125	141	103	139	98.5
Sr[1]	1529	1550	1571	1642	1491
Sr[2]	1515	1527	1494	1601	1458
Ba	203	218	221	222	213
La	6.41	7.08	6.90	7.89	7.63
Ce	10.6	13.3	11.5	13.8	10.1
Pr	0.94	1.59	1.11	1.36	1.05
Nd	3.76	4.26	4.74	3.79	3.46
Eu	2.14	2.55	1.34	1.90	2.26
Pb	3.44	2.40	3.30	2.94	2.96

[1] Calculated 86Sr
[2] Calculated 88Sr

PD-05-02 Plagioclase 1

Distance (um)	335	271	216.8	162.6	108.4
Calculated values (ug/g)					
Li	BDL	15.3	BDL	18.4	10.2
Mg	616	202	144.7	142	116
Si	541000	500500	539300	536700	556200
Ca	195347	126687	142839	132518	129870
Ti	363	453	149	153	172
Sr[1]	1937	1277	1557	1375	1447
Sr[2]	1995	1324	1569	1444	1490
Ba	85.0	128	175	162	200
La	2.15	3.79	6.11	4.65	5.65
Ce	3.48	7.41	13.0	8.73	9.25
Pr	0.51	0.42	1.02	0.50	0.43
Nd	BDL	BDL	2.83	2.78	2.56
Eu	0.92	0.91	2.97	1.18	1.84
Pb	BDL	1.41	4.02	4.57	3.01

PD-05-02 Plagioclase 1 (continued)

Distance (um)	54.2	0
Calculated values (ug/g)		
Li	11.9	19.3
Mg	139	133
Si	546500	541800
Ca	122451	127922
Ti	122	134
Sr[1]	1429	1438
Sr[2]	1453	1509
Ba	181	194
La	5.92	6.35
Ce	9.25	12.7
Pr	0.71	0.98
Nd	2.48	2.54
Eu	1.76	1.35
Pb	3.95	4.15

[1] Calculated 86Sr
[2] Calculated 88Sr

PD-05-02 Plagioclase 3

Distance (um)	770	738.3	706.2	674.1	642
Calculated Values (ug/g)					
Li	17.0	22.4	24.6	16.9	15.3
Mg	674	997	588	163	124
Si	509900	506300	554400	555300	518400
Ca	183362	133138	145358	157636	144304
Ti	663	925	1040	217	151
Sr[1]	1757	1383	1491	1667	1507
Sr[2]	1813	1401	1521	1677	1504
Ba	84.8	205	209	180	185
La	2.34	7.81	9.83	8.23	6.91
Ce	5.44	13.2	14.7	14.1	8.20
Pr	0.77	1.39	1.44	1.54	1.05
Nd	1.74	5.58	5.85	5.39	3.07
Eu	0.28	1.39	2.42	1.31	1.94
Pb	1.09	4.10	3.45	2.88	3.52

PD-05-02 Plagioclase 3 (continued)

Distance (um)	609.9	577.8	545.7	513.6	481.5
Calculated Values (ug/g)					
Li	15.2	17.6	17.9	13.8	23.7
Mg	162	162	147	137	130
Si	560100	571900	567300	555600	561900
Ca	142926	131517	140547	125314	131577
Ti	120	147	137	113	120
Sr[1]	1605	1583	1565	1486	1584
Sr[2]	1635	1637	1593	1560	1582
Ba	201	223	191	206	215
La	6.88	7.65	8.32	6.07	6.91
Ce	11.2	9.74	10.8	10.9	9.97
Pr	0.96	0.97	1.20	1.39	1.02
Nd	3.82	3.90	5.07	2.22	3.85
Eu	1.86	1.69	1.81	1.36	1.37
Pb	3.18	4.30	2.65	3.16	3.04

[1] Calculated 86Sr
[2] Calculated 88Sr

PD-05-02 Plagioclase 3 (continued)

Distance (um)	449.4	417.3	385.2	353.1	321
Calculated Values (ug/g)					
Li	16.9	10.9	10.5	13.5	20.1
Mg	129	170	151	138	172
Si	561100	558000	556600	531400	559900
Ca	127553	130108	121889	121842	140703
Ti	145	167	154	134	151
Sr[1]	1447	1464	1520	1467	1644
Sr[2]	1481	1543	1541	1452	1639
Ba	197	186	224	186	194
La	5.56	6.67	5.51	6.32	8.69
Ce	9.22	11.3	9.58	9.21	11.9
Pr	0.57	0.60	0.62	0.69	1.18
Nd	3.55	0.96	3.75	2.08	6.08
Eu	1.79	1.72	1.55	1.81	1.88
Pb	3.16	2.58	2.58	3.05	2.16

PD-05-02 Plagioclase 3 (continued)

Distance (um)	288.9	256.8	224.7	192.6	160.5
Calculated Values (ug/g)					
Li	BDL	9.16	12.4	9.04	18.9
Mg	148.7	176	145	169	161
Si	556900	540500	529600	533000	521100
Ca	168433	167471	166251	177249	162440
Ti	157	179	173	157	167
Sr[1]	1666	1664	1663	1668	1662
Sr[2]	1699	1612	1687	1721	1687
Ba	167	178	181	168	186
La	9.92	8.46	7.53	9.09	9.41
Ce	12.9	13.1	14.5	12.6	13.0
Pr	1.30	0.92	1.20	1.22	1.03
Nd	3.91	4.02	3.81	3.00	3.83
Eu	1.71	1.11	2.15	1.38	2.08
Pb	2.30	2.85	3.79	4.12	4.22

[1] Calculated 86Sr
[2] Calculated 88Sr

PD-05-02 Plagioclase 3 (continued)

Distance (um)	128.4	96.3	64.2	32.1	0
Calculated Values (ug/g)					
Li	8.82	8.29	9.27	18.9	18.1
Mg	155	157	127	146	145
Si	528600	536200	531500	554200	563700
Ca	149921	132050	127159	125910	122497
Ti	165	136	165	154	162
Sr[1]	1646	1586	1540	1485	1523
Sr[2]	1677	1589	1545	1568	1571
Ba	181	197	198	221	209
La	6.68	7.35	6.62	6.67	6.98
Ce	12.6	11.7	10.6	10.3	10.9
Pr	1.22	0.99	1.00	1.17	0.79
Nd	3.81	3.42	3.92	2.82	3.02
Eu	2.12	1.58	2.03	1.84	1.31
Pb	3.18	2.12	3.26	2.32	3.59

[1] Calculated 86Sr
[2] Calculated 88Sr

WR-05-01 Plagioclase 1

Distance (um)	295	258.3	221.4	184.5	147.6
Calculated Values (ug/g)					
Li	28.4	20.7	26.7	23.4	30.0
Mg	338	113	91.8	132	115
Si	540700	531700	544200	551600	544400
Ca	195009	158175	152381	169145	172761
Ti	253	149	152	121	144
Sr[1]	1790	1693	1827	2135	1847
Sr[2]	1737	1646	1815	2109	1830
Ba	109	159	140	163	152
La	3.10	3.91	5.85	6.45	5.52
Ce	3.41	6.90	7.81	7.97	9.22
Pr	0.80	0.81	1.23	0.93	0.96
Nd	BDL	2.61	1.50	2.97	2.82
Eu	1.20	1.45	0.77	1.52	1.20
Pb	0.73	2.44	2.70	2.32	2.62

WR-05-01 Plagioclase 1 (continued)

Distance (um)	110.7	73.8	36.9	0
Calculated Values (ug/g)				
Li	20.9	34.9	30.6	26.1
Mg	121	127	139	171
Si	540800	549900	540300	540400
Ca	164011	186849	163403	169828
Ti	189	172	211	242
Sr[1]	1711	2000	1685	1777
Sr[2]	1718	1977	1615	1741
Ba	134	161	130	157
La	4.96	5.20	3.88	4.03
Ce	7.15	9.51	6.84	6.87
Pr	0.68	0.78	0.59	0.37
Nd	BDL	2.60	3.08	BDL
Eu	1.51	0.74	0.92	1.23
Pb	1.82	1.84	3.00	1.96

[1] Calculated 86Sr
[2] Calculated 88Sr

WR-05-01 Plagioclase 2

Distance (um)	195	170.8	146.4	122	97.6
Calculated Values (ug/g)					
Li	BDL	39.50	33.47	33.94	38.10
Mg	365.85	351.54	105.38	81.78	65.33
Si	52.70	56.58	59.57	57.62	53.40
Ca	195228.95	169839.46	123601.76	135710.30	170931.51
Ti	279.09	139.74	88.79	89.97	133.04
Sr[1]	1935.99	1717.46	1576.77	1522.25	1734.34
Sr[2]	1870.73	1782.16	1532.06	1518.21	1663.79
Ba	103.44	238.28	347.58	351.45	272.95
La	5.13	5.28	10.97	11.64	6.97
Ce	5.12	11.01	14.44	14.14	14.62
Pr	BDL	1.71	1.20	0.67	1.95
Nd	BDL	BDL	5.13	4.20	BDL
Eu	BDL	1.19	1.25	2.29	2.41
Pb	BDL	4.00	3.87	3.54	8.23

WR-05-01 Plagioclase 2 (continued)

Distance (um)	73.2	48.8	24.4	0
Calculated Values (ug/g)				
Li	20.55	47.35	39.40	18.05
Mg	47.73	71.85	33.59	73.42
Si	54.79	55.47	54.45	54.91
Ca	152826.93	170744.70	182747.69	150223.14
Ti	170.29	172.88	182.39	153.46
Sr[1]	1685.31	1667.13	1853.51	1669.68
Sr[2]	1611.13	1640.10	1746.82	1599.48
Ba	225.04	269.95	278.53	204.88
La	9.64	10.66	10.20	9.24
Ce	10.12	13.71	17.72	13.94
Pr	0.91	2.89	1.15	1.90
Nd	3.07	5.80	7.20	3.09
Eu	2.51	1.65	2.18	1.96
Pb	5.71	3.61	5.02	4.97

[1] Calculated 86Sr
[2] Calculated 88Sr

Appendix C – Crystal Size Distribution Steps

- Standard thin section to X-Ray map on EMPA
  - High and Low Magnifications
    - Al and Fe – Most Important
    - Ca and K – Nice to have for double checking crystal boundaries

- Adobe Photoshop 7.0
  - Prepare Al X-Ray Map
    - Make sure image is flattened[1] and not in grayscale[2]
      1. Layer → Flatten Image
      2. Image → Mode → RGB Color
  - Coloring crystals on Al X-Ray May (High or Low Magnifications
    - Layer → New Layer → Label as "Color"
    - Outline and color every desired whole crystal using *Polygonal Lasso Tool*. Use different colors for crystals that are touching each other in order to measure them as separate crystals. Once desired crystal is outlined use the *Paint Bucket Tool* to color in selected crystal.
      - CMKY Red, CMKY Magenta, Pastle Red Orange are all good colors to use for crystals and are all picked up in NIH Image.
      - Use the *Wand Tool* to highlight already colored crystals to change or fix color.
      - Make sure that crystals are being colored on the layer called "Color" not the Background layer.
    - Outline and color crystals cut off by the edge (optional). These crystals are not measured and can be colored for completion.
      - Use CMKY Blue
    - Outline and color vesicles
      - Use 50% Gray

- ➢ Use Fe X-Ray map to help distinguish vesicles from other minerals (will remain black)
- ➢ Trace over scale bar at bottom of picture with a black line.
  - o Low Magnification = 2 mm
  - o High Magnification = 5 mm
- ▪ When image is completely colored
  - ➢ Save as "*sampleID*_color" as a TIFF file
- ▪ Delete Background and flatten image
  - ➢ Save as "*sampleID*_flat" as a TIFF file
- o Repeat process for other Al X-Ray Map (High or Low Magnification)

- NIH Image 1.63
  - o Open flat image
  - o Set Scale
    - ▪ Use *Straight Line Tool* to trace scale at bottom of picture
    - ▪ Use *Hand Tool* to drag image
      - ➢ Analyze → Set Scale → Insert known distance
  - o Determine whole slide area
    - ▪ Use *Hand Tool* to drag image
    - ▪ Use *Coordinate Tool* to determine X – Y coordinates found in INFO BOX
      - ➢ May have to subtract values if a margin is present. Only want the slide area that contains the rock sample.
  - o Measure Crystals
    - ▪ Analyze → Options
      - ➢ Check the following in Options box
        - o Ellipse Major Axis
        - o Include Interior Holes
        - o Wand Auto Measure
        - o Headings
      - ➢ Max = 8000

- Field Width = 18
- Digits Right of Decimal = 5
- OK

- Double click *Wand Tool*
  - Move red bar on left side to select certain colored crystals
  - Shrink red bar as to not to select random pixels
- Analyze → Analyze Particles
  - Check the following in Analyze Particles Box
    - Include Interior Holes
    - Ignore Particles Touching the Edge
  - Unselect Reset Measurement Counter and Outline Particles
  - Minimum Particle Size
    - Low = 15
    - High = 5
  - Redo steps to analyze all colored crystals

- Analyze → Show Results
  - Edit → Copy Measurements
    - Paste into Excel and save file
- Measure Vesicles
  - Analyze → Options
    - Check the following in Options Box
      - Area
      - Include Interior Holes
      - Wand Auto Measure
      - Headings
    - Max = 8000
    - Field Width = 18
    - Digits Right of Decimal = 5
    - Uncheck all other boxes
  - Double click *Wand Tool* and highlight vesicles
  - Analyze → Analyze Particles

- Check the following in Analyze Particles Box
  - Label Particles
  - Include Interior Holes
- Min Particle Size = 12

- Analyze → Show Results
  - Edit → Copy Measurements
    - Paste into Excel and save file
      - Subtract this the total vesicle area from total slide area to get the total rock area
- Repeat the NIH Image steps for the other magnification of the X-Ray map image for the same sample. Add measurements to the same Excel file but on a different worksheet.

- Excel
  - Highlight column labeled "Major" at the top (include numbers only)
    - Copy column and paste into Kaleidagraph
  - Repeat with data from the other magnification as to have all the measurements from both magnifications in one column.

- Kaleidagraph
  - After the data is pasted click on top to highlight the whole column
    - Functions → Bin Data
      - Adjust the number of bins so that the data resembles a histogram with decreasing frequencies from left to right. Also decrease the number of bins with zeros.
        - Click the Recalculate after each change
      - Check the following
        - Bin Counts
        - Right Bin Edge
        - Histogram
      - Click Copy to Clipboard

- Paste into Excel

- Excel
  - Using the following table as a guide use the histogram bin measurements to create 2D CSD plot
    - 2D plot will have “mid bin” on X-axis and “ln of population density” on Y-axis
      - This will form a rough plot of the CSD data for the sample

- 2D to 3D conversions using CSD Corrections created by Higgins
  - Under “Data Input” Tab
    - Either raw measurement data (Raw Data) or 2D bin data (Frequency Data) can be entered into the right hand side of the screen.
    - Measurement
      - Ellipse Major Axis
    - Fabric
      - Select Appropriate Fabric, Quality of Fabric, and Orientation
    - Shape
      - See Higgins (2000) for Short, Intermediate, and Long ratios
    - Size Scale
      - Log 10
        - 5 per decade
    - Click on “Calculate Pop Dens” at top
  - Under “Results” Tab
    - Copy data results from the area labeled Three dimensional data back into Excel

- Excel

- Re-plot CSD plots
  - Crystal Length (X-axis), Population Density (Y-axis)
- Add trendlines to data points to characterize the different crystal populations if any are present
- Calculate average residence time using following equation

$$t_r = \frac{-1}{G * m * 31,536,000}$$

  - Results in years
  - Assume appropriate growth rate (G)

CSD Setup for Excel spreadsheet.

	A	B	C	D		F	G	H	I	J
1	Right Bin Edge (mm)	Bin Size (mm)	Mid Bin (mm)	Number of Crystals (#)	Crystals per Measured Area (#/mm^2)	2D Cumulative # of Crystals (#/mm^2)	3D Cumulative # of Crystals (#/mm^3)	Change in Cumulative # (#/mm^3)	Population density (#/mm^3/mm)	ln of Population Density (#/mm^4)
2	Bin Data from Kaleidagrap h	= A2 – A1	= (A2 + A1) / 2	= Column A from Kaleidagraph	= D2 / Total Rock Area	= E2 + F1	= F2 ^ 1.5	= G2 – G1	= H2 / B2	= ln (I2)